

# **UNIVERSITÄTSKLINIKUM HAMBURG-EPPENDORF**

Zentrum für Experimentelle Medizin

Institut für Neurophysiologie und Pathophysiologie

Direktor: Prof. Dr. Andreas K. Engel

## **Neuromodulation and the timescale of evidence accumulation during perceptual decision-making**

### **Dissertation**

zur Erlangung des Doktorgrades PhD

an der Medizinischen Fakultät der Universität Hamburg.

vorgelegt von:

Thomas Pfeffer

aus Zwiesel

Hamburg 2017

**(wird von der Medizinischen Fakultät ausgefüllt)**

**Angenommen von der**

**Medizinischen Fakultät der Universität Hamburg am:**

\_\_\_\_\_

**Veröffentlicht mit Genehmigung der**

**Medizinischen Fakultät der Universität Hamburg.**

**Prüfungsausschuss, der/die Vorsitzende:** Prof. Dr. Tobias H. Donner

**Prüfungsausschuss, zweite/r Gutachter/in:** Prof. Dr. Claus C. Hilgetag

**Prüfungsausschuss, dritte/r Gutachter/in:** Prof. Dr. Thilo Womelsdorf

**Datum der mündlichen Prüfung:** 03. November 2017

# Table of contents

<b>1. Synopsis</b>	<b>5</b>
<b>1.1. Introduction</b>	<b>5</b>
<b>1.2. Perceptual decision-making</b>	<b>7</b>
1.2.1. Temporal accumulation	8
1.2.2. Neurophysiological principles of temporal accumulation	9
<b>1.3. Neuromodulation</b>	<b>11</b>
1.3.1. Noradrenaline	12
1.3.2. Acetylcholine	15
1.3.3. Dopamine	17
1.3.4. Other neuromodulators	18
<b>1.4. Study overview and summary of results</b>	<b>18</b>
<b>1.4.1. Study 1: Action Planning and Perceptual Choice</b>	<b>19</b>
1.4.1.1. Background and Aims	19
1.4.1.2. Results and Discussion	21
<b>1.4.2. Study 2: Adaptive Evidence Integration in Perceptual Choice</b>	<b>22</b>
1.4.2.1. Background and Aims	22
1.4.2.2. Results and Discussion	24
<b>1.4.3. Study 3: Neuromodulation and Cortical Excitation-Inhibition Balance</b>	<b>25</b>
1.4.3.1. Background and Aims	25
1.4.3.2. Results and Discussion	26
<b>1.4.4. Study 4: Neuromodulation of Functional Connectivity</b>	<b>28</b>
1.4.4.1. Background and Aims	28
1.4.4.2. Results and Discussion	29
<b>1.4.5. Study 5: Context-dependent neuromodulation of the intrinsic cortical correlation structure</b>	<b>30</b>
1.4.5.1. Background and Aims	30
1.4.5.2. Results and Discussion	31
<b>1.5. General Discussion</b>	<b>31</b>
1.5.1. Top-down control of temporal accumulation	32
1.5.2. Neuromodulation of excitation and inhibition	33
1.5.3. Neuromodulation of large-scale interactions	34
<b>2. Abbreviations</b>	<b>36</b>
<b>3. References</b>	<b>37</b>
<b>4. Experimental chapters</b>	<b>46</b>
<b>4.1. Study 1: Action planning and perceptual choice</b>	<b>46</b>

4.2.	Study 2: Adaptive Evidence Integration in Perceptual Choice .....	68
4.3.	Study 3: Neuromodulation and Cortical Excitation-Inhibition Balance .....	75
4.4.	Study 4: Neuromodulation of Functional Connectivity .....	125
4.5.	Study 5: Context-dependent neuromodulation of the intrinsic cortical correlation structure .....	138
5.	Abstract .....	159
5.1.	English .....	159
5.2.	German.....	160
6.	Acknowledgements.....	163
7.	Curriculum vitae.....	165
8.	Eidesstattliche Versicherung (Declaration of academic integrity).....	166



# 1. Synopsis

## 1.1. Introduction

We are continuously faced with the challenge to make inferences about the state of the world and make choices that guide our behavior based on those inferences. Imagine you are walking down a sidewalk on a busy shopping street. While walking, you are constantly approached by people from different directions moving at different speeds. In order to successfully navigate through such a dynamic crowd and to avoid bumping into other pedestrians, you have to decide continuously whether to swerve left or right. The choices we make in such situations clearly depend on the available sensory information, such as the number of pedestrians approaching from the different directions. The information we gather, however, is not always reliable, but often ambiguous and “noisy”. This ambiguity can be the result of external factors, such as rain, blurring the visual field, but can also arise internally, for example from imperfections along the sensory processing stream. To account for these various sources of noise, perceptual decisions are not based solely on instantaneous estimates of the external sensory information. Instead, mathematical models of decision making posit that sensory information is gradually accumulated (or integrated) over time, in order to attenuate the impact of noisy sensory estimates (Usher and McClelland, 2001; Smith and Ratcliff, 2004; Gold and Shadlen, 2007). This accumulation of information is hypothesized to be carried out until a decision threshold or bound is crossed and a response is initiated (Fig. 1A/B).

The choices we make, however, are not only determined by the (noisy) interpretations of the sensory information provided by the external world. Imagine, you are waking

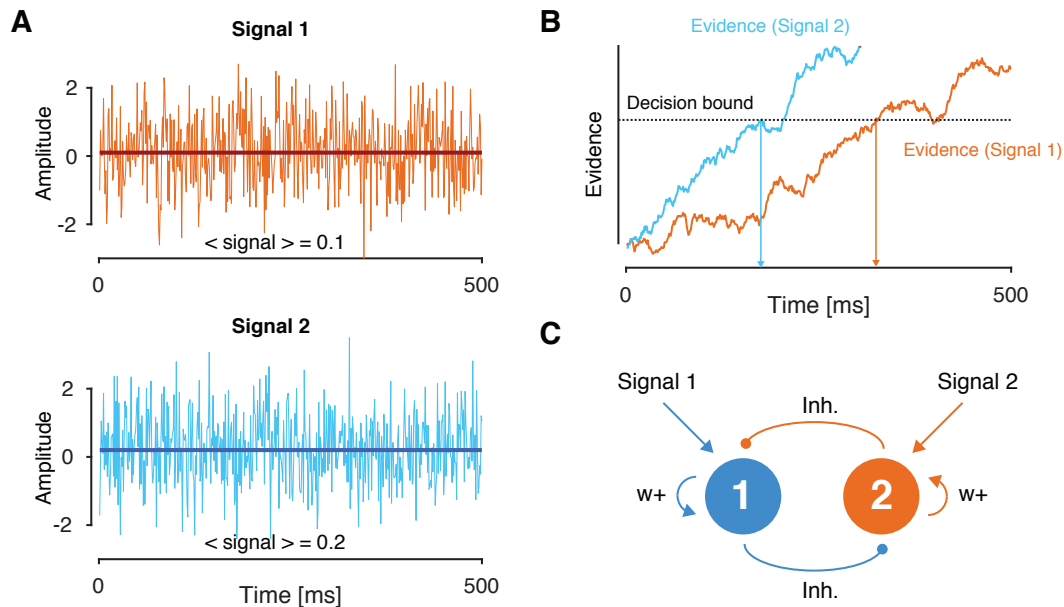


**Figure 1.** Sequential sampling and temporal accumulation. **(A)** Evidence for one choice over an alternative (Choice 1 – Choice 2) is encoded in primary sensory areas. *Top.* Weak evidence for choice 1 with an average strength of +0.1. *Bottom.* Stronger evidence for choice 1 with an average strength of +0.2. **(B)** Instantaneous sensory evidence is accumulated over time until a decision bound (or threshold) is crossed, upon which a choice is made. **(C)** Schematic of an implementation of temporal accumulation within a neural circuit. Two populations, representing different choice alternatives, maintain information through recurrent excitation (denoted with  $w+$ ) and compete with each other through lateral inhibition (Wong and Wang, 2006).

down the same shopping street. The street is just as busy as usual. This time, however, you need to catch a bus, which you can already spot in the distance and which is about to depart shortly. Although the sensory information you gather (i.e., the number of pedestrians approaching you) is, on average, similar to the day before, your choices may differ markedly, as you are rushing down the street. Changes in the levels of arousal, stress and motivation (among others), can substantially alter cortical information processing in general (Aston-Jones and Cohen, 2005; Harris and Thiele, 2011; Zaghera and McCormick, 2014; McGinley et al., 2015b), and decision-making in particular (Eckhoff et al., 2009; Cheadle et al., 2014; de Gee et al., 2014). Previous research demonstrates that these changes in global “brain state” are the result of the action of neuromodulatory systems (Phillis, 1968; Robbins, 1984; Aston-Jones and

Cohen, 2005; Berridge, 2008; Sara, 2009; Lee and Dan, 2012; Zagha and McCormick, 2014), such as the noradrenergic and the cholinergic system. Studies across various species demonstrate that changes in the neuromodulatory levels in the brain are accompanied by profound changes in the computational characteristics of single neurons, local microcircuits as well as distributed networks (Servan-Schreiber et al., 1990; Aston-Jones and Cohen, 2005; Bouret and Sara, 2005; Lee and Dan, 2012; Marder, 2012; Pinto et al., 2013; Chen et al., 2015; McGinley et al., 2015b). Importantly, in contrast to the traditional view of neuromodulatory systems, these changes can occur rapidly, already while a decision is evolving (Aston-Jones and Cohen, 2005; Harris and Thiele, 2011; Martins and Froemke, 2015). Hence, depending on the internal state of the decision maker, her/his choices will be different, even when faced with similar sensory input.

The two mentioned examples roughly outline the scope of this thesis: in the first part, I will review the progress over recent years in the field of decision neuroscience, with a particular focus on the mechanisms and time scales of temporal accumulation of sensory information. The second part will be concerned with three major neuromodulatory systems and their impact on neuronal dynamics and cognitive operations. This is followed by an overview of the studies which are part of this thesis. For each study, I will provide a short summary of the background, the specific aims as well as a summary of the results. In the last section, I will discuss and integrate our findings and provide an outlook into possible future directions.

## **1.2. Perceptual decision-making**

Perceptual tasks are a useful framework to study decision-making, as they allow the experimenter to control the quantity and quality of the information with high precision

(Gold and Shadlen, 2007), but the findings from perceptual decision-making should, in principle, translate to other, more complex forms of decisions, such as value-based economic decisions (Polanía et al., 2014). According to sequential sampling models of decision-making, the formation of a perceptual choice can be roughly divided into three stages (Smith and Ratcliff, 2004; Gold and Shadlen, 2007; Drugowitsch et al., 2016): (i) the initial encoding stage, where incoming sensory information is being processed, probably carried out in primary sensory areas, (ii) the gradual accumulation of this sensory information over time, and (iii) the transformation of sensory evidence into a choice, for example in form of a motor output, once sufficient information has been accumulated and a decision threshold or bound is reached. Over the last decade, investigating the principles behind decision-making emerged as one of the central topics in the field of cognitive and systems neuroscience. Since, the neuronal circuits as well as the computational principles underlying perceptual decision-making have been extensively characterized in studies on rodents (Brunton et al., 2013; Hanks et al., 2015), non-human primates (Gold and Shadlen, 2000; Shadlen and Newsome, 2001; Shadlen and Kiani, 2013), in humans (Donner et al., 2007, 2009; Siegel et al., 2007; Kelly and O’Connell, 2013) as well as theoretically (Ratcliff, 1978; Usher and McClelland, 2001; Wang, 2002; Wong and Wang, 2006; Eckhoff et al., 2009).

### 1.2.1. Temporal accumulation

A hallmark of decision-making is the gradual accumulation of sensory information over time (Ratcliff, 1978; Usher and McClelland, 2001; Gold and Shadlen, 2007). Computational models of decision-making posit a “decision variable”, which encodes the relative evidence for one choice over another. This decision variable shows a gradual build-up during stimulus viewing, with a slope of the build-up being determined

by the quality of the signal (i.e., the strength of the evidence for one choice alternative over another) (Fig. 1B). The decision process is halted, when a decision threshold is reached, upon which a choice is made (Smith and Ratcliff, 2004; Gold and Shadlen, 2007). One indicator that observers indeed accumulate information over time is the decrease in detection threshold (i.e., the lowest signal strength needed in order to be perceived by an observer) as a function of signal duration. This means that very weak signals are likely to be missed if only presented for very short durations. On the other hand, if the same signal is presented for a longer period, the chance of a successful detection increases. In such situations, the strength of the evidence is one key predictor for reaction times, with stronger evidence yielding faster responses as the threshold is reached quicker (Fig. 1B). Errors, for instance false alarms, can arise in this process from the excessive accumulation of noise, which leads to an incidental threshold crossing, whereas misses result when the accumulated signal fails to reach the threshold within the available amount of time. Neurophysiological substrates of temporal accumulation have been identified in various brain regions, many of them linked with the preparation of the motor action that was required to indicate the subjects' choice as well as working memory processes. Among these regions are lateral intraparietal area (Zaborszky et al., 1999; Gold and Shadlen, 2000; Shadlen and Newsome, 2001; Roitman and Shadlen, 2002), prefrontal (Kim and Shadlen, 1999; Philiastides et al., 2011), somatosensory (Romo et al., 2002) and motor cortex (Donner et al., 2009).

### 1.2.2. Neurophysiological principles of temporal accumulation

Given the relatively short time constants of individual synapses and neurons, the time scale of temporal accumulation during decision-making is remarkable: neurons in

association (Shadlen and Newsome, 2001; Roitman and Shadlen, 2002) and (pre-)motor cortices (Gold and Shadlen, 2001; Donner et al., 2009) show ramping activity, reflecting the accumulation of sensory information, for up to several seconds. In contrast, the slowest synaptic time scales are around 100 ms (Wang, 2002). Hence, typically observed integration time scales far exceed this time constant. One key question in decision neuroscience is how the temporal accumulation of information is achieved within neural circuits. The first hints about the neural implementation of temporal accumulation came from the observation that signatures of the decision variable were identified in regions that have previously been linked with processes involving working memory, such as lateral intraparietal area (Wang, 2008). These regions have long been known to exhibit persistent activity during the maintenance of items in working memory (Wang, 1999). This has led to the idea that the mechanisms underlying temporal accumulation might be based on similar principles (Wang, 2002; Wong and Wang, 2006). One hypothesized key component of these accumulator circuits is slow reverberation through recurrent excitation (Fig. 1C) (Douglas et al., 1995; Wang, 2002, 2008, 2012), which can give rise to self-sustained population activity within a neural circuit (Wang, 2001). These slow reverberations observed in such networks are hypothesized to depend critically on slow NMDA receptors at the recurrent excitatory synapses (Wang, 2001; Wong and Wang, 2006). Accordingly, stronger recurrent excitation is associated with longer time scales, facilitating the integration of information over extended periods of time. Recent work described a hierarchy of time scales in the primate cortex, with early sensory areas exhibiting relatively short time constants and higher order areas, which are hypothesized to be involved in working memory as well as decision-making, exhibiting longer time constants (Honey et al., 2012; Murray et al., 2014). The authors show that this

hierarchy can indeed emerge from a gradient of recurrent excitation across the brain, but longer time constants only emerge in combination with long-range structural connections (Chaudhuri et al., 2015). Thus, short time constants can be the result of local recurrence alone, whereas long time constants in the brain may emerge as a consequence of large-scale network interactions in combination with local recurrence (Chaudhuri et al., 2015). Consistent with these findings, it has been observed that the slowest fluctuations in the brain (with longest autocorrelations and, hence, largest time constants) are observed in those areas that exhibit the strongest structural connectivity (Baria et al., 2013).

In sum, over recent years several key principles underlying the temporal accumulation and its neural implementation have emerged, most prominently the reverberation within neural circuits through recurrent excitation, likely mediated through NMDA receptors, as well as long-range connectivity.

### **1.3. Neuromodulation**

Modulatory neurotransmitters, henceforth called “neuromodulators”, are a class of neurotransmitters that, in contrast to regular neurotransmitters, do not alter activity of neurons directly, but rather modulate the response properties of multiple neurons, possibly through a combination of wired transmission and volume transmission (Sarter et al., 2009). The effects of neuromodulatory systems are often described as “spatially diffuse” and unspecific, with a temporal profile that has been characterized as sluggish (Ballinger et al., 2016). More recent studies, however, demonstrated neuromodulatory effects with relatively high spatial precision that unfold on multiple time scales, including very short ones (Aston-Jones and Cohen, 2005; Schultz, 2007; Sarter et al., 2009; Ballinger et al., 2016; Nelson and Mooney, 2016). Several neuromodulatory

systems have been linked with the control of global brain state, and the regulation of behavioral state variables such as arousal and attention (Phillis, 1968; Robbins, 1984; Berridge, 2008; Harris and Thiele, 2011; Lee and Dan, 2012; Zagha and McCormick, 2014). Their role in shaping specific cognitive processes as well as neural computations, however, has long remained unknown. The prominent role of neuromodulatory systems in brain function becomes most evident when considering the consequences associated with their malfunctioning in neuropsychiatric and neurological disorders, such as Parkinson's disease (Burns et al., 1983; Lotharius and Brundin, 2002), schizophrenia (Meltzer and Stahl, 1976) or depression (Fava and Kendler, 2000), which are linked with severe cognitive and/or physical impairments. In the following, I will briefly discuss three neuromodulator systems that are the focus of this thesis: the two catecholamines noradrenaline and dopamine, as well as acetylcholine.

### 1.3.1. Noradrenaline

Noradrenaline (also called norepinephrine) is a catecholaminergic neuromodulator that has been strongly linked with the control of global brain state (Aston-Jones and Cohen, 2005; Lee and Dan, 2012; Zagha and McCormick, 2014) and the regulation of arousal (Aston-Jones and Cohen, 2005; Berridge, 2008; Eldar et al., 2013). The primary source of noradrenaline to the central nervous system is the locus coeruleus (LC), a small structure in the brainstem, which maintains projections throughout almost the entire brain (Foote and Morrison, 1987). The effects of noradrenaline are mediated through different classes of adrenergic receptors, the  $\alpha$ 1- and  $\alpha$ 2- as well as the  $\beta$ -adrenoceptors. Depending on the activated receptor type, the effects of noradrenaline can differ markedly (Foote and Morrison, 1987). On the level of single neurons,



noradrenaline leads to an increase in the signal-to-noise ratio, which manifests as an elevated response of a neuron to synaptic input with respect to spontaneous background noise (Servan-Schreiber et al., 1990; Hasselmo et al., 1997; Aston-Jones and Cohen, 2005; Eldar et al., 2013). Early computational modelling work implemented these changes as an increase in the response gain of the activation function of units in a neural network (Servan-Schreiber et al., 1990). Such an alteration in the input-output function of a neuron means that weak (or inhibitory) input is further suppressed, whereas strong (or excitatory) input is further increased (Fig. 1A, dashed orange line) (Donner and Nieuwenhuis, 2013). In V1, these changes in gain may be the result of a noradrenaline-related depolarization of excitatory pyramidal cells, as well as a depolarization of parvalbumin-positive (PV+) and somatostatin-positive (SOM+) inhibitory interneurons, in combination with a decrease in membrane potential variability (Polack et al., 2013). Whether these observations extend to regions other than V1 is currently not fully understood. In primary auditory cortex A1 of the mouse, for instance, a recent report demonstrated that the pairing of locus coeruleus stimulation with the presentation of a tone of a certain frequency led to an increase in the neuronal response in many neurons, irrespective of the frequency preference of the neurons (Martins and Froemke, 2015). This indicates that noradrenaline, at least

in A1, may cause an increase in the baseline of the neuronal activation function (Fig. 2B, dashed orange line), perhaps in combination with the aforementioned increases in response gain.

Although the involvement of the LC-NE system in the regulation of arousal has long been acknowledged (Robbins, 1984; Berridge, 2008), only recently it began that the neural and computational mechanisms of arousal, as well as its effects on specific cognitive processes, are being investigated (Aston-Jones and Cohen, 2005; Sara, 2009; de Gee et al., 2014; Reimer et al., 2014; McGinley et al., 2015b, 2015a; Vinck et al., 2015; Reimer et al., 2016). This surge in the number of investigations is partly linked to the identification of pupil diameter as a non-invasive index of “neuromodulatory state” in general (Reimer et al., 2016), and of noradrenergic activity, in particular (Murphy et al., 2014; Joshi et al., 2016). The classic view of the noradrenergic involvement in cognitive processes emphasized the slow component, regulating behavioral state over longer time scales. Recent research, however, shows that phasic changes in noradrenaline-related arousal can be fast (Aston-Jones and

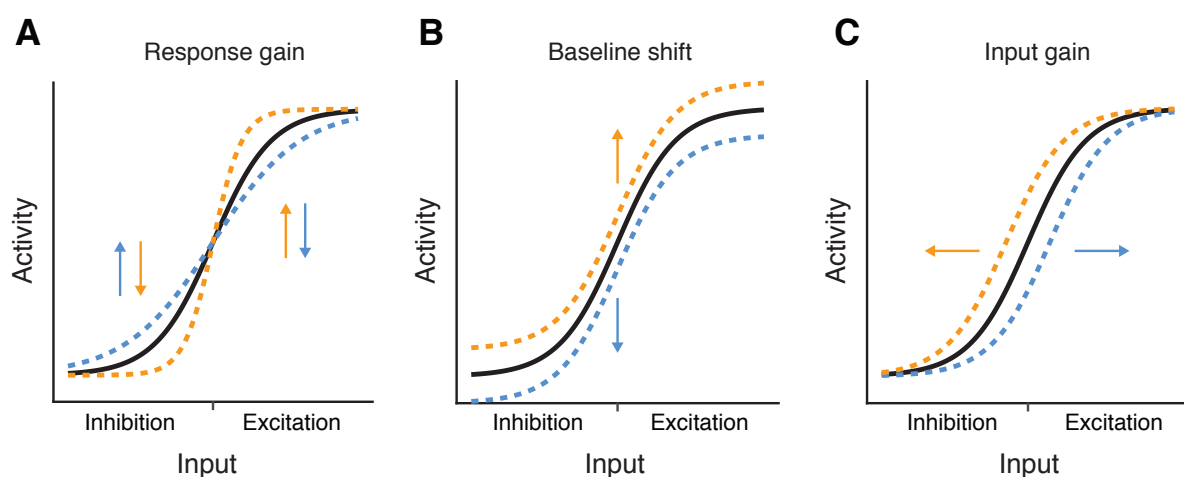


**Figure 2.** Activation or transfer functions and neuromodulation. **(A)** Possible scenarios depicting increases (dashed orange line) and decreases (dashed blue line) in response gain. **(B)** Positive (orange) and negative (blue) baseline shifts of the activation function. **(C)** Increases (orange) and decreases (blue) in input gain.

Cohen, 2005) and alter of specific neural computations already while cognitive processes in general, such as perceptual decisions, are unfolding (de Gee et al., 2014). Taken together, research investigating the impact of noradrenaline on specific cognitive computations has grown substantially over recent years and it is now clear that, in contrast to the classical view, noradrenaline can bias cognitive processes such as decision making while they unfold. However, the exact nature of the role of noradrenaline during such cognitive operations is currently still not sufficiently understood.

### 1.3.2. Acetylcholine

Acetylcholine is hypothesized to play a key role in the control of cortical state as well as in various cognitive processes, most prominently attention, learning and memory (Hasselmo and Sarter, 2010). Moreover, malfunctioning of the cholinergic system is associated with several neurodegenerative and neuropsychiatric diseases (Hasselmo and Bower, 1993; Ballinger et al., 2016). The majority of cholinergic input to the brain is provided by cholinergic cells in the various nuclei of the basal forebrain (Woolf, 1991; Zaborszky et al., 1999, 2015), with the main cortical input being provided by the nucleus basalis of Meynert (Thiele, 2013). Traditionally, the innervation profile of the cholinergic system has been described as diffuse (Ballinger et al., 2016), but projections of basal forebrain cholinergic neurons can exhibit remarkable spatial specificity (Fournier et al., 2004; Sarter et al., 2009; Zaborszky et al., 2015; Kim et al., 2016).

Like other neuromodulators, the effects of acetylcholine depend on specific receptor types. Two prominent classes of cholinergic receptors have been identified in the brain, muscarinic and nicotinic receptors, which can be further divided into several subtypes

that exhibit a heterogeneous distribution across the brain (Disney et al., 2006; Thiele, 2013). Depending on the activated receptor type, the effects of acetylcholine can unfold on different time scales (Parikh et al., 2007) and likely subserve different functions in the brain (Herrero et al., 2008). Earlier research mainly emphasized the slow component, possibly mediated through (metabotropic) muscarinic receptors (Thiele, 2013). However, several studies have reported cholinergic action unfolding much more rapidly, over the course of seconds (Parikh et al., 2007) or even tens of milliseconds (Nelson and Mooney, 2016). These rapid effects may be mediated through fast (ionotropic) nicotinic receptors (Albuquerque et al., 2009; Sarter et al., 2009).

Our understanding of the circuits level mechanism of acetylcholine has grown substantially over recent years, due to advances in imaging, recording as well as stimulation techniques. In visual area V1 of the awake mouse, an intricate circuit involving several subclasses of inhibitory interneurons has been identified as one potential implementation of the effects of acetylcholine (Fu et al., 2014). In this circuit, acetylcholine activates vasoactive intestinal peptide positive (VIP+) inhibitory interneurons, which, in turn, inhibit somatostatin-positive (SOM+) interneurons. SOM+ interneurons, in turn, mainly innervate excitatory pyramidal cells (Pfeffer et al., 2013; Fu et al., 2014; but see Pakan et al., 2016). Hence, the hypothesized net effect of acetylcholine is cortical disinhibition, leading to a net increase in excitation within the targeted microcircuit. This disinhibitory circuit is consistent with the observed increases in response gain under acetylcholine (Disney et al., 2007; Herrero et al., 2008; Fu et al., 2014). However, other studies reported decreases in response gain (Fig. 2A, dashed blue line) along with baseline shifts (Fig. 2B, dashed orange line) (Soma et al., 2012, 2013; Nelson and Mooney, 2016) or even changes in input gain, which manifest

as a shift of the activation function along the x-axis (Fig. 2C, dashed orange and blue lines) (Froemke, 2015). As these latter studies were carried out in A1 of the mouse (as opposed to V1), the discrepancy might point towards dissociable effects of acetylcholine in different regions of the brain, perhaps mediated by different receptors. In sum, acetylcholine can act across multiple spatial and temporal scales, both spatially diffuse and unspecific and spatially precise and rapid. Moreover, the circuit level effects of acetylcholine likely differ, depending on receptor type and target region, which allows the cholinergic system to support a range of functions in the cortex.

### 1.3.3. Dopamine

As a catecholamine, dopamine is structurally strongly related to noradrenaline. In fact, dopamine is the chemical precursor to noradrenaline in the brain. Nonetheless, its functions are markedly different. Traditionally, dopamine has been strongly linked with motor function. This view originates from the observations that the motor deficits that accompany Parkinson's disease are associated with a degeneration of neurons in dopaminergic centers in the brain stem, such as the substantia nigra and the ventral tegmental area (Lotharius and Brundin, 2002). Likewise, experimental lesioning of these areas is reported to result in severe motor deficits (Burns et al., 1983). More recently, dopamine has also been linked with the regulation of reward-related cognitive processes, the control of motivational behavior (Wise, 2004), as well as reinforcement learning (Schultz et al., 1997; Schultz, 2016). The actions of dopamine are mediated by a diverse set of dopaminergic receptors of at least five different types of G protein-coupled receptors (Missale et al., 1998), which are roughly categorized into D1-type and D2-type receptors (with several subclasses each). These different classes of receptors are likely to support the different functional roles of dopamine (Schultz,

2016), which unfold on several (distinct) time scales (Schultz, 2007, 2016). Their individual roles and contributions to the known effects of dopamine are not well understood. Along with noradrenaline, early models of catecholaminergic function proposed that both dopamine increase signal-to-noise ratio and the response gain of neurons (Fig. 2A) (Servan-Schreiber et al., 1990). In contrast to noradrenaline, however, the dopaminergic systems seems to maintain strongest cortical projections to prefrontal regions (Montague et al., 2004), which may explain the involvement in different cognitive operations compared to noradrenaline. Interestingly, dopamine, especially the D1 receptor, has been linked with the control of persistent activity and working memory function (Sawaguchi and Goldman-Rakic, 1991), possibly through a modulation of NMDA-related excitatory currents (Brunel and Wang, 2001). This suggests that dopamine may also play a prominent role in temporal accumulation during perceptual decision-making.

#### **1.3.4. Other neuromodulators**

Many other neuromodulatory systems exist. Prominent examples are serotonin, arising from the dorsal raphe nucleus, and histamine from the tuberomammillary nucleus (Lee and Dan, 2012). Both these systems have been implicated with the control of behavior as well as modulation of cortical excitability (Froemke, 2015). Furthermore, many of these systems are linked to specific neuropsychiatric disorders such as major depressive syndrome. Likely, these systems also impact cognitive processes such as decision-making. However, a detailed discussion is beyond the scope of this thesis.

### **1.4. Study overview and summary of results**

This thesis consists of five experimental chapters. In this paragraph, I will give a short overview of each study, including an outline of the background and aims, followed by

a short summary of the results. For details regarding experimental design, the employed methods as well as results, the reader is referred to the dedicated sections in the experimental chapters below (chapters 4-8).

### **1.4.1. Study 1: Action Planning and Perceptual Choice**

#### **1.4.1.1. Background and Aims**

Computational models of perceptual decision-making posit that decisions are based on the temporal accumulation of sensory information. When the stimulus duration is controlled by the environment, the optimal strategy is to integrate all the available evidence to minimize the influence of noisy estimates. However, if human observers accumulate information optimally, over the entire stimulus period, when provided with sufficiently long streams of information, is unclear. Moreover, in most previous investigations, the subjects knew beforehand which motor response was associated with the available choice alternatives, either from long training (in animals) or explicit instructions (in humans). Under such conditions, the integrated evidence can be continuously mapped onto regions involved in action planning and motor execution. This explains why most signatures of evidence accumulation were consistently identified in brain regions involved in action planning (Gold and Shadlen, 2000, 2003; Donner et al., 2009; de Lange et al., 2013). In contrast, if the sensory-motor mapping was unknown to the subject during the accumulation of information, these neurophysiological signatures were absent (Gold and Shadlen, 2003; O'Connell et al., 2012). Whether the knowledge about sensory-motor contingencies alters the decision-

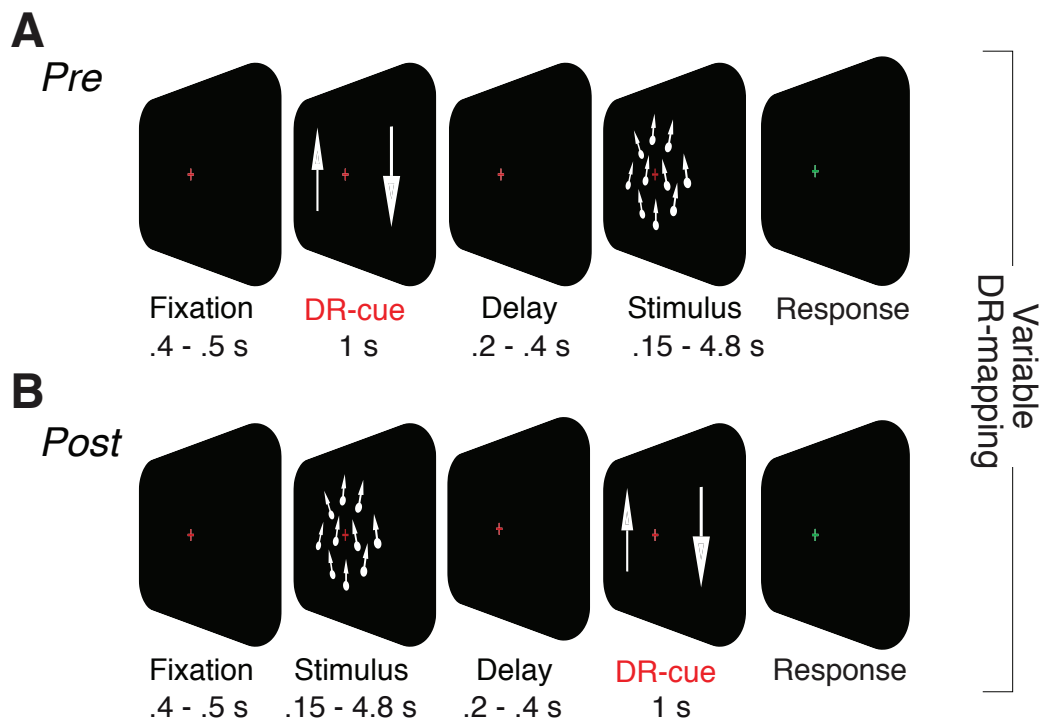


**Figure 3.** Experimental design for study 1. Random dot-kinematograms of varying motion strength were presented to the observer after a variable fixation period. **(A)** In the “Pre” condition, decision-response (DR) mapping (or stimulus-response mapping) was communicated to the subject before stimulus presentation **(B)**. In the “Post” condition, the information about the DR-mapping was communicated to the subject after stimulus presentation. In both conditions, DR-mapping varied from trial to trial.

making process in general, and temporal accumulation in particular, is largely unknown.

In this project, we exploited accumulation time scales as a diagnostic tool of the decision-making process during up/down motion discrimination, where the stimulus-response mapping varied on a trial-by-trial basis. Crucially, in one condition the stimulus-response mapping was communicated to the subject before (“Pre”; Fig. 3A) and in the other condition after stimulus presentation (“Post”; Fig. 3B). Our hypotheses were as follows: if decision-making and evidence accumulation depend on the motor action that is taken, then trial-to-trial fluctuations in the stimulus-response mapping should result in significant alterations of the time scale over which participants accumulate evidence. On the other hand, it is possible that evidence is accumulated



independently of a following motor action. In this case, no such changes are expected. In sum, the aims of the first study were two-fold: (i) investigate if human observers integrate optimally and accumulate all available evidence, even when presented with signals of very long duration, and (ii) investigate whether decision-making and temporal accumulation depend on action planning.

#### 1.4.1.2. Results and Discussion

We first investigated if human observers integrate optimally in a task with prolonged signal durations. In this experiment, signals were of up to 4.8 seconds duration. Thus, in order to maximize performance on this task, our subjects should have accumulated information for the entire length of the signal. While all participants showed clear signatures of evidence accumulation, in form of a decrease of the detection threshold as a function of signal duration, none of the subjects exploited the full duration of the signal. For each condition and subject, we estimated the average time scales of the evidence accumulation process (using both model-free as well as model-based approaches) and found those to be far below the maximum signal duration (with an average time scale across participants of  $\sim 500$ ms).

Furthermore, we found no evidence that temporal accumulation depends on the knowledge about sensory-motor mapping: estimated time scales, independent of the analytic approach (i.e., model-free or model-based), were statistically indistinguishable between the employed task conditions. Hence, we conclude that the rapid acquisition of the sensory-motor mapping after stimulus presentation had no significant impact on the decision mechanism. The result has several implications for the study of decision neuroscience. First, human observers do not integrate all the available sensory information, even if this would optimize performance. This suggests that the

accumulation time scale over which evidence is accumulated may have an upper limit that varies across individuals, just like working memory capacity. Second, it shows that those regions that are involved in motor planning and are usually found to exhibit time courses similar to what is expected from the decision variable itself, likely carry a downstream signal that is generated elsewhere. This indicates that temporal accumulation and action planning as well as motor execution are largely dissociable processes.

## **1.4.2. Study 2: Adaptive Evidence Integration in Perceptual Choice**

### **1.4.2.1. Background and Aims**

The properties of evidence accumulation have commonly been probed in tasks, in which the level of sensory evidence is constant. However, in natural environments the available and relevant sensory information varies in an unpredictable fashion and can be temporally embedded in irrelevant information (i.e., noise). Many models of decision making, such as the drift diffusion model, assume perfect accumulation over time (Ratcliff, 1978; Ratcliff and Gail, 2008). When the sensory information an organism is sampling from is stationary, drift diffusion models predict short response times and optimal accuracy. However, the environment we live in is highly dynamic and contingencies can change at any moment. When faced with non-stationary information, perfect accumulation may be suboptimal, as it can lead to an excessive integration of noise that masks the relevant information. Alternative models of decision-making incorporate leaky or forgetful accumulation (Usher and McClelland, 2001). This means that information that is accumulated, is also subject to decay over time, with a decay rate controlled by the leak term and a time scale given by the inverse of the leak. Using a single accumulator model with leak, we show that there are in fact situations

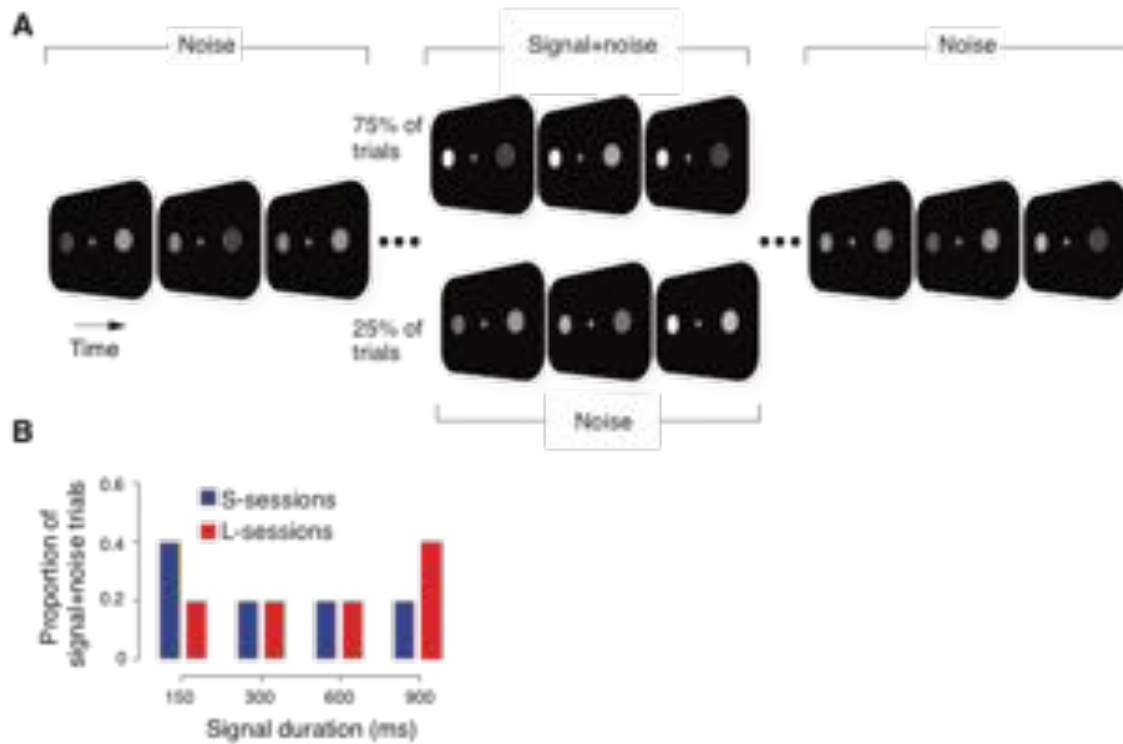


**Figure 4.** Experimental design of study 2. **(A)** Schematic of the time course of the stimulus during an example signal + noise trial. Two discs fluctuated in luminance around a mean level. During the signal interval, at a variable onset latency, the mean luminance level of one of the discs increased. Observers' task was to detect these changes in luminance. **(B)** Distribution of signal durations on signal + noise trials, where the two conditions are highlighted in red (long durations more frequency) and blue (short durations more frequent).

where leaky integration is beneficial over perfect integration. We experimentally tested these predictions, using a novel variant of a signal detection task, in which a signal is embedded in an ongoing stream of noise (Fig. 4A). Crucially, we experimentally manipulated the dominant signal duration in two separate conditions (Fig. 4B). In one condition, short signals were most frequent, whereas in a second condition, long signals were more frequent (and short and long signals were mixed with two medium durations). Based on model simulations, we predicted that observers adapt the time

scale over which they accumulate evidence to the dominant signal duration in order to maximize performance.

#### 1.4.2.2. Results and Discussion

In this study, we showed that under conditions of non-stationary sensory information, perfect integration (using the drift diffusion model) yielded suboptimal results and is not the strategy employed by human observers. Instead, human observers increased their performance during the task by adapting the time scale over which they accumulate sensory information to the dominant (or expected) signal duration, consistent with predictions derived from simulations of a leaky accumulation process (Usher and McClelland, 2001). This adaptation of the time scale manifests in clear differences in performance: for short signals, observers show higher performance when short signals dominate (and the time scale is short) compared to when long signals dominate (and the time scale is long). For long signals, on the other hand, performance is better when long signals dominate, compared to when short signals dominate.

This study has a number of important implications. First, our results provide strong support for models of perceptual choice that are based on leaky integration of perceptual evidence. This is consistent with fundamental principles of neural computation (Wang, 2002). Furthermore, it shows that in ecologically more valid situations, forgetful accumulation can in fact be advantageous. Second, our results shed new light on the question of how “top-down” mechanisms shape decision computations in the brain. Our results reveal a novel top-down mechanism that can already shape decision-making at the level of evidence accumulation. This shows that the time scale of evidence accumulation is not just a fixed circuit property, but exhibits a high degree of flexibility.

### 1.4.3. Study 3: Neuromodulation and Cortical Excitation-Inhibition Balance

#### 1.4.3.1. Background and Aims

Cortical activity fluctuates continuously, even in the absence of changes in sensory input or motor output (Faisal et al., 2008). These intrinsic fluctuations exhibit a characteristic temporal structure, which is evident as 1/f-like power spectra and long-range temporal autocorrelations (Linkenkaer-Hansen et al., 2001; Miller et al., 2009; He et al., 2010; Palva et al., 2013; Zhigalov et al., 2015). The temporal structure of intrinsic cortical activity varies widely across individuals, partly due to variations in the balance between anatomical excitatory and inhibitory connections. Excitation and inhibition, however, are not determined solely by the anatomy of cortical circuits, but are a dynamic property that fluctuates continuously as a function of brain state (Isaacson and Scanziani, 2011; Froemke, 2015). Previous animal work points to two key factors involved in shaping cortical excitation-inhibition: first, thalamic drive of the cortex, for instance due to sensory stimulation (Zagha and McCormick, 2014). Evidence suggests that excitatory feedforward drive is accompanied by intracortical inhibition of comparably strong (Shadlen and Newsome, 1998), or even stronger (Haider et al., 2013), magnitude. Second, modulatory brainstem systems, such as the noradrenergic and the cholinergic system (Froemke, 2015). Despite an increase in our understanding of the effects of neuromodulation at the level of neural microcircuits, their net effects on excitation and inhibition in large-scale cortical circuits have remained unknown. In this study, we employed a combination of computational modelling, selective pharmacological manipulation of acetylcholine and catecholamines (noradrenaline and dopamine), as well as magnetoencephalography in healthy humans (during rest and task) to address this question (Fig. 5A/B). We

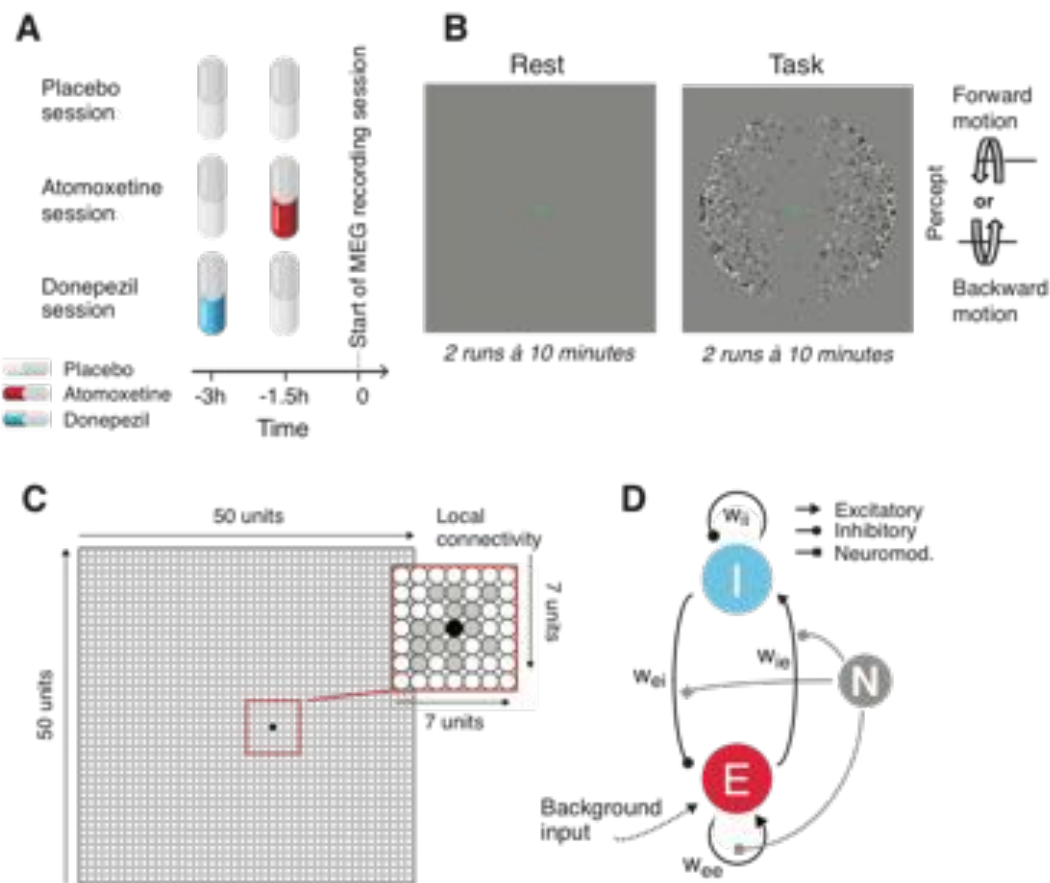


**Figure 5.** Experimental design for study 3 **(A)** Neuromodulation levels were pharmacologically manipulated within subjects. To ensure a valid double-blind design, drugs and placebo pills were administered at different points in time. **(B)** Brain activity was recorded during rest (left) and during task (right), which entailed constant visual stimulation by means of a structure-from-motion rotating sphere stimulus. **(C)** Layout of neural network model, consisting of 2500 units arranged on a 50x50 grid, with local connectivity. **(D)** Neuromodulatory effects (grey lines) were implemented as a multiplicative increase in the connection weights between excitatory (E) and inhibitory (I) units.

hypothesized that, if neuromodulators alter the net ratio between excitation and inhibition systematically, this should be evident in form of an alteration of the temporal correlation structure of cortical oscillations.

#### 1.4.3.2. Results and Discussion

We first simulated neural activity, using a modified version of a network model of a simplified cortical circuit (Poil et al., 2012). In this model, we separately manipulated excitatory as well as inhibitory synapses in the model through multiplicative modulation

of the connection weights (Fig. 5C/D) and determined their impact on long-range temporal correlations of intrinsic network oscillations. We found that dynamic modulation of the connection weights led to changes in the temporal correlation structure of alpha-band amplitude fluctuations.

Next, we tested the influence of neuromodulation on brain activity recorded with MEG experimentally. We found that increased levels of catecholamines were associated with significant increases in temporal correlations of intrinsic cortical activity in parietal and occipital regions, indicative of changes in the ratio of excitation and inhibition. By contrast, acetylcholine had no effects on long-range temporal correlations. In principle, the observed changes in temporal correlations can have multiple causes: both increases and decreases in excitation or inhibition can lead to the observed effects. In order to get a better idea of the net effects of catecholamines, we compared the changes in temporal correlations induced by pharmacological treatments with those induced by sensory/task drive. Sensory stimulation is associated with profound increases in inhibition and, in our experiment, with pronounced decreases in temporal correlations (compared to rest). This specific pattern enabled us to infer that the catecholamine-related increase in temporal correlations is likely the result of an increase in excitation-inhibition ratio.

We conclude that catecholamines, but not acetylcholine, change temporal correlations of intrinsic cortical activity, possibly by increasing the ratio between excitation and inhibition, which may be the result of a decrease in inhibition (Martins and Froemke, 2015).

## 1.4.4. Study 4: Neuromodulation of Functional Connectivity

### 1.4.4.1. Background and Aims

Intrinsic brain activity not only exhibits remarkable temporal structure, but is also highly coordinated in space. This coordination is reflected in the organization of intrinsic activity into distributed networks of correlated activity (Fox et al., 2005; Raichle and Snyder, 2007; de Pasquale et al., 2010; Deco et al., 2011). The neurophysiological mechanisms behind such widespread network fluctuations, however, are not well understood. Due to their global innervation profile and effects across multiple time scales, neuromodulatory systems, such as the catecholaminergic system, are in an ideal position to shape brain activity spatially widespread, in a temporally coordinated manner. Catecholamines have been hypothesized to increase the gain of the activation function of targeted neurons (Servan-Schreiber et al., 1990). Using a simple network model, it has been shown that such changes in response gain lead to a global increase in the correlations across the units in such a network (Eldar et al., 2013). Indeed, during the execution of a simple perceptual task, periods of increased pupil dilation, reflecting increases in neuromodulatory activity (Murphy et al., 2014; Joshi et al., 2016; Reimer et al., 2016), are associated with spatially widespread increases in activity correlations as measured using BOLD-fMRI (Eldar et al., 2013). In this project, we increased the levels of catecholamines, through pharmacological manipulation, during BOLD-fMRI measurements of resting state activity in healthy human participants. The main objectives in this study were (i) to investigate if and how pharmacological manipulation of catecholamines alters whole-brain BOLD correlations during rest and (ii) investigate the functional topology that is associated with increased levels of catecholamines.



#### 1.4.4.2. Results and Discussion

Previous research, using pupil dilation as an index of noradrenergic activity (Eldar et al., 2013) and studies employing pharmacological manipulation of catecholamine levels (Warren et al., 2016), reported increases in brain-wide correlations measured using fMRI. In stark contrast, in this study, we found that increased levels of catecholamines were associated with a strong decrease of inter-regional BOLD correlations. These decreases exhibited spatial specificity, indicating that catecholamines can exert spatially distinct effects on the correlations between particular brain regions. How can the discrepancy between the previous results, reporting increases in correlations and our current findings be reconciled? One key difference between the discussed studies and the current study was the behavioral context. Here, we recorded brain activity during rest, that is, in absence of external stimulation or overt behavior. In contrast, in the earlier studies, participants were engaged in a perceptual task (Eldar et al., 2013; Warren et al., 2016). Noradrenaline has been shown to depend on the level of glutamate in the system, exerting stronger effect when more glutamate is available (Polack et al., 2013; Mather et al., 2015). Hence, it is possible that during a perceptual task, glutamate levels are elevated due to strong feedforward excitation. In turn, this may have amplified the effects of noradrenaline in those previous studies, while the absence of strong stimulation and, thus, lower levels of glutamate, led to a decrease in activity correlations.

Our findings have two key implications. First, catecholamines reshape functional network topology spatially widespread, yet spatially specific. This supports the findings that locus coeruleus coupling and receptor distribution across the brain can exhibit a high degree of spatial specificity. Second, the observed decrease in whole-brain correlations is inconsistent with a simple catecholamine-related increase in response

gain. Thus, the effects of catecholamines may be more diverse than previously assumed.

#### **1.4.5. Study 5: Context-dependent neuromodulation of the intrinsic cortical correlation structure**

##### **1.4.5.1. Background and Aims**

The noradrenergic and the cholinergic system have long been implicated with the regulation of global brain state (Harris and Thiele, 2011; Lee and Dan, 2012; Zagha and McCormick, 2014). These systems are made up of brainstem centers, the locus coeruleus (containing noradrenergic neurons) and the basal forebrain (containing cholinergic), who have widespread projections to most parts of the entire cerebral cortex (Foote and Morrison, 1987; Aston-Jones and Cohen, 2005; Ballinger et al., 2016). Work from theoretical neuroscience postulates that both neuromodulatory systems, despite their overall similar functional organization, play distinct computational roles in learning, inference, and decision-making (Yu & Dayan, 2005; Dayan, 2012). However, there is so far, little evidence for distinct functional roles of these two neuromodulatory systems. Previous research suggests that catecholamines, possibly through changes in the balance between excitation and inhibition (Murphy and Miller, 2003), increase neural gain, i.e., the responsivity of neurons towards input (Servan-Schreiber et al., 1990). Similar effects have been described for acetylcholine (Fu et al., 2014; but see Nelson & Mooney, 2016). Here, we manipulated the levels of both catecholamines and acetylcholine with selective pharmacological interventions and measured intrinsic cortical activity fluctuations during rest and continuous task drive, by means of whole-brain MEG recordings. This study is based on the data presented in chapter 3 (see Fig. 5A/B).

#### 1.4.5.2. Results and Discussion

In this study, we present a striking double-dissociation between the effects of catecholamines and acetylcholine on the global correlation structure of intrinsic ('steady-state') cortical activity in the human brain. Catecholamines strongly increased brain-wide correlations, but only during task. By contrast, acetylcholine strongly decreased correlations, but only during rest (i.e., in absence of external drive). These results reveal a novel context-dependence of the large-scale effects of both key neuromodulators on human brain activity. For both neuromodulators, the effects were spatially widespread. Moreover, these results help to resolve the seemingly inconsistent results reported earlier (see 1.4.4.2.). Here, we provide evidence that the observed discrepancies of catecholaminergic effects on global BOLD correlations indeed arise from different behavioral contexts.

### 1.5. General Discussion

Our choices depend on the information we infer from the external world and accumulate over time. However, the computations that are carried out in order to arrive at a choice also critically depend on the brain's internal state, which fluctuates due to factors such as arousal and attention. These fluctuations in brain state are controlled by neuromodulatory systems (Aston-Jones and Cohen, 2005; Harris and Thiele, 2011; Lee and Dan, 2012), such as noradrenaline, acetylcholine and dopamine. The traditional view of neuromodulatory function assumed that the effects they exert unfold over relatively long time scales. By contrast, recent research demonstrates that phasic changes in neuromodulation can occur rapidly and bias decision-making already during the evolution of a choice (Aston-Jones and Cohen, 2005; Sarter et al., 2009; Cheadle et al., 2014; de Gee et al., 2014).

### 1.5.1. Top-down control of temporal accumulation

A number of previous studies have investigated the top-down effects in perceptual decision-making. Most such studies have focused on top-down adjustments of the decision threshold, for example in studies investigating the speed-accuracy trade-off (Ratcliff, 1978; Bogacz et al., 2010; Heitz and Schall, 2012). By contrast, top-down control of the time scale over which observers integrate information has rarely been studied experimentally.

In study 2, we show that temporal accumulation of sensory evidence can be flexibly adjusted to environmental contingencies (Ossmy et al., 2013), although the time scale might have an upper limit, as shown in study 1 (Tsetsos et al., 2015). These findings have several implications. First, many investigations on decision-making employed stimuli with prolonged signal durations, with the implicit assumption that observers accumulate over the entire signal. We show that human observers instead accumulate over time scales that are much shorter than the typical stimulus durations, despite resulting in suboptimal performance. This suggests that the time scale over which evidence is accumulated has an upper bound, just like working memory capacity. Yet, the time scale over which humans accumulate information is also not a fully hard-wired property of neural circuits. In study 2 (Ossmy et al., 2013), we show that the accumulation time scale can in fact be adapted to the statistics of a task, in order to optimize task performance. The discrepancy between study 1 and 2 in this respect may arise from the fact that signal durations in study 2 were much shorter. Thus, time scale adaption may only be possible, when signal durations are close to or below the upper limit of an individual.

Based on observations from studies on working memory, theoretical work hypothesized a key role for recurrent excitation, mediated by NMDA receptors, in

temporal information accumulation (Wang, 2002; Wong and Wang, 2006). Interestingly, dopamine has been shown to enhance NMDA related excitatory currents in prefrontal cortex, via D1 receptors (Seamans et al., 2001). Consistent with this finding, dopaminergic D1 receptors within dorsolateral prefrontal cortex (dlPFC) of the macaque monkey were shown to be crucial for the maintenance of items over time during a working memory task (Sawaguchi and Goldman-Rakic, 1991). Dorsolateral PFC was also shown to be causally involved in perceptual decision-making: in a recent study, repetitive transcranial magnetic stimulation of dlPFC led to reduced accuracy (Philiastides et al., 2011) during a perceptual decision-making task. Computational modeling based on drift diffusion revealed that these changes in performance are mainly attributable to changes in drift rate, which reflects the efficiency of the accumulation mechanism. Future research should address the role of dopamine within dlPFC and specifically assess its role in the temporal accumulation mechanism during decision-making in general, and its role in time scale adaptation, in particular.

### 1.5.2. Neuromodulation of excitation and inhibition

Our results from study 3 demonstrate that atomoxetine, which increases the levels of catecholamines (noradrenaline and dopamine), increases the ratio between excitation and inhibition ratio, which can be achieved through a decrease in inhibition (Martins and Froemke, 2015) or an increase in excitation. It is possible that this change in the excitation-inhibition ratio also affects temporal accumulation during decision making. Interestingly, it has been shown that atomoxetine acts on NMDA receptors (Udvardi et al., 2013; Di Miceli and Gronier, 2015), which have been strongly linked with recurrent excitation and temporal accumulation (see above). This suggests that the observed

changes in cortical dynamics could reflect an increase in recurrent excitation, possibly mediated by an increase in dopamine (Seamans et al., 2001).

A recent network modelling study strongly links the balance of excitation and inhibition with mechanisms underlying decision-making (Lam et al., 2017). The authors found an inverted-U relation between decision-making performance of their biophysically plausible network model and the underlying ratio between excitation and inhibition. More specifically, under high levels of excitation-inhibition ratio, activity build-up towards the decision threshold during temporal accumulation was much faster compared to lower E:I ratios. This means when the ratio is (too) high, decisions become impulsive. In contrast, low E:I ratios led to very slow ramping activity, which resulted in indecisiveness. Two testable prediction can be derived from this result. In our study, catecholamines were associated with an increase in the ratio between excitation and inhibition. This increase in E:I should facilitate more impulsive behavior during decision-making compared to the placebo condition. Moreover, future studies can exploit signatures of E:I ratio, such as the one we employed in this study (i.e., long range temporal correlations of cortical activity), to determine baseline levels of E:I ratio across individuals. These should predict the level of impulsivity/indecisiveness during decision-making.

### **1.5.3. Neuromodulation of large-scale interactions**

Recent research indicates that the timescale over which evidence is accumulated within a region does not only depend on local properties of the circuit, such as the recurrent excitation, but also strongly on the large-scale structural and functional network the regions is embedded on (Chaudhuri et al., 2015). In two separate studies (Studies 4 and 5), we show that catecholamines and acetylcholine cause large-scale

network reconfigurations, with a striking context-dependence (Study 5). This shows that neuromodulators can potentially alter the temporal accumulation of sensory information, even without changing in the local properties of the accumulation mechanism. The model by Chaudhuri et al. predicts that long time scales are the result of network reverberation, whereas shorter time scales can emerge from local dynamics only. Hence, longer time scales should may also be evident in stronger functional coupling across regions. In this scenario, increased interactions during task, as observed in study 5 during atomoxetine, could give the potential for prolonged integration time scales.

## 2. Abbreviations

AAL	Automated anatomical labelling
Ach	Acetylcholine
BOLD	Blood oxygen level dependent
DA	Dopamine
DDM	Drift diffusion model
dIPFC	Dorsolateral Prefrontal Cortex
E/I	Excitation/Inhibition
EEG	Electroencephalography
eLORETA	Exact low resolution tomography
EPSCs	Excitatory postsynaptic current
FC	Functional connectivity
fMRI	Functional Magnetic Resonance Imaging
ICA	Independent component analysis
IPSCs	Inhibitory postsynaptic current
LC-NE	Locus Coeruleus-norepinephrine
LCMV	Linearly constrained minimum variance
LCA	Leaky competing accumulation model
LFP –	Local field potential
MEG	Magnetoencephalography
NA	Noradrenaline (also NE, norepinephrine)
PV+	Parvalbumin positive
ROI	Region of interest
SOM+	Somatostatin positive
VIP+	Vasoactive intestinal peptide positive



### 3. References

- Albuquerque EX, Pereira EFR, Alkondon M, Rogers SW (2009) Mammalian Nicotinic Acetylcholine Receptors: From Structure to Function *Physiol Rev* 89:73–120.
- Aston-Jones G, Cohen JD (2005) An integrative theory of locus coeruleus-norepinephrine function: adaptive gain and optimal performance. *Ann Rev. Neurosci* 28:403–450.
- Ballinger EC, Ananth M, Talmage DA, Role LW (2016) Basal Forebrain Cholinergic Circuits and Signaling in Cognition and Cognitive Decline. *Neuron* 91:1199–1218.
- Baria AT, Mansour A, Huang L, Baliki MN, Cecchi GA, Mesulam MM, Apkarian AV (2013) Linking human brain local activity fluctuations to structural and functional network architectures. *Neuroimage* 73:144–155.
- Berridge C (2008) Noradrenergic modulation of arousal. *Brain Res Rev* 58(1), 1-17.
- Bogacz R, Wagenmakers E-J, Forstmann BU, Nieuwenhuis S (2010) The neural basis of the speed–accuracy tradeoff. *Trends Neurosci* 33:10–16.
- Bouret S, Sara SJ (2005) Network reset: a simplified overarching theory of locus coeruleus noradrenaline function. *Trends Neurosci* 28(11):574–582.
- Brunel N, Wang X (2001) Effects of neuromodulation in a cortical network model of object working memory dominated by recurrent inhibition. *J Comput Neurosci* 11:63–85.
- Brunton BW, Botvinick MM, Brody CD (2013) Rats and humans can optimally accumulate evidence for decision-making. *Science* 340: 95–98.
- Burns RS, Chiueh CC, Markey SP, Ebert MH, Jacobowitz DM, Kopin IJ (1983) A primate model of parkinsonism: selective destruction of dopaminergic neurons in the pars compacta of the substantia nigra by N-methyl-4-phenyl-1,2,3,6-tetrahydropyridine. *Proc Natl Acad Sci U S A* 80:4546–4550.
- Chaudhuri R, Knoblauch K, Gariel M-A, Kennedy H, Wang X-J (2015) A Large-Scale Circuit Mechanism for Hierarchical Dynamical Processing in the Primate Cortex. *Neuron* 88:419–431.
- Cheadle S, Wyart V, Tsetsos K, Myers N, de Gardelle V, Herculano-Houzel S, Summerfield C (2014) Adaptive Gain Control during Human Perceptual Choice. *Neuron* 81:1429-1441.
- Chen N, Sugihara H, Sur M (2015) An acetylcholine-activated microcircuit drives temporal dynamics of cortical activity. *Nat Neurosci* 18:892–902.
- de Gee J, Knapen T, Donner TH (2014) Decision-related pupil dilation reflects upcoming choice and individual bias. *Proc Natl Acad Sci U S A* 111:E618-25.

- de Lange FP, Rahnev DA, Donner TH, Lau H (2013) Prestimulus oscillatory activity over motor cortex reflects perceptual expectations. *J Neurosci* 33:1400–1410.
- de Pasquale F, Penna S, Snyder AZ, Lewis C, Mantini D, Marzetti L, Belardinelli P, Ciancetta L, Pizzella V, Romani GL, Corbetta M (2010) Temporal dynamics of spontaneous MEG activity in brain networks. *Proc Natl Acad Sci U S A* 107:6040–6045.
- Deco G, Jirsa VK, R M Anthony (2011) Emerging concepts for the dynamical organization of resting-state activity in the brain. *Nat Rev Neurosci* 12:43–56.
- Di Miceli M, Gronier B (2015) Psychostimulants and atomoxetine alter the electrophysiological activity of prefrontal cortex neurons, interaction with catecholamine and glutamate NMDA receptors. *Psychopharmacology* 232:2191–2205.
- Disney AA, Aoki C, Hawken MJ (2007) Gain Modulation by Nicotine in Macaque V1. *Neuron* 56:701–713.
- Disney AA, Domakonda KV, Aoki C (2006) Differential expression of muscarinic acetylcholine receptors across excitatory and inhibitory cells in visual cortical areas V1 and V2 of the macaque monkey. *J Comp Neurol* 499:49–63.
- Donner TH, Nieuwenhuis S (2013) Brain-wide gain modulation: the rich get richer. *Nat Neurosci* 16:989–990.
- Donner TH, Siegel M, Fries P, Engel AK (2009) Buildup of choice-predictive activity in human motor cortex during perceptual decision making. *Current Biology* 19:1581–1585.
- Donner TH, Siegel M, Oostenveld R, Fries P, Bauer M, Engel AK (2007) Population activity in the human dorsal pathway predicts the accuracy of visual motion detection. *J Neurophys* 98:345–359.
- Douglas RJ, Koch C, Mahowald M, Martin KA, Suarez HH (1995) Recurrent excitation in neocortical circuits. *Science* 269:981–985.
- Drugowitsch J, Wyart V, Devauchelle A-D, Koechlin E (2016) Computational Precision of Mental Inference as Critical Source of Human Choice Suboptimality. *Neuron* 92:1398–1411.
- Eckhoff P, KF W-L, Holmes P (2009) Optimality and robustness of a biophysical decision-making model under norepinephrine modulation. *J Neurosci* 29:4301-4311.
- Eldar E, Cohen JD, Niv Y (2013) The effects of neural gain on attention and learning. *Nat Neurosci* 16:1146–1153.
- Faisal A, Selen LP, Wolpert DM (2008) Noise in the nervous system. *Nat Rev Neurosci* 9:292–303.

- Fava M, Kendler KS (2000) Major Depressive Disorder. *Neuron* 28:335–341.
- Foote S, Morrison J (1987) Extrathalamic modulation of cortical function. *Annu Rev Neurosci* 10: 67-95,
- Fournier GN, Semba K, Rasmusson DD (2004) Modality- and region-specific acetylcholine release in the rat neocortex. *Neuroscience* 126:257–262.
- Fox MD, Snyder AZ, Vincent JL, Corbetta M, Essen DC, Raichle ME (2005) The human brain is intrinsically organized into dynamic, anticorrelated functional networks. *Proc Natl Acad Sci U S A* 102:9673–9678.
- Froemke R (2015) Plasticity of cortical excitatory-inhibitory balance. *Annu Rev Neurosci.* 38: 195-219.
- Fu Y, Tucciarone JM, Espinosa SJ, Sheng N, Darcy DP, Nicoll RA, Huang JZ, Stryker MP (2014) A cortical circuit for gain control by behavioral state. *Cell* 156:1139–1152.
- Gold J, Shadlen M (2000) Representation of a perceptual decision in developing oculomotor commands. *J Neurosci* 404:390–394.
- Gold JI, Shadlen MN (2001) Neural computations that underlie decisions about sensory stimuli. *J Neurosci* 5.
- Gold JI, Shadlen MN (2003) The influence of behavioral context on the representation of a perceptual decision in developing oculomotor commands. *J Neurosci* 23:632–651.
- Gold JI, Shadlen MN (2007) The neural basis of decision making. *Ann Rev Neurosci* 30:535–574.
- Haider B, Häusser M, Carandini M (2013) Inhibition dominates sensory responses in the awake cortex. *Nature* 493(7430):97-100.
- Hanks TD, Kopec CD, Brunton BW, Duan CA, Erlich JC, Brody CD (2015) Distinct relationships of parietal and prefrontal cortices to evidence accumulation. *Nature* 520:220–223.
- Harris KD, Thiele A (2011) Cortical state and attention. *Nat Rev Neurosci* 12:509–523.
- Hasselmo M, Linster C, Patil M (1997) Noradrenergic suppression of synaptic transmission may influence cortical signal-to-noise ratio. *J Neurophys* 77(6): 3326-39
- Hasselmo ME, Bower JM (1993) Acetylcholine and memory. *Trends Neurosci* 16:218–222.
- Hasselmo ME, Sarter M (2010) Modes and Models of Forebrain Cholinergic Neuromodulation of Cognition. *Neuropsychopharmacol* 36:52–73.

- He B, Zempel J, Snyder A, Raichle M (2010) The temporal structures and functional significance of scale-free brain activity. *Neuron* 66(3):353-69.
- Heitz RP, Schall JD (2012) Neural Mechanisms of Speed-Accuracy Tradeoff. *Neuron* 76:616–628.
- Herrero JL, Roberts MJ, Delicato LS, Gieselmann MA, Dayan P, Thiele A (2008) Acetylcholine contributes through muscarinic receptors to attentional modulation in V1. *Nature* 454:1110–1114.
- Honey C, Theisen T, Donner T, Silbert L (2012) Slow cortical dynamics and the accumulation of information over long timescales. *Neuron* 76(2): 423-34.
- Isaacson J, Scanziani M (2011) How inhibition shapes cortical activity. *Neuron* 72(2):231-43.
- Joshi S, Li Y, Kalwani R, Gold J (2016) Relationships between pupil diameter and neuronal activity in the locus coeruleus, colliculi, and cingulate cortex. *Neuron* 89(1):221-34.
- Kelly S, O’Connell R G (2013) Internal and External Influences on the Rate of Sensory Evidence Accumulation in the Human Brain. *J Neurosci* 33:19434-19441.
- Kim J-HH, Jung A-HH, Jeong D, Choi I, Kim K, Shin S, Kim SJ, Lee S-HH (2016) Selectivity of Neuromodulatory Projections from the Basal Forebrain and Locus Ceruleus to Primary Sensory Cortices. *J Neurosci* 36:5314–5327.
- Kim JN, Shadlen MN (1999) Neural correlates of a decision in the dorsolateral prefrontal cortex of the macaque. *Nat Neurosci* 2:176–185.
- Lam NH, Borduqui T, Hallak J, Roque AC, Anticevic A, Krystal JH, Wang X-J, Murray JD (2017) Effects of Altered Excitation-Inhibition Balance on Decision Making in a Cortical Circuit Model. *bioRxiv*.
- Lee S, Dan Y (2012) Neuromodulation of brain states. *Neuron* 76:209–222.
- Leopold DA, Murayama Y, Logothetis NK (2003) Very slow activity fluctuations in monkey visual cortex: implications for functional brain imaging. *J Neurosci* 23:422–433.
- Linkenkaer-Hansen K, Nikouline VV, Palva JM, Ilmoniemi RJ (2001) Long-range temporal correlations and scaling behavior in human brain oscillations. *J Neurosci* 21(4):1370-7.
- Lotharius J, Brundin P (2002) Pathogenesis of parkinson’s disease: dopamine, vesicles and  $\alpha$ -synuclein. *Nat Rev Neurosci* 3:932–942.
- Marder E (2012) Neuromodulation of neuronal circuits: back to the future. *Neuron* 76:1–11.
- Martins AR, Froemke RC (2015) Coordinated forms of noradrenergic plasticity in the locus coeruleus and primary auditory cortex. *Nat Neurosci* 18:1483–1492.

- Mather M, Clewett D, Sakaki M, Harley CW (2015) Norepinephrine ignites local hot spots of neuronal excitation: how arousal amplifies selectivity in perception and memory. *Brain Beh Sci*:1–100.
- McGinley M, David S, McCormick D (2015a) Cortical membrane potential signature of optimal states for sensory signal detection. *Neuron* 87(1):179-92..
- McGinley M, Vinck M, Reimer J, R B-B (2015b) Waking state: rapid variations modulate neural and behavioral responses. *Neuron* 87(6):1143-61..
- Meltzer HY, Stahl SM (1976) The Dopamine Hypothesis of Schizophrenia: A Review\*. *Schizophr Bull* 2:19–76.
- Miller KJ, Sorensen LB, Ojemann JG, Nijs M (2009) Power-law scaling in the brain surface electric potential. *PLoS Comput Biol* 5:e1000609.
- Missale C, Nash SR, Robinson SW, Jaber M, Caron MG (1998) Dopamine receptors: from structure to function. *Physiol Rev* 78:189–225.
- Montague PR, Hyman SE, Cohen JD (2004) Computational roles for dopamine in behavioural control. *Nature* 431:760–767.
- Murphy BK, Miller KD (2003) Multiplicative gain changes are induced by excitation or inhibition alone. *J Neurosci* 23:10040–10051.
- Murphy PR, G O Redmond, Michael O, Robertson IH, Balsters JH (2014) Pupil diameter covaries with BOLD activity in human locus coeruleus. *Hum Brain Mapp* 35:4140–4154.
- Murray JD, Bernacchia A, Freedman DJ, Romo R, Wallis JD, Cai X, Padoa-Schioppa C, Pasternak T, Seo H, Lee D, Wang X-J (2014) A hierarchy of intrinsic timescales across primate cortex. *Nat Neurosci* 17:1661–1663.
- Nelson A, Mooney R (2016) The Basal Forebrain and Motor Cortex Provide Convergent yet Distinct Movement-Related Inputs to the Auditory Cortex. *Neuron* 90:635–648.
- O’Connell R G, Dockree PM, Kelly SP (2012) A supramodal accumulation-to-bound signal that determines perceptual decisions in humans. *Nat Neurosci* 15:1729–1735.
- Ossmy O, Moran R, Pfeffer T, Tsetsos K, Usher M, Donner TH (2013) The timescale of perceptual evidence integration can be adapted to the environment. *Curr Biol* 23:981–986.
- Pakan JM, Lowe SC, Dylida E, Keemink SW, Currie SP, Coutts CA, Rochefort NL (2016) Behavioral-state modulation of inhibition is context-dependent and cell type specific in mouse visual cortex. *Elife* 5.

- Palva J, Zhigalov A, Hirvonen J, Korhonen O, Klaus L-H, Palva S (2013) Neuronal long-range temporal correlations and avalanche dynamics are correlated with behavioral scaling laws. *Proc Natl Acad Sci U S A* 110(9):3585-90.
- Parikh V, Kozak R, Martinez V, Sarter M (2007) Prefrontal Acetylcholine Release Controls Cue Detection on Multiple Timescales. *Neuron* 56:141–154.
- Pfeffer CK, Xue M, He M, Huang Z, Scanziani M (2013) Inhibition of inhibition in visual cortex: the logic of connections between molecularly distinct interneurons. *Nat Neurosci* 16:1068–1076.
- Philiastides MG, Auksztulewicz R, Heekeren HR, Blankenburg F (2011) Causal Role of Dorsolateral Prefrontal Cortex in Human Perceptual Decision Making. *Curr Biol* 21:980–983.
- Phillis JW (1968) Acetylcholine release from the cerebral cortex: Its role in cortical arousal. *Brain Res* 7:378–389.
- Pinto L, Goard MJ, Estandian D, Xu M, Kwan AC, Lee S-HH, Harrison TC, Feng G, Dan Y (2013) Fast modulation of visual perception by basal forebrain cholinergic neurons. *Nat Neurosci* 16:1857–1863.
- Poil S-S, Hardstone R, Mansvelder HD, Klaus L-H (2012) Critical-State Dynamics of Avalanches and Oscillations Jointly Emerge from Balanced Excitation/Inhibition in Neuronal Networks. *J Neurosci* 32:9817–9823.
- Polack P-OO, Friedman J, Golshani P (2013) Cellular mechanisms of brain state-dependent gain modulation in visual cortex. *Nat Neurosci* 16:1331–1339.
- Polanía R, Krajbich I, Grueschow M, Ruff CC (2014) Neural oscillations and synchronization differentially support evidence accumulation in perceptual and value-based decision making. *Neuron* 82:709–720.
- Raichle M, Snyder A (2007) A default mode of brain function: a brief history of an evolving idea. *Neuroimage* 37(4):1083-90..
- Ratcliff R (1978) A theory of memory retrieval. *Psychol Rev* 85:59–108.
- Ratcliff R, Gail M (2008) The diffusion decision model: theory and data for two-choice decision tasks. *20:873–922*.
- Reimer J, Froudarakis E, Cadwell C, Yatsenko D (2014) Pupil fluctuations track fast switching of cortical states during quiet wakefulness. *Neuron* 84(2):355-62.
- Reimer J, J M Matthew, Liu Y, Rodenkirch C, Wang Q, A M David, Tolias AS (2016) Pupil fluctuations track rapid changes in adrenergic and cholinergic activity in cortex. *Nat Commun* 7:13289.
- Robbins TW (1984) Cortical noradrenaline, attention and arousal. *Psychol Med* 14:13–21.

- Roitman JD, Shadlen MN (2002) Response of neurons in the lateral intraparietal area during a combined visual discrimination reaction time task. *J Neurosci* 22:9475–9489.
- Romo R, Hernández A, Zainos A, Lemus L, Brody CD (2002) Neuronal correlates of decision-making in secondary somatosensory cortex. *Nat Neurosci* 5:1217–1225.
- Sara S (2009) The locus coeruleus and noradrenergic modulation of cognition. *Nat Rev Neurosci.* 10(3):211-23.
- Sarter M, Parikh V, Howe WM (2009) Phasic acetylcholine release and the volume transmission hypothesis: time to move on. *Nat Rev Neurosci* 10:383–390.
- Sawaguchi T, Goldman-Rakic PS (1991) D1 dopamine receptors in prefrontal cortex: involvement in working memory. *Science* 251:947–950.
- Scholvinck ML, Maier A, Ye FQ, Duyn JH, Leopold DA (2010) Neural basis of global resting-state fMRI activity. *Proc Natl Acad Sci* 107:10238–10243.
- Schultz W (2007) Multiple Dopamine Functions at Different Time Courses. *Annu Rev Neurosci* 30:259–288.
- Schultz W (2016) Dopamine reward prediction-error signalling: a two-component response. *Nat Rev Neurosci.* 17(3):183-95.
- Schultz W, Dayan P, Montague PR (1997) A neural substrate of prediction and reward. *Science* 275:1593–1599.
- Seamans JK, Durstewitz D, Christie BR, Stevens CF, Sejnowski TJ (2001) Dopamine D1/D5 receptor modulation of excitatory synaptic inputs to layer V prefrontal cortex neurons. *Proc Natl Acad Sci U S A* 98:301–306.
- Servan-Schreiber D, Printz H, Cohen J (1990) A network model of catecholamine effects: gain, signal-to-noise ratio, and behavior. *Science* 249:892–895.
- Shadlen M, Newsome W (2001) Neural basis of a perceptual decision in the parietal cortex (area LIP) of the rhesus monkey. *J Neurophys* 86(4):1916-36.
- Shadlen MN, Kiani R (2013) Decision making as a window on cognition. *Neuron* 80:791–806.
- Shadlen MN, Newsome WT (1998) The variable discharge of cortical neurons: implications for connectivity, computation, and information coding. *J Neurosci* 18:3870–3896.
- Siegel M, Donner TH, Oostenveld R, Fries P, Engel AK (2007) High-frequency activity in human visual cortex is modulated by visual motion strength. *Cereb Cortex* 17:732–741.
- Smith PL, Ratcliff R (2004) Psychology and neurobiology of simple decisions. *Trends Neurosci* 27:161–168.

- Soma S, Shimegi S, Osaki H, Sato H (2012) Cholinergic modulation of response gain in the primary visual cortex of the macaque. *J Neurophysiol* 107:283–291.
- Soma S, Shimegi S, Suematsu N, Sato H (2013) Cholinergic modulation of response gain in the rat primary visual cortex. *Sci Rep* 3:1138.
- Thiele A (2013) Muscarinic signaling in the brain. *Annu Rev Neurosci* 36:271–294.
- Tsetsos K, Pfeiffer T, Jentgens P, Donner T (2015) Action planning and the timescale of evidence accumulation. *PLoS One* 10(7):e0133332.
- Udvardi PT, Föhr KJ, Henes C, Liebau S, Dreyhaupt J, Boeckers TM, Ludolph AG (2013) Atomoxetine affects transcription/translation of the NMDA receptor and the norepinephrine transporter in the rat brain--an in vivo study. *Drug Des Devel Ther* 7:1433–1446.
- Usher M, McClelland J (2001) The time course of perceptual choice: the leaky, competing accumulator model. *Psychol Rev* 108(3):550–592.
- Vinck M, R B-B, Knoblich U, Cardin J (2015) Arousal and locomotion make distinct contributions to cortical activity patterns and visual encoding. *Neuron* 86(3):740-54.
- Wang XJ (1999) Synaptic basis of cortical persistent activity: the importance of NMDA receptors to working memory. *J Neurosci* 19:9587–9603.
- Wang X-J (2001) Synaptic reverberation underlying mnemonic persistent activity. *Trends Neurosci* 24(8):455-63.
- Wang X-JJ (2002) Probabilistic decision making by slow reverberation in cortical circuits. *Neuron* 36:955–968.
- Wang X-JJ (2008) Decision making in recurrent neuronal circuits. *Neuron* 60:215–234.
- Wang X-JJ (2012) Neural dynamics and circuit mechanisms of decision-making. *Curr Opin Neurobiol* 22:1039–1046.
- Warren C, Eldar E, van den Brink R (2016) Catecholamine-mediated increases in gain enhance the precision of cortical representations. *J Neurosci* 36(21):5699-708.
- Wise R (2004) Dopamine, learning and motivation. *Nat Rev Neurosci*. 5(6):483-94.
- Wong K-F, Wang X-J (2006) A Recurrent Network Mechanism of Time Integration in Perceptual Decisions. *J Neurosci* 26:1314–1328.
- Woolf NJ (1991) Cholinergic systems in mammalian brain and spinal cord. *Prog Neurobiol* 37:475–524.
- Zaborszky L, Csordas A, Mosca K, Kim J (2015) Neurons in the basal forebrain project to the cortex in a complex topographic organization that reflects



corticocortical connectivity patterns: an experimental study Based on Retrograde Tracing and 3D Reconstruction. *Cereb Cortex* 25(1):118-137.

Zaborszky L, Pang K, Somogyi J, Nadasdy Z, Kallo I (1999) The Basal Forebrain Corticopetal System Revisited. *Ann N Y Acad Sci* 877:339–367.

Zagha E, McCormick D (2014) Neural control of brain state. *Curr Opin Neurobiol.* 0:178-186.

Zhigalov A, Arnulfo G, Nobili L, Palva S (2015) Relationship of Fast-and Slow-Timescale Neuronal Dynamics in Human MEG and SEEG. *Journal of Neuroscience*, 35(13): 5385-5396.

## 4. Experimental chapters

### 4.1. Study 1: Action planning and perceptual choice

#### Author contributions:

1. Conceptualization
  2. Investigation
  3. Formal analysis
  4. Writing – Original draft
  5. Writing – Review
  6. Supervision
- \* Contributed equally

Tsetsos, K.:	*,3,4,5
<b>Pfeffer, T.:</b>	<b>*,1,2,3,4,5</b>
Jentgens, P.:	*,1,2,3,4,5
Donner, T.H.:	1,4,5,6

**Status: Published**

RESEARCH ARTICLE

# Action Planning and the Timescale of Evidence Accumulation

Konstantinos Tsetsos<sup>1</sup>, Thomas Pfeffer<sup>2,3,4</sup>, Pia Jentgens<sup>2,5</sup>, Tobias H. Donner<sup>2,3,6\*</sup>

**1** Department of Experimental Psychology, Oxford University, 9 South Parks Road, Oxford, OX1 3UD, United Kingdom, **2** Department of Psychology, University of Amsterdam, Weesperplein 4, 1018 XA, Amsterdam, The Netherlands, **3** Amsterdam Brain and Cognition, University of Amsterdam, Nieuwe Achtergracht 129, 1018 WS, Amsterdam, The Netherlands, **4** Department of Neurophysiology and Pathophysiology, University Medical Center Hamburg- Eppendorf, 20246, Hamburg, Germany, **5** Netherlands Institute for Neuroscience, Meibergdreef 47, 1105 BA, Amsterdam Zuidoost, The Netherlands, **6** Bernstein Center for Computational Neuroscience, Charitein Center for Comput, Haus 6, Philippstrast 13, 10115, Berlin, Germany

☞ These authors contributed equally to this work.

\* [T.H.Donner@uva.nl](mailto:T.H.Donner@uva.nl)



OPEN ACCESS

**Citation:** Tsetsos K, Pfeffer T, Jentgens P, Donner TH (2015) Action Planning and the Timescale of Evidence Accumulation. PLoS ONE 10(6): e0129473. doi:10.1371/journal.pone.0129473

**Academic Editor:** James A.R. Marshall, University of Sheffield, UNITED KINGDOM

**Received:** May 10, 2014

**Accepted:** May 12, 2015

**Published:** June 12, 2015

**Copyright:** © 2015 Tsetsos et al. This is an open access article distributed under the terms of the [Creative Commons Attribution License](https://creativecommons.org/licenses/by/4.0/), which permits unrestricted use, distribution, and reproduction in any medium, provided the original author and source are credited.

**Data Availability Statement:** All raw data files in Ascii format, and a brief description of how the data is structured, are available from the Open Science Framework database: (<https://osf.io/ju95a/>).

**Funding:** This work was funded by the Amsterdam Brain and Cognition Priority Program (Grant number: ABC2014-01, <http://abc.uva.nl/research/hav>) and the European Union FP7, Human Brain Project (Grant number: Call-ID FP7-ICT-2013-FET-F, Project ID: 604102(v1), <http://www.humanbrainproject.eu>). The funders had no role in study design, data collection and analysis, decision to publish, or preparation of the manuscript.

## Abstract

Perceptual decisions are based on the temporal integration of sensory evidence for different states of the outside world. The timescale of this integration process varies widely across behavioral contexts and individuals, and it is diagnostic for the underlying neural mechanisms. In many situations, the decision-maker knows the required mapping between perceptual evidence and motor response (henceforth termed “sensory-motor contingency”) before decision formation. Here, the integrated evidence can be directly translated into a motor plan and, indeed, neural signatures of the integration process are evident as build-up activity in premotor brain regions. In other situations, however, the sensory-motor contingencies are unknown at the time of decision formation. We used behavioral psychophysics and computational modeling to test if knowledge about sensory-motor contingencies affects the timescale of perceptual evidence integration. We asked human observers to perform the same motion discrimination task, with or without trial-to-trial variations of the mapping between perceptual choice and motor response. When the mapping varied, it was either instructed before or after the stimulus presentation. We quantified the timescale of evidence integration under these different sensory-motor mapping conditions by means of two approaches. First, we analyzed subjects’ discrimination threshold as a function of stimulus duration. Second, we fitted a dynamical decision-making model to subjects’ choice behavior. The results from both approaches indicated that observers (i) integrated motion information for several hundred ms, (ii) used a shorter than optimal integration timescale, and (iii) used the same integration timescale under all sensory-motor mappings. We conclude that the mechanisms limiting the timescale of perceptual decisions are largely independent from long-term learning (under fixed mapping) or rapid acquisition (under variable mapping) of sensory-motor contingencies. This conclusion has implications for neurophysiological and neuroimaging studies of perceptual decision-making.

**Competing Interests:** The authors have declared that no competing interests exist.

## Introduction

A hallmark of perceptual decision-making is the integration of evidence for different states of the world [1]. Imagine driving your car on a rainy day and reading a street sign to decide whether to turn left or right. Since the “sensory evidence” you are trying to interpret is noisy (i.e., it fluctuates randomly), you can improve your judgment by integrating evidence over time [1,2,3].

The timescale of this integration process is a key psychophysical parameter quantifying perceptual decision-making as it reflects the network mechanisms underlying the accumulation of sensory information in the brain [4–7]. While many studies of non-sensory (top-down) effects in perceptual decision-making have focused on strategic adjustments of the decision threshold that terminates the decision process [3,6,8,9,10], only few previous studies have investigated direct top-down effects on the evidence integration process *per se*, as indicated by the integration timescale [11–14]. Only two of these studies were conducted in human observers [11,13] whose integration mechanisms may differ from those of other species [15]. Here, we examined the effect of one important top-down factor that has not been previously examined: knowledge of sensory-motor contingencies.

In the above example, the integrated evidence is continuously mapped onto a plan to select and execute a motor movement. The same holds for most previous neurophysiological laboratory studies of perceptual decision-making [1,16,17,18]. Under such conditions, build-up signatures of evidence integration are found in brain regions involved in action planning. In particular, when perceptual choices are reported as saccades [12,19,20] or hand movements [21,22] choice-specific activity ramps up in the corresponding (pre-)motor brain regions. These premotor build-up signatures are not evident if the sensory-motor contingencies are broken up by instructing the mapping between perceptual choice and motor response only after stimulus presentation [12], or by eliminating the motor response altogether (in a covert counting task) [23]. This raises the question whether knowledge about sensory-motor contingencies might also improve (i.e., prolong) integration timescales observed behaviorally. Further, it has been shown that learning of fixed sensory-motor contingencies (over hundreds of trials or more) improves the selectivity of the read-out of sensory information by the association cortex [24,25]. But it remains unknown whether such learning also improves the integration timescale.

We addressed these questions in six human observers performing the same motion discrimination task under three different sensory-motor mapping conditions. In one experiment, the mapping between decision outcome and motor response varied on a trial-by-trial basis. In different conditions, this mapping was instructed before or after stimulus presentation. While the first condition allowed the integration of evidence directly towards action plans, the second did not. We found that integration timescales were generally shorter than the maximum stimulus duration, and thus shorter than the timescale required to maximize the fraction of correct choices in the task. But integration timescales were indistinguishable between conditions. We then reasoned that sensory-motor mapping might only improve integration timescales if fixed over many trials, due to a slow learning process. Thus, we asked the same observers to perform the task under fixed mapping in another experiment. Again, despite extensive practice, integration timescales were indistinguishable from the other two conditions. We conclude that the integration of perceptual evidence does not depend on sensory-motor contingencies.

## Materials and Methods

### Ethics Statement

The ethical committee of the University of Amsterdam approved the study (reference number 2011-OP-1588). Written informed consent was obtained from all participants.

## Observers

Six healthy human observers were recruited for this study (2 males, mean age: 25; range: 22–29 years). All observers had normal or corrected-to-normal vision. The pool included four observers who were naïve with respect to the purpose of the experiment, and two authors (P.J. and T.P.). Observers received either course credits or were paid a small amount of money (€10/hour) for their participation.

## Stimuli

We used an established psychophysical approach for quantifying the perceptual evidence integration timescale [12,13,26–29], which entailed the following two aspects of the sensory input: First, we systematically manipulated the duration of the stimulus (i.e., the maximal evidence integration time available to the observer) and prompted the response after that time (“interrogation protocol”). Second, we systematically manipulated the strength of the perceptual evidence to estimate the observer’s perceptual discrimination threshold for each stimulus duration. This enabled us to quantify discrimination thresholds as function of stimulus duration (see below).

Using this general approach, we performed two experiments. Below, we first describe all general aspects, followed by the specifics of each experiment. Motion stimuli consisted of “random dot kinematograms” (RDK), consisting of 785 white dots (on average) within a circular aperture  $9.1^\circ$  in diameter (dot density: 12.07 dots per  $\text{deg}^2$ ), centered on a red fixation cross ( $0.4^\circ \times 0.4^\circ$ ), and displayed against a black background. Individual dots subtended  $0.04^\circ \times 0.04^\circ$ . On each frame, the dots were randomly assigned to either a population of “signal dots” or of “noise dots”. The signal dots were randomly selected on each frame and were displaced from frame to frame with a fixed spatiotemporal offset, creating a coherent motion signal with upward or downward direction (separated by  $180^\circ$ ) and a speed of  $2.6^\circ/\text{s}$ . We used “random position” noise. That is, the noise dots were re-drawn on a randomly selected position, creating spatiotemporal white noise, which comprised a mixture of directions and speeds [30]. On each trial, three different “sets” of RDKs of the selected direction and coherence were plotted in an interleaved fashion, where the dot pattern from each set was shown for one frame and followed by the next pattern from the same set only after three successive video frames, and so forth. This version of the RDK stimulus corresponds to the one used in many of the seminal monkey physiology studies on temporal integration of visual motion information (e.g. [31]). This was to encourage integration of motion information across space and time. The percentage of coherently moving dots (“motion coherence”; 0.05, 1.26, 3.15, 7.92, 19.91, and 50%), viewing duration (150, 300, 600, 1200, 2400, and 4800 ms), direction (“up/down”), and “decision-to-response-mapping” (“DR-mapping”; e.g. upward motion left button and downward motion right button) were randomly chosen on each trial, under the constraint that each combination of these parameters occurred equally often within a block of 144 trials. The six coherence levels listed above were determined in extensive pilot sessions, tailored to sample the full psychometric function for all stimulus durations. New stimuli were generated for each experimental block, including six different variations of the interleaved RDK sequences.

Stimuli were displayed on a 22-inch CRT monitor (resolution:  $800 \times 600$  pixels) at a rate of 100 Hz. The viewing distance was 68 cm. Experiments were conducted in a dimly illuminated room. Subjects were seated in an adjustable chair with their chin resting comfortably in a chin cup and additional support was provided by a head restraint mounted on the table. The height of the monitor placed the center of the display at approximately eye level.

## Task and procedure

Throughout all experimental conditions, subjects were required to fixate the red cross in the center of the screen and classify the net motion in a stimulus as upward (50% of trials) or downward motion by pressing one of two buttons (left or the right index finger) when a response prompt was provided. The RDK presentation was followed by a variable delay interval, after which the response was prompted. Observers were under no time pressure to respond. Auditory feedback of 100 ms duration (a 1000 Hz tone) was provided for incorrect responses.

**Variable DR-mapping experiment.** The decision-response mapping (e.g., left-hand button press for indicating “upward” choice) varied randomly from trial to trial. We will henceforth abbreviate this as “DR-mapping”. The experiment consisted of two conditions, which differed only in the timing of the cue instructing observers about the DR-mapping, relative to presentation of the RDK stimuli (Fig 1A and 1B). The cue indicated the motion direction corresponding to each response button in terms of two white arrows (one upward, one downward pointing) presented on the left and right half of the screen (11° from fixation).

In the pre-cueing (“Pre”) condition (Fig 1A), the arrows were presented after a variable period of fixation for 1000 ms, and were followed by a second random delay (200–400 ms) and the onset of the motion stimulus (150–4800 ms). After stimulus offset and another random delay (200–400 ms) the fixation cross turned green, which prompted the subject to report their choice.

The post-cueing (“Post”) condition was identical, except that DR-mapping cue was presented after the motion stimulus and second delay (Fig 1B). In both conditions, the inter-trial intervals were 900 ms. “Pre”- and “Post”-conditions were conducted in alternating blocks of 144 trials (see *General design* below).

**Fixed DR-mapping experiment.** This experiment consisted of a single condition, which was identical to the “Pre”-condition, with the exception that the DR-mapping was kept constant across all trials (Fig 1C). Although the DR-mapping was instructed at the start of the experiment and remained constant thereafter, the DR-cue was shown at the beginning of each trial to keep the visual input and trial duration identical to the “Pre”- from the variable DR-mapping experiment. Each subject was first trained on the task for a minimum of 432 trials and then completed between 2448 and 7632 trials (distributed over 3–9 experimental sessions), which were used for the analyses reported in this paper.

**General design.** All statistical analyses reported in this paper were performed within individual observers. Given the large number of trials required from each observer per condition (minimum: 2016) and the clear effect evident in Subjects 1–3 who participated in all conditions (see [Results](#)), the remaining three observers were asked to only participate in a subset of conditions. Subjects 4 and 5 were used to replicate the comparison between “Pre” and “Post”. Subject 6 was used to replicate the comparison between the variable and “Fixed” mappings.

The experimental conditions were arranged as follows. Subjects 1–5 first performed the Variable DR-mapping experiment, in which they alternated between “Pre” and “Post” conditions in a pseudorandom order. Each experimental session consisted of 6 blocks: 3 blocks of each condition (“Pre” and “Post”). Subjects 1–3 then performed the Fixed DR-mapping experiment. General order effects would have (if anything) predicted an improvement (prolongation) of integration timescales in the “Fixed” condition, due to the extensive practice of the task (under variable and fixed mapping). By contrast, we found no change of integration timescale in these subjects. Nonetheless, to rule out any order effects, we flipped the order in one additional observer (subject 6), who started with “Fixed”, followed by “Post”. Each subject was first trained on the task for a minimum of 432 trials per condition. Subjects then completed between 2110 and 5760 trials of each condition (distributed over 3–7 experimental sessions in total).

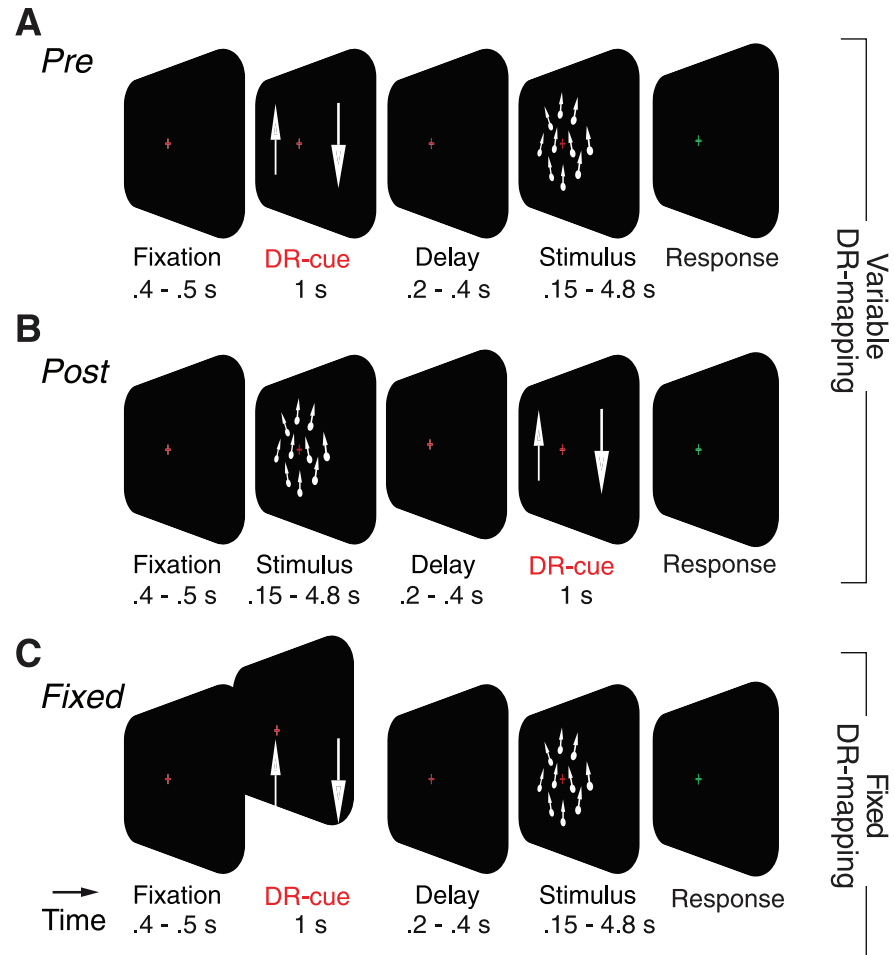


**Fig 1. Experimental design.** On each trial, the observer was required to discriminate the direction (upward or downward) of the random dot kinematogram (RDK), while fixating the central crosshair. The RDK was presented for one of a number of different durations and levels of motion strength **(A)** Variable “Pre” DR-mapping condition. The DR-mapping cue (two arrows mapping up/down motion directions onto left/right hand button presses) was presented before the RDK (separated by a variable delay), and it varied randomly from trial to trial. After another variable delay, a color switch of the fixation cross prompted the observer to indicate the choice with a button press. **(B)** Variable “Post” DR-mapping condition. Identical to “Pre”, except that the DR-mapping cue was presented after the RDK (“Post”). **(C)** “Fixed” DR-mapping condition. Identical to “Pre”, except that the DR-mapping cue was kept constant throughout the experiment, enabling long-term learning of sensory-motor associations.

doi:10.1371/journal.pone.0129473.g001

### Model-independent analysis of integration timescale

**Quantifying psychophysical thresholds.** Given the task design (interrogation protocol with different levels of stimulus strength), our analyses focused on proportion correct data, rather than response times [3]. We fitted the observers’ proportion of correct choices as a function of motion coherence, denoted  $P(C)$  below, by means of a cumulative Weibull function [32], separately for each experimental condition and stimulus duration. See Fig 2 for example fits from one subject in both conditions of Experiment 2. The cumulative Weibull distribution function was defined as

$$P_{t_1 \leq t \leq t_2}(C) = 0.5 + (0.5 - \lambda) \left( 1 - \exp \left[ - \left( \frac{C}{a} \right)^\beta \right] \right) \quad (1)$$

where  $\lambda$ ,  $\alpha$  and  $\beta$  are free parameters and the value 0.5 represents chance performance. The lapse rate ( $\lambda$ ) represents stimulus-independent errors, corresponding to the fraction of incorrect choices at the highest motion strength and longest viewing duration.  $\lambda$  was determined by fitting eq (1) to data from the longest viewing duration in each experiment, and then inserted in eq 2 to find best fits of  $\alpha$ , and  $\beta$  to the data from all conditions. The value of  $\alpha$  is the psychophysical threshold corresponding to the coherence level that elicits 82% correct responses when asymptotic performance is perfect (i.e.,  $\lambda = 0$ ). Parameter  $\beta$  determines the steepness of the psychometric function for a particular threshold. Best-fitting values for the free parameters were obtained by means of a maximum likelihood procedure [33]. To obtain the best-fitting values for the free parameters, we minimized the negative log-likelihood, which yields the exact same parameters as maximizing the likelihood.

Confidence intervals for the proportion of correct choices were obtained by employing a non-parametric bootstrap [34], in which the original set of trials was resampled with replacement a large number of times ( $N = 10,000$ ) and the proportion of correct responses was computed for each iteration. The confidence intervals of the parameters of the cumulative Weibull functions and of the regression-based threshold vs. duration functions (see below, eqs 2–5) were obtained by means of a parametric bootstrap procedure [35]. We used a binary process to generate a new set of data based on the binomially distributed noise and estimated Weibull parameters from the observed data set. We repeated the maximum likelihood procedure for each bootstrap iteration to find the best parameter fits for the “mock” data set and calculated the corresponding parameters anew. The resulting distributions indicated the likely spread of all parameters for the original data set.

**Fitting threshold versus duration functions.** Perfect integration predicts a linear decrease in threshold with duration with a slope of -0.5 in log-log coordinates. A lack of integration predicts a flat line (slope of 0). Hence, to analyze the dependence of thresholds on duration, we fitted a bilinear function to the log of the best fits of  $\alpha$  and viewing duration [26–28]. The slope of the first line was constrained to -0.5 and the slope of the second line was constrained to 0. We determined the best fitting value for the intercept  $\beta_0$  of the linear function. The general fit was evaluated by calculating the sum of squared errors (SSE) and the best fit of the bilinear function was determined by means of an iterative least squares method [36].

With a number of durations  $n$ , the relationship between thresholds and viewing duration for each  $i = 1, \dots, n$  was expressed as

$$y_i = \beta_0 - 0.5\log(t_i) + e_i, \text{ if } \log(t_i) \leq A_i$$

and

$$y_i = \beta'_0 + e_i, \text{ if } \log(t_i) > A_i \tag{2}$$

where  $\beta_0$  correspond to the  $y$ -intercept of the first line,  $\beta'_0$  corresponds to the  $y$ -intercept of the second line,  $A$  represents the abscissa of the joint point. In order to ensure that the two lines join at the value  $x = A$ , we applied the following restriction:

$$\beta_0 - 0.5A = \beta'_0 + e_i \tag{3}$$

The error terms (i.e.  $e_i$ 's for  $i = 1, \dots, n$ ) were independent and identically distributed normal random variables with mean equal to zero and constant variance. Due to the restriction from



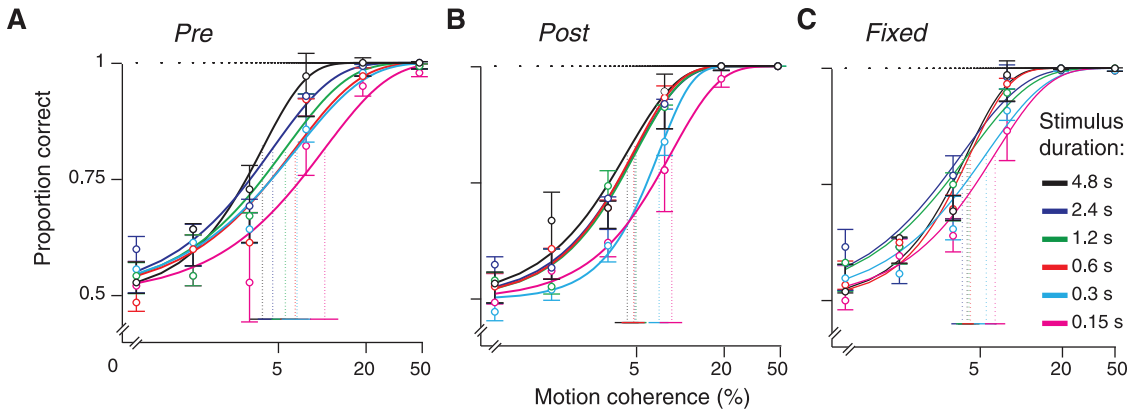


**Fig 2. Example psychometric functions of one observer in all conditions.** Solid curves are maximum likelihood fits of cumulative Weibull functions to the proportion correct data. Vertical dashed lines represent estimated threshold parameters (solid horizontal lines at bottom, 95% confidence intervals). The horizontal dashed line represents the lapse rate. **(A)** “Pre”- condition. The performance data and psychometric functions are shown separately for all stimulus durations. **(B)** As in A, but for “Post”. **(C)** As in A, but for “Fixed”.

doi:10.1371/journal.pone.0129473.g002

eq (3), the abscissa of the joint point could be estimated as

$$A = \frac{(\beta_0 - \beta'_0)}{0.5} \tag{4}$$

Eq (4) held only for cases in which  $A$  lied between two consecutive values of  $\log(t_j)$ ,  $\log(t_{j+1})$  and  $\log(a_j)$ . In this case, the first line included  $n_j$  number of  $\log(t_i)$  and  $\log(a_i)$  pairs up to and including  $\log(t_j)$  and  $\log(a_j)$ , whereas the second line included all values from  $\log(t_{j+1})$  and  $\log(a_{j+1})$  on to  $n'_j$ . If the estimated joint point was indeed  $\log(t_j)$ , and  $\log(t_{j+1})$ , we computed the ordinary least squares solutions and determined the joint point by substituting the observed  $\beta$ 's with the estimated  $\beta$ 's. The SSE was computed as the sum of the individual SSEs from the two lines

$$SSE_j = \sum_{i=1}^j [\log(a_i) - (\beta_0 - 0.5\log(t_i))]^2 + \sum_{i=j+1}^n [\log(a_i) - \beta'_0]^2 \tag{5}$$

If the estimate of the joint point was not between  $\log(t_j)$ , and  $\log(t_{j+1})$ , we modified the computation such that  $A$  occurred exactly at  $\log(t_j)$ . Since the minimization of SSE in this case is constrained to only one possible joint point  $\log(t_j)$ , this constrained least squares solution was computed as a modification of the two separate ordinary least squares solutions [36].

In a control analysis, we relaxed the constraints on the slopes of the bi-linear fits, by allowing the first slope to be in the range from -0.5 to 0, and the second slope was constrained to any value larger than the first slope. These fits required two additional constraints. 1. If the estimated joint point exceeded the longest signal duration in the experiment, it was set to the longest signal duration (4.8 s). 2. If the first slope was smaller than 0.001, we assumed that participants did not integrate and set the joint point to the shortest signal duration of 0.15 s.

Given the six stimulus durations, the joint point could only be estimated for the four intermediate durations, which corresponded to the limited interval 0.3–2.4 s. We verified that in all cases, the bi-linear fits provided a significantly better match to the data than a single linear fit, with or without slopes constrained to -0.5 (data not shown). Further, in all cases were the joint point estimates significantly shorter than the longest possible timescale estimates of 2.4 s (see Results, Fig 3). Thus, it is unlikely that the short timescale estimates obtained are due to the limitations of the procedure.

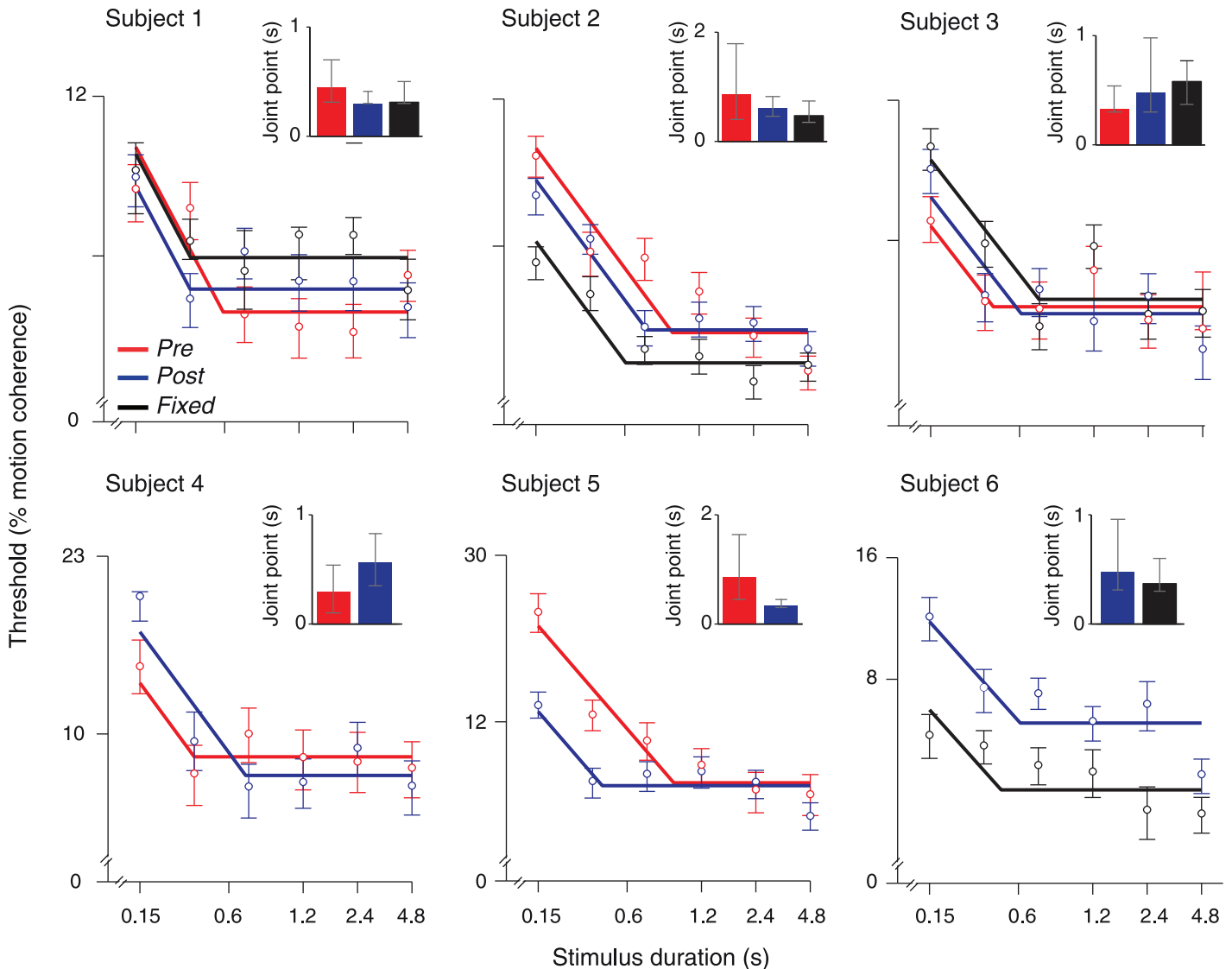


**Fig 3. Model-independent characterization of integration timescales.** Threshold vs. duration functions from all conditions. Circles represent psychophysical thresholds for each stimulus duration. Solid lines: best fitting bilinear function, with the slopes constrained to -0.5 (first branch) and 0 (second branch; see text for details). Error bars, 60% confidence intervals (bootstrap). Inset: bar graphs of the joint point estimates of the best fitting bilinear function. Error bars, 95% confidence intervals (bootstrap).

doi:10.1371/journal.pone.0129473.g003

**Statistical comparisons of joint points.** To compare integration time scales and lapse rates between conditions within individual observers (i.e., “Pre”- versus “Post”-conditions; “Post” vs. “Fixed”; “Post” vs. “Fixed”), we compared the joint point estimates  $A$  by means of non-parametric permutation tests [34]. For each permutation, all trials were combined into one set of  $N_{pre}/N_{fixed} + N_{post}$  trials and shuffled 10,000 times. Then the shuffled set was split into 2 sets of  $N_{pre}/N_{fixed}$  and  $N_{post}$  trials, the proportion correct was recalculated and the Weibull functions were fitted to determine the new thresholds and lapse rates. Based on these,  $A$  was iteratively computed to obtain the permuted difference between the two sets. Finally, we compared the observed difference lapse rates and in  $A$  with the permuted differences.

P-values were obtained by calculating the fractions of repetitions (10,000), in which the absolute value of the permuted difference was larger than the absolute value of the measured difference.

## Computational modeling of psychophysical performance

**General model description.** We fitted the leaky-competing accumulator model (LCA) [37,38] to the behavioral data of each individual observer. The LCA is a neurophysiologically inspired sequential sampling model of decision-making and has successfully accounted for behavioral data from a wide variety of perceptual tasks [2]. Similar to other models, LCA assumes that noisy evidence for different hypotheses is accumulated towards a decision criterion. A separate accumulator, corresponding to the pooled neuronal activity of a dedicated population, represents each competing hypothesis. Thus, in choices between two options, two pools of neurons integrate the momentary evidence for each alternative and compete with each other via lateral inhibition, while their activity is subject to slow decay (“leak”). The activation states of the accumulators are described by the following finite difference equations:

$$\begin{aligned}
 x_1(t+1) &= \max(0, x_1(t) + Dx_1); \\
 x_2(t+1) &= \max(0, x_2(t) + Dx_2); \\
 Dx_1 &= I_1 - \kappa x_1 - \beta x_2 + I_0 + N(0, \sigma); \\
 Dx_2 &= I_2 - \kappa x_2 - \beta x_1 + I_0 + N(0, \sigma).
 \end{aligned}
 \tag{6}$$

In the above equation  $x_i$  corresponds to the activation states of the accumulator associated to alternative  $i$ . The  $\max$  function prevents activation states (which correspond to population firing rates) from going below a predefined value, implementing in this case a lower reflecting boundary at 0. Constant input to both accumulators (controlling for the degree of non-linearity in the activation states) is denoted by  $I_0$  while  $\Delta$  is the momentary change of each accumulator on each time step. This change or increment is driven by three factors: i) the external input in favor of the corresponding accumulator, ii) the activation state of the accumulator on the preceding moment and iii) the activation state of the competing accumulator. The external momentary input, denoted by  $I_i$ , is subject to Gaussian noise fluctuations with zero mean and standard deviation  $\sigma$ . The accumulators compete with each other via lateral inhibition of strength  $\beta$ , and their activation is subject to leak of  $\kappa$ . For the interrogation protocol used in this study, the activation states of the two accumulators are read out at the end of the trial (corresponding to the response cue presentation), and the alternative with the highest activation state, up to that point, is chosen.

In the simulations presented here, we fixed the standard deviation of noise to  $\sigma = 1$ . We further assumed that  $I_1 = C \times s$ , with  $C$  corresponding to the motion coherence for the corresponding alternative and  $s$  being the sensitivity parameter that modulates the signal to noise ratio. We let  $I_0$  be a free parameter, and we assumed that motion coherence is subject to power-law saturation with exponent  $m$ :  $I_1 = C^m \times s$ . The experimental time units were converted into simulation time steps with 1 second corresponding to 250 time-steps. The coherence level ( $C$ ) was determined by the experimental condition and ranged from 0 (no coherent motion) to 1 (all dots move coherently towards a given direction). The input to the first unit ( $I_1$ ) was always proportional to the coherence level  $c$ , while the input to the second unit ( $I_2$ ) was always set to 0. In sum, the decision-making model had five free parameters: inhibition ( $\beta$ ), leak ( $\kappa$ ), sensitivity ( $s$ ), constant activity ( $I_0$ ) and coherence saturation ( $m$ ).

**Model fits to behavioral data.** We fitted the model described above to the data of each individual observer. Specifically, the model was fitted to the individual proportion correct data

for  $N$  coherencies  $\times$   $M$  duration levels ( $N = 5$  and  $M = 6$ ). We excluded the lowest coherence level (0.05) because performance indistinguishable from chance for all durations at that coherence and we found that including this coherence yielded worse fits. Assuming that the correct responses follow a binomial distribution, we computed the likelihood for a given parameterization of the model, for the  $K = N \times M$  data points as:

$$L = \prod_i^k \binom{n_i}{y_i} p_i^{y_i} (1 - p_i)^{n_i - y_i} \tag{7}$$

where  $n_i$  was the number of trials for the  $i$ -th data point,  $y_i$  was the corresponding number of correct responses and  $p_i$  the probability of correct response predicted by the model (obtained by running 5000 iterations of the model for the given condition/ parameterization). The cost function was the negative logarithm of  $L$ :

$$-LL = -\log_e(L) \tag{8}$$

and was minimized using SUBPLEX minimization routine [39]. For each subject and each model we ran the optimization 400 times with starting points randomly sampled from uniform distributions within a parameter-specific range.

In order to assess the goodness of fit for the best parameters of a given model, we calculated the chi-square statistic as follows:

$$\chi^2 = \sum_{i=1}^K \frac{(O_i - E_i)^2}{E_i} \tag{9}$$

where  $K$  was the number of bins corresponding to the experimental conditions,  $O_i$  was the observed frequency of correct responses at condition  $i$ , and  $E_i$  the corresponding frequency predicted by the model. Because the number of experimental and simulated trials was different,  $E_i$  was calculated by multiplying  $p_i$  (the probability of correct response predicted by the model) by the number of experimental trials. The chi-square statistic had  $K-1$  degrees of freedom. P-values indicated the probability that the chi-square statistic is at least as extreme as the obtained one, under the null hypothesis that the data and the predictions of the model follow the same distribution. We rejected the null hypothesis at a significance level of  $\alpha = 0.05$ .

**Model-based estimation of integration time constants.** In order to obtain a model-based estimate of the time constant of evidence integration, we fitted shifted exponential functions [40] to the  $d'$  transformed psychometric functions of the LCA model fits of each observer. The shifted exponential function has been shown to accurately track the stimulus sensitivity increase as a function of time of human observers [40]. Fitting shifted exponential functions to the simulated (rather than the measured)  $d'$  vs. duration functions provided more robust time constant estimates (Fig 4) by discounting noise in the behavioral data. We applied this procedure after ensuring that the LCA provided a reasonable fit to the behavioral (proportion correct) data of each subject (MLE,  $\chi^2$  and  $p$  values for assessment of goodness of fit). We fitted the following shifted exponential function to the predicted average sensitivity across all coherences  $d'$  ( $d' = \Phi^{-1}(0.99 \cdot p_i)$ ) vs. duration (Fig 4):

$$d'(t) = D' \left( 1 - \exp\left(-\frac{t - t_0}{\tau}\right) \right) \tag{10}$$

with  $D'$  denoting the average asymptotic sensitivity level for all coherences,  $t_0$  the period during which sensitivity was zero and  $\tau$  the time constant (Fig 5).

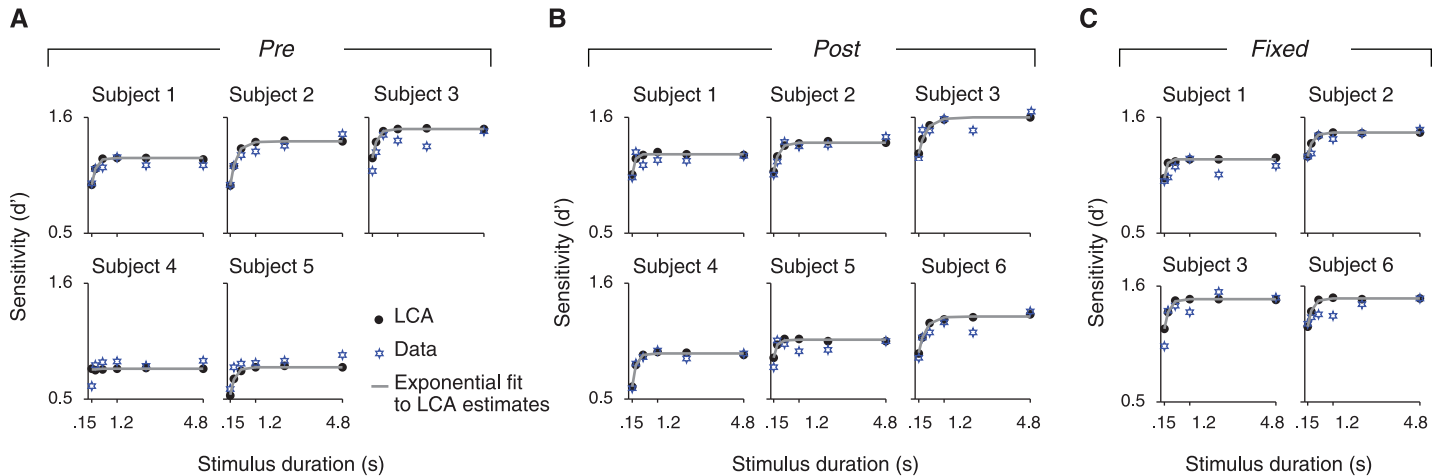


**Fig 4. Model-based characterization of integration timescales.** Simulated  $d'$  vs. duration functions, and exponential fits. Filled dots are the best-fitting LCA model estimates for each subject; solid curves: shifted exponential functions on the predicted average sensitivity across all coherences; blue stars: measured average sensitivity across all coherences. **(A)** “Pre”. **(B)** “Post”. **(C)** “Fixed”.

doi:10.1371/journal.pone.0129473.g004

## Results

We examined the impact of sensory-motor contingencies [41,42] on the timescale of perceptual evidence integration in a total of six human observers. To this end, we used a standard psychophysical task, coarse discrimination of visual motion direction, and quantified the integration timescale under variable (Fig 1A and 1B) or fixed (Fig 1C) DR-mapping. For the variable mapping, the mapping was instructed either before (“Pre”; Fig 1A) or after decision formation (“Post”; Fig 1B). Subjects 1–3 were asked to perform all three mapping conditions, to establish the main result in terms of three independent within-subject comparisons. Subjects 4 and 5 were measured to replicate the results of the “Pre” vs. “Post” comparison. Subject 6 was measured to replicate the result of the variable (only “Post”) vs. fixed comparison.

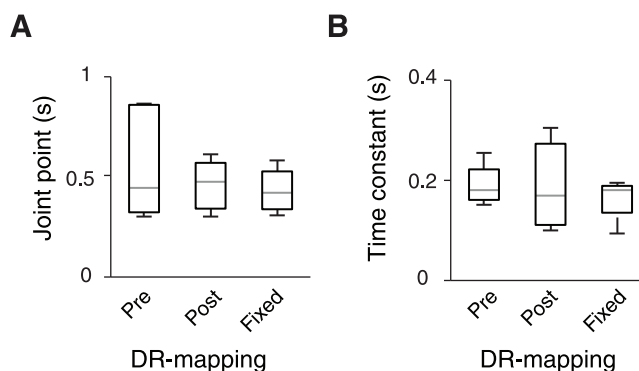


**Fig 5. Summary of integration times using model-independent (A) and model-based (B) characterization of time-constants.** Summary of integration times under the three DR-mappings tested. The gray horizontal line marks the median, the upper and lower edges of the box mark the 25<sup>th</sup> and 75<sup>th</sup> percentiles, and the whiskers extend to the most extreme data points, excluding outliers. **(A)** Joint points of the bilinear fit to threshold vs. duration functions. **(B)** Time constants derived from LCA model fits.

doi:10.1371/journal.pone.0129473.g005

## Overall performance

In all observers and experimental conditions, performance depended lawfully on both, the strength and the duration of the visual motion signal (see Fig 2 for an example observer). The proportion of correct choices was generally about chance-level (~0.5) for the lowest level of coherently moving dots (0.05) and about perfect (~1) for the highest coherence level (0.5). This was true for all stimulus durations, except for the shortest (150 ms), at which even the highest coherence did not yield perfect performance in some subjects. We quantified the dependency on motion coherence by fitting cumulative Weibull functions to the proportion correct data. The psychometric functions generally shifted leftwards with increasing stimulus duration, as reflected by the decrease of the threshold parameter (inverse of sensitivity; Fig 2), meaning that observers could integrate the motion information over time and even discriminate patterns with a low percentage of coherently moving dots. The thresholds reached less than 0.1 motion coherence in all observers for the longer durations (Fig 3). This decrease of psychophysical thresholds with stimulus duration is an index of temporal integration of stimulus information (see below).

To assess whether observers made more “non-perceptual” errors (i.e., choosing the incorrect buttons irrespective of signal strength) in any of the three experimental conditions, we compared the “lapse rate” estimates (i.e., the upper asymptote of best-fitting cumulative Weibull functions) between conditions. Lapse rates quantify processes independent of the perceptual decision per se, such as lapses of attention or motor errors. Lapse rates were generally negligible in all three conditions (Table 1), and there were no systematic differences between the three conditions in most observers. One observer (subject 5) exhibited a significant difference in lapse rates between “Pre” and “Post” ( $p = 0.02$ ), but also evident in the joint point (see below). There were also no differences in the overall threshold levels between the conditions when tested separately for all but the first (0.15 s) stimulus durations (Table 2).

In sum, all six observers exhibited a high sensitivity and were able to adjust the sensory-motor associations and even rapidly (on a trial-by-trial basis) under the variable DR-mappings. There were no systematic differences in the occurrence of motor errors, as well as in overall performance, between the three conditions. Finally, the lawful shift in psychometric functions with stimulus duration indicates that observers indeed integrated stimulus information over time and thus became better in discriminating motion directions with low coherences the longer the observation period [12,13,26–28]. We next quantified the timescale of this integration process, and its dependence on DR-mapping, based on two complementary approaches: a model-independent and a model-based approach.

**Table 1. Lapse rates.**

Subject	“Pre“	“Post“	“Fixed”
1	0.014 (0.000, 0.033)	0.000 (0.000, 0.004)	0.000 (0.000, 0.008)
2	0.000 (0.000, 0.000)	0.000 (0.000, 0.003)	0.000 (0.000, 0.000)
3	0.011 (0.000, 0.028)	0.000 (0.000, 0.000)	0.006 (0.000, 0.017)
4	0.049 (0.000, 0.070)	0.029 (0.030, 0.062)	-
5	0.052 (0.009, 0.070)	0.014 (0.000, 0.029)	-
6	-	0.000 (0.000, 0.000)	0.028 (0.000, 0.059)

Numbers are estimates of lapse rate ( $\lambda$ ) and by 95% confidence intervals.

doi:10.1371/journal.pone.0129473.t001

**Table 2. Comparisons of threshold estimates between conditions.**

Subject	Comparison	0.15s	0.30s	0.60s	1.2s	2.4s	4.8s
1	Pre/Post	0.356	0.002	0.079	0.174	0.204	0.284
	Post/Fixed	0.465	0.001	0.436	0.451	0.810	0.237
2	Pre/Post	<b>0.000</b>	0.277	0.002	0.163	0.374	0.363
	Post/Fixed	0.001	0.000	0.147	0.070	0.060	0.393
3	Pre/Post	0.004	0.447	0.311	0.090	0.316	0.401
	Post/Fixed	0.082	0.069	0.199	0.009	0.352	0.331
4	Pre/Post	0.005	0.293	0.175	0.332	0.403	0.414
5	Pre/Post	<b>0.000</b>	0.004	0.183	0.403	0.393	0.378
6	Post/Fixed	<b>0.000</b>	0.005	0.004	0.230	0.005	0.304

Numbers are p-values based on two-sided permutation tests. Significant p-values (after Bonferroni-correction for multiple comparisons) are printed in bold.

doi:10.1371/journal.pone.0129473.t002

### Model-independent characterization of integration timescales

The model-independent approach was based on the following rationale. The integral of the “signal” embedded in the noisy stimulus increases linearly with the stimulus duration, while the “noise” (i.e., standard deviation) increases with the square root of the stimulus duration. Consequently, the signal-to-noise ratio increases with the square root of duration and perfect integration of the sensory evidence implies that the observers’ psychophysical threshold (the inverse of their signal-to-noise ratio) decreases as a function of the square root of stimulus duration, yielding a straight line with a slope of -0.5 on log-log axes. Conversely, no integration of sensory evidence implies that the observers’ threshold does not change as a function of stimulus duration (i.e., a straight line with a slope of 0). Consequently, integration of evidence across a limited time window predicts an initial linear decrease of the threshold vs. duration function with a slope of -0.5, followed by gradual deceleration towards a second (asymptotic) linear portion with a slope of 0. Note that such a timescale limitation may be due to leaky integration [37,38], or perfect (i.e., without leak) integration towards absorbing bounds [28] (see [Discussion](#)). Based on this rationale, the duration situated in between the -0.5- and 0-slope portions of the threshold vs. duration function can be used as an estimate of the integration timescale. We fitted bilinear functions to the individual threshold vs. duration functions, whereby the slope of the first line was constrained to -0.5 and the slope of the second to 0 and used the joint point between both lines as time scale estimate.

In all three conditions, the threshold vs. duration functions decreased with stimulus duration, but only for a limited range ([Fig 3](#)). The individual joint points ranged from 300 to 870 ms for “Pre” (presumably involving the highest short-term memory demands, see [Discussion](#)), from 300 to 610 ms for “Post”, and from 310 to 580 ms for “Fixed”. Any two frames of one of the three interleaved sequences of coherent motion were separated by 30 ms (at the monitor refresh rate of 100 Hz; see [Materials and Methods](#)), across which the observers’ visual motion system could pair dots to extract motion. Thus, the physical evidence fluctuated over 30 ms. Under the assumption that visual cortical regions like MT that encode visual motion track this stimulus information with high temporal precision [43], the shortest integration timescale observed here (300 ms) implies integration of ten samples of sensory evidence provided by visual cortex into the decision. The longest timescale of 870 ms corresponds to integration of close to 30 samples of sensory evidence.

Given the experimental design and fitting procedure, possible estimates of the joint point were confined to the interval 0.3–2.4 s (see [Materials and Methods](#)). All joint point estimates in



the insets [Fig 3](#) were shorter than the upper bound of 2.4 s, and the 95% confidence intervals of these joint point also estimates excluded 2.4 s. Thus, in all cases were the timescale significantly shorter than the one that would have maximized performance in this task entailing the maximum stimulus duration of 4.8 s.

In sum, all subjects showed temporal integration of perceptual evidence, but their integration timescale were consistently smaller than the optimal timescale for this task (defined as the timescale that would have maximized the overall fraction of correct choices). Possible mechanistic accounts of the timescale limitation are described in Discussion. We next explored if and how the timescale was affected by our manipulations of the sensory-motor contingencies.

**Integration timescale for “Pre” vs. “Post” under variable DR-mapping.** If the integration timescales depended on subjects’ ability to directly translate the integrated evidence into an action plan, then precluding the sensory-motor contingency in the “Post”-condition might be expected to shorten the integration timescale, relative to the “Pre”-condition. We found no consistent evidence for this scenario. Only one observer (subject 5 who also had a difference in lapse rates; [Table 1](#)) exhibited a significant difference in joint points between “Pre”- and “Post”-conditions ( $p < 0.01$ ; two-tailed permutation test). In the remaining four observers (subjects 1–4) the joint points did not differ significantly between “Pre”- and “Post”-(range of p-values: 0.07–0.37; two-tailed permutation test).

Separate bi-linear fits with relaxed constraints on the two slopes (see [Materials and Methods](#)) yielded qualitatively identical results. The joint point estimates obtained from this procedure were generally less precise (larger confidence intervals, data not shown). Importantly, however, there was again no robust difference between joint points from the different conditions in all of the five observers (range of p-values across subjects 1–5: 0.09–0.77; two-tailed permutation test). Taken together, the results suggest that the evidence integration timescale is largely independent of the “Pre” vs. “Post” condition.

**Integration timescale for fixed vs. variable DR-mapping.** In previous studies reporting neural signatures of evidence integration in brain regions involved in motor planning [[12,19–22,44,45](#)], subjects were typically practiced with one specific sensory-motor contingency for at least hundreds of trials. It is possible that sensory-motor contingencies only improve the integration timescale after extensive practice, due to slow learning mechanisms. The trial-to-trial variation of DR-mapping in the “Pre”-condition of the previous experiment may have not have enabled such learning and, therefore, no improvement in integration timescale. To test this idea, we next explored the effect of long-term practice of one specific fixed DR-mapping on the integration timescale ([Fig 1C](#)), and compared this with the timescale under the variable DR-mapping.

The joint points obtained from the constrained fits (first slope: -0.5, second slope: 0) were statistically indistinguishable between the “Fixed” and “Pre” (range of p-values across three observers: 0.07–0.19; two-tailed permutation test) and the “Fixed” and “Post” conditions (range of p-values across four observers: 0.31–0.70; two-tailed permutation test) and. The bi-linear fits with relaxed constraints on the slopes yielded similar results: There was no significant difference in the joint points for two out of three observers in the “Fixed” vs. “Pre” comparison (subject 1:  $p = 0.81$ ; subject 2:  $p = 0.02$ ; subject 3:  $p = 0.21$ ) and three out of four observers in the “Fixed” vs. “Post” comparison (subject 1:  $p = 0.41$ ; subject 2:  $p = 0.68$ , subject 3:  $p = 0.66$ ; subject 6  $p < 0.01$ ). Thus, even extensive practice of a specific sensory-motor association across several thousands of trials did not seem to robustly improve the temporal integration process.

**Model-based characterization of integration timescales.** One concern may be that our model-independent assessment of integration timescale may not have been sufficiently sensitive to reveal subtle effects of the sensory-motor contingencies. To address this, and to obtain a more theoretically motivated estimate of the integration timescale, we used a computational



model of the decision process to fit the behavioral performance data (see [Materials and Methods](#)). The LCA is a neurophysiologically inspired model of the collective dynamics of two populations of “decision neurons”, which has been successfully applied to behavioral data from a wide variety of decision tasks [2,37,38,40]. For our interrogation protocol, the model assumed that the observers kept integrating for the whole stimulus interval and made a decision in favor of the alternative with the largest integrated evidence after that interval. Limitations of integration time scale resulted from the balance between “leaking away” of past evidence (biasing choices towards the most recent evidence) and mutual inhibition (biasing choices towards the early evidence).

The LCA model provided a reasonable fit to the behavioral performance of all observers in all three experimental conditions ([Table 3](#)). The goodness of fit was assessed by means of comparing the empirical and model-predicted psychometric functions using the chi-square statistic (see [Materials and Methods](#)). For an alpha value of 0.05, the null hypothesis that the two compared distributions (e.g. psychometric functions) are the same was not rejected for any of the participants ( $p > 0.95$  for all participants, see [Table 3](#)).

We used the model with the best-fitting parameters for each observer to generate accuracy ( $d'$ ) vs. duration functions and fitted the average (across coherence levels) sensitivity with a shifted exponential function ([Fig 4](#)). The LCA fit of subject 4 in the “Pre”-condition was invariant to increases of duration and thus meaningful exponential fits could not be obtained. For the remaining subjects and conditions the obtained time constants were typically around 200 ms ([Table 4](#), [Fig 5B](#)), consistently shorter than the around 500 ms timescale estimates obtained from the bi-linear fits (compare [Fig 5A](#) and [5B](#)). This difference is expected since the time constant of the exponential fit represents the time it takes for the sensitivity to reach ~62% of its asymptotic value while the joint point indicates the exact moment of asymptotic saturation; by simulating a leaky integrator model we confirmed that the bilinear joint point is expected to be 2–2.5 times higher than the exponential time constant. The exact, analytical correspondence between the two measures of integration timescale should be addressed in future theoretical work. Despite the quantitative difference between the two timescale measures, there was a consistent qualitative correspondence across subjects (compare insets in [Fig 3](#) with [Table 4](#)).

Most importantly, in line with the analysis of joint points, comparison of the model-based integration time constants between conditions did not yield any significant difference between DR-mapping contexts, as assessed by comparing the 95% confidence intervals between conditions ([Table 4](#)).

To assess the sensitivity of the model-based time constant estimation, we simulated a leaky integration model to generate many psychometric functions and repeated the same time constant estimation procedure (i.e., based on exponential fits as described in [Materials and Methods](#)) on these psychometric functions. In a simple leaky integration model, the integration time constant is known precisely (inverse of the leak parameter), whereas the time constant is a combination of leak and mutual inhibition in the more complex non-linear LCA described above (see [Materials and Methods](#) and [37]). We used three different levels of leak corresponding to time constants of 200, 400, and 600 ms, whereby 200 ms corresponds roughly to the median time constant estimate obtained from our behavioral data in all conditions ([Fig 5B](#)). Using three motion coherence levels (7%, 11%, 15%) and six stimulus durations (as in our behavioral experiments) we generated 300 simulated model responses per condition and repeated the time constant estimation process 10,000 times, for each of the three different time constants. The 95% confidence intervals of the resulting distributions of estimated time constants did not overlap ([Fig 6](#)). We conclude that our estimation procedure was sufficiently sensitive for distinguishing differences in time constants of 200 ms.

**Table 3. LCA model parameters and goodness of fit.**

Condition	Subject	$\beta$	$\kappa$	$s$	$l_0$	$m$	-LL	$\chi^2(1, N = 29)$	$p$
"Pre"	1	0.282	0.133	1.528	0.646	0.837	73.041	3.78	1.000
	2	0.497	0.020	1.696	-0.021	0.806	74.444	7.70	1.000
	3	0.436	0.028	2.379	-0.055	0.767	70.6333	7.17	1.000
	4	0.270	0.557	1.909	-0.064	0.381	88.095	6.03	1.000
	5	0.359	0.006	0.929	0.129	0.883	100.468	10.87	0.999
"Post"	1	0.126	0.090	2.403	0.507	0.985	61.137	4.33	1.000
	2	0.019	0.036	2.613	0.858	1.033	62.749	4.69	1.000
	3	0.061	0.063	9.181	1.125	1.371	40.263	2.06	1.000
	4	0.173	0.123	0.532	0.818	0.591	96.489	15.19	0.989
	5	0.257	0.110	2.178	0.484	1.083	76.182	6.17	1.000
	6	0.772	0.002	1.680	-0.237	0.732	61.299	3.79	1.000
"Fixed"	1	0.155	0.084	1.025	0.403	0.728	83.117	17.68	0.951
	2	0.179	0.011	1.622	-0.136	0.663	74.168	4.86	0.999
	3	0.176	0.093	1.449	0.456	0.672	65.839	8.25	0.999
	6	0.447	0.046	2.739	0.118	1.012	64.579	10.80	0.999

Parameters: inhibition  $\beta$ , leak  $k$ , sensitivity  $s$ , baseline activity ( $l_0$ ) and coherence saturation ( $m$ ). See [Materials](#) for description of the meaning of these parameters. -LL,  $\chi^2$  and  $p$  are the negative log likelihood of the best-fitting parameters, the chi-square value and the p-value respectively.

doi:10.1371/journal.pone.0129473.t003

## Discussion

Here, we examined how knowledge of sensory-motor contingencies [41,42] affects the time-scale of perceptual evidence integration into visual motion discrimination decisions, on a short-term (trial-by-trial) or long-term (across thousands of trials) basis. We found that all subjects integrated visual motion signals across time, and that their behavioral performance was well accounted by a leaky competing accumulator [37] model. However, integration time-scales were generally shorter than optimal for the task (median joint points of ~450 ms), in which subject had to integrate evidence for up to 4.8 s. Finally, we found that neither subjects' knowledge of a (variable) sensory-motor contingency, nor their long-term learning of one (fixed) contingency, had a significant and consistent effect on their integration timescale. Although we used two independent analytic approaches (model-independent and model-based) for estimating integration timescales which yielded consistent results, and established the sensitivity of our analyses, there was no evidence for a difference in integration timescales between the experimental conditions. We, therefore, conclude that long-term learning (under fixed

**Table 4. Model-based time constant estimates.**

Subject	"Pre"	"Post"	"Fixed"
1	0.151 (0.112, 0.212)	0.100 (0.038, 0.162)	0.093 (0.017, 0.169)
2	0.255 (0.221, 0.314)	0.197 (0.145, 0.251)	0.195 (0.152, 0.237)
3	0.170 (0.142, 0.192)	0.305 (0.251, 0.360)	0.178 (0.146, 0.210)
4	N/A	0.141 (0.087, 0.196)	—
5	0.190 (0.124, 0.255)	0.111 (0.032, 0.190)	—
6	—	0.273 (0.137, 0.409)	0.184 (0.124, 0.243)

Numbers are estimates of time constant ( $\tau$ ) and 95% confidence intervals.

doi:10.1371/journal.pone.0129473.t004

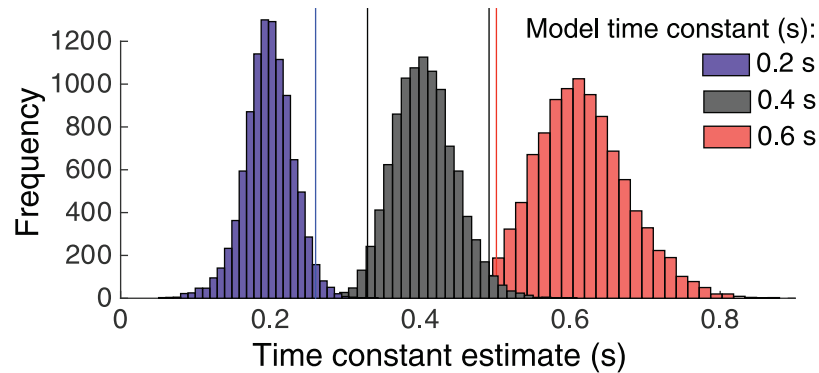


**Fig 6. Sensitivity of the model-based timescale estimation.** Sensitivity of the model-based timescale estimation. Three distributions of estimated time constants obtained by simulating leaky integrator models with three different time constants (0.2, 0.4, 0.6 s). Vertical lines indicate the 2.5% and 97.5% quantiles. The overlap between the distributions is small (<5%).

doi:10.1371/journal.pone.0129473.g006

mapping) or rapid acquisition (under variable mapping) of sensory-motor contingencies have only a small, if any, effect on the mechanisms limiting the timescale of perceptual decisions.

Many studies have used free response protocols, in which the observer controls the decision time, to study the dynamics of perceptual decision-making [8,9,31,37,46]. Evidence integration is then inferred from fitting a decision model to the reaction time distributions [2,3,8,37]. Reaction times do not only reflect the integration process, but also the observer’s speed-accuracy tradeoff [3,6,8,9,47]. By contrast, in the interrogation protocol used in the present study, the optimal strategy is to integrate all available evidence (perhaps subject to inevitable leak), and then choose the option that is best supported by the integrated evidence when the response is prompted [3,37]. Thus, the improvement of threshold as a function of stimulus duration should directly reflect the evidence integration process.

Previous studies of perceptual decision-making in humans and animals using this approach yielded a wide range of integration timescales. Some studies of human motion discrimination found timescales on the order of several seconds [26,27]. One study in rats and humans showed close-to-perfect integration, within a range of ~1 s using a task where participants had to discriminate the relative frequency of discrete events [29]. Another human study showed threshold decreases throughout a range of 900 ms—crucially, this decrease was steeper when subjects expected longer signals compared to when they expected shorter signals [13]. The relatively short timescales observed in the current study are in line with previous results from monkeys [28] in motion discrimination: In particular, using stimuli and tasks analogous to our fixed DR-mapping condition, Kiani et al. [28] found that monkeys exhibited a joint point of ~420 ms, just like our current human results. The human studies with larger samples sizes performing the same task also observed a substantial inter-individual variability in integration timescales [13]. Taken together, these results may suggest that integration timescale may, just like short-term memory capacity, be an individual trait with an upper limit, which can only be adapted to task demands within that limited range [13]. Additionally, the length of the temporal integration window may differ across different tasks.

Limited integration timescales are consistent with two mechanistically distinct scenarios. First, the decision process may terminate prematurely, once the integrated evidence has reached an implicit absorbing bound (termed “bounded diffusion”) [28]. This strategy can be compared to “closing the eyes” after an initial decision is made, thus eliminating the impact of the subsequently presented evidence. Second, the limit may be explained using a leaky

competing accumulation process, as postulated by the LCA model that we used here [38,48]. If the leak parameter exceeds inhibition then the model implements a stable Ornstein-Uhlenbeck (leaky integration) process, with integration taking place only until the stable state is reached [3]. When the inhibition parameter is larger than leak, the model has unstable dynamics and is maximally sensitive to early evidence, in close resemblance to the bounded diffusion model. Both the implicit boundary and LCA dynamics might also work in concert, and to different extent in different individuals. The current findings establish that, whatever the mechanism limiting the integration time scale, this mechanism seems unaffected by sensory-motor mapping.

The variable DR-mapping forced observers to establish and remember a new association between decision and response on each trial, whereas the fixed mapping allowed them to establish an automatic sensory-motor transformation, presumably after a few hundred trials of practice [49]. Specifically, maintaining a new DR-mapping rule online during the decision formation (“Pre”-condition) increased short-term memory load [49,50], which may have interfered with the integration process. This difference in task demand seemed not to affect the behavioral performance measures—neither the mean integration timescales, nor the frequency of simple motor errors (lapse rates; Table 1).

Our results have a number of implications for neurophysiological studies of perceptual decision-making. First, several studies into the neural basis of decision-making have used a manipulation analogous to our “Post-condition” to decouple decision-making from action planning [12,23,42,51–54]. Our present results indicate that these studies, in fact, probe decision dynamics analogous to those occurring in the classical tasks with fixed mapping. Second, our observation of limited integration time scales question an assumption that has been implicit in several fMRI and neurophysiological studies using interrogation protocols [16,20,21,30,50,53–55]: that observers integrate all sensory information provided, even for extended (> 1 s) stimulus durations. Our results indicate that this assumption should be verified for each experimental condition and subject. Finally, our findings shed new light on the build-up activity commonly observed during decision formation in motor structures of the human brain [21,22,23,45,56]: Albeit providing a useful neural marker of the evolving integration process, this activity seems to be a downstream consequence of the integration process rather than a direct correlate of that process. Our results are consistent with a growing body of physiological evidence [23,53,57–59] indicating that evidence integration during decision-making is distinct from action planning.

## Author Contributions

Conceived and designed the experiments: TP PJ THD. Performed the experiments: TP PJ. Analyzed the data: KT TP PJ. Contributed reagents/materials/analysis tools: PJ KT TP THD. Wrote the paper: KT TP PJ THD.

## References

1. Gold JI, Shadlen MN (2007) The neural basis of decision making. *Annu Rev Neurosci* 30:535–574. PMID: [17600525](#)
2. Smith P, Ratcliff R (2004) Psychology and neurobiology of simple decisions. *Trends in Neurosci* 27:161–168. PMID: [15036882](#)
3. Bogacz R, Brown E, Moehlis J, Holmes P, Cohen JD (2006) The physics of optimal decision making: A formal analysis of models of performance in two-alternative forced-choice tasks. *Psychol Rev* 113:700–765. PMID: [17014301](#)
4. Honey CJ, Theisen T, Donner TH, Silbert LJ, Carlson CE, Devinsky O, et al. (2012) Slow cortical dynamics and the accumulation of information over long time scales. *Neuron* 76:423–434. doi: [10.1016/j.neuron.2012.08.011](#) PMID: [23083743](#)

5. Brody CD, Romo R, Kepecs A (2003) Basic mechanisms for graded persistent activity: discrete attractors, continuous attractors, and dynamic representations. *Curr Opin Neurobiol* 13:204–11. PMID: [12744975](#)
6. Uchida N, Kepecs A, Mainen ZF (2006) Seeing at a glance, smelling in a whiff: rapid forms of perceptual decision making. *Nat Rev Neurosci* 7:485–491. PMID: [16715056](#)
7. Wang XJ (2002) Probabilistic decision making by slow reverberation in cortical circuits. *Neuron* 36:955–968. PMID: [12467598](#)
8. Ratcliff R (1978) A theory of memory retrieval. *Psychol Rev* 85:59–108.
9. Palmer J, Huk AC, Shadlen MN (2005) The effect of stimulus strength on the speed and accuracy of perceptual decisions. *J Vis* 5:376–404. PMID: [16097871](#)
10. Bogacz R, Wagenmakers EJ, Forstmann BU, Nieuwenhuis S (2010) The neural basis of speed-accuracy tradeoff. *TICS* 33: 10–16.
11. Carrasco M, McElree B (2001) Covert attention accelerates the rate of visual information processing. *Proc Natl Acad Sci U S A*. 98:5363–7 PMID: [11309485](#)
12. Gold JI, Shadlen MN (2003) The influence of behavioral context on the representation of a perceptual decision in developing oculomotor commands. *J Neurosci* 23:632–651. PMID: [12533623](#)
13. Ossmy O, Moran O, Pfeffer T, Tsetsos K, Usher M, Donner TH (2013) The timescale of perceptual evidence integration can be adapted to the environment. *Curr Biol*. 23: 981–6. doi: [10.1016/j.cub.2013.04.039](#) PMID: [23684972](#)
14. Zariwala HA, Kepecs A, Uchida N, Hirokawa J, Mainen ZF (2013) The Limits of deliberation in a perceptual decision task. *Neuron* 78:339–351. doi: [10.1016/j.neuron.2013.02.010](#) PMID: [23541901](#)
15. Rorie AE, Newsome WT (2005) A general mechanism for decision-making in the human brain? *Trends Cogn Sci*. 9:41–43. PMID: [15668095](#)
16. Heekeren HR, Marrett S, Bandettini PA, Ungerleider LG (2004) A general mechanism for perceptual decision-making in the human brain. *Nature* 431:859–862. PMID: [15483614](#)
17. Siegel M, Engel AK, Donner TH (2011) Cortical network dynamics of perceptual decision-making in the human brain. *Front Hum Neurosci* 5:21. doi: [10.3389/fnhum.2011.0021](#) PMID: [21427777](#)
18. Siegel M, Donner TH, Engel AK (2012) Spectral fingerprints of large-scale neuronal interactions. *Nat Rev Neurosci* 13:121–134. doi: [10.1038/nrn3137](#) PMID: [22233726](#)
19. Schall JD, Thompson KG (1999) Neural selection and control of visually guided eye movements. *Annu Rev Neurosci* 22:241–259. PMID: [10202539](#)
20. Horwitz GD, Newsome WT (2001) Target selection for saccadic eye movements: prelude activity in the superior colliculus during a direction discrimination task. *J Neurophysiol* 86:2543–2558. PMID: [11698541](#)
21. Donner TH, Siegel M, Fries P, Engel AK (2009) Build-up of choice-predictive activity in human motor cortex during perceptual decision-making. *Curr Biol* 19:1581–1585. doi: [10.1016/j.cub.2009.07.066](#) PMID: [19747828](#)
22. de Lange F, Dobromir Rahnev D, Donner TH, Lau H (2013) Pre-stimulus oscillatory activity over motor cortex reflects perceptual expectations. *J Neurosci*. 33:1400–1410.
23. O'Connell RG, Dockree PM, Kelly SP (2012) A supramodal accumulation-to-bound signal that determines perceptual decisions in humans. *Nat Neurosci*. 15: 1729–35. doi: [10.1038/nn.3248](#) PMID: [23103963](#)
24. Law CT, Gold JI (2008) Neural correlates of perceptual learning in a sensory-motor, but not a sensory, cortical area. *Nat Neurosci* 11:505–513. doi: [10.1038/nn2070](#) PMID: [18327253](#)
25. Connolly PM, Bennur S, Gold JI (2009) Correlates of perceptual learning in an oculomotor decision variable. *J Neurosci* 29:2136–2150. doi: [10.1523/JNEUROSCI.3962-08.2009](#) PMID: [19228966](#)
26. Watamaniuk SNJ, Sekuler R (1992) Temporal and spatial integration in dynamic random-dot stimuli. *Vision Res* 32:2341–2347. PMID: [1288010](#)
27. Burr DC, Santoro L (2001) Temporal integration of optic flow, measured by contrast and coherence thresholds. *Vision Res* 41:1891–1899. PMID: [11412882](#)
28. Kiani R, Hanks TD, Shadlen MN (2008) Bounded integration in parietal cortex underlies decisions even when viewing duration is dictated by the environment. *J Neurosci* 28:3017–3029. doi: [10.1523/JNEUROSCI.4761-07.2008](#) PMID: [18354005](#)
29. Brunton BW, Botvinick MM, Brody CD (2013) Rats and humans can optimally accumulate evidence for decision-making. *Science* 6128: 95–98. doi: [10.1126/science.1233912](#) PMID: [23559254](#)
30. Britten KH, Shadlen MN, Newsome WT, Movshon JA (1992) The analysis of visual motion: a comparison of neuronal and psychophysical performance. *J Neurosci* 12:4745–4765. PMID: [1464765](#)

31. Roitman JD, Shadlen MN (2002) Response of neurons in the lateral intraparietal area during a combined visual discrimination reaction time task. *J Neurosci* 22:9475–9489.
32. Quick RF Jr (1974) A vector-magnitude model of contrast detection. *Kybernetik* 16:65–67. PMID: [4453110](#)
33. Wichmann FA, Hill JN (2001) The psychometric function: I Fitting, sampling, and goodness of fit. *Perception & Psychophysics* 63:1314–1329.
34. Efron B, Tibshirani R (1993) *An Introduction to the Bootstrap*. New York: Chapman and Hall.
35. Wichmann FA, Hill JN (2001) The psychometric function: II Bootstrap-based confidence intervals and sampling. *Perception & Psychophysics* 63:1314–1329.
36. Nickerson DM, Douglas EF, Grossman GD (1989) Estimating physiological thresholds with continuous two-phase-regression. *Physiological Zoology* 62:866–887.
37. Usher M, McClelland JL (2001) The time course of perceptual choice: the leaky, competing accumulator model. *Psychol Rev* 108:550–592. PMID: [11488378](#)
38. Tsetsos K, Gao J, McClelland JL, Usher M (2012) Using time-varying evidence to test models of decision dynamics: bounded diffusion vs. the leaky competing accumulator model. *Front Decis Neurosci* 6:79. doi: [10.3389/fnins.2012.00079](#)
39. Bogacz R, Cohen JD (2004) Parameterization of connectionist models. *Behav Res Methods Instrum Comput* 36:732–741. PMID: [15641419](#)
40. Gao J, Tortell R, McClelland JL (2011) Dynamic Integration of Reward and Stimulus Information in Perceptual Decision-Making. *PLoS One* 6: e16749. doi: [10.1371/journal.pone.0016749](#) PMID: [21390225](#)
41. Bennur S, Gold JI (2011) Distinct representations of perceptual decisions and the associated oculomotor plan in the monkey lateral ontraparietal area. *J Neurosci* 31: 913–921. doi: [10.1523/JNEUROSCI.4417-10.2011](#) PMID: [21248116](#)
42. Freedman DJ, Assad JA (2011) A proposed common neural mechanism for categorization and perceptual decisions. *Nat Neurosci* 14: 143–146. doi: [10.1038/nn.2740](#) PMID: [21270782](#)
43. Bair W, Koch C (1996) Temporal precision of spike trains in extrastriate cortex of the behaving macaque monkey. *Neural Comput* 15:1185–1202. PMID: [8845004](#)
44. Horwitz GD, Batista AP, Newsome WT (2004) Representation of an abstract perceptual decision in macaque superior colliculus. *J Neurosci* 91:2281–2296.
45. Wyart V, de Gardelle V, Scholl J, Summerfield C (2012) Rhythmic fluctuations in evidence accumulation during decision making in the human brain. *Neuron* 76(4): 847–858 doi: [10.1016/j.neuron.2012.09.015](#) PMID: [23177968](#)
46. Luce RD (1986) *Response times: Their role in inferring elementary mental organization*. Belfast, UK: Oxford UP.
47. Marshall JAR, Bogacz R, Gilchrist ID (2012) Consistent implementation of decisions in the brain. *PLoS ONE* 7(9): e43443. doi: [10.1371/journal.pone.0043443](#) PMID: [22984425](#)
48. Tsetsos K, Usher M, McClelland JL (2011) Testing multi-alternative decision models with non-stationary evidence. *Front Decis Neurosci* 5:63. doi: [10.3389/fnins.2011.00063](#)
49. Miller EK, Cohen JD (2001) An integrative theory of prefrontal cortex function. *Ann Rev Neurosci* 14:167–202.
50. Schneider W, Shiffrin RM (1977) Controlled and automatic human information processing: I. Detection, search, and attention. *Psychol Rev* 84:1–66.
51. Rahnev D, Lau H, de Lange FP (2011) Prior Expectation modulates the interaction between sensory and prefrontal regions in the human brain. *J Neurosci* 31:10741–10748. doi: [10.1523/JNEUROSCI.1478-11.2011](#) PMID: [21775617](#)
52. Merten K, Nieder A (2012) Active encoding of decisions about stimulus absence in primate prefrontal cortex neurons. *Proc Natl Acad Sci U S A*. 109: 6289–94. doi: [10.1073/pnas.1121084109](#) PMID: [22460793](#)
53. Hebart MN, Donner TH, Haynes JD (2012) Human visual and parietal cortex encode visual choices independent of motor plans. *NeuroImage*. 63: 1392–1403.
54. Hebart MN, Schriever Y, Donner TH, Haynes JD (2014) The relationship between perceptual decision variables and confidence in the human brain. *Cereb Cortex*. pii: bhu181. [Epub ahead of print].
55. Donner TH, Siegel M, Oostenveld R, Fries P, Bauer M, Engel AK (2007) Population activity in the human dorsal pathway predicts the accuracy of visual motion Detection. *J Neurophysiol* 98, 345–359 PMID: [17493916](#)



56. Gould IC, Nobre AC, Wyart V, Rushworth MF (2012) Effects of decision variables and intraparietal stimulation on sensorimotor oscillatory activity in the human brain. *J Neurosci.* 32:13805–18. doi: [10.1523/JNEUROSCI.2200-12.2012](https://doi.org/10.1523/JNEUROSCI.2200-12.2012) PMID: [23035092](https://pubmed.ncbi.nlm.nih.gov/23035092/)
57. Liu T, Pleskac TJ (2011) Neural correlates of evidence accumulation in a perceptual decision task. *J Neurophysiol.* 106:2383–98. doi: [10.1152/jn.00413.2011](https://doi.org/10.1152/jn.00413.2011) PMID: [21849612](https://pubmed.ncbi.nlm.nih.gov/21849612/)
58. Filimon F, Philiastides MG, Nelson JD, Kloosterman NA, Heekeren HR (2013) How embodied is perceptual decision making? Evidence for separate processing of perceptual and motor decisions. *J Neurosci.* 33:2121–36. doi: [10.1523/JNEUROSCI.2334-12.2013](https://doi.org/10.1523/JNEUROSCI.2334-12.2013) PMID: [23365248](https://pubmed.ncbi.nlm.nih.gov/23365248/)
59. Hanks TD, Kopec CD, Brunton BW, Duan CA, Erlich JC, Brody CD (2015) Distinct relationships of parietal and prefrontal cortices to evidence accumulation. *Nature.* 520:220–3. doi: [10.1038/nature14066](https://doi.org/10.1038/nature14066) PMID: [25600270](https://pubmed.ncbi.nlm.nih.gov/25600270/)

## 4.2. Study 2: Adaptive Evidence Integration in Perceptual Choice

### Author contributions:

1. Conceptualization
  2. Investigation
  3. Formal analysis
  4. Writing – Original draft
  5. Writing – Review
  6. Supervision
- \* Contributed equally

Ossmy, O.:	*,1,2,3,4,5
Moran, R.:	*,3,4,5
<b>Pfeffer, T.:</b>	<b>1,3,5</b>
Tsetsos, K.:	1,5
Usher, M.:	1,4,5,6
Donner, T.H.:	1,4,5,6

**Status: Published**



# The Timescale of Perceptual Evidence Integration Can Be Adapted to the Environment

Ori Ossmy,<sup>1,7</sup> Rani Moran,<sup>1,7</sup> Thomas Pfeffer,<sup>2,3,4</sup> Konstantinos Tsetsos,<sup>5</sup> Marius Usher,<sup>1,8,\*</sup> and Tobias H. Donner<sup>2,3,6,8,\*</sup>

<sup>1</sup>School of Psychology and Sagol School of Neuroscience, Tel-Aviv University, 69978 Ramat-Aviv, Israel

<sup>2</sup>Department of Psychology, University of Amsterdam, Weesperplein 4, 1018 XA Amsterdam, the Netherlands

<sup>3</sup>Cognitive Science Center Amsterdam, University of Amsterdam, 1018 WS Amsterdam, the Netherlands

<sup>4</sup>Department of Neurophysiology and Pathophysiology, University Medical Center Hamburg- Eppendorf, 20246 Hamburg, Germany

<sup>5</sup>Department of Experimental Psychology, University of Oxford, 9 South Parks Road, Oxford OX1 3UD, UK

<sup>6</sup>Bernstein Center for Computational Neuroscience, Charité-Universitätsmedizin, Haus 6, Philippstraße 13, 10115 Berlin, Germany

## Summary

A key computation underlying perceptual decisions is the temporal integration of “evidence” in favor of different states of the world. Studies from psychology and neuroscience have shown that observers integrate multiple samples of noisy perceptual evidence over time toward a decision [1–11]. An influential model posits perfect evidence integration (i.e., without forgetting), enabling optimal decisions based on stationary evidence [2, 3, 12]. However, in real-life environments, the perceptual evidence typically changes continuously. We used a computational model to show that, under such conditions, performance can be improved by means of leaky (forgetful) integration, if the integration timescale is adapted toward the predominant signal duration. We then tested whether human observers employ such an adaptive integration process. Observers had to detect visual luminance “signals” of variable strength, duration, and onset latency, embedded within longer streams of noise. Different sessions entailed predominantly short or long signals. The rate of performance improvement as a function of signal duration indicated that observers indeed changed their integration timescale with the predominant signal duration, in accordance with the adaptive integration account. Our findings establish that leaky integration of perceptual evidence is flexible and that cognitive control mechanisms can exploit this flexibility for optimizing the decision process.

## Results

Numerous studies of perceptual decision-making in psychology and neuroscience have shown that human and animal decision-makers integrate multiple samples of noisy “evidence”

about the state of the outside world over time [1–11]. An influential model, the drift diffusion model, posits a perfect integration (i.e., without forgetting) of evidence toward a critical level, henceforth termed “decision bound.” Crossing the decision bound triggers the response and hence determines reaction time [2, 3, 12–14]. When the evidence is stationary (i.e., its mean does not vary over time), this model produces the fastest decisions for a fixed error rate [1, 2, 15]. In most real-life perceptual decisions, however, we face changing environments that yield changes in evidence over time (Figure 1A). Consider a radar operator who has to decide whether the trace displayed on the monitor corresponds to a missile, a passenger plane, or just “noise”: the operator has to search for a weak signal that emerges from a continuous stream of noise, at an unknown time, and needs to respond to it as soon as she detects the signal. Henceforth, we will refer to this situation as signal detection under nonstationary evidence and temporal uncertainty.

Here, we used a computational model of the decision process to show that, in this situation, perfect integration is sub-optimal, because it results in an excessive level of “false alarms” due to integration of presignal noise. Instead, we show that leaky (i.e., forgetful) integration, which limits the integration of presignal noise, is more suitable, provided that the decision-maker can adapt the integration time constant to the typical signal duration (e.g., the typical duration of the signal emitted by a missile). We simulated a leaky integrator model that detected signals of varying duration in protracted streams of noise using different integration time constants (Figure 1B; see also Figure S1 and Supplemental Experimental Procedures). The time constant corresponded to the time it took the integrator’s response to a sudden signal increase (step function) to reach  $1 - (1/e)$  of its final, asymptotic value. The model’s detection threshold (the inverse of sensitivity, not to be confused with the decision bound shown in Figure S1) decreased as a function of signal duration in an approximately linear fashion in log-log coordinates [16]. This linear decrease of the logarithm of the threshold (i.e., the increase of sensitivity) with the logarithm of signal duration is a hallmark of temporal integration of sensory evidence [1, 4, 17, 18]. Its slope provides an index of the integration time constant (Figure S1C). For large time constants (approaching perfect integration), the slope was close to  $-1$ . For small time constants (leak approaching 1), the decrease was shallower, governed by “probability summation” of correct detection events, rather than temporal integration [19]. Intermediate time constants yielded slopes between about  $-0.3$  and  $-1$ , like the ones shown in Figure 1B. As expected, the long time constant was better suited than the short time constant (i.e., yielded a lower threshold) for detecting the longest signals (compare red and blue lines in Figure 1B). However, crucially, for the shortest signals, the short time constant (blue line) was advantageous over the long time constant (i.e., lower threshold than for red line). Consequently, the threshold versus duration functions produced by the two different time constants intersected.

If human observers are able to adapt to the statistics of signal durations to enhance their performance, then they should, likewise, shift their integration timescale toward the

<sup>7</sup>Co-first authors

<sup>8</sup>Co-senior authors

\*Correspondence: [marius@post.tau.ac.il](mailto:marius@post.tau.ac.il) (M.U.), [t.h.donner@uva.nl](mailto:t.h.donner@uva.nl) (T.H.D.)



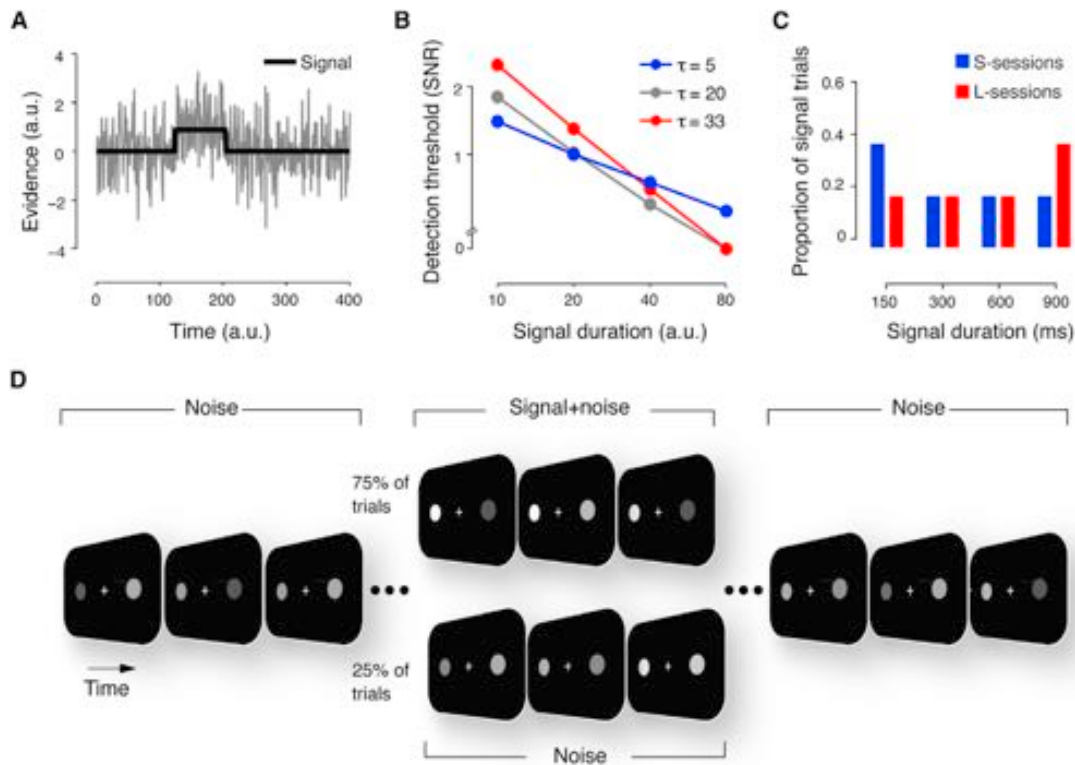


Figure 1. Model Predictions and Behavioral Detection Task

(A) Example time course of evidence for a detection decision with temporal uncertainty. A “signal” (an increment in the mean level, black line) is superimposed onto a continuous stream of random fluctuations (“noise”) at a random time, resulting in the noisy evidence (gray line). This time course describes any type of evidence that a decision-maker might integrate (e.g., the luminance of a visual stimulus or the value of a stock). (B) Detection thresholds as a function of signal duration for a leaky integrator model employing different time constants  $\tau$ . Thresholds correspond to the signal strength yielding a hit rate of 80%. The decision bound was adjusted for each  $\tau$  to maintain a fixed false alarm rate of 20%. The linear slope on log-log axes provides an estimate of  $\tau$ . See also Figures S1–S3. (C) Histograms of the signal durations on signal + noise trials during S- and L-sessions of the psychophysical detection task. Observers were informed about these contingencies at the start of each session. (D) Schematic of the time course of the stimulus during an example signal + noise trial. The two discs fluctuated in luminance around a common mean level. During the signal interval, the mean luminance level of one of the discs increased (variable onset latency, magnitude, and duration). The signal is exaggerated for illustration. In the actual experiments, signal strengths were selected to span observers’ psychophysical detection threshold.

typical signal duration. This should be evident in the rate of observers’ performance (measured in terms of hit rate and detection threshold, respectively) improvement as a function of signal duration (Figure 1B): one should find a stronger improvement when long signals predominate compared to when short signals predominate. Thus, the hit rate versus duration functions (and threshold versus duration functions, respectively) measured under different predominant signal durations should intersect.

To test this prediction, we asked 12 human observers to detect visual “signals” embedded in a longer “noise” stream (Figures 1C and 1D; Experimental Procedures). On each “signal + noise” trial, the signal was an increment in mean luminance level of one of two fluctuating discs, which occurred at different latencies within the longer noise stream and varied (across trials) in duration and intensity (Figure 1D). Critically, we systematically manipulated the typical signal duration (and, thereby, presumably the observers’ expectation of signal duration) by presenting either predominantly the shortest or the longest signal durations within each of a number of different experimental sessions (henceforth referred to as “S-” or “L-sessions,” respectively; Figure 1C). Observers were informed about the predominant signal duration at the start of each session. We hypothesized that they would

integrate the difference between the two input streams on the left and right, respectively, and respond whenever this accumulated difference surpassed one of two symmetric decision bounds (a positive and negative one for left and right, respectively). More importantly, we further hypothesized that observers would employ a longer integration timescale in the L- than in the S-sessions.

This is what we found (Figures 2 and 3). All observers performed the task with low rate of false alarms (mean across observers: 14%; range: 8%–24%) and other errors (Table S1). Across the group, there was no significant difference in false alarms between L and S sessions ( $t_{11} = 0.94$ ;  $p = 0.36$ ). Hit rates increased monotonically with signal duration, indicating temporal integration of the signal. Importantly, for the shortest signals (150 ms), hit rates were significantly higher in the S- than in the L-sessions, while the opposite was the case for the longest signals (900 ms; Figure 2). Accordingly, in signal trials, there was a highly significant interaction between the session type (L versus S) and signal duration (two-way repeated-measures ANOVA with factors signal duration and session type;  $F_{3,33} = 17.91$ ;  $p < 10^{-3}$ ). This interaction was not evident in the reaction times (RTs). Although RTs increased with signal duration (main effect of signal duration:  $F_{3,33} = 6.81$ ;  $p = 0.02$ ; effect of session type:  $F_{3,33} = 2.32$ ;

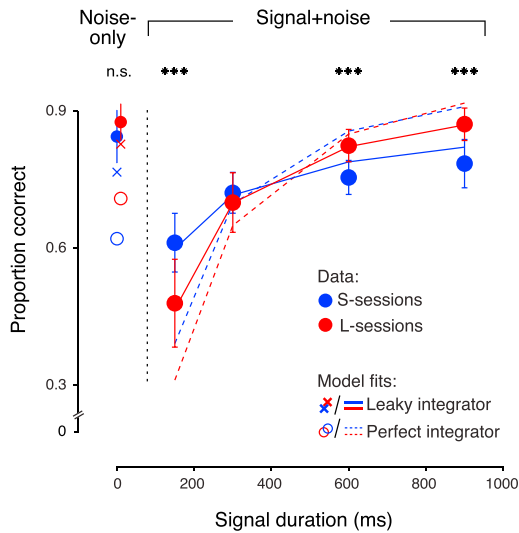


Figure 2. Interacting Effects of Expectation and Signal Duration on Hit Rate Reveal Adaptation of Integration Time Constant

The group average ( $n = 12$ ) of proportion of correct choices for the noise-only trials and signal + noise trials are shown separately for the different signal durations and for L-sessions (red) and S-sessions (blue). For noise-only trials, numbers correspond to the correct rejection rate (no response). For signal + noise trials, numbers correspond to hit rates, collapsed across the five different signal strengths. Solid lines, average prediction of best-fitting leaky integrator model; dashed lines, average prediction of best-fitting drift diffusion model; error bars represent 95% confidence intervals; \*\*\* $p < 10^{-3}$  (paired t test). See also Figure S2 and Tables S1–S3.

$p = 0.15$ ), there was no statistically significant interaction between signal duration and session type ( $F_{3,33} = 0.9$ ;  $p = 0.45$ ). Therefore, we focused our subsequent analyses on the accuracy data.

The behavioral results in Figure 2 indicate that observers indeed changed their integration time constant, depending on which signal duration predominated in a given session. We used two complementary approaches to quantify this effect and link it to our theoretical predictions. First, we compared alternative computational models of the decision process in their ability to account for the observers' behavioral data (i.e., the false alarm rates, and the hit rates as a function of signal strength and duration; Figures 2 and S2; Tables S2 and S3). One class of models incorporated our theoretical predictions: a leaky integrator, the timescale of which was free to vary with the session type (see Supplemental Experimental Procedures). This model provided a reasonable account of the psychophysical data (solid lines in Figure 2; see Figure S2A and Table S2 for individual observers). The integration time constants estimated by this model were consistently longer for L- than for S-sessions (group average: S: 80 ms; L: 490 ms; Wilcoxon signed-rank test:  $10^{-3}$ ).

The variant of the leaky integrator model shown in Figure 3 had different parameters for the internal “noise” in both session types and for an exponent describing the nonlinear relationship between physical signal intensity and neuronal input to the integrator at the decision stage. A simpler variant of this model, without these additional parameters, provided qualitatively identical results (Figure S2B).

We also fitted a perfect integrator (drift diffusion) model to the behavioral data (Supplemental Experimental Procedures). As expected, this model (dashed lines in Figure 2) consistently

provided a worse performance level (low correct rejection rates for noise-only trials) and a worse account of the data (underestimation of hit rate at short signals and overestimation of hit rate at long signals) than the leaky integrator model with variable time constant (see Figure S2A and Table S3 for individual observers). Quantitative model comparison was consistently in favor of the leaky integrator model (Table 1). The difference in the Bayesian information criterion (BIC, which takes into account both the goodness of fit and the number of model parameters) values, ranged between 82 and 766 across observers, providing strong support for the leaky integrator. In sum, fitting alternative models of the decision process strengthens the case for leaky integration with adaptive timescale.

In the second, model-independent approach, we estimated observers' psychophysical detection thresholds for all signal durations (see Figure 3A for an example observer; Supplemental Experimental Procedures). For all observers individually (Figure S3A), as well as for the group (Figure 3B), the thresholds were approximately linear in duration (in log-log coordinates). Just as for the model in Figure 1, the slopes of observers' empirical threshold versus duration functions depended on the expected signal duration (Figures 3B and 3C and Figure S3A). Slopes were significantly larger (i.e., more negative) in the L- than S-sessions in nine of the 12 individual observers ( $p < 0.05$ ; one-sided permutation test). Further, the difference in slopes was highly significant when tested for the group (Wilcoxon signed-rank test;  $p < 10^{-3}$ ; Figure 3C). We obtained qualitatively similar results when using an alternative, more constrained, approach for estimating the slopes of the threshold versus duration functions (see Supplemental Experimental Procedures and Figures S3B–S3D). Taken together, our results provide strong and complementary support for our hypothesis that observers changed their integration timescale with the predominant signal duration, in line with a decision process employing an adaptive timescale.

## Discussion

The temporal integration of pieces of evidence supporting different choice options is a fundamental computational process underlying all decisions. This process operates during perceptual decisions like the one studied here [1–11], as well as during valued-based, economic decisions (e.g., a stock-buyer choosing stock options by integrating their fluctuating values) [14, 17, 20]. Here, we show that under conditions of nonstationary evidence with temporal uncertainty, perfect evidence integration is suboptimal and is not the computation employed by human decision-makers. To this end, we used an experimental protocol, which, albeit still far from real-life decisions, extends the standard laboratory tasks used for probing evidence integration in an important way. Our results demonstrate that human observers can boost their decision performance by flexibly changing the timescale of a leaky integration process according to changes in the expected signal duration.

Our estimates of integration timescales showed a consistent separation between long and short expected signals. But these timescales also varied substantially across observers and tended to be shorter than the actual duration of the typical signal, especially during the S-sessions. One possible explanation for the latter is that, in the S-sessions, some observers may have based their decision, in addition to the integrated signal, on transient responses at signal on- and offsets (see

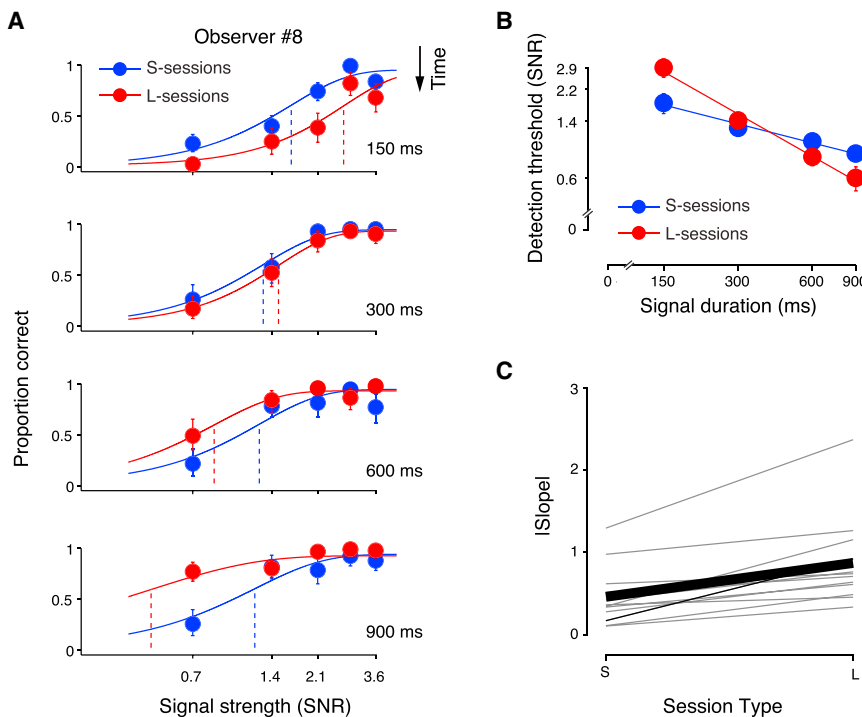


Figure 3. Change of Psychophysical Thresholds with Signal Duration Reveals Adaptation of Integration Time Constant

(A) Psychometric functions of one example observer, separately for the four signal durations and two session types. Psychophysical detection thresholds (expressed in units of signal-to-noise ratio; SNR) decreased with duration but more strongly in L- than in S-sessions. Solid lines, best-fitting cumulative Weibull functions. Vertical dashed lines indicate location of threshold parameter on the x axis. Error bars represent 95% bootstrap confidence intervals. (B) Group average thresholds, plotted on log-log scales as a function of signal duration. Error bars represent SEM. (C) Individual (thin lines) and group average (thick black line), best-fitting regression slopes for S- versus L-sessions. The absolute value of the slopes is shown (all fitted individual slopes were negative; see Figure S3A). The thin black line corresponds to the observer shown in (A). See also Figure S3.

legend of Figure S2A for details). In general, a substantial fraction of the interindividual variability in the performance of our 12 observers may reflect differences between strategies (or integration capacities) among individuals. Future studies should examine more complex models of the decision process to capture such individual differences.

Our results have a number of implications for understanding the mechanisms of decision-making. First, they provide strong support for models of perceptual choice that are based on leaky, rather than perfect, integration of perceptual evidence. The notion of leaky integration is inspired by fundamental principles of neural computation [4, 18], and it is consistent with neurophysiological data suggesting a reservoir of time constants in the cerebral cortex [21, 22]. Leaky integration is also consistent with a common finding in psychophysical experiments, which manipulated the stimulus duration and hence available decision time, showing that observers integrate sensory evidence only across limited periods of time ([8, 10, 11, 23, 24], but see [8] for an alternative interpretation involving perfect integration). While information leak has so far been regarded as a limitation in perceptual decision-making, our results reveal that it is, in fact, advantageous for real-life decisions: the integration timescale provides a critical degree of freedom for adapting the decision process to the environmental contingencies. Similar conclusions have been reached for the temporal integration of reward (across trials) in a dynamic foraging task, in which monkeys used a time constant that was closely matched to the statistics of the environment [25]. However, in this study, the optimal timescale was not systematically manipulated.

Our results also shed new light on the question of how “top-down” cognitive control mechanisms shape decision computations [26]. Since the emergence of signal detection theory in perceptual psychophysics [16], perceptual decision-making has been viewed as a two-component process: (1) the encoding and integration of sensory evidence and (2) the criterion

level (decision bound), against which the integrated evidence is compared to reach a decision. In this view, decision-makers exert control over the decision process only by adapting the decision bound [1–3, 27, 28], while the evidence integration operates automatically. By contrast, our results reveal that adaptive control mechanisms can directly shape the evidence integration computation.

Further, the results imply that the brain is remarkably flexible in selecting an integration timescale suitable for the environmental context at hand. Timescales of several hundreds of milliseconds, like the ones observed here, are probably an emergent property of dynamic network interactions rather than a fixed property of individual neurons [4, 18, 24]. Physiological evidence suggests that such network interactions during decision-making span multiple regions that are widely distributed across the brain [29–31]. The adaptive changes in integration timescales found in the present study may, therefore, reflect the flexible adjustment of such large-scale decision networks, which might be achieved by neuromodulation [32–34].

Finally, our study sets the stage for future neurophysiological studies of the biophysical circuit mechanisms underlying perceptual evidence integration. Such studies could exploit our experimental protocol to experimentally manipulate integration timescale, while characterizing neurophysiological signatures of the evidence integration mechanism [22, 29].

#### Experimental Procedures

Below, we describe the psychophysical experiments and provide a brief summary of the psychometric fitting procedures. All data analysis and modeling procedures are described in detail in the [Supplemental Experimental Procedures](#).

#### Observers

Twelve healthy observers (eight females, age range: 20–37 years, normal or corrected-to-normal vision) participated in this study after informed consent. The observers were psychology students at TAU, who were naive to the purpose of the study, did the experiment for credit, and were, in addition, paid for their participation in proportion to task performance (20–40 NIS per hr). The study was approved by the local ethics committee.



Table 1. Comparison between Leaky and Perfect Integrator Models

Observer	Perfect Integrator	Leaky Integrator	Leaky Better?
1	468.06	298.32	TRUE
2	596.55	263.14	TRUE
3	527.07	300.60	TRUE
4	505.74	278.92	TRUE
5	436.49	244.50	TRUE
6	483.94	313.87	TRUE
7	1,144.75	379.02	TRUE
8	737.00	358.21	TRUE
9	1,016.56	494.46	TRUE
10	346.15	263.81	TRUE
11	470.75	332.18	TRUE
12	624.11	445.98	TRUE

Values correspond to Bayesian information criterion (BIC). BIC differences perfect integrator – leaky integrator of >6 are considered strong support for the leaky integrator model.

### Stimuli

Stimuli were presented on a linearized CRT screen (frame rate: 100 Hz). On each trial, two discs were presented in the right and left visual hemifields on a black background, for a total duration of 5 s (Figure 1C). Discs were presented at an eccentricity of 5° and subtended about 2.85° of visual angle. We controlled the level of (external) noise entering the decision process by randomly and independently changing each disc's luminance level at each monitor refresh (10 ms). These random luminance fluctuations were drawn from a truncated Gaussian noise (SD after truncation = 0.11), and they were added to each disc's mean luminance level. The truncation was used to prevent the luminance variable to exceed the (0,1) boundaries (see below). Throughout each trial, the mean luminance level had one of two values. Twenty-five percent of the trials ("noise-only" trials) contained only fluctuations around the same baseline level (0.40, on a 0–1 scale). This was constructed by using RGB values with equal components. In the remaining 75% ("signal + noise" trials), both discs fluctuated around the same baseline level for most of the trial, and a luminance increment was added to the baseline level of one of the discs at various different latencies within the noise stream (uniform distribution of signal onsets; range: 0.6–3.5 s). This increment was the signal that observers had to detect. The signal's location (left or right), strength (0.08, 0.16, 0.24, 0.32, or 0.40), and duration (150, 300, 600, or 900 ms) were randomly selected on each signal + noise trial.

### Procedure

Observers' task was to maintain fixation throughout the whole trial and to respond whenever they judged that one of the discs had increased in brightness (the signal; Figure 1D). They had to indicate the location of the signal by pressing a left or a right button within a predetermined response window (from signal onset to 600 ms after signal offset). Responses to signals were classified as correct ("hits") if they were made within the response window and with the correct button. There were four possible types of errors: "false alarms" (response on noise-only trials or before the response window on signal + noise trials), "slow responses" (response on signal + noise trials after the response window), "misses" (no response whatsoever on signal + noise trials), or "mislocalization" (response on signal + noise trials within response window but with incorrect button). At the end of "mislocalization" trials, a sound feedback was provided. At the end of the other error trials, a text on the screen informed observers about the type of error. After the completion of each trial, observers pressed a key to continue to the next trial. In the absence of any key press, the next trial started automatically after 2.5 s. Every 100 trials, observers were allowed to pause.

After a short practice session, each observer performed several experimental sessions of 500 trials each (duration: ~1 hr). All sessions consisted of 125 noise-only trials and 375 signal + noise trials. To manipulate the observers' expectation of signal duration, we introduced a predominance of a factor of two (rate of occurrence: 0.4 versus 0.2) of either the longest or the shortest signal duration over the other three durations (Figure 1C). In one type of session ("S-sessions"), there were 150 trials (5 signal strengths × 30 trials) of the shortest duration (150 ms). In the other type of session ("S-sessions"), there were 150 trials of the longest duration (900 ms). In all sessions, there were 75 trials (5 signal strengths × 15 trials) of the remaining three durations (see Supplemental Experimental Procedures for rationale behind these distributions of signal durations.)

The two types (S/L) were alternated from session to session, with the order counterbalanced across observers. Observers received an explicit instruction about each session's type before the start of testing. Nine observers performed four sessions. Three observers performed six sessions.

### Data Analysis and Model Fits

We computed observers' psychophysical detection performance as the percentage of hits on signal + noise trials, separately for each signal duration and intensity, and as the percentage of no responses ("correct rejections") on noise-only trials (Figure 2). We fitted two different classes of computational models of the decision process (leaky integrator and drift diffusion) to the complete performance data of each individual observer (including noise-only trials). To estimate observers' detection thresholds, we fitted a cumulative Weibull function to the hit rates as a function of signal strength and extracted the threshold parameter of the best fits (Figure 3). See Supplemental Experimental Procedures for details of the data analysis and model fitting procedures.

### Supplemental Information

Supplemental Information includes Supplemental Experimental Procedures, three figures, and three tables and can be found with this article online at <http://dx.doi.org/10.1016/j.cub.2013.04.039>.

### Acknowledgments

We thank Michael Herrmann for helpful discussions on the computational model. M.U. is funded by the Israeli Science Foundation (grant: 743/12) and by the German Israeli Foundation (grant, 1130-158.4/2010).

Received: November 22, 2012

Revised: April 11, 2013

Accepted: April 15, 2013

Published: May 16, 2013

### References

- Bogacz, R., Brown, E., Moehlis, J., Holmes, P., and Cohen, J.D. (2006). The physics of optimal decision making: a formal analysis of models of performance in two-alternative forced-choice tasks. *Psychol. Rev.* 113, 700–765.
- Gold, J.I., and Shadlen, M.N. (2007). The neural basis of decision making. *Annu. Rev. Neurosci.* 30, 535–574.
- Smith, P.L., and Ratcliff, R. (2004). Psychology and neurobiology of simple decisions. *Trends Neurosci.* 27, 161–168.
- Usher, M., and McClelland, J.L. (2001). The time course of perceptual choice: the leaky, competing accumulator model. *Psychol. Rev.* 108, 550–592.
- de Lange, F.P., Jensen, O., and Dehaene, S. (2010). Accumulation of evidence during sequential decision making: the importance of top-down factors. *J. Neurosci.* 30, 731–738.
- Donner, T.H., Siegel, M., Fries, P., and Engel, A.K. (2009). Buildup of choice-predictive activity in human motor cortex during perceptual decision making. *Curr. Biol.* 19, 1581–1585.
- Gold, J.I., and Shadlen, M.N. (2000). Representation of a perceptual decision in developing oculomotor commands. *Nature* 404, 390–394.
- Kiani, R., Hanks, T.D., and Shadlen, M.N. (2008). Bounded integration in parietal cortex underlies decisions even when viewing duration is dictated by the environment. *J. Neurosci.* 28, 3017–3029.
- van Ravenzwaaij, D., van der Maas, H.L., and Wagenmakers, E.J. (2012). Optimal decision making in neural inhibition models. *Psychol. Rev.* 119, 201–215.
- Tsetsos, K., Gao, J., McClelland, J.L., and Usher, M. (2012). Using time-varying evidence to test models of decision dynamics: bounded diffusion vs. the leaky competing accumulator model. *Front Neurosci.* 6, 79.
- Gao, J., Tortell, R., and McClelland, J.L. (2011). Dynamic integration of reward and stimulus information in perceptual decision-making. *PLoS ONE* 6, e16749.
- Ratcliff, R., and McKoon, G. (2008). The diffusion decision model: theory and data for two-choice decision tasks. *Neural Comput.* 20, 873–922.
- Roitman, J.D., and Shadlen, M.N. (2002). Response of neurons in the lateral intraparietal area during a combined visual discrimination reaction time task. *J. Neurosci.* 22, 9475–9489.

14. Krajbich, I., and Rangel, A. (2011). Multialternative drift-diffusion model predicts the relationship between visual fixations and choice in value-based decisions. *Proc. Natl. Acad. Sci. USA* *108*, 13852–13857.
15. Wald, A., and Wolfowitz, J. (1948). Optimum characteristic of sequential probability ratio test. *Ann. Math. Stat.* *19*, 326–339.
16. Green, D.M., and Swets, J.A. (1966). *Signal Detection Theory and Psychophysics* (New York: Wiley).
17. Busemeyer, J.R., and Townsend, J.T. (1993). Decision field theory: a dynamic-cognitive approach to decision making in an uncertain environment. *Psychol. Rev.* *100*, 432–459.
18. Wang, X.J. (2002). Probabilistic decision making by slow reverberation in cortical circuits. *Neuron* *36*, 955–968.
19. Watson, A.B. (1979). Probability summation over time. *Vision Res.* *19*, 515–522.
20. Tsetsos, K., Chater, N., and Usher, M. (2012). Saliency driven value integration explains decision biases and preference reversal. *Proc. Natl. Acad. Sci. USA* *109*, 9659–9664.
21. Bernacchia, A., Seo, H., Lee, D., and Wang, X.J. (2011). A reservoir of time constants for memory traces in cortical neurons. *Nat. Neurosci.* *14*, 366–372.
22. Honey, C.J., Thesen, T., Donner, T.H., Silbert, L.J., Carlson, C.E., Devinsky, O., Doyle, W.K., Rubin, N., Heeger, D.J., and Hasson, U. (2012). Slow cortical dynamics and the accumulation of information over long timescales. *Neuron* *76*, 423–434.
23. Burr, D.C., and Santoro, L. (2001). Temporal integration of optic flow, measured by contrast and coherence thresholds. *Vision Res.* *41*, 1891–1899.
24. Uchida, N., Kepecs, A., and Mainen, Z.F. (2006). Seeing at a glance, smelling in a whiff: rapid forms of perceptual decision making. *Nat. Rev. Neurosci.* *7*, 485–491.
25. Sugrue, L.P., Corrado, G.S., and Newsome, W.T. (2004). Matching behavior and the representation of value in the parietal cortex. *Science* *304*, 1782–1787.
26. Miller, E.K., and Cohen, J.D. (2001). An integrative theory of prefrontal cortex function. *Annu. Rev. Neurosci.* *24*, 167–202.
27. Botvinick, M.M., Braver, T.S., Barch, D.M., Carter, C.S., and Cohen, J.D. (2001). Conflict monitoring and cognitive control. *Psychol. Rev.* *108*, 624–652.
28. Lo, C.C., and Wang, X.J. (2006). Cortico-basal ganglia circuit mechanism for a decision threshold in reaction time tasks. *Nat. Neurosci.* *9*, 956–963.
29. Donner, T.H., Siegel, M., Oostenveld, R., Fries, P., Bauer, M., and Engel, A.K. (2007). Population activity in the human dorsal pathway predicts the accuracy of visual motion detection. *J. Neurophysiol.* *98*, 345–359.
30. Pesaran, B., Nelson, M.J., and Andersen, R.A. (2008). Free choice activates a decision circuit between frontal and parietal cortex. *Nature* *453*, 406–409.
31. Siegel, M., Donner, T.H., and Engel, A.K. (2012). Spectral fingerprints of large-scale neuronal interactions. *Nat. Rev. Neurosci.* *13*, 121–134.
32. Aston-Jones, G., and Cohen, J.D. (2005). An integrative theory of locus coeruleus-norepinephrine function: adaptive gain and optimal performance. *Annu. Rev. Neurosci.* *28*, 403–450.
33. Eckhoff, P., Wong-Lin, K.F., and Holmes, P. (2009). Optimality and robustness of a biophysical decision-making model under norepinephrine modulation. *J. Neurosci.* *29*, 4301–4311.
34. Usher, M., and Davelaar, E.J. (2002). Neuromodulation of decision and response selection. *Neural Netw.* *15*, 635–645.

### 4.3. Study 3: Neuromodulation and Cortical Excitation-Inhibition Balance

#### Author contributions:

1. Conceptualization
  2. Investigation
  3. Formal analysis
  4. Writing – Original draft
  5. Writing – Review
  6. Supervision
- \* Contributed equally

<b>Pfeffer, T.:</b>	<b>1,3,5</b>
Armivea, A.E.:	3,5
Nolte, G.:	5,6
Engel, A.K.:	5
Linkenkaer-Hansen, K.:	5,6
Donner, T.H.:	1,4,5,6

**Status: In preparation**

1 **Catecholaminergic Shaping of Fluctuations of Human**  
2 **Cortical Activity Is Indicative of Changes in Excitation-**  
3 **Inhibition Ratio**

4

5 Thomas Pfeffer (1), Arthur-Emil Armivea (2), Guido Nolte (1), Andreas K. Engel (1),  
6 Klaus Linkenkaer-Hansen (2), Tobias H. Donner (1,3,4)

7

8 1 Department of Neurophysiology and Pathophysiology, University Medical Center Hamburg,  
9 Germany

10 2 Center for Neurogenomics and Cognitive Research, Neuroscience Campus Amsterdam,  
11 Free University Amsterdam, The Netherlands

12 3 Department of Psychology, University of Amsterdam, The Netherlands

13 4 Amsterdam Brain and Cognition, University of Amsterdam, The Netherlands

14

15 Address for correspondence:

16 Thomas Pfeffer

17 thms.pffr@gmail.com

18 Tobias H. Donner

19 t.donner@uke.de

20 Dept. of Neurophysiology and Pathophysiology

21 University Medical Center Hamburg-Eppendorf

22 Martinistr. 52, 20246 Hamburg

23

24



25 **Abbreviated title:** Neuromodulation and Cortical Excitation-Inhibition Balance

26

27 **Author contributions:**

28 Conceptualization, T.P. and T.H.D.; Investigation, T.P.; Formal analysis T.P.; Model

29 simulations: A.-E.; Writing - Original draft, T.P., T.H.D.; Writing – Review & Editing, T.P., A-

30 E.A., G.N., A.K.E., K.L-H. and T.H.D. - Funding Acquisition, K.L-H., A.K.E. and T.H.D.;

31 Supervision, G.N., K.L-H. and T.H.D.

32

33

34

35 **Introduction**

36 Cortical activity fluctuates continuously, even in the absence of changes in sensory input or  
37 motor output (Faisal et al., 2008). These intrinsic fluctuations in cortical activity are evident  
38 from the level of single neurons to large-scale networks of distant cortical areas (Shadlen  
39 and Newsome, 1998; Fox et al., 2005; Deco et al., 2011). Fluctuations in cortical mass  
40 activity exhibit temporal structure characteristic of so-called “scale-free” behavior: “1/f-like”  
41 power spectra (Miller et al., 2009; He et al., 2010) and long-range temporal autocorrelations  
42 (Linkenkaer-Hansen et al., 2001; He, 2011; Palva et al., 2013; Zhigalov et al., 2015). This  
43 characteristic temporal structure of cortical activity fluctuations varies widely across people,  
44 partly explained by genetics (Linkenkaer-Hansen et al., 2007) and exhibits marked changes  
45 in brain disorders, such as depression or Alzheimer’s disease (Linkenkaer-Hansen et al.,  
46 2005; Montez et al., 2009).

47         The large variability of cortical neurons is not only due to the biophysics of individual  
48 cells (Faisal et al., 2008), but also due to the balance between excitatory and inhibitory  
49 inputs to each (van Vreeswijk and Sompolinsky, 1996; Shadlen and Newsome, 1998) – a  
50 key determinant of the computational properties of cortical circuits (Murphy and Miller, 2003;  
51 Polack et al., 2013; Martins and Froemke, 2015), and the behavior of the organism (Wang,  
52 2008; Eckhoff et al., 2009). The balance between excitatory and inhibitory interactions  
53 seems also essential for the characteristic temporal structure of spontaneous cortical  
54 activity: Variations of the degree of excitatory and inhibitory connectivity change the long-  
55 range temporal correlation structure of activity in a cortical circuit model (Poil et al., 2012).  
56 Such differences in cortical microcircuitry might account for the large differences in the  
57 temporal structure of activity fluctuations between people, and between the healthy and  
58 diseased brain.

59         However, there is an important factor other than the fixed structural circuitry, which  
60 might also shape cortical excitation-inhibition balance and thus variability: dynamic

61 neuromodulatory state (Marder, 2012). Modulatory systems of the brainstem regulate  
62 cortical state through widespread ascending projections (Aston-Jones and Cohen, 2005;  
63 Berridge, 2008; Harris and Thiele, 2011; Lee and Dan, 2012; Froemke, 2015). The  
64 neurotransmitters released from these projections, such as noradrenaline or acetylcholine,  
65 modulate specific elements of cortical microcircuits (Polack et al., 2013; Fu et al., 2014) and  
66 alter the variability of cortical neurons (Polack et al., 2013; Eggermann et al., 2014; Chen et  
67 al., 2015). Thus, neuromodulators might dynamically “tune” the net ratio between cortical  
68 excitation and inhibition within an individual, and variations in neuromodulatory tone between  
69 people, in addition to variations in structure, might account for individual differences. The net  
70 effects of neuromodulatory systems on cortical excitation-inhibition balance, and on the  
71 temporal structure of activity fluctuations, have so far remained unknown. Unraveling these  
72 effects across cortex is critical for bridging between the modulations of specific microcircuit  
73 elements on the one hand and the gross effects of neuromodulatory state on cognition and  
74 behavior on the other hand (Aston-Jones and Cohen, 2005; Sara, 2009; Harris and Thiele,  
75 2011).

76         Here, we investigated if, how, and where, catecholaminergic and cholinergic  
77 modulation shape the temporal structure of intrinsic activity fluctuations in human cortex. We  
78 hypothesized that neuromodulatory effects that modulate net cortical excitation-inhibition  
79 balance should also alter the temporal correlation structure of intrinsic activity fluctuations.  
80 We solidified this prediction through simulations of a simplified cortical circuit model under  
81 modulation of excitatory or inhibitory synapses. We then tested this prediction by combining  
82 pharmacological intervention and magnetoencephalographic (MEG) recordings of human  
83 cortical steady-state activity during two conditions: “rest” and continuous, strong visual input  
84 combined with a simple task. Comparing the changes in temporal correlations induced by  
85 pharmacological treatments with those induced by external drive, enabled us to infer the

86 alterations in net cortical excitation-inhibition balance induced by catecholaminergic  
87 neuromodulation.

88

## 89 **Methods**

### 90 **Pharmacological MEG experiment**

#### 91 *Subjects*

92 30 healthy human participants (16 females, age range 20-36, mean 26.7) participated in the  
93 study after informed consent. The study was approved by the Ethical Committee responsible  
94 for the University Medical Center Hamburg-Eppendorf. One participant was excluded from  
95 subsequent analysis due to excessive extra-cranial artifacts in the MEG recording. Another  
96 participant only completed 2 out of 3 recording sessions and was also excluded, resulting in  
97 a total of 28 participants (15 females).

98

#### 99 *General design*

100 We pharmacologically manipulated the levels of catecholamines (noradrenaline and  
101 dopamine) and acetylcholine in a double-blind, randomized, placebo-controlled, and cross-  
102 over experimental design (Fig. 1A, B). Each participant completed three experimental  
103 sessions, consisting of drug (or placebo) intake at two time points, a waiting period of 3  
104 hours, and an MEG recording of about 1.5 hours. During MEG, participants were seated on  
105 a chair inside a magnetically shielded MEG chamber. All instructions and stimuli were  
106 projected onto a screen (distance: 60 cm) inside the chamber. Each session consisted of 6  
107 runs of 10 minutes each.

108

#### 109 *Pharmacological intervention*

110 We used the selective noradrenaline reuptake inhibitor atomoxetine (dose: 40 mg) to boost  
111 the levels of catecholamines noradrenaline and (at least in prefrontal cortex) dopamine

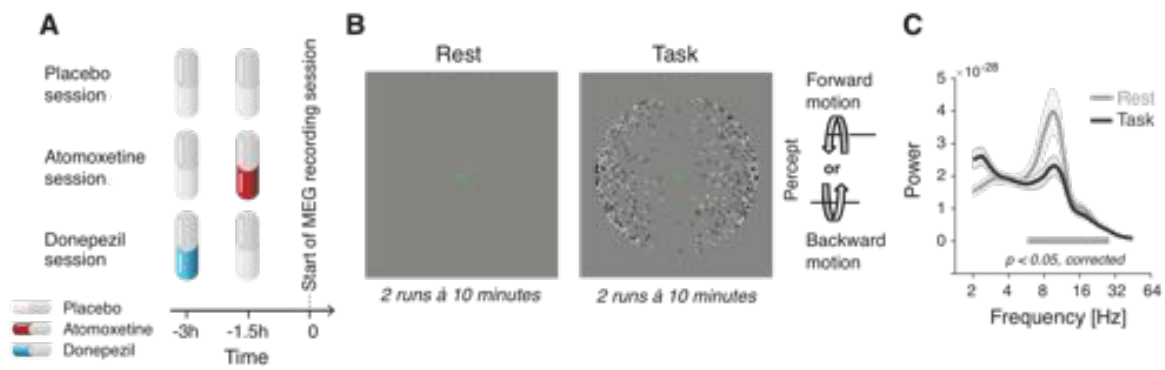


**Figure 1.** Experimental design. **(A, B)** Types and time course of experimental sessions. **(A)** Each subject participated in three sessions, involving administration of placebo, atomoxetine, or donepezil (session order randomized across subjects). Each session entailed the administration of two pills, in the order depicted for the different session types. **(B)** Within each session, subjects alternated between two steady-state conditions, Rest and Task, during MEG (runs of 10 min each). See Materials and Methods for details. **(C)** Group average power spectrum, averaged across all MEG sensors, for Rest and Task (Placebo condition only).

112 (Robbins and Arnsten, 2009). We used the cholinesterase inhibitor donepezil (dose: 5 mg)  
 113 to boost acetylcholine levels. A mannitol-aerosil mixture was administered as placebo. All  
 114 substances were encapsulated identically in order to render them visually indistinguishable.  
 115 Peak plasma concentration are reached after ~3-4 hours after administration for donepezil  
 116 (Tiseo et al., 1998) and 1-2 hours for atomoxetine (Sauer et al., 2005). We adopted the  
 117 following procedure to account for the different pharmacokinetics (Fig. 1A): participants  
 118 received two pills in each session, one 3 h and another 1.5 h before the start of MEG  
 119 recording. In the Atomoxetine condition, they first received a placebo pill (t = -3 h) followed  
 120 by the atomoxetine pill (t = -1.5 h). In the Donepezil condition, they first received the  
 121 donepezil pill (t = -3 h), followed by placebo (t = -1.5 h). In the Placebo condition, they  
 122 received placebo at both time points. The half-life is ~ 5 h for atomoxetine (Sauer et al.,  
 123 2005) and ~ 82 h for donepezil, respectively (Tiseo et al., 1998). The three recording  
 124 sessions were scheduled at least 2 weeks apart in order to allow plasma concentration

125 levels to return to baseline. This design ensured maximum efficacy of both pharmacological  
126 manipulations, while effectively blinding participants as well as experimenters.

127

128 *Stimulus and task conditions*

129 In each session, participants alternated between three different stimulus and task conditions  
130 (2 runs à 10 minutes per condition).

131 *Rest condition.* During the Rest condition, participants' task was to fixate a green  
132 fixation dot (radius =  $0.45^\circ$  visual angle) presented in the center of an otherwise grey screen.

133 *Task-counting condition.* During the Task-counting condition, subjects viewed a  
134 seemingly rotating sphere giving rise to the kinetic depth effect (Wallach and O'connell,  
135 1953; Sperling et al., 1990), spontaneous changes in the perceived rotation direction (Fig.  
136 1B). The stimulus subtended  $21^\circ$  of visual angle. It consisted of 1000 dots (500 black and  
137 500 white dots, radius:  $0.18^\circ$  of visual angle) arranged on a circular aperture presented on a  
138 mean-luminance gray background, with the green fixation dot in the center. The speed of  
139 rotation of the sphere was 2.6 °/s or 3.3 °/s, in different sessions (same speed for 24 out of  
140 28 subjects). In order to minimize tracking eye movements, the sphere rotation was either  
141 "forward" (towards the observer) or "backward" (away from the observer), and the dot  
142 density decreased along the horizontal axis towards the center of the stimulus. Participants  
143 were instructed to count the number of perceived changes in rotation direction and report the  
144 total number of perceived transitions at the end of the run. Taken together, just like the Rest  
145 condition, the Task condition minimized any external (sensory or motor) transients, but it  
146 produced well-constrained endogenous transients associated with the spontaneous  
147 perceptual changes.

148 *Task-pressing condition.* This condition was identical to Task-counting, except that  
149 participants were instructed to press and hold one of two buttons with their index finger to  
150 indicate the currently perceived rotation direction of the sphere.

151 Here, we only analyzed the Rest and Task-counting conditions. For simplicity, the  
152 latter will be referred to as Task condition in the following.

153

#### 154 **Data acquisition**

155 MEG was recorded using a whole-head CTF 275 MEG system (CTF Systems, Inc.,  
156 Canada) at a sampling rate of 1200 Hz. In addition, eye movements and pupil dilation were  
157 recorded with an MEG-compatible EyeLink 1000 Long Range Mount system (SR Research,  
158 Osgoode, ON, Canada) and electrocardiogram (ECG) was acquired using two Ag/AgCl  
159 electrodes.

160

#### 161 **Data analysis**

##### 162 *Preprocessing*

163 *Eye data.* Eye blinks were detected using the manufacturer's standard algorithm with default  
164 settings.

165

166 *MEG data.* First, all data were cleaned of strong transient muscle artifacts and squid jumps  
167 through visual inspection and manual as well as semi-automatic artifact rejection procedures,  
168 as implemented in the FieldTrip toolbox for MATLAB (Oostenveld et al., 2011). To this end,  
169 data segments contaminated by such artifacts ( $\pm 500$  ms) were discarded from the data  
170 (across all channels). Subsequently, data were downsampled to 400 Hz the data were split  
171 into low (2-40 Hz) and high ( $\geq 40$  Hz) frequency components, using a 4th order (low- or  
172 high-pass) Butterworth filter. Both signal components were separately submitted to  
173 independent component analysis (Bell and Sejnowski, 1995) using the FastICA algorithm  
174 (Hyvärinen, 1999). Artifactual components (eye blinks/movements, sustained muscle  
175 artifacts, heartbeat and other extra-cranial artifacts) were identified based on three criteria as  
176 described in detail in (Hipp and Siegel, 2013): power spectrum, fluctuation in signal variance

177 over time (in bins of 1s length), and topography. Artifactual components were reconstructed  
178 and subtracted from the raw signal and low- and high frequencies were combined into a  
179 single data set. On average, 20 (+/- 14) artifactual components were identified for the low-  
180 frequencies and 13 (+/- 7) artifactual components were identified for the high frequencies.

181

### 182 *Spectral analysis and motivation of frequency bands of interest*

183 Sensor-level spectral estimates (power spectra and cross spectral density matrices) were  
184 computed by means of the multi taper method using a sequence of discrete prolate Slepian  
185 tapers (Mitra and Pesaran, 1999). For the power spectrum shown in Fig. 1C, power spectra  
186 were computed using a window length of 5s and a frequency smoothing of 2 Hz, yielding 19  
187 orthogonal tapers. For all remaining analyses, spectral estimates were computed for the  
188 following, coarsely defined frequency bands: 2-8 Hz ('delta/theta'), 8-12 Hz ('alpha') and 12-  
189 45 Hz ('beta/gamma').

190 The focus of this paper was on the fluctuations of the amplitude envelopes, rather  
191 than on the (oscillatory) fluctuations of the carrier signals *per se*. The temporal correlation  
192 structure of the amplitude envelope fluctuations of cortical activity seems similar across  
193 different carrier frequency bands (Zhigalov et al., 2015). For most analyses reported in the  
194 following, we focused on amplitude envelope fluctuations in the alpha-band because (i) the  
195 cortical power spectra exhibited a clearly discernible alpha-peak, which robustly modulated  
196 with task, as expected from previous work (Donner & Siegel, 2011) (Fig. 1C); and (ii) the  
197 computational model used to study the effect of synaptic gain modulation on cortical activity  
198 fluctuations was tuned to produce alpha-band oscillations (see above and Poil et al., 2012).  
199 The two lower and higher frequency bands were defined coarsely for simplicity, such as to  
200 cover the complete range of the power spectrum with reliable signal during task and rest.  
201 They were analyzed as control for frequency dependence of any effects observed in the  
202 alpha-band.



203

204 *Source reconstruction: general approach*

205 The cleaned sensor level signal ( $N$  sensors) was projected onto a grid consisting of  $M =$   
 206  $3000$  voxels covering the cortical surface (mean distance: 6.3 mm) with spatial filters  
 207 computed using the exact low-resolution brain electromagnetic tomography (eLORETA;  
 208 (Pascual-Marqui and Lehmann, 2011) method. The magnetic leadfield was calculated,  
 209 separately for each subject and session, using a single shell head model constructed from  
 210 the individual structural MRI scans and the head position relative to the MEG sensors at the  
 211 beginning of the run (Nolte, 2003). In case no MRI was available (4 subjects), the leadfield  
 212 was computed from a standard MNI template brain transformed to an estimate of the  
 213 individual volume conductor using the measured fiducials (located at the nasion, the left and  
 214 the right ear).

215

216 *Computation of source level estimates of amplitude envelopes and power*

217 For comparing amplitude envelope and power estimates between experimental conditions in  
 218 source space we aimed to select a single direction of the spatial filter for each voxel across  
 219 pharmacological conditions (i.e., MEG sessions), but separately for Rest and Task  
 220 conditions. The rationale was to avoid filter-induced biases in the comparisons between the  
 221 pharmacological conditions, while allowing that external task drive might systematically  
 222 change the dipole orientations.

223 To this end, we first computed the mean source-level cross-spectral density matrix  
 224  $C(r, f)$  for each frequency band  $f$ , averaged across the three MEG sessions, as follows:

$$225 \quad C(r, f) = \frac{1}{3} \sum_{i=1}^3 \left( A_i^T(r) C_i(f) A_i(r) \right) \quad (1)$$

226 where  $A_i$  denotes the subject-specific spatial filter for session  $i$  and  $C_i(f)$  was the (sensor-  
 227 level) session- and frequency-specific cross-spectral density matrix. We then extracted the

228 first eigenvector  $u_1(r, f)$  of the session-average matrix  $C(r, f)$  and computed the unbiased  
 229 filter selective for the dominant dipole orientation,  $B_i(r, f)$ , as:

$$230 \quad B_i(r, f) = A_i(r)u_1(r, f) \quad (2)$$

231 Please note that this filter was now frequency-specific, whereas the previous filters,  
 232  $A_i$ , were not. To obtain instantaneous estimates of source-level amplitudes, the sensor-level  
 233 signal for session  $i$ ,  $X_i(t)$ , was band-pass filtered (using a finite impulse response filter) and  
 234 Hilbert-transformed, yielding a complex-valued signal  $H_i(f, t)$  for each frequency band. This  
 235 signal was projected into source space through multiplication with the unbiased spatial filter,  
 236  $B_i(r, f)$ , and the absolute value taken:

$$237 \quad Env_i(r, f, t) = |(H_i(f, t) B_i(r, f))| \quad (3)$$

238 where  $Env_i(r, f, t)$  was the estimated amplitude envelope time course of source location  $r$   
 239 and frequency  $f$ . Next, for each session, unbiased source-level cross spectral density  
 240 estimates were obtained from the sensor-level cross-spectral density matrix  $C_i(f)$  and the  
 241 frequency-specific, unbiased spatial filter  $B_i(f)$ . The main diagonal of the resulting matrix  
 242 contains source-level power estimates for all source locations:

$$243 \quad S_i(f) = diag(B_i^T(f)C_i(f)B_i(f)) \quad (4)$$

244 These computations were repeated separately for the Task and Rest conditions,  
 245 session by session. The differences in amplitude envelope fluctuations and power estimates  
 246 between pharmacological and task conditions reported in this paper were robust with  
 247 respect to the specifics of the analysis approach. In particular, we obtained qualitatively  
 248 similar pharmacological effects in sensor space, as reported in an earlier conference  
 249 abstract (Pfeffer et al, SfN, 2015).

250

### 251 *Detrended fluctuation analysis of MEG data*

252 The source-level amplitude envelopes  $Env_i(r, f, t)$  were submitted to detrended fluctuation  
 253 analysis (Peng et al., 1994; Hardstone et al., 2012) in order to quantify long-range temporal

254 correlations. Detrended fluctuation analysis quantifies the scaling with time-window length of  
 255 the fluctuation of a (locally detrended) cumulative signal. Different from the analysis of the  
 256 (more widely known) autocorrelation function (Honey et al., 2012; Murray et al., 2014),  
 257 detrended fluctuation analysis provides robust estimates of the autocorrelation structure for  
 258 stationary and non-stationary signals. Non-stationarities in the signal may originate from  
 259 artifacts that are time-locked to the onset of a recording, such as head movements that are  
 260 more pronounced at the beginning of a recording compared to the end. The procedure of  
 261 detrended fluctuation analysis is illustrated for an example subject in Figure 2.

262 For simplicity, in the following, we re-write the amplitude envelope  $Env_i(r, f, t)$  as  $x_i$ , with  $i$   
 263 indicating time points. First, we computed the cumulative sum of the demeaned  $x_i$ , (Fig. 2B):

$$264 \quad X_t = \sum_{i=1}^t (x_i - \langle x \rangle) \quad (5)$$

265 The cumulative signal  $X_t$  was then cut into  $k$  segments (overlap: 50%) of length  $T$ , where  
 266  $k = \text{floor}[(N - T)/(0.5 T)]$  and  $N$  was the length of the complete signal  $X_t$  (Fig. 2B, top).  
 267 Within each segment, the linear trend  $X_{trend}$  (least squares fit) was subtracted from  $X_t$  (Fig.  
 268 2B, middle, blue vs. red lines), and the average fluctuation computed as the root of the sum  
 269 of squared differences, averaged across windows of equal length (root-mean-square):

$$270 \quad \langle F \rangle = \left[ \frac{1}{N} \sum_{n=1}^N (X_t - X_{trend})^2 \right]^{\frac{1}{2}} \quad (6)$$

271 where  $n$  indicated windows of equal length  $T$ . The procedure was repeated for different  
 272 window lengths, yielding the fluctuation function  $\langle F(T) \rangle$  (Fig. 2B, bottom). As expected for  
 273 scale-free time series (Hardstone et al., 2012), this function of window size followed a  
 274 power-law of the form:

$$275 \quad \langle F(T) \rangle \propto T^\alpha \quad (7)$$

276 The “scaling exponent”  $\alpha$  was computed through a linear regression fit of  $\langle F(T) \rangle$  in log-log  
 277 coordinates (Fig. 2B, bottom). We estimated the scaling exponent  $\alpha$  for 15 logarithmically  
 278 spaced windows ranging from 3 s to 50 s. These bounds were chosen such as to achieve an

279 upper bound of 10% of the total data length and to avoid spurious long-range temporal  
280 correlations introduced by band-pass filtering (Hardstone et al., 2012).

281 A scaling exponent of  $0.5 < \alpha < 1$  is indicative of scale-free behavior (also referred to  
282 as “power-law scaling”) and long-range temporal correlations (Hardstone et al., 2012). The  
283 scaling exponents for alpha-band MEG amplitude envelopes estimated in this study ranged  
284 (across experimental conditions, behavioral contexts, and participants) from 0.40 and 1.04,  
285 with 99.4% of all estimates in the range between 0.5 and 1, indicative of scale-free behavior  
286 and consistent with a growing body of evidence (Linkenkaer-Hansen et al., 2001, 2005;  
287 Montez et al., 2009; He, 2011; Palva et al., 2013; Tagliazucchi et al., 2013; Zhigalov et al.,  
288 2015).

289

#### 290 *Coefficient of variation of MEG data*

291 As another aspect of intrinsic fluctuations in cortical activity, we also computed the  
292 coefficient of variation of the amplitude envelopes. The coefficient of variation, the standard  
293 deviation of a signal over its mean, quantified the overall magnitude of the fluctuations of  
294 amplitude envelope, irrespective of the frequency or time-scale, at which these fluctuations  
295 were expressed.

296

#### 297 *Relationship between measures of variability*

298 Scale-free behavior of neural time series has also been quantified via analysis of the power  
299 spectrum (Miller et al., 2009; He et al., 2010; Honey et al., 2012). There is a straightforward  
300 relationship between both approaches, which we explain below and illustrate in Fig. 2C and  
301 D, to help appreciate our results in the context of these previous studies. The power  
302 spectrum of the amplitude envelope of cortical activity is typically well approximated by  
303  $p(f) \propto f^\beta$ , where  $\beta$  is referred to as the power-law exponent. For power-law decaying

304 autocorrelations, the relationship between the power-law exponent  $\beta$  and the scaling  
 305 exponent  $\alpha$  (estimated through DFA) of a time series is:

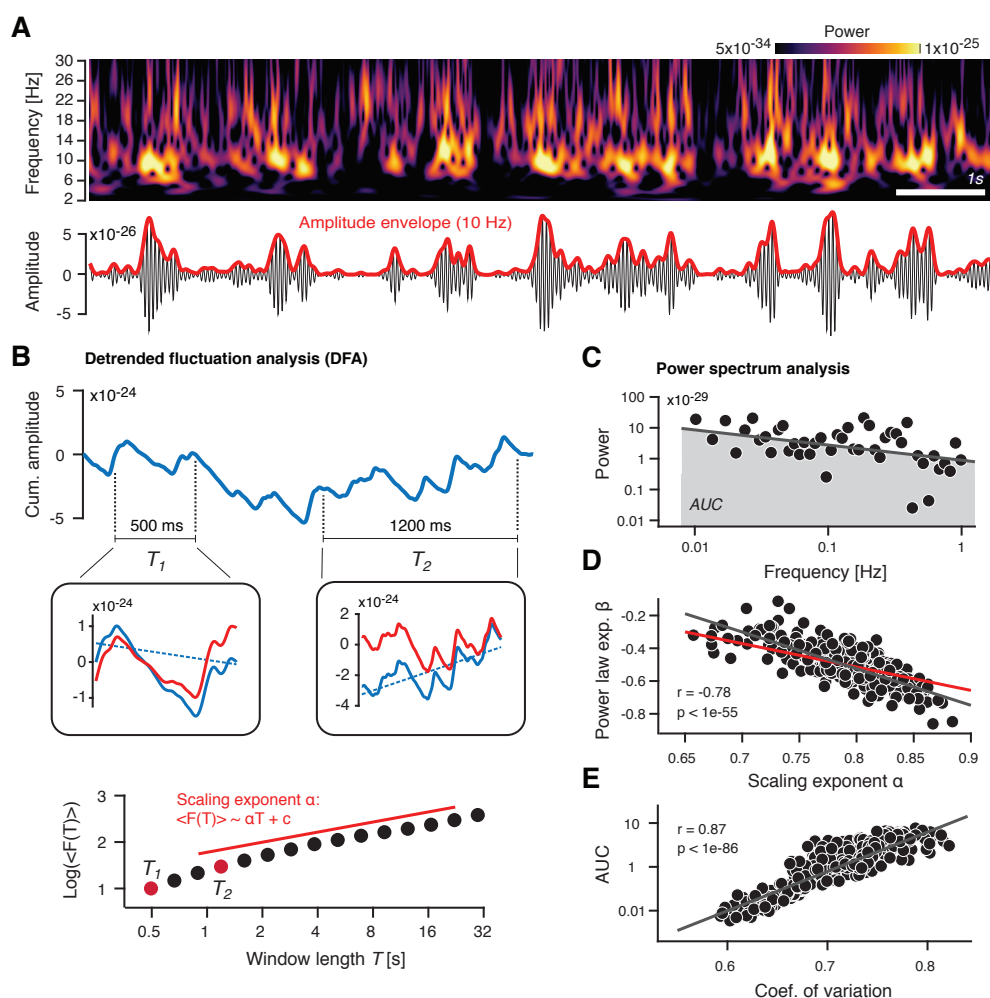


**Figure 2.** Quantifying fluctuations in cortical activity. **(A)** *Top*. Time-frequency representation of MEG power fluctuations during Rest (example subject). *Bottom*. Filtered signal (at 10 Hz; black) and the corresponding amplitude envelope (red). **(B)** Illustration of detrended fluctuation analysis. See main text (Materials and Methods) for details. *Top*. Cumulative sum of the amplitude envelope. *Center*. Detrending of cumulative sum within segments, shown for two different window lengths  $T$ . *Bottom*. Root-mean-square fluctuation function  $\langle F(T) \rangle$ . In log-log coordinates,  $\langle F(T) \rangle$  increases approximately linearly as a function of  $T$ , with a slope that is the scaling exponent  $\alpha$ . **(C)** Illustration of power spectrum analysis. In log-log coordinates, the power spectrum can be approximated by a straight line, with a slope  $\beta$  (power-law exponent) and an area under the curve (gray) that quantifies the overall variance of the signal. **(D)** Analytical and empirical relationship between scaling exponent  $\alpha$  and power-law exponent  $\beta$  from the analyses shown in (B) and (C). Exponents are strongly correlated across sensors in one example subject. Red line, analytically predicted relation for a scale-free signal. **(E)** Empirical relationship between coefficient of variation of amplitude envelope signal (red in panel A, bottom) and the area under the curve of power spectrum in (C). Both measures are strongly correlated across sensors. AUC, area under the curve.

$$\beta = 2\alpha - 1 \quad (9)$$

306  
307 To illustrate this relation with our empirical data, we computed the double-logarithmic power  
308 spectrum of the amplitude envelopes of the band-pass filtered signal (8-12 Hz; finite impulse  
309 response filter). Fig. 2D shows the relation between power-law exponent  $\beta$  and the scaling  
310 exponent  $\alpha$  for subject #27 across all 274 MEG channels. As expected, we observed a  
311 highly significant negative correlation between the two measures ( $r=-0.78$ ;  $p<1e-55$ ). The  
312 analytically derived values for  $\alpha$ , depicted in red, corresponded reasonable well with the  
313 empirically measured ones (black).

314 Likewise, the coefficient of variation, a measure of the overall fluctuation of the  
315 amplitude envelope signals, was linearly related to the area under the curve (AUC) of the  
316 power spectrum. Figure 2E depicts this relation, across sensors, for subject 27 ( $r = -0.87$ ;  $p$   
317  $< 1e-87$ ).

318

### 319 *Analysis of ECG data*

320 ECG data were used to extract average heart rate and scaling behavior of the R-R time  
321 series (Palva et al., 2013; Zhigalov et al., 2015). To this end, we used an adaptive  
322 thresholding procedure to reliably capture the R-component of each QRS-complex in the  
323 ECG time series. Heart rate was estimated by computing the total number of R-components  
324 divided by time. To investigate scaling behavior, we determined the temporal intervals  
325 between all consecutive heartbeats. Next, we estimated long-range temporal correlations in  
326 the resulting interval time series using detrended fluctuation analysis described for MEG  
327 above (see *Detrended fluctuation analysis*). Here, we used windows ranging from 3 to 50  
328 heartbeats (roughly corresponding to 3 - 50 s).

329

### 330 *Statistical tests*

331 *Cluster-based permutation test.* To identify significant alterations in space, we computed a  
332 non-parametric permutation test based on spatial clustering (Nichols and Holmes, 2002;  
333 Maris and Oostenveld, 2007). This procedure has been shown to reliably control for Type I  
334 errors arising from multiple comparisons. First, a paired t-test was performed to identify  
335 voxels with significant changes (voxel with  $p < 0.05$ ). Subsequently, significant voxels are  
336 combined into clusters based on their spatial adjacency. Here, a voxel was only included  
337 into a cluster when it had at least two significant neighbors. Subsequently, the t-values of all  
338 voxels comprising a cluster were summed, which yields a cluster statistic (i.e., a cluster t-  
339 value) for each identified cluster. Next, a randomization null distribution was computed using  
340 a permutation procedure (N=10000). On each permutation, the experimental labels (i.e., the  
341 pharmacological conditions) were randomly re-assigned within participants and the  
342 aforementioned procedure was repeated. For each iteration, the maximum cluster statistic  
343 was determined and a distribution of maximum cluster statistics was generated. Eventually,  
344 the cluster statistic of all empirical clusters was compared to the values obtained from the  
345 permutation procedure. All voxels comprising a cluster with a cluster statistic smaller than  
346 2.5% or larger than 97.5% of the permutation distribution were labeled significant,  
347 corresponding to a corrected threshold of  $\alpha = 0.025$ .

348

349 *Bayes Factor.* Wherever null effects were conceptually important, results obtained from a  
350 regular (paired) t-test (Rouder et al., 2009) and Pearson correlations (Wetzels and  
351 Wagenmakers, 2012) were used to derive corresponding Bayes factors. The Bayes Factor is  
352 useful, as it allows to estimate the strength of the evidence in support (or against) the null  
353 hypothesis with respect to the alternative hypothesis and takes effect size into account. Here,  
354 we computed Bayes Factors to quantify null effects, which are difficult to interpret using  
355 regular null hypothesis significance testing.

356

357 **Computational model simulations**

358 To simulate the effects of synaptic gain modulation on cortical activity fluctuations, we  
 359 extended a previously described, simplified computational model of a local cortical patch  
 360 (Poil et al., 2012) by means of multiplicative modulation of synaptic gain. The model  
 361 consisted of 2500 integrate-and-fire (75% excitatory, 25% inhibitory) with local connectivity  
 362 within a square (width = 7 units) and a connection probability that decayed exponentially with  
 363 distance (Fig. 3A). The dynamics of the units were governed by:

$$364 \quad I_i = I_0 + \sum_j N_{ij} W_{ij} S_j \quad (8)$$

$$365 \quad \tau_i \frac{dI_i}{dt} = I_0 - I_i \quad (9)$$

366 where subscripts  $i, j$  indicated different units,  $W_{ij}$  were the connection weights between two  
 367 units, and  $S_j$  a binary spiking vector representing whether unit  $j$  did or did not spike on the  
 368 previous time step, and  $I_0 = 0$ .  $N_{ij}$  was a multiplicative gain factor, which was the main  
 369 difference to the model described by (Poil et al., 2012), and which was introduced to  
 370 simulate the effects of neuromodulation on synaptic interactions in the cortical network  
 371 (Eckhoff et al., 2009). On each time step,  $I_i$  was updated for each unit  $i$ , with the summed  
 372 input from all other (connected) units  $j$  and scaled by a time constant  $\tau_i = 9 \text{ ms}$ , which was  
 373 the same for excitatory and inhibitory units. The connection weights were  $W_{IE} =$   
 374  $-0.569$ ,  $W_{II} = -2.0$ ,  $W_{EE} = 0.0085$  and  $W_{EI} = 0.0085$ , whereby subscript  $E$  indicated  
 375 excitatory, subscript  $I$  indicated inhibitory, and the first and second subscript referred to the  
 376 receiving and sending unit, respectively. The probability of a unit generating a spike output  
 377 was given by:

$$378 \quad P_{si} = P_0 + I_i \quad (10)$$

$$379 \quad \tau_P \frac{dP_{si}}{dt} = P_0 - P_{si} \quad (11)$$

380 with the time constant for excitatory units  $\tau_P = 6 \text{ ms}$  and for inhibitory  $\tau_P = 12 \text{ ms}$ .  $P_0$  was the  
 381 background spiking probability, with  $P_0(\text{exc.}) = 0.000001 [1/\text{ms}]$  and  $P_0(\text{inh.}) = 0 [1/\text{ms}]$ .  
 382 For each time step, it was determined whether a unit did or did not spike. If it did, the spiking



383 probability of that unit spiking was reset to  $P_r(\text{excitatory}) = -2 [1/ms]$  and  $P_r(\text{inhibitory}) =$   
 384  $-20 [1/ms]$ .

385 We quantified the power-law scaling of neuronal avalanche distributions using the  
 386 kappa-index, as described in (Shew et al., 2009). To simulate the models' "local field  
 387 potential", we summed the activity across all (excitatory and inhibitory) neurons. We band-  
 388 pass filtered the local field potential in the alpha-band (8-16 Hz) and computed long-range  
 389 temporal correlations in the alpha-band amplitude envelopes following the procedure  
 390 described above (see *Detrended fluctuation analysis of MEG data*), using windows sizes  
 391 ranging from 5 s to 30 s.

392 For the simulations reported in this paper, we chose the connection weights and  
 393 synaptic decay constants for all simulations, such that the network exhibited alpha-band  
 394 oscillations, long-range temporal correlations, and neuronal avalanches (see Discussion).  
 395 From this baseline level, we systematically varied the synaptic gain factors  $N_{EE}$ ,  $N_{IE}$ , and  $N_{EI}$

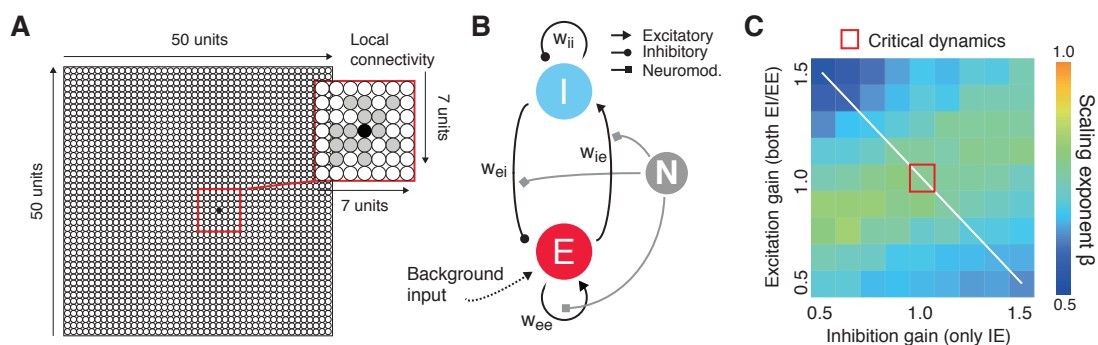


**Figure 3.** Dynamic modulation of excitation-inhibition balance simplified model of cortical patch. **(A)** Schematic of the computational model. The network consists of 2500 excitatory and inhibitory integrate-and-fire units and random, local (within an area of 7x7 units) connectivity (magnified within the red square). **(B)** Neuromodulation was simulated as gain modulation term multiplied with excitatory and/or inhibitory synaptic weights. **(C)** Scaling exponent as a function of excitatory and inhibitory synaptic gain modulation. Red square, baseline state. White line, axis of parameter combinations corresponding to changes in excitation-inhibition ratio re-plotted schematically in Fig. 7.

396 (Fig. 3B).  $N_{EI}$  was modulated independently from  $N_{EE}$ , and  $N_{IE}$ , which in turn were co-  
397 modulated by the same factor. This was intended to simulate modulations GABA receptors  
398 in the former case (mediating the effects of inhibitory neurons on others), as opposed  
399 (AMPA or NMDA) glutamate receptors in both of the latter two cases (mediating the effects  
400 of excitatory neurons on others).  $N_{EE}$ , and  $N_{IE}$  were co-modulated by the same factor for  
401 simplicity, because we did not assume that excitatory (glutamatergic) synapses would be  
402 differentially modulated depending on whether they were situated on excitatory or inhibitory  
403 target neurons.  $N_{II}$  was not modulated because we found this to cancel the effects of  
404 modulating  $N_{EI}$ . Per parameter combination, we ran 10 simulations with a random global  
405 input noise. In this paper, we focus on the effects of neuromodulation on the scaling  
406 exponent  $\alpha$  which served as a reference for interpretation of the MEG effects.

407

## 408 **Results**

409 We simulated a simplified model of a cortical patch under systematic variations in synaptic  
410 gain modulations. We then compared the simulation results to empirically measured  
411 changes in the fluctuations of human MEG activity under placebo-controlled  
412 pharmacological interventions with the cholinergic and catecholaminergic systems.  
413 Importantly, cortical activity fluctuations were measured during two steady-state conditions:  
414 “rest” and continuous, visual task drive. This allowed us to build on animal work which  
415 established that strong external (sensory) drive of cortex is accompanied by intracortical  
416 inhibition of comparably strong (Shadlen and Newsome, 1998a), or even stronger (Haider et  
417 al., 2013a), magnitude than the excitatory drive. Consequently, we assumed that the net  
418 excitation-inhibition ratio was either unchanged or reduced (but not increased) during task  
419 compared to rest. This assumption constrained the baseline level for the pharmacological  
420 manipulations.

421           The Results section is organized as follows. We first present results from simulations  
422 of a cortical circuit model under neuromodulation. These helped solidify the prediction that  
423 dynamic modulations of (excitatory and/or inhibitory) synaptic gain, alter long-range temporal  
424 correlations of intrinsic fluctuations in the amplitude of cortical oscillations, similar to those  
425 observed experimentally with EEG or MEG recordings. Next, we show how manipulating  
426 catecholaminergic and cholinergic neuromodulation (through atomoxetine and donepezil,  
427 respectively), affects fluctuations in cortical activity – specifically, the temporal correlation  
428 structure of intrinsic fluctuations in the amplitude of cortical oscillations. The  
429 neuromodulatory effects were quantified during both, “rest” (passive fixation) and external  
430 task drive; the task- and drug-induced effects on the temporal structure of activity  
431 fluctuations enabled inferences about the change in the net excitation-to-inhibition ratio  
432 under neuromodulation. Finally, we demonstrate that the observed pharmacological effects  
433 on central (cortical) activity fluctuations were not explained by effects on the peripheral  
434 (vegetative) nervous system.

435

436 **Asymmetric modulation of excitatory and inhibitory synaptic gain alters long-range**  
437 **temporal correlations in cortical circuit model**

438 We simulated neural network activity using a modified version of a cortical circuit model that  
439 has previously been analyzed to demonstrate effects of variations in structural connectivity  
440 (i.e., the percentage of excitatory and inhibitory connections) on intrinsic fluctuations in  
441 cortical activity (Poil et al., 2012). The previous work has shown that the model, despite its  
442 simplicity, accounts for the joint emergence of two empirically established phenomena (Poil  
443 et al., 2012): (i) neuronal avalanches (Beggs and Plenz, 2003), which are dissipations of  
444 activity across cortical neurons, with an event size distribution that roughly follows a power-  
445 law; and (ii) long-range temporal correlations of cortical mass activity, the focus of the  
446 present study (Linkenkaer-Hansen et al., 2001). Both phenomena unfold on different spatial

447 scales (single neurons vs. mass activity summed across neurons) and temporal scales (tens  
448 of milliseconds vs. several hundred seconds). Yet, both phenomena emerge at the same  
449 ratio of excitatory and inhibitory connectivity.

450         Here, we first determined the structural connectivity and the time scale parameters  
451 such that the network generated intrinsic alpha-band oscillations with amplitude fluctuations  
452 that exhibited robust long-range temporal correlations (with  $\alpha \sim 1$ ), as well as neuronal  
453 avalanches (Materials and Methods). We then independently manipulated both excitatory  
454 (EE and IE) as well as inhibitory synapses (only EI, see Materials and Methods) through  
455 multiplicative modulation of the connection weights (Fig. 3B), and evaluated the effects on  
456 the scaling exponent  $\alpha$  of the amplitude envelopes of alpha-band activity. Dynamic  
457 modulation of excitatory and inhibitory gain altered the scaling exponent of intrinsic  
458 amplitude fluctuations in a non-monotonic fashion (Fig. 3C, white line). Changes in both,  
459 excitatory as well as inhibitory gain resulted in alterations of  $\alpha$ . Importantly, the effect of  
460 changes in excitation or inhibition depended on the starting point: increases in excitation  
461 increased in  $\alpha$  from an inhibition-dominant starting point but decreased  $\alpha$  from an excitation-  
462 dominant starting point.

463         Overall, the effects of excitatory and inhibitory gain modulation on the temporal  
464 correlation structure of the simulated activity were qualitatively similar to the effects of  
465 (structural) changes in the fraction of excitatory and inhibitory synapses simulated previously  
466 (Poil et al., 2012). We conceptualize the latter as simulations of individual differences in  
467 cortical anatomical microstructure, and the former as simulations of within-subject, state-  
468 dependent changes in cortical dynamics, which are the focus of the current study. The new  
469 simulation results provided a solid theoretical foundation for the interpretation of the  
470 pharmacological effects on fluctuations of alpha-band amplitude envelope signals in human  
471 MEG data, as described next.

472

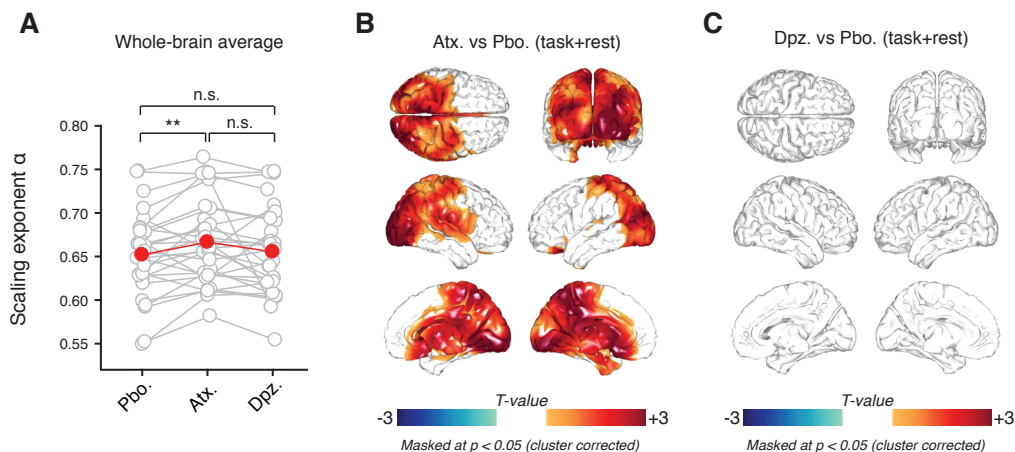


**Figure 4.** Scaling exponent  $\alpha$  for the pharmacological conditions, pooled across behavioral contexts. **(A)** Mean scaling exponent across all cortical voxels ( $N = 3000$ ) for all three pharmacological conditions. Compared to placebo, the exponent exhibits a significant increase under atomoxetine, but not under donepezil. **(B, C)** Spatial distributions of drug-induced changes (threshold: at  $p = 0.05$ , two-sided cluster-based permutation test). **(B)** atomoxetine vs. placebo; **(C)** donepezil vs. placebo.

#### 473 **Atomoxetine increases temporal correlations of intrinsic cortical activity**

474 We focused on amplitude envelope fluctuations in the alpha (8-12 Hz) band for most  
 475 analyses reported in the following because (i) as expected from previous work (Donner and  
 476 Siegel, 2011), the cortical power spectra exhibited a clearly discernible alpha-peak, which  
 477 robustly modulated with task (Fig. 1C); and (ii) alpha-band were used in the above model  
 478 simulations to read out the effect of synaptic gain modulation on cortical activity fluctuations  
 479 was tuned to produce oscillations (see above and (Poil et al., 2012)).

480 We assessed the effect of catecholaminergic and cholinergic neuromodulation on  
 481 long-range temporal correlations (as indicated by the scaling exponent  $\alpha$ ) of amplitude  
 482 envelope fluctuations in the alpha (8-12 Hz) band, during both rest and task. The average  
 483 scaling exponent during rest (placebo only) was  $\alpha = 0.67$  ( $\sigma = 0.09$ ) and during task (placebo  
 484 only)  $\alpha = 0.64$  ( $\sigma = 0.07$ ), indicative of robust long-range temporal correlations during both  
 485 behavioral contexts. In order to evaluate the main effect of the drugs, we pooled the data  
 486 across the behavioral contexts (rest and task). Averaged across voxels, we found a

487 significant increase in  $\alpha$  ( $p = 0.0068$ ;  $t = 2.93$ ; paired t-test) under atomoxetine ( $\alpha = 0.67$ ,  $\sigma =$   
 488  $0.05$ ), compared to placebo ( $\alpha = 0.65$ ,  $\sigma = 0.05$ ; Fig. 4A). There was no overall significant  
 489 difference between donepezil ( $\alpha = 0.66$ ,  $\sigma = 0.05$ ) and placebo ( $p = 0.50$ ;  $t = 0.68$ ;  $bf = 0.68$ ;  
 490 paired t-test; Fig. 4A). We next assessed the spatial profile of the atomoxetine-induced  
 491 changes. A cluster-based permutation test revealed significant increases in  $\alpha$  across  
 492 distributed cortical regions, comprising central, parietal and occipital cortex (Fig. 4B,  $p =$   
 493  $0.0022$ ; cluster-based permutation test). By contrast, we found no significant effect of  
 494 donepezil on  $\alpha$  in any cortical region ( $p = 0.22$ ; cluster-based permutation test; Fig. 4C).

495

#### 496 **Similar effects of atomoxetine on temporal correlation during rest and task**

497 To assess whether the drug effects depended on the behavioral context, we repeated the  
 498 above comparisons, separately for the two behavioral contexts. This revealed significant  
 499 effects of atomoxetine on  $\alpha$  during both rest (Fig. 5A;  $p = 0.0245$ ; cluster-based permutation  
 500 test) and task (Fig. 5B;  $p = 0.0035$ ; cluster-based permutation test), with a large number of  
 501 voxels that exhibited significant effects during both rest and task (Fig. 5C). Correspondingly,  
 502 there was no evidence for a significant interaction between task and atomoxetine effects

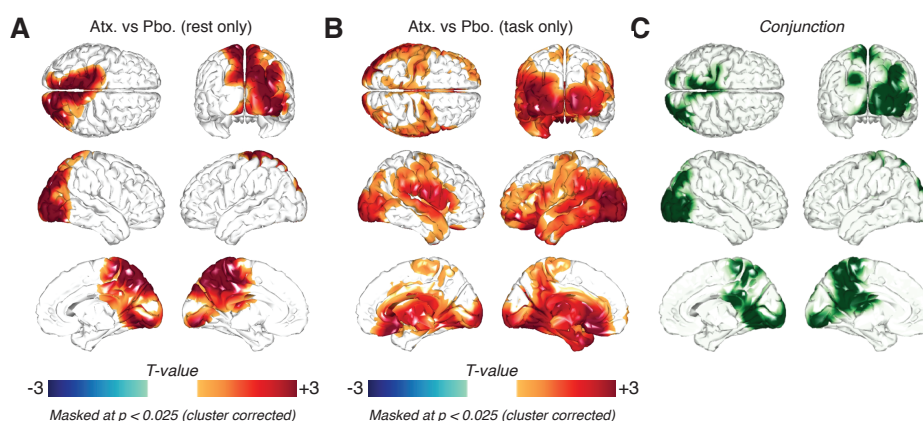


**Figure 5.** Spatial distribution of the atomoxetine-induced changes in scaling exponent  $\alpha$ . **(A)** Rest; **(B)** Task. **(C)** Conjunction of maps in (A) and (B), highlighting (in green) voxels with significant increases in both conditions.

503 anywhere in cortex: when directly comparing the contrast maps from rest with the maps from  
 504 task, we did not find any significant cluster ( $p > 0.081$  for all clusters; cluster-based  
 505 permutation test), indicating that the effects of atomoxetine were largely independent of  
 506 context. Again, no effects were evident for donepezil, neither during rest nor during task (Fig.  
 507 5 – figure supplement 1A/B). The control analyses presented below establish clear effects of  
 508 donepezil on both, cortical activity as well as markers of peripheral nervous system activity,  
 509 thus ruling out concerns that the drug may have been less effective overall than atomoxetine  
 510 (see Discussion).

511

### 512 Task drive decreases temporal correlations of intrinsic cortical activity

513 Averaged across voxels, we observed a significantly larger  $\alpha$  during rest compared to task ( $p$   
 514 = 0.0062;  $t = 2.97$ ; paired t-test; placebo condition only; Fig. 6A). The effect was spatially  
 515 more widespread than the reported increase due to atomoxetine, covering large parts of the  
 516 cortical surface ( $p < 0.01$ ; cluster-based permutation test; Fig. 6B). This task-related  
 517 decrease was also observed consistently across pharmacological conditions (Fig. 6C/D). As  
 518 expected (Donner and Siegel, 2011), the task condition also exhibited significantly lower

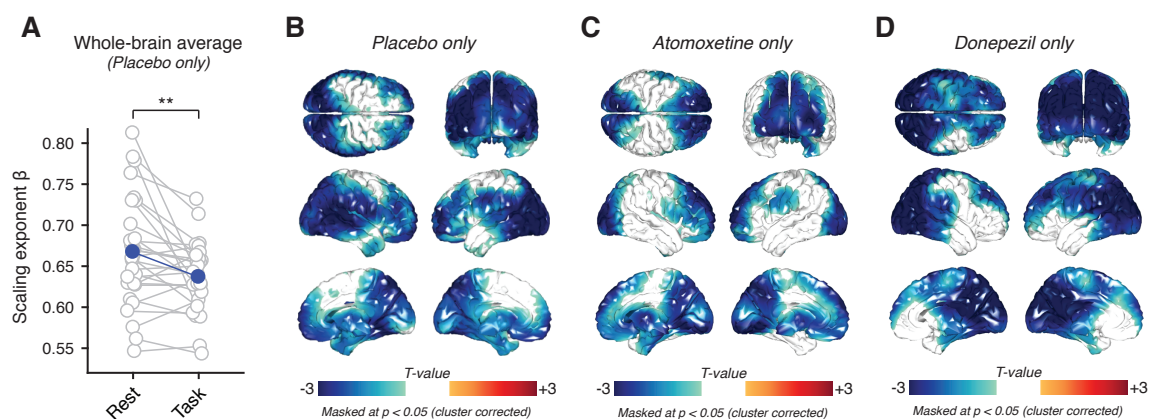


**Figure 6.** External task drive decreases long-range temporal correlations. **(A)** Mean scaling exponent across all cortical voxels ( $N = 3000$ ) for Rest and Task conditions (placebo only). The exponent is significantly reduced during Task. **(B)** Spatial distributions of task-induced changes in scaling exponents (placebo only; thresholded at  $p = 0.05$ , two-sided cluster-based permutation test).

519 alpha-band power averaged across the brain ( $p < 0.05$ ; two-sided cluster-based permutation  
520 test; Fig. 1C), but also across large parts of the cortical surface ( $p < 0.01$  for all clusters; two-  
521 sided cluster-based permutation test; Fig. 6 – figure supplement 1).

522

523 **Pattern of effects on temporal correlation indicate that catecholamines increase net**  
524 **excitation-inhibition ratio in the cortex**

525 In our model, the scaling exponent  $\alpha$  exhibited a non-monotonic dependence on excitation-  
526 inhibition ratio (see the white diagonal line in Fig. 3C, and schematic depiction in Fig. 7).  
527 Consequently, changes in in excitation-inhibition ratio are generally impossible to infer from  
528 changes in  $\alpha$  without knowing the baseline state (i.e., excitation- or inhibition-dominance).  
529 Specifically, the observed increase in  $\alpha$  following the administration of atomoxetine at rest  
530 could have been due to an increase or a decrease in excitation-inhibition ratio. However,  
531 well-established findings about the changes in cortical excitation-inhibition ratio induced by  
532 sensory drive combined with the measured changes in  $\alpha$  during task compared to rest,  
533 (Figures 6), put strong constraints on the baseline state during task, which, in turn, allowed  
534 us to infer the change in net cortical excitation-inhibition ratio induced by atomoxetine.

535 The rationale is illustrated in Figure 7. Findings from animal physiology indicate that,  
536 counter-intuitively, strong sensory drive as in our experiment does not increase cortical  
537 excitation-inhibition ratio, but rather keeps it constant or even shifts it toward stronger  
538 inhibition (Haider et al., 2013a). This assumption is illustrated by the two blue arrows in  
539 Figure 7. Thus, the observed decrease in  $\alpha$  must have been due to a shift towards inhibition-  
540 dominance from rest to task (yellow point Fig. 7A). This inference, in turn, determines the  
541 baseline state for the atomoxetine manipulation during task (i.e., inhibition-dominance).  
542 From observing the atomoxetine-induced increase in  $\alpha$ , we can then infer that atomoxetine  
543 must have increased the excitation-inhibition ratio during task (Fig. 7B). Because the effects



544 of atomoxetine on  $\alpha$  were the same during task and rest, it is likely that the same  
 545 mechanism was at play during rest, where the baseline state was unknown.

546

547 **Distinct (or absent) drug effects on features of fluctuations in cortical activity other**  
 548 **than long-range temporal correlations**

549 We next investigated drug-induced changes in power. Pooled across contexts, we find no  
 550 significant changes in power in the alpha-band due to atomoxetine (Fig. 8A;  $p > 0.025$  for all  
 551 clusters; cluster-based permutation test). In contrast, donepezil decreases alpha-band  
 552 power, although locally confined (Fig. 8B;  $p < 0.01$ ; cluster-based permutation test). Next, we  
 553 assessed the drug-related effects on alpha power separately for the two behavioral contexts:  
 554 first, during rest, both atomoxetine and donepezil reduced alpha-band power compared to  
 555 placebo in occipito-parietal regions (Fig. 8 – figure supplement 1A/B;  $p < 0.025$  for all

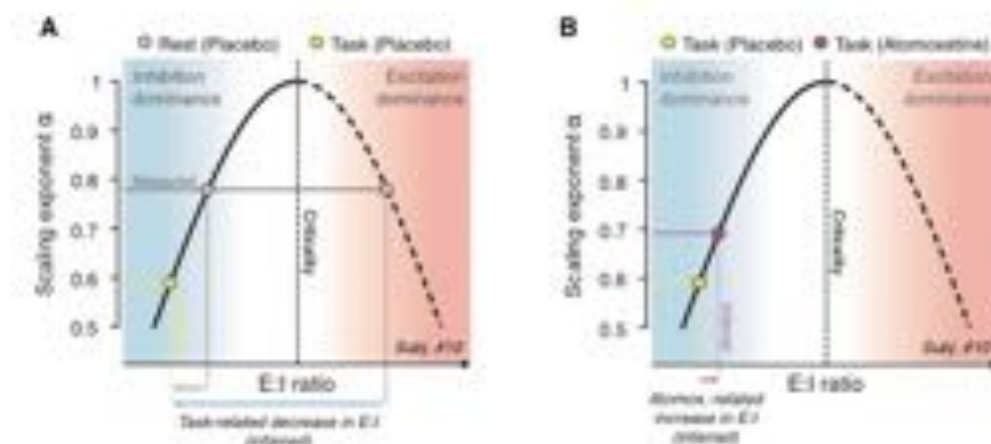


**Figure 7.** Schematic illustration of the inference from observed change in exponent to (hidden) change in net E:I ratio (see main text for details). The non-monotonic dependence of scaling exponent  $\alpha$  on E:I ratio (white line in Fig. 3C) is replotted schematically. **(A)** The measured scaling exponent  $\alpha$  during Rest (gray) can result from both, inhibition- or excitation-dominant regimes; the baseline is unknown. We assume that external drive (task; yellow dot) does not increase E:I ratio (Shadlen and Newsome, 1998). Thus, the observed decrease in scaling exponent during Task (yellow) must reflect a shift towards the inhibition-dominance (blue arrows), consistent with animal physiology (Haider et al., 2013). **(B)** This constrains the baseline state for the interpretation of the atomoxetine-induced increase in scaling exponent during Task (red): The latter increase must reflect an increase in E:I ratio (red arrow).

556 clusters; cluster-based permutation tests). During task, in contrast, neither atomoxetine nor  
557 donepezil changed alpha-power significantly (Fig. 8 – figure supplement 1C/D,  $p > 0.025$  for  
558 all clusters; cluster-based permutation test). In sum, elevating the levels of both,  
559 catecholamines and acetylcholine, suppressed cortical alpha-band oscillations during rest  
560 (but not task), which is largely consistent with previous pharmacological work in rodents  
561 (Chen et al., 2015) and humans (Bauer et al., 2012). This is also consistent with recent  
562 studies on single neuron correlates of non-luminance-mediated fluctuations in pupil diameter  
563 (Reimer et al., 2014; McGinley et al., 2015; Vinck et al., 2015), a marker of the activity of  
564 neuromodulatory brainstem centers (Joshi et al., 2016).

565         Critically, the atomoxetine-induced changes in alpha-band power had a different  
566 spatial pattern than those of the atomoxetine-induced changes in the scaling exponent  $\alpha$ :  
567 within the cluster of the significant main effect of atomoxetine on  $\alpha$ , power did not show a  
568 significantly correlate with the changes in  $\alpha$  (group average spatial correlation between  
569 pooled difference maps within cluster;  $r = 0.073$ ;  $p = 0.129$ ,  $bf = 1.065$ ).

570         Next, we evaluated the drug-related changes on the coefficient of variation of the  
571 amplitude envelopes. Again, we find no main effect of atomoxetine, pooled across  
572 behavioral contexts (Fig. 8C;  $p > 0.025$  for all clusters; cluster-based permutation test),  
573 whereas donepezil led to a significant reduction in coefficient of variation, mainly in temporal  
574 regions of the left hemisphere (Fig. 8D;  $p < 0.025$  for all clusters; cluster-based permutation  
575 test). We assessed the drug-related effects separately for the behavioral contexts: during  
576 rest, atomoxetine slightly decreased the coefficient of variation in frontal cortex (Fig. 8 –  
577 figure supplement 2A;  $p < 0.025$ ; cluster-based permutation test), whereas donepezil  
578 exhibited a decrease across several areas comprising (left) temporal and frontal cortex (Fig.  
579 8 – figure supplement 2B;  $p < 0.025$  for all clusters; cluster-based permutation test). We  
580 observed no significant changes in coefficient of variation during task (Fig. 8 – figure  
581 supplement 2C/D;  $p > 0.025$  for all clusters; cluster-based permutation test).

582 Taken together, these control analyses indicate that the above-shown effect of  
 583 atomoxetine on the scaling exponent  $\alpha$  was a specific effect and may largely be resulting  
 584 from independent factors.

585

586 **Atomoxetine-induced change of cortical fluctuations not explained by peripheral**  
 587 **effects**

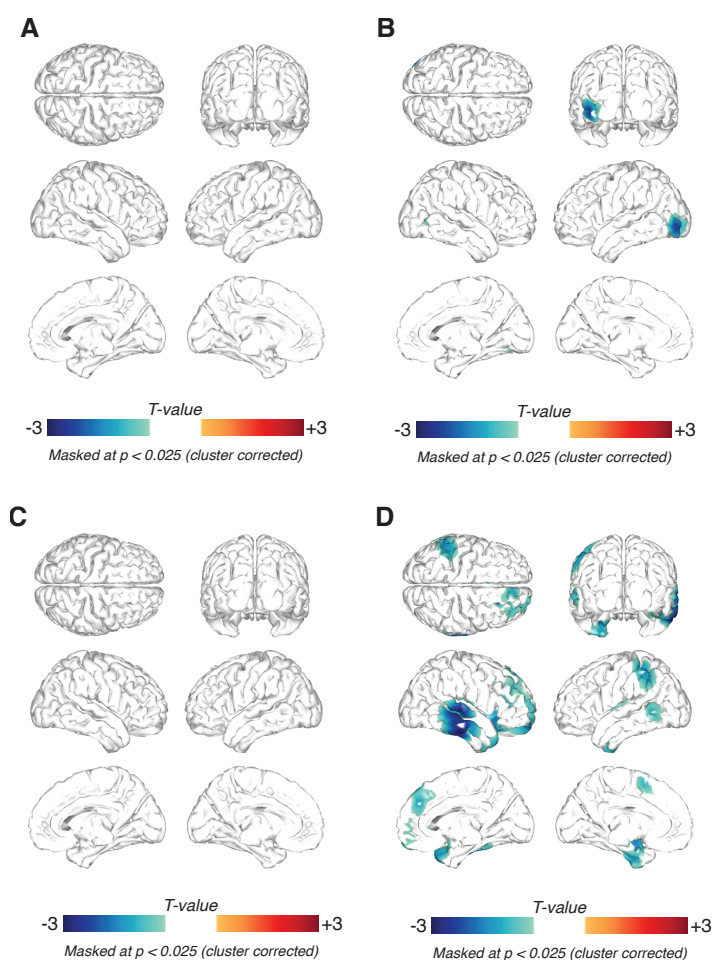


**Figure 8.** Drug-related changes in power and coefficient of variation. **(A)** Spatial distribution of atomoxetine-related power changes, pooled across behavioral contexts (thresholded at  $p = 0.05$ , two-sided cluster-based permutation test). **(B)** Same as (A), but for donepezil. **(C)** Spatial distribution of atomoxetine-related changes in coefficient of variation, pooled across behavioral contexts (thresholded at  $p = 0.05$ , two-sided cluster-based permutation test). **(D)** Same as (C), but for donepezil.

588 Atomoxetine and donepezil also affect catecholamine and noradrenaline levels at synapses  
589 of the peripheral vegetative nervous system. Atomoxetine increased average heart rate,  
590 both during rest ( $p < 0.001$ ;  $t = 3.83$ ; paired t-test; Fig. 8A) and task ( $p < 0.0001$ ;  $t = 5.56$ ;  
591 paired t-test; Fig 8B). Donepezil had no significant effect on average heart rate, neither  
592 during rest ( $p = 0.8676$ ;  $t = 0.16$ ; paired t-test;  $bf = 0.8676$ ; Fig. 8A) nor during task ( $p =$   
593  $0.3274$ ;  $t = 1.0$ ; paired t-test;  $bf = 0.3139$ ; Fig. 8B). We evaluated also the effects on the  
594 scaling behavior of the time intervals between consecutive heart beats, as assessed in  
595 previous studies (Palva et al., 2013; Zhigalov et al., 2015b). During both rest and task, and  
596 for both drugs, we found significant increases the scaling exponent  $\alpha$  compared to placebo  
597 (atomoxetine/rest:  $p = 0.0012$ ,  $t = 3.62$ ; atomoxetine/task:  $p = 0.0167$ ;  $t = 2.55$ ; Fig. 8C;  
598 donepezil/rest:  $p = 0.0076$ ,  $t = 2.88$ ; donepezil/task  $p = 0.0049$ ,  $t = 3.06$ ; Fig. 8D; all paired t-  
599 tests).

600 Previous studies of intrinsic cortical fluctuations reported a significant relation  
601 between the scaling behavior of inter-heartbeat intervals and the scaling behavior of cortical  
602 activity (Palva et al., 2013; Zhigalov et al., 2015b). Here, atomoxetine-induced changes in  
603 heart rate showed no (task:  $r = 0.00$ ;  $p = 0.99$ ; Person correlation;  $bf = 0.15$ ) or only very  
604 weak and non-significant ( $r = 0.24$ ;  $p = .21$ ; Person correlation;  $bf = 0.31$ ) correlations with  
605 the changes in cortical activity (8A/B, right). Similarly, the atomoxetine-related changes in  
606 the scaling behavior of inter-heartbeat intervals were only weakly (and not significantly)  
607 correlated with the changes in cortical scaling behavior (rest:  $r = 0.22$ ;  $p = 0.26$ ;  $bf = 0.27$ ;  
608 task:  $p = 0.26$ ;  $p = 0.19$ ;  $bf = 0.35$ ; Fig. 8C/D, right).

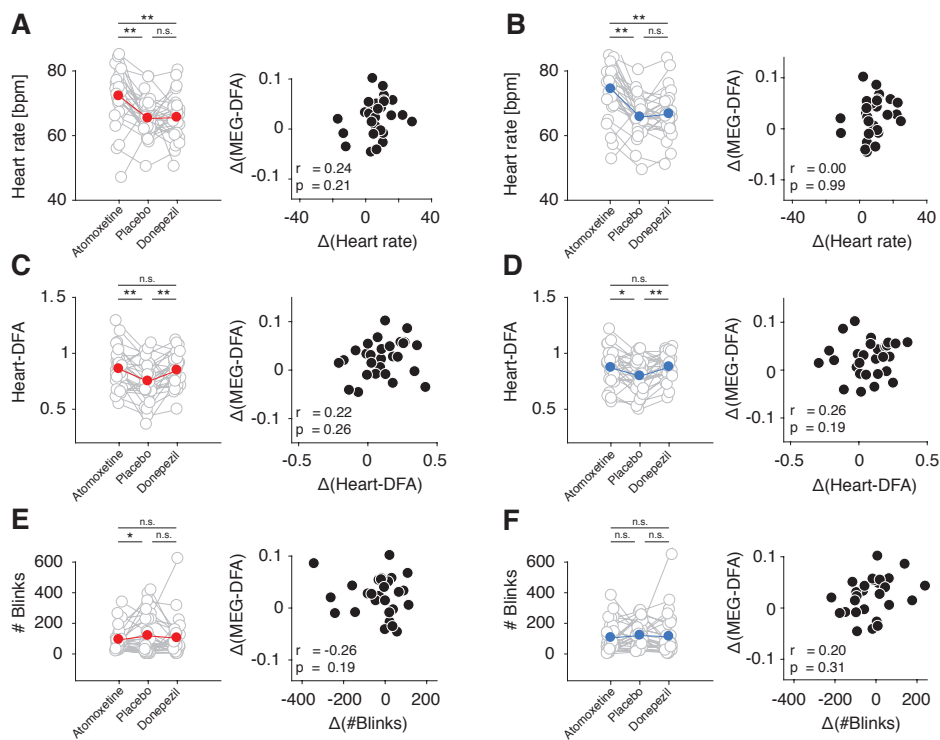


**Figure 9.** Drug effect on cortical scaling exponent not explained by peripheral drug effects. **(A) Left.** Heart rate for atomoxetine, placebo and donepezil during Rest. **Right.** Correlation of atomoxetine-related changes in heart rate (x-axis) with atomoxetine-related changes in MEG scaling exponent  $\alpha$  (y-axis) (within significant cluster during Rest). **(B)** As (A), but during Task **(C) Right.** Scaling behavior of inter-heartbeat intervals (Heart-DFA). **Left.** Heart-DFA for all pharmacological conditions during Rest. **Right.** Correlation of atomoxetine-related changes in Heart-DFA (x-axis) with atomoxetine-related changes in MEG scaling exponent  $\alpha$  (y-axis). **(D)** Same as (C), but during task. **(E) Left.** Number of blinks during rest for all drug conditions. **Right.** Correlation of atomoxetine-related changes in number of blinks (x-axis) with atomoxetine-related changes in MEG scaling exponent  $\alpha$  (y-axis) (within significant cluster during rest). **(F)** As (E), but for Task.

609 As an additional measure of peripheral activity, we also assessed the drug effects on  
 610 subjects' rate of spontaneous eye blinks. This was an important control for two reasons. First,  
 611 it has been speculated that spontaneous blink rate might reflect dopamine levels (Karson,  
 612 1983; Jongkees and Colzato, 2016), which, in turn, might also be altered by atomoxetine  
 613 (Robbins and Arnsten, 2009). Second, blinks evoke transients in cortical activity, even in the  
 614 absence of retinal input (Bristow et al., 2005), which might have contributed to our estimates

615 of intrinsic cortical variability, although blink-related effects were minimized through our  
616 artifact rejection (see Materials and Methods). Indeed, atomoxetine, but not donepezil,  
617 significantly altered spontaneous blink rate during rest ( $p = 0.034$ ;  $t = 2.24$ ; paired t-test; Fig.  
618 6E, left). However, this change was a decrease, rather than an increase, of spontaneous  
619 blink rate. This contrasts with the previously reported increase in spontaneous blink rate due  
620 to increased levels of dopamine. Further, there was no effect of atomoxetine on blink rate  
621 during task ( $p = 0.53$ ;  $t = -0.63$ ; paired t-test;  $bf = 0.676$ ; Fig. 6F, left), and no significant  
622 correlation between changes in blink-rate and changes in cortical scaling behavior (rest:  $r = -$   
623  $0.26$ ;  $p = 0.19$ ;  $bf = 0.35$ ; Fig. 6E/F, right).

624         Taken together, we found no evidence for drug-induced changes in peripheral  
625 activity (read out via heart rate) or in spontaneous blinking behavior underlying the  
626 atomoxetine-induced changes in the temporal structure of cortical fluctuations shown in  
627 Figures 4 and 5.

628

## 629 **Discussion**

630 Cortical circuits maintain a tight balance between excitation and inhibition (Denève and  
631 Machens, 2016). This balance shapes the computational properties of cortical neurons and  
632 circuits (Murphy and Miller, 2003; Polack et al., 2013; Martins and Froemke, 2015), and  
633 thereby the behavior of the organism (Wang, 2008; Eckhoff et al., 2009). Deviations from  
634 this balance have been linked to schizophrenia and autism and might also be at play in  
635 various other neuropsychiatric disorders (Yizhar et al., 2011; Lisman, 2012; Nelson and  
636 Valakh, 2015). The exact ratio between excitation and inhibition changes continuously in  
637 cortex (Isaacson and Scanziani, 2011; Froemke, 2015), presumably due to the effects of  
638 neuromodulators, such as noradrenaline and acetylcholine (Froemke et al., 2007; Eckhoff et  
639 al., 2009; Polack et al., 2013; Eggermann et al., 2014; Fu et al., 2014; Martins and Froemke,

640 2015). Neuromodulators also regulate ongoing changes in the operating mode of behavior  
641 (Aston-Jones and Cohen, 2005; Sara, 2009; Harris and Thiele, 2011; Dayan, 2012).

642 Here, we unraveled the effect of neuromodulation-controlled microcircuit level  
643 changes on the net ratio between excitation and inhibition across the cortical sheet. To this  
644 end, we combined computational modeling, pharmacological intervention, and MEG  
645 recordings of neural mass activity in humans. We found that catecholamines (noradrenaline,  
646 possibly also dopamine) altered the temporal structure of intrinsic cortical activity in a  
647 consistent way during both rest and under external (sensory and task) drive. Together with  
648 knowledge about the effect of strong external drive on the cortical excitation-inhibition ratio,  
649 the model and MEG results enabled us to infer that catecholamines increased the net ratio  
650 between excitation and inhibition (see Results and Fig. 7). We propose that combining  
651 measurements of changes in intrinsic cortical fluctuations under task and pharmaceuticals  
652 provides a novel potential non-invasive read-out of drug effects on cortical excitation-  
653 inhibition balance. Our general approach might also be useful for inferences about changes  
654 in cortical excitation-inhibition balance in neuropsychiatric disorders.

655

#### 656 **Microcircuit basis of catecholaminergic increase of net excitation-inhibition ratio**

657 An increase in excitation-inhibition ratio could have been realized through either a net  
658 increase in excitatory currents, a net decrease in inhibitory currents, or both. Results from  
659 recent invasive work in rodents are consistent with this conclusion. One study found that  
660 locus coeruleus stimulation, and thus noradrenaline release in cortex, yielded a decrease in  
661 the rate of tonic inhibitory postsynaptic currents in cortical neurons, whereas the rates and  
662 amplitudes of tonic excitatory currents remained unaffected (Martins and Froemke, 2015).  
663 Another study showed found noradrenaline (but not acetylcholine) to mediate a locomotion-  
664 induced, tonic depolarization of V1 pyramidal cells, possibly through a reduction in  
665 membrane leak conductance (Polack et al., 2013). Provided no (or weaker) depolarization of

666 inhibitory interneurons through noradrenaline, this observation is consistent with a net  
667 increase in excitation in the local microcircuit. Both results are consistent with an increase in  
668 net excitation-inhibition ratio within local cortical circuits.

669

#### 670 **Cortical distribution of catecholaminergic effects on cortical fluctuations**

671 The atomoxetine effects on the scaling exponent were widespread across cortex, but they  
672 were not entirely homogenous, pronounced across parietal cortex but not robust in frontal  
673 cortex (see Fig. 4B). It is unlikely that this distribution simply reflected where signal-to-noise  
674 of alpha-band activity is highest (commonly most pronounced in occipito-parietal cortex)  
675 because the drug-induced changes in power (which should be equally affected by signal-to-  
676 noise) were spatially uncorrelated with the changes in long-range temporal correlations (see  
677 Results). The observed distribution of effects points to a noradrenergic, rather than  
678 dopaminergic origin. Atomoxetine increases the levels of both catecholamines,  
679 noradrenaline and dopamine (Robbins and Arnsten, 2009). But the dopaminergic system  
680 mainly projects to prefrontal cortex (Montague et al., 2004), whereas the noradrenergic  
681 projections are more widespread, with a focus on parietal and occipital cortex (Morrison and  
682 Foote, 1986). Another possibly important aspect is the receptor composition of different  
683 cortical regions, which is heterogeneous (Ramos and Arnsten, 2007; Salgado et al., 2016):  
684 The relative frequency of different adrenoceptors ( $\alpha$ 1-,  $\alpha$ 2 or  $\beta$ -adrenoceptor) differs strongly  
685 between frontal and posterior cortex, which, in turn, can result in distinct effects of  
686 noradrenaline on the dynamics of neural activity in these different cortical regions (Ramos  
687 and Arnsten, 2007), in particular persistent activity. Future studies should investigate  
688 whether the observed differences of noradrenergic effects on long-range temporal  
689 correlations in cortical activity are due to these differences in adrenoceptor composition  
690 across cortex.

691



692 **No evidence for cholinergic effects of net excitation-inhibition ratio**

693 In contrast to atomoxetine, we observed no robust effect of increased acetylcholine levels on  
694 cortical long-range temporal correlations. This absence of an effect was unlikely due to an  
695 ineffective pharmacological manipulation through donepezil: The latter had equally strong  
696 effects as atomoxetine on alpha-band power in some cortical regions, as well as on heart  
697 rate variability. Rather, the absence of robust donepezil effects might reflect specific  
698 properties of cholinergic action, which may leave the cortical net excitation-inhibition ratio  
699 largely unchanged. Substantial evidence points to the rapid disinhibition of (excitatory)  
700 pyramidal cells by acetylcholine, by activating a circuit made up of a chain two inhibitory  
701 interneurons (VIP+ and SOM+) (Pfeffer et al., 2013; Fu et al., 2014; Pakan et al., 2016). The  
702 cholinergic activation of this disinhibitory circuit would be expected to shift the net excitation-  
703 inhibition ratio towards excitation, just as we inferred for catecholamines. However, this  
704 disinhibitory circuit seems to mainly affect transient, stimulus-evoked responses (Froemke et  
705 al., 2007), whereas noradrenaline also alters the tonic levels of inhibition (Martins and  
706 Froemke, 2015). This may explain the relative lack of donepezil effects during the steady-  
707 state conditions (rest and continuous task drive) employed in our present study. Alternatively,  
708 the cholinergic activation of this disinhibitory circuit might be balanced by other, inhibitory  
709 effects of acetylcholine on the local microcircuit, thus leaving the net excitation-inhibition  
710 ratio unchanged.

711

712 **Functional consequences of changes in net excitation-inhibition ratio**

713 A net increase in excitation may have behaviorally relevant effects on the dynamics of  
714 parietal and prefrontal cortical circuits involved in working memory and decision-making  
715 (Wang, 2008). These circuits are characterized by slow intrinsic fluctuations of activity  
716 (Honey et al., 2012; Murray et al., 2014; Chaudhuri et al., 2015). The catecholaminergic  
717 increase in long-range temporal correlations of intrinsic activity fluctuations in parietal circuits

718 that we observed in the current study may reflect a relative increase specifically in the  
719 recurrent excitation in ‘accumulator’ circuits. Recurrent excitation, in turn, is essential for  
720 both the computational capacities (Wang, 2002) as well as the timescale of intrinsic activity  
721 fluctuations of these circuits (Murray et al., 2014; Chaudhuri et al., 2015). Simulations of  
722 synaptic gain modulation of such ‘accumulator’ circuits indicate that the most robust  
723 behavior emerges from co-modulation of both, excitatory and inhibitory synapses, but with  
724 different factors (Eckhoff et al., 2009).

725         Consistent with our current results, previous studies also found a decrease in  
726 temporal autocorrelations of cortical activity due to external drive, even during intermittent  
727 presentation of stimuli and tasks, entailing more external transients than the steady-state  
728 task condition used here (Linkenkaer-Hansen et al., 2004; He, 2011). Indeed, simulations of  
729 large-scale biophysical models of cortical networks show that the driven state is associated  
730 with shortened temporal autocorrelations as well as a decrease in the entropy of activity  
731 states in the network (Ponce-Alvarez et al., 2015). This suggests that the increased long-  
732 range temporal autocorrelations with catecholaminergic modulation we observed here may  
733 be associated with an increase in entropy, in other words, a tendency of the cortex to  
734 explore a larger set of activity states. It is tempting to link this to a prominent idea about the  
735 function of noradrenaline, which postulates that high tonic noradrenaline levels promote  
736 exploratory, and more distractible, behavior (Aston-Jones and Cohen, 2005).

737

### 738 **Catecholamines may act as a control parameter for critical network dynamics**

739 Long-range temporal correlations in the fluctuations of neural mass activity (i.e., activity  
740 summed across the entire local network) (Linkenkaer-Hansen et al., 2001) and avalanches  
741 within the neuronal network (Beggs and Plenz, 2003) jointly emerge at the same ratio  
742 between excitatory and inhibitory connectivity in the simplified cortical patch model used  
743 here. Both phenomena, long-range temporal correlations and neuronal avalanches, are

744 commonly interpreted as hallmarks of “criticality” (Linkenkaer-Hansen et al., 2001; Beggs  
745 and Plenz, 2003; Beggs, 2008; Zhigalov et al., 2015b). Criticality refers to a complex  
746 dynamical system poised between order and chaos (Bak et al., 1987; Bak, 1996; Chialvo,  
747 2010).

748         The cortex might operate in a narrow regime around this critical point (Chialvo, 2010;  
749 Hesse and Gross, 2015). This operating mode, in turn, might yield computational capabilities  
750 superior to those of the “sub-“ or “supercritical” modes (Kinouchi and Copelli, 2006; Beggs,  
751 2008; Shew et al., 2009b, 2011; Shriki and Yellin, 2016). A number of recent reports have  
752 indicated that cortical dynamics may fluctuate around the critical state (Priesemann et al.,  
753 2013; Arviv et al., 2015; Fagerholm et al., 2015; Shew et al., 2015), but these fluctuations  
754 have, so far, been spontaneous. Here, we identified two key factors (task drive and  
755 catecholaminergic neuromodulation) to bring these changes under experimental control.

756         Complex systems can self-organize towards criticality (Bak et al., 1987), e.g. through  
757 plasticity and/or feedback connections. However, critical dynamics can also be achieved  
758 through an external control parameter that fine-tunes the system. The tuning of temperature  
759 in the Ising model of spin magnetization is a common example (Chialvo, 2010). We propose  
760 that noradrenaline may serve as such a control parameter in the cerebral cortex.

761

## 762 **Conclusion**

763 In summary, we demonstrated that catecholamines increase the long range-temporal  
764 correlations of intrinsic cortical activity. The combination of computational modeling with  
765 MEG measurements changes in temporal correlations related to task drive and those  
766 induced by selective pharmaceuticals, allowed us to infer that catecholamines increase the  
767 net excitation-inhibition ratio in the cortex. Our approach can be readily applied to other  
768 studies investigating drug-related effects on excitation-inhibition balance or clinical studies of  
769 neuropsychiatric diseases associated with disturbances thereof.

770

771 **References**

772 Arviv O, Goldstein A, Shriki O (2015) Near-Critical Dynamics in Stimulus-Evoked Activity of  
773 the Human Brain and Its Relation to Spontaneous Resting-State Activity. *J Neurosci.*  
774 35(41):13927-42.

775 Aston-Jones G, Cohen JD (2005) An integrative theory of locus coeruleus-norepinephrine  
776 function: adaptive gain and optimal performance. *Ann Rev Neurosci* 28:403–450.

777 Bak P (1996) *The Discovery of Self-Organized Criticality. How Nature Works.*

778 Bak, Tang, Wiesenfeld (1987) Self-organized criticality: An explanation of the 1/f noise. *Phys*  
779 *Rev Let* 59:381–384.

780 Bauer M, Kluge C, Bach D, Bradbury D, Heinze HJ, Dolan RJ, Driver J (2012) Cholinergic  
781 enhancement of visual attention and neural oscillations in the human brain. *Curr Biol*  
782 22:397–402.

783 Beggs J (2008) The criticality hypothesis: how local cortical networks might optimize  
784 information processing. *Philos Trans A Math Phys Eng Sci* 366(1864):329-43.

785 Beggs J, Plenz D (2003) Neuronal avalanches in neocortical circuits. *J Neurosci.*  
786 23(35):11167-77.

787 Bell AJ, Sejnowski TJ (1995) An information-maximization approach to blind separation and  
788 blind deconvolution. *Neural Comput* 7:1129–1159.

789 Berridge C (2008) Noradrenergic modulation of arousal. *Brain Res Rev* 58(1):1-17.

790 Bristow D, Haynes J-D, Sylvester R, Frith CD, Rees G (2005) Blinking suppresses the  
791 neural response to unchanging retinal stimulation. *Curr Biol* 15:1296–1300.

- 792 Chaudhuri R, Knoblauch K, Gariel M-A, Kennedy H, Wang X-J (2015) A Large-Scale Circuit  
793 Mechanism for Hierarchical Dynamical Processing in the Primate Cortex. *Neuron*  
794 88:419–431.
- 795 Chen N, Sugihara H, Sur M (2015) An acetylcholine-activated microcircuit drives temporal  
796 dynamics of cortical activity. *Nat Neurosci* 18:892–902.
- 797 Chialvo D (2010) Emergent complex neural dynamics. *Nat Phys.* 6(1):744-750.
- 798 Dayan P (2012) Twenty-five lessons from computational neuromodulation. *Neuron* 76:240–  
799 256.
- 800 Deco G, Jirsa VK, R M Anthony (2011) Emerging concepts for the dynamical organization of  
801 resting-state activity in the brain. *Nat Rev Neurosci* 12:43–56.
- 802 Denève S, Machens C (2016) Efficient codes and balanced networks. *Nat Neurosci*  
803 19(3):375-382.
- 804 Donner TH, Siegel M (2011) A framework for local cortical oscillation patterns. *Trends Cogn*  
805 *Neurosci* 15:191–199.
- 806 Eckhoff P, KF W-L, Holmes P (2009) Optimality and robustness of a biophysical decision-  
807 making model under norepinephrine modulation. *J Neurosci* 29(13):4301-11.
- 808 Eggermann E, Kremer Y, Crochet S, Petersen C (2014) Cholinergic signals in mouse barrel  
809 cortex during active whisker sensing. *Cell Rep* 9(5):1654-60.
- 810 Fagerholm ED, Lorenz R, Scott G, Dinov M, Hellyer PJ, Mirzaei N, Leeson C, Carmichael  
811 DW, Sharp DJ, Shew WL, Leech R (2015) Cascades and Cognitive State: Focused  
812 Attention Incurs Subcritical Dynamics. *J Neurosci* 35:4626–4634.
- 813 Faisal A, Selen LP, Wolpert DM (2008) Noise in the nervous system. 9(5):292–303.

- 814 Fox MD, Snyder AZ, Vincent JL, Corbetta M, Essen DC, Raichle ME (2005) The human  
815 brain is intrinsically organized into dynamic, anticorrelated functional networks. Proc  
816 Natl Acad Sci U S A 102:9673–9678.
- 817 Froemke R (2015) Plasticity of cortical excitatory-inhibitory balance. *Annu Rev Neurosci.* 38:  
818 195-219.
- 819 Froemke R, Merzenich M, Schreiner C (2007) A synaptic memory trace for cortical receptive  
820 field plasticity. *Nature.*
- 821 Froemke R, Merzenich M, Schreiner C (2007b) A synaptic memory trace for cortical  
822 receptive field plasticity. *Nature.*
- 823 Fu Y, Tucciarone JM, Espinosa SJ, Sheng N, Darcy DP, Nicoll RA, Huang JZ, Stryker MP  
824 (2014) A cortical circuit for gain control by behavioral state. *Cell* 156:1139–1152.
- 825 Haider B, Häusser M, Carandini M (2013a) Inhibition dominates sensory responses in the  
826 awake cortex. *Nature.*
- 827 Haider B, Häusser M, Carandini M (2013b) Inhibition dominates sensory responses in the  
828 awake cortex. *Nature* 493(430):97-100..
- 829 Hardstone R, Poil S-SS, Schiavone G, Jansen R, Nikulin VV, Mansvelder HD, Klaus L-H  
830 (2012) Detrended fluctuation analysis: a scale-free view on neuronal oscillations.  
831 *Front Fract Neurophys* 3:450.
- 832 Harris KD, Thiele A (2011) Cortical state and attention. *Nat Rev Neurosci* 12:509–523.
- 833 He B (2011) Scale-free properties of the functional magnetic resonance imaging signal  
834 during rest and task. *J Neurosci* 31(39):13786-95..

- 835 He B, Zempel J, Snyder A, Raichle M (2010) The temporal structures and functional  
836 significance of scale-free brain activity. *Neuron* 66(3): 353-69.
- 837 Hesse J, Gross T (2015) Self-organized criticality as a fundamental property of neural  
838 systems. *Front Syst Neurosci* 8:166
- 839 Hipp JF, Siegel M (2013) Dissociating neuronal gamma-band activity from cranial and ocular  
840 muscle activity in EEG. *Front Hum Neurosci* 7:338.
- 841 Honey C, Theisen T, Donner T, Silbert L (2012) Slow cortical dynamics and the accumulation  
842 of information over long timescales. *Neuron* 76(2):423-34.
- 843 Hyvärinen A (1999) The fixed-point algorithm and maximum likelihood estimation for  
844 independent component analysis. *Neural Processing Letters* 10(1):1-5.
- 845 Isaacson J, Scanziani M (2011) How inhibition shapes cortical activity. *Neuron* 72(2):231-43.
- 846 Jongkees BJ, Colzato LS (2016) Spontaneous eye blink rate as predictor of dopamine-  
847 related cognitive function-A review. *Neurosci Biobehav Rev* 71:58–82.
- 848 Joshi S, Li Y, Kalwani R, Gold J (2016) Relationships between pupil diameter and neuronal  
849 activity in the locus coeruleus, colliculi, and cingulate cortex. *Neuron* 89(1):221-34.
- 850 Karson CN (1983) Spontaneous eye-blink rates and dopaminergic systems. *Brain J Neurol*  
851 106 (Pt 3):643–653.
- 852 Kinouchi O, Copelli M (2006) Optimal dynamical range of excitable networks at criticality.  
853 *Nat Phys* 2: 348-351.
- 854 Lee S, Dan Y (2012) Neuromodulation of brain states. *Neuron* 76:209-222.

- 855 Linkenkaer-Hansen K, Monto S, Rytysälä H, Suominen K, Isometsä E, Kähkönen S (2005)  
856 Breakdown of long-range temporal correlations in theta oscillations in patients with  
857 major depressive disorder. *J Neurosci* 25:10131–10137.
- 858 Linkenkaer-Hansen K, Nikouline VV, Palva JM, Ilmoniemi RJ (2001) Long-range temporal  
859 correlations and scaling behavior in human brain oscillations. *J Neurosci* 21(4):1370-  
860 7.
- 861 Linkenkaer-Hansen K, Nikulin VV, Palva JM, Kaila K, Ilmoniemi RJ (2004) Stimulus-induced  
862 change in long-range temporal correlations and scaling behaviour of sensorimotor  
863 oscillations. *Eur J Neurosci* 19(1):203-11.
- 864 Linkenkaer-Hansen K, Smit D, Barkil A, Beijsterveldt T, Brussaard A, Boomsma D, Ooyen A,  
865 Geus E (2007) Genetic Contributions to Long-Range Temporal Correlations in  
866 Ongoing Oscillations. *J Neurosci* 27:13882–13889.
- 867 Lisman J (2012) Excitation, inhibition, local oscillations, or large-scale loops: what causes  
868 the symptoms of schizophrenia? *Curr Opin Neurobiol* 22:537–544.
- 869 Marder E (2012) Neuromodulation of neuronal circuits: back to the future. *Neuron* 76:1–11.
- 870 Maris E, Oostenveld R (2007) Nonparametric statistical testing of EEG-and MEG-data. *J*  
871 *Neurosci Methods* 165(1):177-190.
- 872 Martins AR, Froemke RC (2015) Coordinated forms of noradrenergic plasticity in the locus  
873 coeruleus and primary auditory cortex. *Nat Neurosci* 18:1483–1492.
- 874 McGinley M, David S, McCormick DA (2015) Cortical membrane potential signature of  
875 optimal states for sensory signal detection. *Neuron*.



- 876 Miller KJ, Sorensen LB, Ojemann JG, Nijs M (2009) Power-law scaling in the brain surface  
877 electric potential. *PLoS Comp Biol* 5:e1000609.
- 878 Mitra P, Pesaran B (1999) Analysis of dynamic brain imaging data. *Biophys J* 76(2):691-708.
- 879 Montague PR, Hyman SE, Cohen JD (2004) Computational roles for dopamine in  
880 behavioural control. *Nature* 431:760–767.
- 881 Montez T, Poil S-S, Jones BF, Manshanden I, Verbunt JPA, van Dijk BW, Brussaard A, van  
882 Ooyen A, Stam CJ, Scheltens P, Linkenkaer-Hansen K (2009) Altered temporal  
883 correlations in parietal alpha and prefrontal theta oscillations in early-stage Alzheimer  
884 disease. *Proc Natl Acad Sci U S A* 106(5):1614-9.
- 885 Murphy BK, Miller KD (2003) Multiplicative gain changes are induced by excitation or  
886 inhibition alone. *J Neurosci* 23:10040–10051.
- 887 Murray JD, Bernacchia A, Freedman DJ, Romo R, Wallis JD, Cai X, Padoa-Schioppa C,  
888 Pasternak T, Seo H, Lee D, Wang X-J (2014) A hierarchy of intrinsic timescales  
889 across primate cortex. *Nat Neurosci* 17:1661–1663.
- 890 Nelson S, Valakh V (2015) Excitatory/inhibitory balance and circuit homeostasis in autism  
891 spectrum disorders. *Neuron* 87(4):684-98.
- 892 Nichols T, Holmes A (2002) Nonparametric permutation tests for functional neuroimaging: a  
893 primer with examples. *Hum Brain Mapp* 15(1):1-25.
- 894 Oostenveld R, Fries P, Maris E (2011) FieldTrip: open source software for advanced  
895 analysis of MEG, EEG, and invasive electrophysiological data. *Comput Intell*  
896 *Neurosci* 2011:156869.

- 897 Pakan JM, Lowe SC, Dylida E, Keemink SW, Currie SP, Coutts CA, Rochefort NL (2016)  
898 Behavioral-state modulation of inhibition is context-dependent and cell type specific  
899 in mouse visual cortex. *Elife* 5.
- 900 Palva J, Zhigalov A, Hirvonen J, Korhonen O, Klaus L-H, Palva S (2013) Neuronal long-  
901 range temporal correlations and avalanche dynamics are correlated with behavioral  
902 scaling laws. *Proc Natl Acad Sci U S A* 110(9):3585-90.
- 903 Pascual-Marqui RD, Lehmann D (2011) Assessing interactions in the brain with exact low-  
904 resolution electromagnetic tomography. *Philos Trans A Math Phys Eng Sci*  
905 369(1952):3768-84.
- 906 Peng C, Buldyrev S, Havlin S, Simons M (1994) Mosaic organization of DNA nucleotides.  
907 *Phys Rev E* 49(2):1685-9.
- 908 Pfeiffer CK, Xue M, He M, Huang Z, Scanziani M (2013) Inhibition of inhibition in visual  
909 cortex: the logic of connections between molecularly distinct interneurons. *Nat*  
910 *Neurosci* 16:1068–1076.
- 911 Poil S-S, Hardstone R, Mansvelder HD, Klaus L-H (2012) Critical-State Dynamics of  
912 Avalanches and Oscillations Jointly Emerge from Balanced Excitation/Inhibition in  
913 Neuronal Networks. *J Neurosci* 32:9817–9823.
- 914 Polack P-OO, Friedman J, Golshani P (2013a) Cellular mechanisms of brain state-  
915 dependent gain modulation in visual cortex. *Nat Neurosci* 16:1331–1339.
- 916 Polack P-OO, Friedman J, Golshani P (2013b) Cellular mechanisms of brain state-  
917 dependent gain modulation in visual cortex. *Nat Neurosci* 16:1331–1339.

- 918 Ponce-Alvarez A, He B, Hagmann P, Deco G (2015) Task-Driven Activity Reduces the  
919 Cortical Activity Space of the Brain: Experiment and Whole-Brain Modeling. *Plos*  
920 *Comput Biol* 11:e1004445.
- 921 Priesemann V, Valderrama M, Wibral M, Quyen M (2013) Neuronal avalanches differ from  
922 wakefulness to deep sleep—evidence from intracranial depth recordings in humans.  
923 *PLoS Comput Biol* 9:e1002985.
- 924 Ramos BP, Arnsten AFT (2007) Adrenergic pharmacology and cognition: focus on the  
925 prefrontal cortex. *Pharmacol Ther* 113:523–536.
- 926 Reimer J, Froudarakis E, Cadwell C, Yatsenko D (2014) Pupil fluctuations track fast  
927 switching of cortical states during quiet wakefulness. *Neuron* 84(2):355-62.
- 928 Robbins TW, Arnsten AFT (2009) The neuropsychopharmacology of fronto-executive  
929 function: monoaminergic modulation. *Annu Rev Neurosci* 32:267–287.
- 930 Rouder J, Speckman P, Sun D, Morey R (2009) Bayesian t tests for accepting and rejecting  
931 the null hypothesis. *Psychon Bull Rev* 16(2):225-37.
- 932 Salgado H, Treviño M, Atzori M (2016) Layer-and area-specific actions of norepinephrine on  
933 cortical synaptic transmission. *Brain Res* 1641:163–176.
- 934 Sara S (2009) The locus coeruleus and noradrenergic modulation of cognition. *Nat Rev*  
935 *Neurosci* 10(3):211-23.
- 936 Sauer J-M, Ring BJ, Witcher JW (2005) Clinical pharmacokinetics of atomoxetine. *Clin*  
937 *Pharmacokinet* 44:571–590.
- 938 Shadlen MN, Newsome WT (1998) The variable discharge of cortical neurons: implications  
939 for connectivity, computation, and information coding. *J Neurosci* 18:3870–3896.

- 940 Shew W, Clawson W, Pobst J, Karimippanah Y (2015) Adaptation to sensory input tunes  
941 visual cortex to criticality. *Nat Phys*. 11:659-663.
- 942 Shew W, Yang H, Petermann T, Roy R (2009a) Neuronal avalanches imply maximum  
943 dynamic range in cortical networks at criticality. *J Neurosci* 29(49):15596-600.
- 944 Shew W, Yang H, Yu S, Roy R (2011) Information capacity and transmission are maximized  
945 in balanced cortical networks with neuronal avalanches. *J Neurosci* 31(1):55-63.
- 946 Shriki O, Yellin D (2016) Optimal Information Representation and Criticality in an Adaptive  
947 Sensory Recurrent Neuronal Network. *PLoS Comput Biol* 12(2):e1004698.
- 948 Sperling G, Doshier BA, Landy MS (1990) How to study the kinetic depth effect  
949 experimentally. *J Exp Psychol Hum Percept Perform* 16:445–450.
- 950 Tagliazucchi E, von Wegner F, Morzelewski A, Brodbeck V, Jahnke K, Laufs H (2013)  
951 Breakdown of long-range temporal dependence in default mode and attention  
952 networks during deep sleep. *Proc Natl Acad Sci U S A* 110:15419–15424.
- 953 Tiseo PJ, Rogers SL, Friedhoff LT (1998) Pharmacokinetic and pharmacodynamic profile of  
954 donepezil HCl following evening administration. *Br J Clin Pharmacol* 46 Suppl 1:13–  
955 18.
- 956 van Vreeswijk C, Sompolinsky H (1996) Chaos in neuronal networks with balanced  
957 excitatory and inhibitory activity. *Science* 274:1724–1726.
- 958 Vinck M, R B-B, Knoblich U, Cardin J (2015) Arousal and locomotion make distinct  
959 contributions to cortical activity patterns and visual encoding. *Neuron* 86(3):740-54.
- 960 Wallach H, O'connell DN (1953) The kinetic depth effect. *J Exp Psychol* 45:205–217.
- 961 Wang X-JJ (2008) Decision making in recurrent neuronal circuits. *Neuron* 60:215–234.

- 962 Wetzels R, Wagenmakers E (2012) A default Bayesian hypothesis test for correlations and  
963 partial correlations. *Psychon Bull Rev* 19(6):1057-64.
- 964 Yizhar O, Fenno L, Prigge M, Schneider F (2011) Neocortical excitation/inhibition balance in  
965 information processing and social dysfunction. *Nature* 477(7363):171-8.
- 966 Zhigalov A, Arnulfo G, Nobili L, Palva S (2015) Relationship of Fast-and Slow-Timescale  
967 Neuronal Dynamics in Human MEG and SEEG. *J Neurosci* 35(13): 5385-5396.
- 968

## Supplementary material

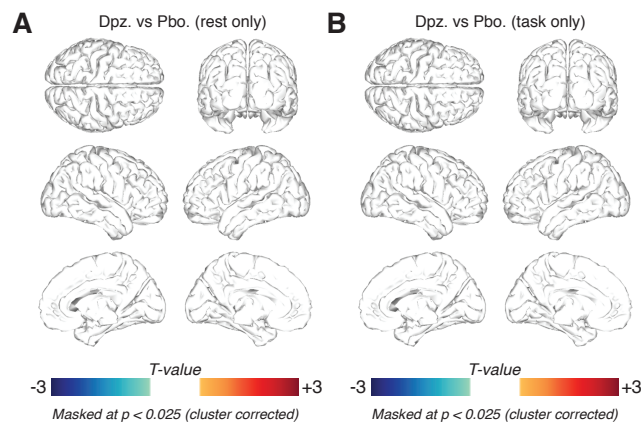


**Figure 5 - Supplemental Figure 1.** No donepezil-related changes in scaling exponent. **(A)** Spatial distribution of donepezil-induced changes in scaling exponent  $\alpha$  during Rest, thresholded at  $p = 0.05$  (two-sided cluster-based permutation test). **(B)** As (A), but for Task.

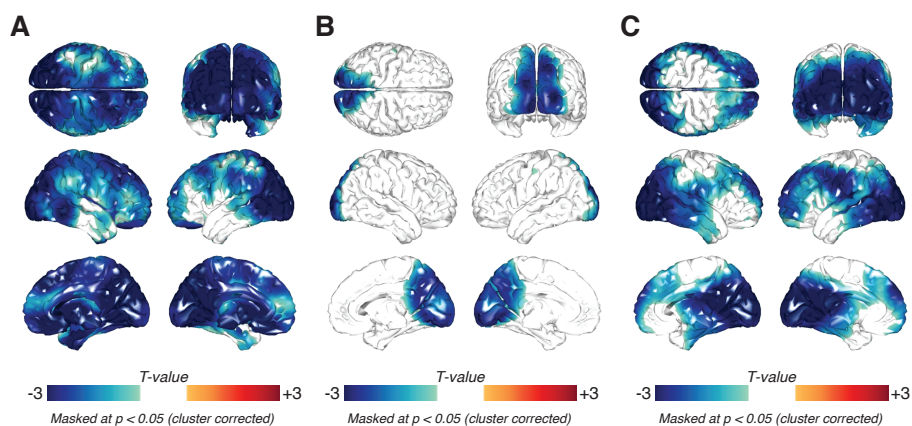


**Figure 6 - Supplemental Figure 1.** External task drive decreases alpha-band power. **(A)** Spatial distribution of task-induced changes in scaling exponents (placebo only; thresholded at  $p = 0.05$ , two-sided cluster-based permutation test). **(B)** Same as (A), but for atomoxetine condition. **(C)** Same as (A) and (B), but for donepezil condition.

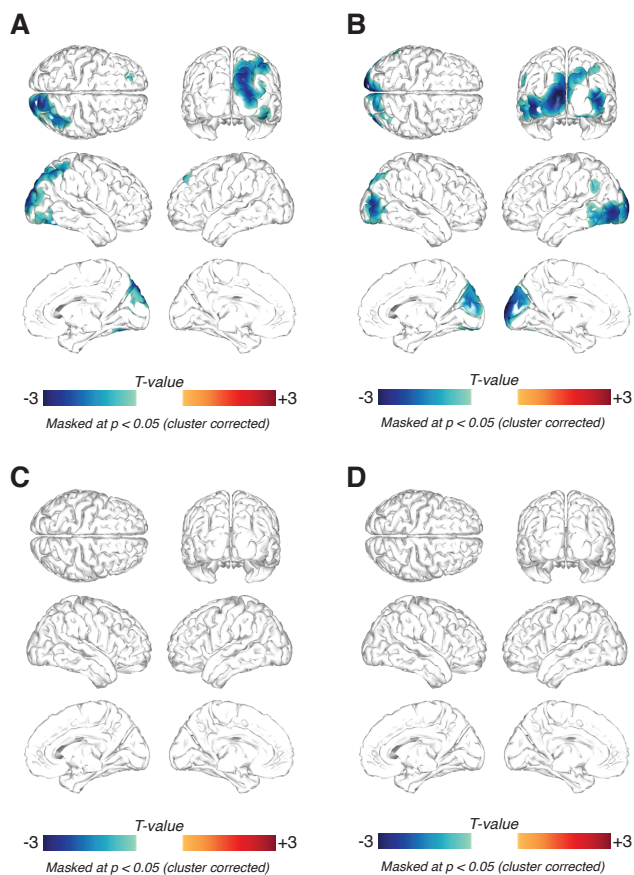


**Figure 8 - Supplemental Figure 1.** Drug-related alpha-band power changes. **(A)** Spatial distribution of atomoxetine-related power changes during rest, thresholded at  $p = 0.05$  (two-sided cluster-based permutation test). **(B)** Same as (A), but for donepezil. **(C)** Spatial distribution of atomoxetine-related power changes during task, thresholded at  $p = 0.05$  (two-sided cluster-based permutation test). **(D)** Same as (C), but for donepezil.

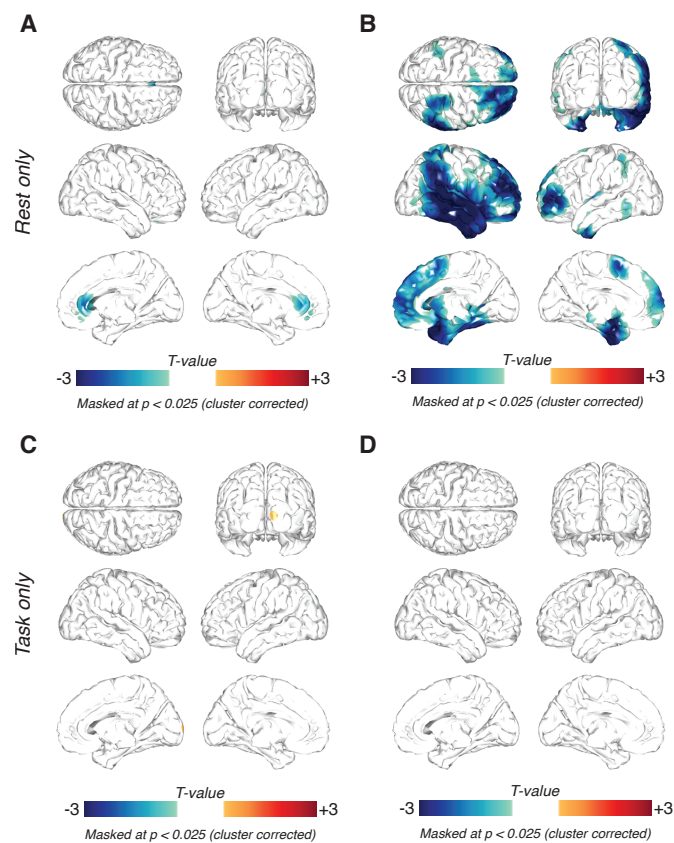


**Figure 8 - Supplemental Figure 2.** Drug-related changes in coefficient of variation. **(A)** Spatial distribution of atomoxetine-related changes in coefficient of variation during rest, thresholded at  $p = 0.05$  (two-sided cluster-based permutation test). **(B)** Same as (A), but for donepezil. **(C)** Spatial distribution of atomoxetine-related changes in coefficient of variation during task, thresholded at  $p = 0.05$  (two-sided cluster-based permutation test). **(D)** Same as (C), but for



#### 4.4. Study 4: Neuromodulation of Functional Connectivity

##### Author contributions:

1. Conceptualization
  2. Investigation
  3. Formal analysis
  4. Writing – Original draft
  5. Writing – Review
  6. Supervision
- \* Contributed equally

Van den Brink, R.L.:	1,2,3,4,5
<b>Pfeffer, T.:</b>	<b>3,5</b>
Warren, C.M.:	2,5
Murphy, P.R.:	2,5
Tona, K.D.:	2
Van der Wee, N.J.A.:	2,5
Giltay, E.:	2,5
Van Noorden, M.S.:	2,5
Rombouts, S.A.R.B.:	1,5
Donner, T.H.:	*,4,5,6
Nieuwenhuis, S.:	*,1,4,5,6

**Status: Published**

# Catecholaminergic Neuromodulation Shapes Intrinsic MRI Functional Connectivity in the Human Brain

 Ruud L. van den Brink,<sup>1,2</sup>  Thomas Pfeffer,<sup>3</sup>  Christopher M. Warren,<sup>1,2</sup>  Peter R. Murphy,<sup>1,2</sup> Klodiana-Daphne Tona,<sup>1,2</sup> Nic J. A. van der Wee,<sup>2,4</sup>  Eric Giltay,<sup>4</sup> Martijn S. van Noorden,<sup>4</sup>  Serge A.R.B. Rombouts,<sup>1,2,5</sup> Tobias H. Donner,<sup>3,6,7\*</sup> and  Sander Nieuwenhuis<sup>1,2\*</sup>

<sup>1</sup>Institute of Psychology, Leiden University, 2333AK Leiden, The Netherlands, <sup>2</sup>Leiden Institute for Brain and Cognition, 2333AK Leiden, The Netherlands, <sup>3</sup>Department of Neurophysiology and Pathophysiology, University Medical Center Hamburg-Eppendorf, 20246, Hamburg, Germany, <sup>4</sup>Department of Psychiatry and <sup>5</sup>Department of Radiology, Leiden University Medical Center, Albinusdreef 2, 2333 ZA Leiden, The Netherlands, <sup>6</sup>Department of Psychology, University of Amsterdam, 1012 WX, Amsterdam, The Netherlands, and <sup>7</sup>Amsterdam Center for Brain and Cognition, Institute for Interdisciplinary Studies, 1001 NK Amsterdam, The Netherlands

The brain commonly exhibits spontaneous (i.e., in the absence of a task) fluctuations in neural activity that are correlated across brain regions. It has been established that the spatial structure, or topography, of these intrinsic correlations is in part determined by the fixed anatomical connectivity between regions. However, it remains unclear which factors dynamically sculpt this topography as a function of brain state. Potential candidate factors are subcortical catecholaminergic neuromodulatory systems, such as the locus ceruleus-norepinephrine system, which send diffuse projections to most parts of the forebrain. Here, we systematically characterized the effects of endogenous central neuromodulation on correlated fluctuations during rest in the human brain. Using a double-blind placebo-controlled crossover design, we pharmacologically increased synaptic catecholamine levels by administering atomoxetine, an NE transporter blocker, and examined the effects on the strength and spatial structure of resting-state MRI functional connectivity. First, atomoxetine reduced the strength of inter-regional correlations across three levels of spatial organization, indicating that catecholamines reduce the strength of functional interactions during rest. Second, this modulatory effect on intrinsic correlations exhibited a substantial degree of spatial specificity: the decrease in functional connectivity showed an anterior–posterior gradient in the cortex, depended on the strength of baseline functional connectivity, and was strongest for connections between regions belonging to distinct resting-state networks. Thus, catecholamines reduce intrinsic correlations in a spatially heterogeneous fashion. We conclude that neuromodulation is an important factor shaping the topography of intrinsic functional connectivity.

**Key words:** catecholamines; functional connectivity; gain; neuromodulation; norepinephrine; resting-state fMRI

## Significance Statement

The human brain shows spontaneous activity that is strongly correlated across brain regions. The factors that dynamically sculpt these inter-regional correlation patterns are poorly understood. Here, we test the hypothesis that they are shaped by the catecholaminergic neuromodulators norepinephrine and dopamine. We pharmacologically increased synaptic catecholamine levels and measured the resulting changes in intrinsic fMRI functional connectivity. At odds with common understanding of catecholamine function, we found (1) overall reduced inter-regional correlations across several levels of spatial organization; and (2) a remarkable spatial specificity of this modulatory effect. Our results identify norepinephrine and dopamine as important factors shaping intrinsic functional connectivity and advance our understanding of catecholamine function in the central nervous system.

## Introduction

The resting-state, here defined as periods during which a participant is not engaged in a complex explicit task, is characterized by

fluctuations in neural activity that are correlated across brain regions (Biswal et al., 1995; Leopold et al., 2003; Fox and Raichle, 2007; Hiltunen et al., 2014). Such spontaneous, correlated fluctu-

Received March 2, 2016; revised May 18, 2016; accepted June 2, 2016.

Author contributions: R.L.v.d.B., S.R., and S.N. designed research; R.L.v.d.B., C.M.W., P.R.M., K.-D.T., N.J.v.d.W., E.G., and M.S.v.N. performed research; R.L.v.d.B., T.P., and T.H.D. analyzed data; R.L.v.d.B., T.P., C.M.W., P.R.M., N.J.v.d.W., E.G., M.S.v.N., S.R., T.H.D., and S.N. wrote the paper.

This work was supported by a European Research Council Consolidator Grant. We thank Elena Allen for her helpful comments; and Henk van Steenbergen and Janna Marie Bas-Hoogendam for help with preprocessing the data. The authors declare no competing financial interests.

\*T.H.D. and S.N. contributed equally to this study as co-senior authors.

tuations exhibit a rich spatial (Yeo et al., 2011) and temporal (Allen et al., 2014; Zalesky et al., 2014) structure that is reflective of the brain's functional organization (Tavor et al., 2016). The strength and spatial distribution of these correlated fluctuations are predictive of behavior and pathological conditions (Greicius et al., 2004; De Luca et al., 2005). Moreover, the global structure, or topography, of correlated activity changes dynamically with alterations in conscious state (Barttfeld et al., 2015) and task conditions (Nir et al., 2006; Sepulcre et al., 2010). While the existence and overall spatiotemporal structure of the spontaneous inter-regional correlations are well established (Fox and Raichle, 2007), uncertainty remains regarding the underlying physiological mechanisms. It has been proposed that correlations across distant brain regions could be induced by brainstem neuromodulatory systems, and in particular the locus ceruleus-norepinephrine (LC-NE) system, which sends diffuse, ascending projections to the forebrain (Leopold et al., 2003; Drew et al., 2008; Schölvink et al., 2010), where noradrenergic terminals corelease dopamine (DA) (Devoto and Flore, 2006). Here, we examined whether and how the catecholaminergic neuromodulators NE and DA shape correlated fluctuations during rest in the human brain.

A number of observations suggest that catecholamines should generally increase the strength of functional connectivity. Both iontophoretic NE application and DA agonism enhance neuronal responses to excitatory synaptic input (Rogawski and Aghajanian, 1980; Seamans et al., 2001b; Wang and O'Donnell, 2001). Furthermore, NE and DA can amplify synaptic GABAergic inhibition (Moises et al., 1979; Seamans et al., 2001a). These and other findings have led to the view that catecholamines boost the efficacy of synaptic interactions between neurons (Berridge and Waterhouse, 2003; Winterer and Weinberger, 2004), resulting in an increased difference in firing rates between strongly and weakly active neurons. Such signal amplification yields a systematic facilitation of signal transmission (Waterhouse et al., 1998). Recent computational work suggests that this effect of catecholamines should boost both positive and negative temporal correlations between the activities of local groups of neurons, resulting in stronger and increasingly clustered network connectivity (Donner and Nieuwenhuis, 2013; Eldar et al., 2013). Putative behavioral and pupillary indices of heightened NE activity have accordingly been shown to co-occur with stronger functional coupling throughout the brain (Eldar et al., 2013). A first consideration of the anatomy of the LC-NE system suggests that these changes in functional connectivity might show little spatial specificity. LC neurons exhibit tightly synchronous firing and collateralize broadly, resulting in largely homogeneous catecholaminergic innervation throughout the brain (Swanson and Hartman, 1975; Aston-Jones et al., 1984; Ishimatsu and Williams, 1996; Berridge and Waterhouse, 2003).

In the present study, we systematically characterized catecholamine effects on the strength and spatial structure of resting-state inter-regional correlations, measured with fMRI. Using a double-blind placebo-controlled crossover design, we manipulated catecholamine activity by administering a single dose of atomoxetine, a selective NE transporter (NET) blocker. Within the cortex, NET is also responsible for DA reuptake, due to the

cortical paucity of DA transporters (Devoto and Flore, 2006). Thus, NET blockers increase both central NE and cortical DA availability (Bymaster et al., 2002; Devoto et al., 2004; Swanson et al., 2006; Koda et al., 2010). We systematically quantified catecholamine effects on functional connectivity: globally, between brain networks, and at the level of individual connections between brain regions. In contrast to the notion of a catecholamine-induced homogeneous increase in functional connectivity, we found that atomoxetine reduced correlations across most pairs of brain regions. Most remarkably, atomoxetine altered the strength of inter-regional correlations in a highly spatially specific manner. These results have important ramifications for our understanding of resting-state activity and central catecholaminergic function.

## Materials and Methods

**Participants.** Neurologically healthy right-handed individuals ( $N = 24$ , age 19–26 years, 5 male) were recruited and medically screened by a physician for physical health and drug contraindications. Exclusion criteria included: standard contraindications for MRI; current use of psychoactive or cardiovascular medication; a history of psychiatric illness or head trauma; cardiovascular disease; renal failure; hepatic insufficiency; glaucoma; hypertension; drug or alcohol abuse; learning disabilities; poor eyesight (myopia  $\leq -6$  diopters); smoking  $>5$  cigarettes a day; and pregnancy. All participants gave written informed consent before the experiment and screening, and were compensated with €135 or course credit.

**Design and functional MRI data.** We used a double-blind placebo-controlled crossover design. In each of two sessions, scheduled 1 week apart at the same time of day, participants received either a single oral dose of atomoxetine (40 mg) or placebo (125 mg of lactose monohydrate with 1% magnesium stearate, visually identical to the drug). Elsewhere, we report data showing that the atomoxetine treatment significantly increased salivary levels of cortisol and  $\alpha$  amylase, reliable markers of sympathetic nervous system and hypothalamus-pituitary-adrenal axis activation, respectively (C. M. Warren, R. L. van den Brink, S. Nieuwenhuis, and J. A. Bosch, unpublished observations), thus confirming drug uptake. In both sessions, participants were scanned once before pill ingestion ( $t = -20$  min) and once at  $t = 90$  min, when approximate peak-plasma levels are reached. The interaction contrast (postatomoxetine – preatomoxetine) minus (postplacebo – preplacebo) allowed us to examine the effects of atomoxetine while controlling for other session-related differences. Each scan comprised 8 min of eyes-open resting-state fMRI. During scanning, the room was dark, and participants fixated on a black fixation cross presented on a gray background.

**MRI data collection and preprocessing.** All MRI data were collected with a Philips 3T MRI scanner. In each of the scanning sessions, we collected a T2\*-weighted EPI resting-state image (echo time 30 ms, repetition time 2.2 s, flip angle 80°, FOV 80 × 80 × 38 voxels of size 2.75 mm isotropic, and 216 volumes). To allow magnetic equilibrium to be reached, the first 5 volumes were automatically discarded.

In addition, each time the participant entered the scanner, we collected a  $B_0$  field inhomogeneity scan (echo time 3.2 ms, repetition time 200 ms, flip angle 30°, and FOV 256 × 256 × 80 voxels with a reconstructed size of 0.86 × 0.86 mm with 3-mm-thick slices). Finally, at the start of the first session, we collected a high-resolution anatomical T1 image (echo time 4.6 ms, repetition time 9.77 ms, flip angle 8°, and FOV 256 × 256 × 140 voxels with size 0.88 × 0.88 mm with 1.2-mm-thick slices).

We used tools from the FMRIB Software Library for preprocessing of the MRI data (Smith et al., 2004; Jenkinson et al., 2012). EPI scans were first realigned using MCFLIRT motion correction and skull-stripped using BET brain extraction. We used  $B_0$  unwarping to control for potential differences in head position each time the participant entered the scanner and resulting differences in geometric distortions in the magnetic field. The  $B_0$  scans were first reconstructed into an unwrapped phase angle and magnitude image. The phase image was then converted to units radians per second and median-

filtered, and the magnitude image was skull-stripped. We then used FEAT to unwarped the EPI images in the  $y$ -direction with a 10% signal loss threshold and an effective echo spacing of 0.332656505.

The unwarped EPI images were then high-pass filtered at 100 s, pre-whitened, smoothed at 5 mm FWHM, and coregistered with the anatomical T1 to 2 mm isotropic MNI space (degrees of freedom: EPI to T1, 3; T1/EPI to MNI, 12). Any remaining artifacts (e.g., motion residual, susceptibility-motion interaction, cardiac and sinus artifacts) were removed using FMRIB's ICA-based X-noiseifier (Griffanti et al., 2014; Salimi-Khorshidi et al., 2014) with pretrained weights (Standard.RData). Noise classification performance was checked afterward, by manually classifying components as "signal," "noise," or "unknown." Then, the accuracy of the automated artifact detection algorithm was quantified as the percentage of components that had the label "noise" in both classifications. The accuracy was found to be 96.4% correct. All subsequent analyses were conducted in MATLAB 2012a (The MathWorks).

**Physiological recordings and correction.** We recorded heart rate using a pulse oximeter and breath rate using a pneumatic belt at 500 Hz during acquisition of each EPI scan. We used these time series for retrospective image correction (RETROICOR) (Glover et al., 2000). This method assigns cardiac and respiratory phases to each volume in each individual EPI time series, which can then be removed from the data. The physiological time series were first down-sampled to 100 Hz. Next, the pulse oximetry data were bandpass filtered between 0.6 and 2 Hz, and the respiration data were low-pass filtered at 1 Hz, using a two-way FIR filter. We then extracted peaks in each time series corresponding to maximum blood oxygenation and maximum diaphragm expansion. The interpeak intervals were then converted to phase time by linearly interpolating across the intervals to between 0 and  $2\pi$ . Next, we used these phase time series to extract the sine- and co-sine components of the dominant and first harmonic Fourier series of each signal. After down-sampling to the EPI sample rate, this yielded 8 regressors (4 cardiac and 4 respiratory) that could then be used to remove cardiac and respiratory effects from the BOLD time series using multiple linear regression. The findings reported here were based on noncorrected data, but we replicated all of our results using the RETROICOR-corrected data (see Results).

**Pupillometry.** Pupil size was measured from the right eye at 500 Hz with an MRI-compatible Eyelink 1000 eye tracker. Blinks and other artifacts were interpolated offline using shape-preserving piecewise cubic interpolation. Pupil data were low-pass filtered at 5 Hz to remove high-frequency noise and  $Z$ -scored across conditions. Five participants were excluded from pupil-related analyses due to poor signal quality (>50% of continuous time series interpolated) or missing data. Of the remaining participants, on average 20% (SD 9%) of the data were interpolated.

**Brain parcellation and connectivity.** Time series of brain regions were extracted for the 90 regions of the Automated Anatomical Labeling (AAL) atlas (Tzourio-Mazoyer et al., 2002) (see Fig. 1a). We did not include the cerebellum because it was not fully inside the FOV for all participants. Following averaging across voxels within each brain region, time series ( $M$ ) for each run  $i$  were  $Z$ -scored and correlation matrices ( $R$ ) were computed between them via the following:

$$R_i = \frac{M_i' \cdot M_i}{nTR - 1}$$

where  $'$  denotes transposition and  $nTR$  is the number of volumes (211). Because positive and negative correlations jointly determine a network's functional organization (Fox et al., 2005), many prior studies have used the absolute value of the correlation coefficient to describe functional interactions (Achard and Bullmore, 2007; Eldar et al., 2013; Li et al., 2013). Moreover, computational work suggests that catecholamines should boost temporal correlations regardless of their sign (Donner and Nieuwenhuis, 2013; Eldar et al., 2013). We therefore used the absolute correlation coefficient as our measure of connectivity strength. The signed and absolute matrices were very similar because anticorrelations were rare (mean 3.4% of all connections, SD 3.5%), as is common when no global signal regression has been performed. In the group- and condition-averaged correlation matrix, 0.28% were anticorrelations (11 of 4005 unique connections; see Fig. 1b). To facilitate comparisons of

values across participants, we range-normalized each participant's absolute correlation matrices between 0 and 1 across the 4 conditions. This procedure discarded the between-participant variance while leaving the spatial structure and between-condition variance intact.

In addition, for the postatomoxetine condition time-resolved connectivity (Allen et al., 2014) was computed for 189 tapered windows  $w$  of length  $nw$  (22 volumes) via the following:

$$R_{wi} = \frac{M'_{wi} \cdot M_{wi}}{nw - 1}$$

The taper was created by convolving a Gaussian (SD 3 TRs) with a rectangle.  $R_{wi}$  was Fisher-transformed to stabilize variance across windows. We then again used the absolute value as our measure of connectivity strength. An identical sliding window was applied to the pupil diameter data in the postatomoxetine condition such that for each window in  $R_{wi}$  there was a corresponding value of pupil size during that window. Then, we divided up pupil size into 3 equal-sized bins and averaged the corresponding values in  $R_{wi}$  for each pupil bin separately. To rule out the possibility that the results depended on the choice of bin size, we also tried alternate bin sizes (2, 5, and 7 bins) and found similar effects.

**Graph-theoretical analysis of global correlation structure.** For each condition, we constructed a binary undirected (adjacency) matrix  $A$ . We did this by first concatenating the correlation matrices across participants such that for each condition we had a brain region by brain region by  $N$  ( $90 \times 90 \times 24$ ) matrix of connectivity. We then assessed with a  $t$  test across the participant dimension for each element  $y, x$  in the connectivity matrix whether its value differed significantly from the average of its row  $y$  or column  $x$  (Hipp et al., 2012). In other words, for each connection, we obtained a distribution across participants of weighted values, and two distributions corresponding to the mean weighted values of each brain region that was linked by that particular connection. The connection distribution was then compared with each of the brain region distributions with a  $t$  test. If either of the two comparisons was significant, the connection was scored as 1, and otherwise it was scored as 0. The  $\alpha$  level was set to 0.01, Bonferroni-corrected for two comparisons to 0.005 (Hipp et al., 2012).

This procedure, as opposed to simply applying a fixed-percentage threshold, results in adjacency matrices that can differ in the number of connections between conditions, and therefore allows the assessment of correlation structure, or degree. We thus quantified the global degree  $k$  in each condition as the average across the adjacency matrix (Hipp et al., 2012) via the following:

$$k = n^{-1} \sum_{x=1}^n n^{-1} \sum_{y=1}^n A(x, y)$$

where  $n$  is the number of brain regions in the AAL atlas.

To test the prediction that increased catecholamine levels should result in stronger functional connectivity, we used  $k$  as our measure of connectivity strength rather than relying on the mean weighted values (i.e., the average of  $R_i$ ). The binarization of weighted graphs is common in functional network analysis (Achard and Bullmore, 2007; Rubinov and Sporns, 2010; Hipp et al., 2012; Li et al., 2013) and is intended to preserve only the strongest (most probable) connections. This ensures that weak edges, which are more likely to be spurious (Rubinov and Sporns, 2010), do not convolute the global mean. Given that these edges are less likely to reflect true neurophysiological interactions, they are less likely to be sensitive to any experimental manipulation that is specifically intended to alter neurophysiology (in our case, drug intake). Thus, excluding these connections decreases the likelihood of false negatives in between-condition comparisons of the global mean. In addition, by treating each connection equally (either present or absent), the global mean is not disproportionately influenced by extremely strong connections that are more likely to decrease in strength after an experimental manipulation by virtue of regression toward the mean.

Furthermore, by defining adjacency matrices using a statistical test across participants, each connection that is present in the adjacency matrix is ensured to be reliably expressed across the group of participants for a given condition. Thus, the adjacency matrices are representative of the



group-level topography of connectivity. We used two measures of clustering, defined using these group-level adjacency matrices, to test the prediction that an increase in central catecholamine levels should be accompanied by more strongly clustered network connectivity. The clustering coefficient  $C$  was quantified as the average fraction of triangles  $\tau$  around a node, the latter given by the following:

$$\tau_x = 2^{-1} \sum A(x, y) A(x, z) A(y, z), \text{ where } y, z \in N$$

and  $N$  represents the total set of nodes.  $C$  was then given by the following:

$$C = n^{-1} \sum_{y=1}^n n^{-1} \sum_{x=1}^n \frac{2\tau_x}{k_x(k_x - 1)}$$

The clustering coefficient here is equivalent to the average proportion of the node's neighbors that are in turn neighbors to each other (Watts and Strogatz, 1998; Rubinov and Sporns, 2010). Thus, the clustering coefficient represents the mean fraction of clustering around each node.

Because  $C$  is normalized by degree ( $k$ ) individually per node, it may be biased by nodes with a relatively low  $k$ . We therefore also included a measure of clustering that is normalized by  $k$  collectively and hence does not suffer from the same potential bias. This measure is known as transitivity ( $T$ ), and is given by the following:

$$T = \frac{\sum_{x=1}^n 2\tau_x}{\sum_{x=1}^n k_x(k_x - 1)}$$

This is equivalent to the ratio of triangles to triplets in the network. Both clustering coefficient and transitivity capture the extent to which the network is segregated in terms of processing because a large number of triangles implies functional clustering. These two measures were computed using the Brain Connectivity Toolbox (Rubinov and Sporns, 2010). Both clustering and transitivity are (partially) dependent on global degree (van Wijk et al., 2010).

To test statistically whether degree, clustering coefficient and transitivity differed between conditions, we used nonparametric permutation testing. We shuffled the condition labels for each participant before computing the adjacency matrices and then computed the graph-theoretical measures. This was done for 10,000 iterations to produce a null distribution. We then derived a  $p$  value for each contrast by dividing the number of null observations less extreme than the observed contrast by the total number of null observations, and subtracting this value from 1.

**Network identification via community detection.** We used the Louvain method for community detection optimized for stability (Blondel et al., 2008; Le Martelot and Hankin, 2013) to classify each brain region as belonging to a particular network, or module. This method works by maximizing the number of within-group connections (edges) while minimizing the number of between-group connections via greedy optimization. We first defined an adjacency matrix  $A_s$  by concatenating the condition-averaged correlation matrices across participants, and then statistically comparing each element  $y, x$  to the average of its row  $y$  or column  $x$ , similar as described above. However, to accurately classify networks, we needed to retain only those connections that were most informative about community structure. We therefore promoted sparsity in the condition-averaged adjacency matrix by defining it using a one-tailed  $t$  test with a conventional  $\alpha$  level (0.05) and a correction for multiple comparisons using the false discovery rate (FDR). This preserved only those connections that were consistently the strongest across participants (16.9% of all possible connections). We then submitted this sparse condition-averaged adjacency matrix to the Louvain community detection algorithm. The optimization procedure (Le Martelot and Hankin, 2013) ensured a stable solution across multiple runs of the algorithm. In the optimization procedure, the Markov time acts as a resolution parameter that determines the community scale, and thus the number of modules that the algorithm will return. This parameter was set to 0.9, resulting in 6 separate modules. We set the number of modules to be detected to 6 because, given the relatively coarse anatomical layout of the AAL atlas, this number yielded a relatively reliable modular organi-

zation. The community detection and optimization resulted in a “module number” for each AAL brain region indicating to which module it belonged, and a single  $Q$  value indicating the strength of modularity.

We first verified whether the  $Q$  value was significantly higher than chance. To do so, we generated 10,000 randomized null networks with an identical size, density, and degree distribution as  $A_s$  (Maslov and Sneppen, 2002), and submitted them to Louvain community detection and optimization to produce a null-distribution of  $Q$  values. We then derived a  $p$  value for the observed modularity by dividing the number of null  $Q$  values less extreme than the empirical  $Q$  value by the total number of null  $Q$  values, and subtracting it from 1.

The observed  $Q$  value of 0.46 was significantly higher than chance ( $p < 0.001$ ), showing that group-average connectivity was strongly modular. We then visualized the modular structure by rearranging the condition-averaged correlation matrix by module. The assignment of brain regions to modules corresponded closely to a number of well-characterized intrinsic connectivity networks, indicating that the modular structure reflected a functionally meaningful grouping of brain regions.

**Graph-theoretical analysis of network structure.** The procedure described above allowed us to group brain regions into modules of intrinsically coupled AAL brain regions. We could then use these modules to assess changes in the structure of intrinsic correlations at the within- and between-network level, rather than as a function of the system in its entirety. To do this, we first rearranged the condition-specific adjacency matrices by their module number, and computed average degree of elements within and between modules via the following:

$$k_m = n_a^{-1} \sum_{x_a=1}^{n_a} n_b^{-1} \sum_{y_b=1}^{n_b} A_s(x_a, y_b)$$

where  $n_a$  is the number of brain regions belonging to module  $a$  and  $n_b$  is the number of brain regions in module  $b$ . This yielded, for each condition, a symmetric and module-by-module matrix of continuous average degree values, in which values on the diagonal indicated the average number of connections within each module, and each value around the diagonal indicated the average number of connections between a combination of modules.

We could then use these “module matrices” to test for atomoxetine-related changes in degree of the connections within modules, and the connections linking different modules. This allowed us to characterize changes in connectivity in a spatially more specific way than for global degree. We again used nonparametric permutation testing, similar as described for global degree, except that it was done for individual elements within the module matrices.

**Control analyses using an alternate atlas and multiple thresholds.** To rule out the possibility that our results were specific to the use of the AAL atlas, we repeated all of our key analyses using the atlas made available by Craddock et al. (2012), which comprised 87 distinct regions after excluding the cerebellum, and found similar effects in terms of both direction and significance. Moreover, to verify that our results were independent of the statistical threshold used to define the adjacency matrices, we conducted a control analysis in which a range of adjacency matrices was created per condition with varying condition-averaged connection densities (40%–75%). This was done by progressively raising/lowering the  $\alpha$  level of the  $t$  test that was used to determine whether a connection is present or absent (see above). Then, for each threshold we computed the graph-theoretical measures, and for each condition and measure separately calculated the area under the curve across thresholds. This allowed us to compare the area under the curve between conditions with permutation testing (10,000 iterations). For all measures, the critical interaction contrast was significant and in the same direction as our original findings (see Results).

**Controlling for regression toward the mean.** The correlation between baseline coupling strength and the atomoxetine-related change in coupling strength (see Fig. 3e; see Results) is confounded by regression toward the mean. That is, if two particular brain regions show strong baseline coupling, then simply by chance they are more likely to show a reduction under atomoxetine, and so a negative correlation is likely to occur. We therefore controlled for regression toward the mean using

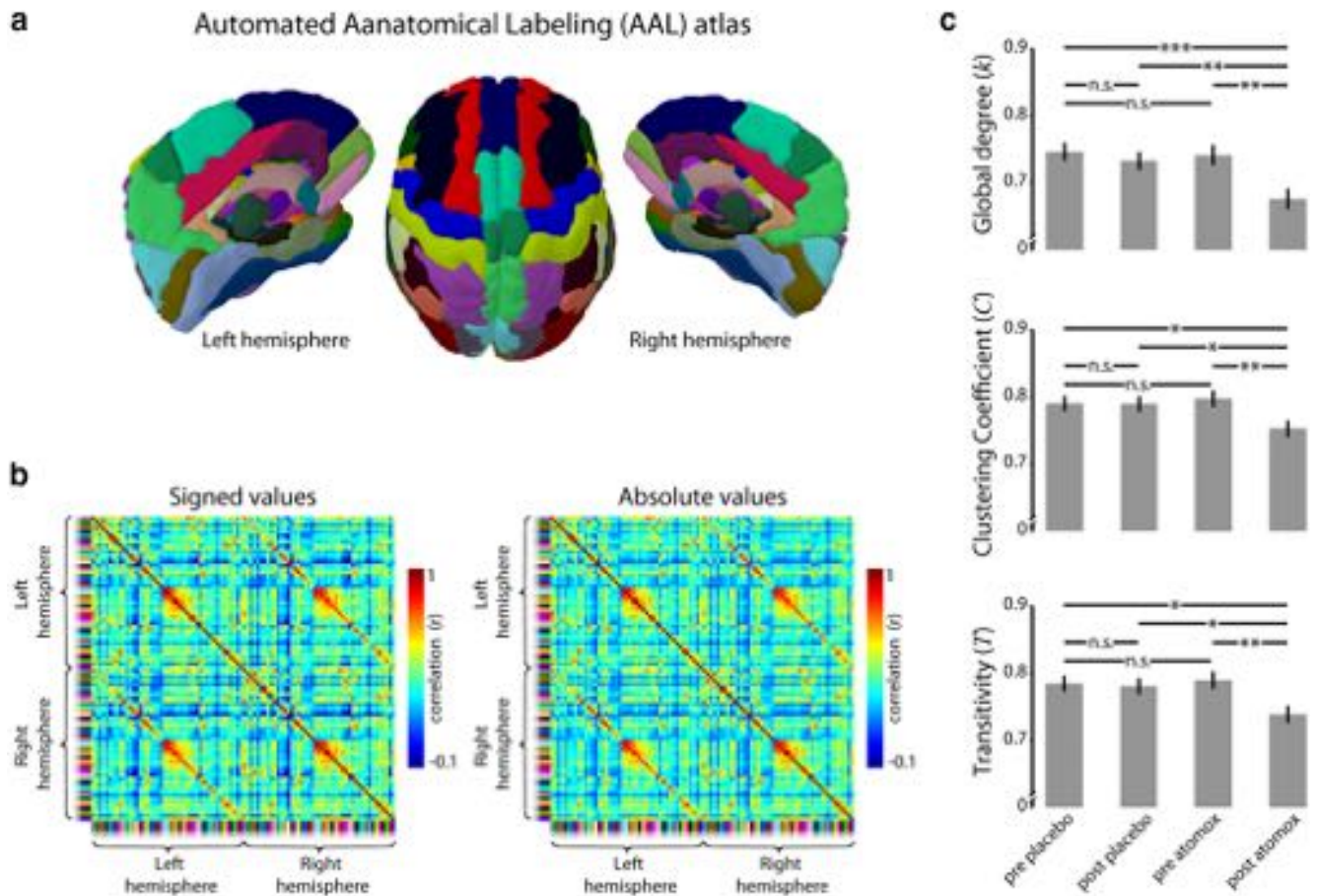


**Figure 1.** Inter-regional correlation and global graph-theoretical results. *a*, Topography of the AAL atlas. Each brain region within hemispheres has a unique color. *b*, Condition-averaged inter-regional correlation. Both the signed and absolute values are shown. Color labels on the left and bottom axes represent brain regions in *a*. *c*, Atomoxetine-related effects on global graph-theoretical measures. Error bars indicate the SD of the bootstrapped null-distribution. n.s., Not significant. \* $p < 0.05$ . \*\* $p < 0.01$ . \*\*\* $p < 0.001$ .

permutation testing. For 10,000 permutations, we shuffled the condition labels across participants before computing the atomoxetine-related change in coupling strength. We then computed the correlation between baseline coupling and atomoxetine-related change in coupling to produce a distribution of correlation coefficients under the null hypothesis of regression toward the mean. Finally, we derived a  $p$  value for the empirical correlation coefficient by dividing the number of null observations less extreme than the correlation coefficient by the total number of null observations, and subtracting this value from 1. This  $p$  value indicated the significance of the observed correlation coefficient beyond regression toward the mean.

**Analysis of BOLD signal variance.** We calculated for each participant and each AAL brain region the fractional amplitude (i.e., variance) of low-frequency fluctuations in the non-Z-scored BOLD time series (fALFF) (Zou et al., 2008). This measure indexes the relative contribution of low-frequency (0.01–0.08 Hz) fluctuations to the total amplitude spectrum. We compared fALFF between conditions using repeated-measures ANOVA. Additionally, for each participant, we correlated the atomoxetine-related change in fALFF with the atomoxetine-related change in inter-regional correlation strength across AAL brain regions. We then compared the distribution of Fisher-transformed correlation coefficients to zero using a two-tailed  $t$  test. Very similar results were obtained using alternative measures of variance (e.g., average 0.01–0.08 Hz amplitude or the signal SD rather than fractional amplitude).

## Results

### Atomoxetine reduces global degree and clustering

In a first set of analyses, we examined the effect of atomoxetine on graph-theoretical summary measures of functional connectivity

strength. We parcellated each participant's brain into 90 separate regions according to the AAL atlas (Tzourio-Mazoyer et al., 2002) (Fig. 1*a*) and computed the correlation between the Z-scored time series of all pairs of regions (Fig. 1*b*). We then took the absolute correlation coefficient as our measure of functional connectivity strength (see Materials and Methods). In general, functional connectivity was strongest between visual cortical areas and between homolog areas in both hemispheres (Fig. 1*b*), consistent with a host of previous work (Fox and Raichle, 2007).

For each condition (preplacebo, postplacebo, preatomoxetine, postatomoxetine), we constructed a binary matrix of connections (edges) between pairs of brain regions that consistently differed in strength across participants from the average of other connections involving either of the two brain regions (following Hipp et al., 2012). Graph theory allowed us to capture different properties of these matrices of intrinsic correlations in a small number of diagnostic scalar quantities (Bullmore and Sporns, 2009; Rubinov and Sporns, 2010). Specifically, we assessed three such measures: the global degree, which indexes the number of strongly correlated regions (above a certain threshold; see Materials and Methods) in the network, and two descriptors of the extent to which network connectivity is clustered in segregated local groups of brain regions: clustering coefficient and transitivity, both of which are (partially) dependent on the strength of connectivity (van Wijk et al., 2010; Eldar et al., 2013). If cat-

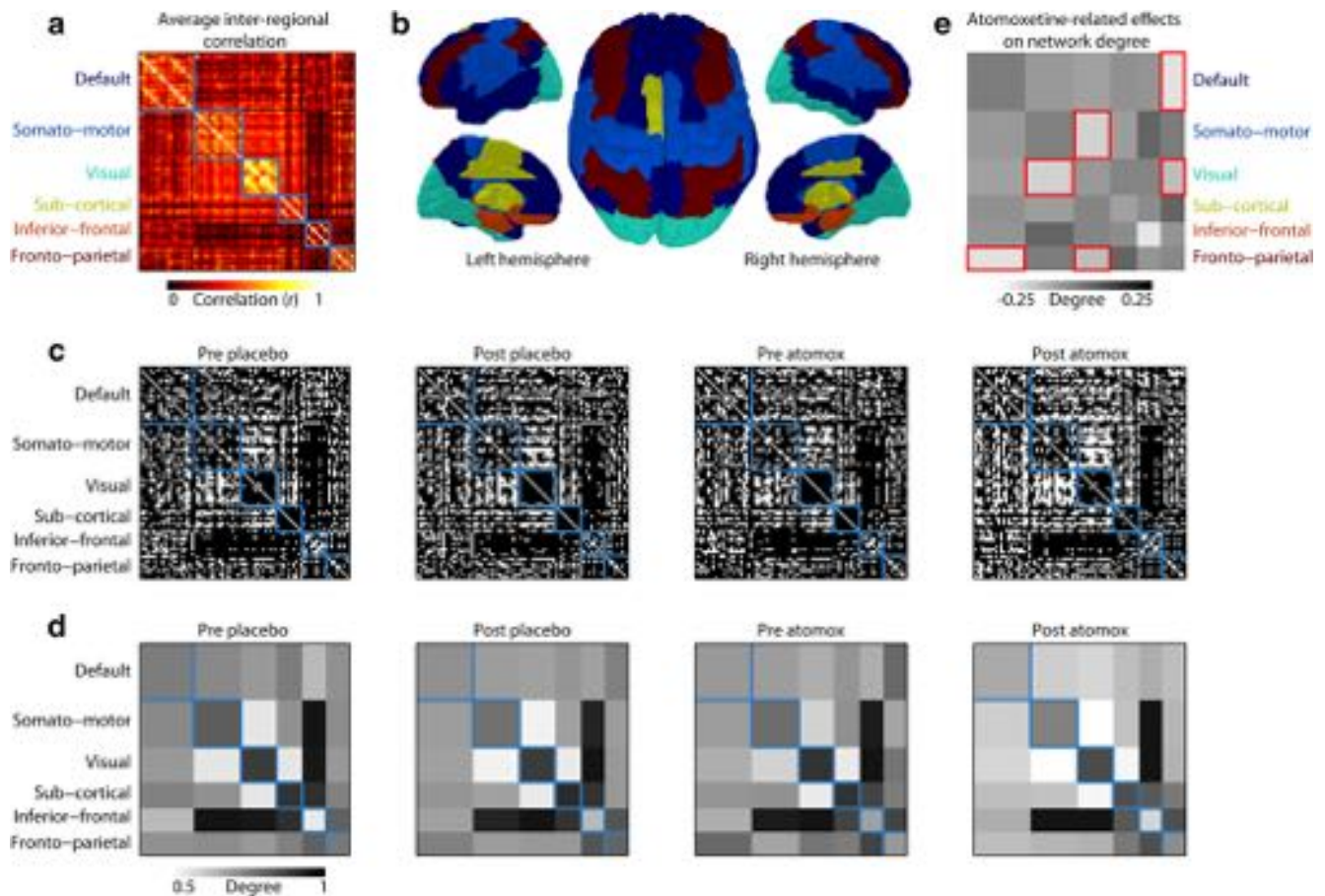


**Figure 2.** Intrinsic connectivity networks and changes in graph-theoretical measures of network structure. *a*, Condition-averaged inter-regional correlation arranged by network. The networks are outlined in blue. *b*, Topography of functional networks. Colors correspond to the labels in *a*. *c*, Condition-specific adjacency matrices arranged by network. Black elements indicate that a connection is present. *d*, Average degree for within- and between-network connections. To facilitate visual comparison, the size of each network is the same as in *c*. However, all statistical comparisons were conducted on symmetrically sized matrices in which each network contributed equally to the global mean. *e*, Atomoxetine-induced changes in degree for connections within and between networks. Shades of gray represent the value of the interaction contrast (postatomoxetine – preatomoxetine) minus (postplacebo – preplacebo). Significant ( $p < 0.05$ ) changes in degree are outlined in red.

echolamines increase global functional connectivity, then atomoxetine should increase all three measures.

Figure 1c shows that atomoxetine significantly *reduced* the number of strong correlations present in the network, as indicated by lower global degree. This was reflected in a significant interaction between treatment and time ( $p = 0.039$ ). A similar pattern of results was found for the two measures of clustering, both of which decreased in magnitude (Fig. 1c): clustering coefficient ( $p = 0.043$ ) and transitivity ( $p = 0.048$ ). Thus, atomoxetine reduced the number of strongly correlated brain regions, as well as the extent to which correlated brain regions formed local functional ensembles. Together, these results show that atomoxetine decreases, rather than increases, overall inter-regional correlations in the brain at rest.

#### Atomoxetine reduces internetwork degree

Many studies of resting-state activity in humans have revealed a consistent set of groups, or modules, of brain regions that are characterized by strong coupling between brain regions belonging to the same module, and weaker coupling between brain regions belonging to different modules (Bullmore and Sporns, 2009). These modules are often referred to as “intrinsic functional connectivity networks” (Fox and Raichle, 2007). In a next set of analyses, we investigated atomoxetine-related changes in

the strength of functional connectivity within and between these networks.

To do this, we arranged the connectivity matrix by network (Fig. 2a) (Blondel et al., 2008). This resulted in 6 functional networks that correspond closely to previously reported resting-state networks (Yeo et al., 2011; Zalesky et al., 2014). Based on their topography (Fig. 2b), we termed them: default; somatomotor; visual; subcortical; inferior-frontal; and frontoparietal networks. We then calculated the average number of connections within and between these networks, resulting in a  $6 \times 6$  network degree matrix for each condition (Fig. 2c,d). Finally, we examined atomoxetine-related changes in within- and between-network degree using permutation testing. This allowed us to explore whether changes in functional connectivity occurred in intranetwork or internetwork connections. The atomoxetine-related reduction in global degree (Fig. 1c) is visible in the network degree matrices as an overall increase in “brightness” in Figure 2d (right).

Consistent with the decrease in global degree reported above, we observed only atomoxetine-related reductions in network degree (Fig. 2e). The interaction between treatment and time was significant for the connections between the visual and somatomotor networks ( $p < 0.001$ ), between the visual and frontoparietal networks ( $p = 0.044$ ), and between the frontoparietal and default networks ( $p < 0.001$ ). After using the FDR ( $q = 0.05$ ) to



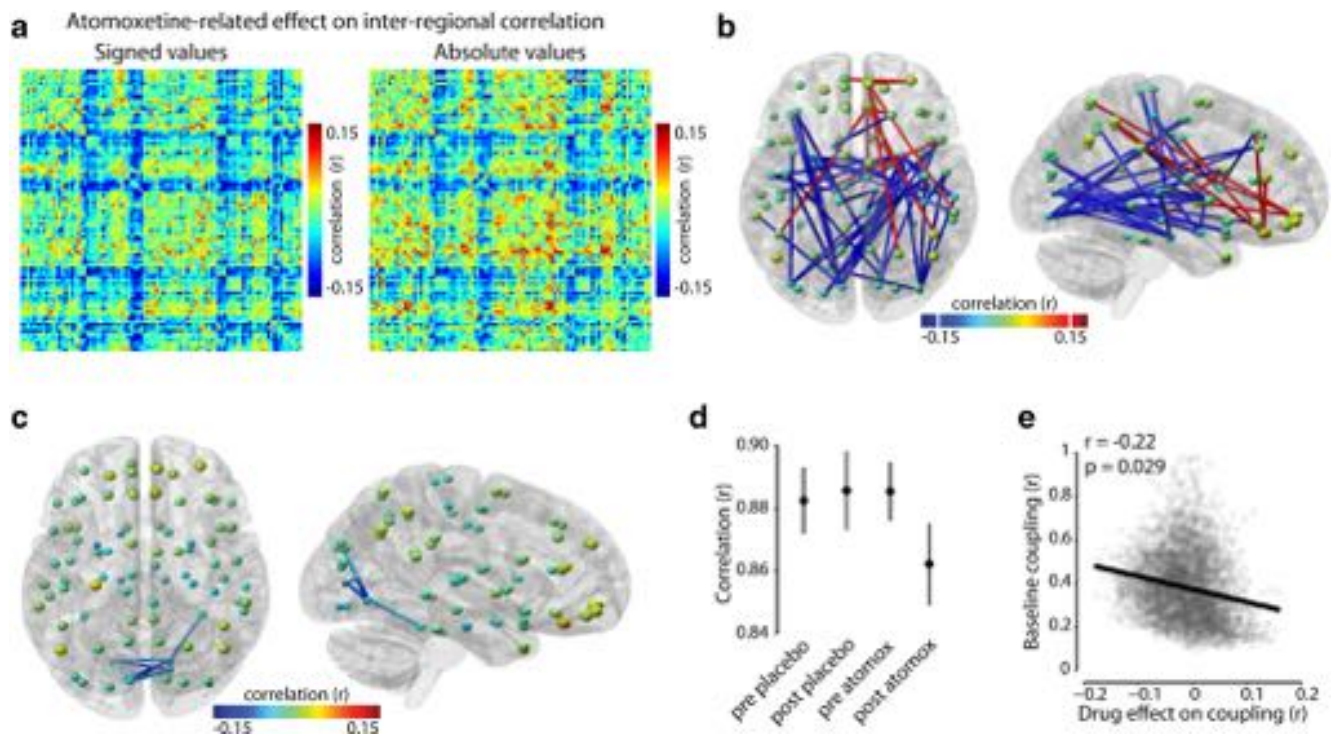


**Figure 3.** Atomoxetine-related effects on inter-regional correlation. **a**, Region-by-region matrix of atomoxetine-related changes in inter-regional correlation strength. Colors represent the value of the interaction contrast (postatomoxetine — preatomoxetine) minus (postplacebo — preplacebo). Blue represents reduced correlation following atomoxetine. The matrices are organized following Figure 1b. **b**, Atomoxetine-related effect on the absolute inter-regional correlation coefficient, rendered in 3D with an arbitrary threshold applied. White dashes in the color bar indicate threshold. Spheres are placed in the center of mass of their respective AAL atlas regions. Both the size and color indicate the average atomoxetine-related effect on coupling (i.e., the average across rows or columns in **a**). **c**, Transverse (top is anterior) and sagittal (right is anterior) view on 3D rendering of significant correlation changes, resulting from the whole-brain two-step analysis. Individual connections that changed significantly with atomoxetine are plotted as cylinders between the corresponding regions. **d**, Inter-regional correlation in each condition, averaged across the significant connections shown in **c**. Error bars indicate the SEM. **e**, Correlation between baseline inter-regional correlation strength (collapsed across preplacebo and preatomoxetine) and change with atomoxetine. Each dot represents a unique region-by-region connection. Self-connections were excluded.

correct for multiple comparisons, all connections, except the connection between the visual and frontoparietal networks, remained significant. However, when comparing the area under the curve across a range of thresholds (see Materials and Methods), all connections remained significant after FDR correction.

Interestingly, all significant reductions in network degree were in connections between (as opposed to within) functional networks. Thus, the most robust decreases in functional coupling occurred for connections linking functionally dissociable groups of brain regions. These results corroborate the conclusion drawn above: that atomoxetine decreased inter-regional correlations in the brain at rest. More importantly, these results provide a first indication that this reduction in inter-regional correlations is not spatially homogeneous across the brain. In the following, we further characterize the spatial heterogeneity of the atomoxetine-induced reductions in inter-regional correlations.

#### Regionally specific reductions and baseline-dependent changes in connectivity with atomoxetine

Having assessed the topographical changes induced by atomoxetine at the global level and the level of functional networks, we next assessed differences in the strength of inter-regional correlations at the level of individual connections between brain regions, using the absolute correlation coefficient. We found that atomoxetine altered correlation strength in a strikingly structured fashion (Fig. 3a): In general, connectivity was reduced by atomoxetine, especially in posterior brain regions (Fig. 3b). These observations align with our findings of reductions in internet-

work degree involving the visual system. To quantify these effects, we used a two-step procedure. Specifically, we first derived a set of data-driven hypotheses by identifying, in the first half of the fMRI volumes, the limited number of individual connections that exhibited an atomoxetine-related change in connectivity that was reliable across participants ( $p < 0.05$ , using a two-tailed  $t$  test), thereby reducing the number of comparisons for the subsequent step. We then retested those connections using the (independent) second half of the volumes and selected those that again showed a systematic atomoxetine-related change in correlation strength ( $p < 0.005$ , two-tailed). Atomoxetine significantly lowered correlation strength in a cluster of occipital brain regions (Fig. 3c,d), specifically correlations between left calcarine cortex and right calcarine cortex/bilateral lingual gyrus; between left cuneus and right calcarine cortex/lingual gyrus; between left lingual gyrus and right calcarine cortex/lingual gyrus; and between right lingual gyrus and right calcarine cortex/right fusiform gyrus. These contiguous connections remained significant after applying a highly conservative cluster size threshold ( $p < 0.0001$ ), obtained by generating a distribution of maximum cluster sizes under the null hypothesis with permutation testing (Nichols and Holmes, 2002). Thus, the cluster involved significantly more connections than would be expected by chance.

We did not find significant changes in connectivity between structures of the basal ganglia, which have been widely studied in relation to catecholaminergic drug effects (Sulzer et al., 2016). This lack of an atomoxetine-related effect in the human basal ganglia is consistent with the observation that the basal ganglia



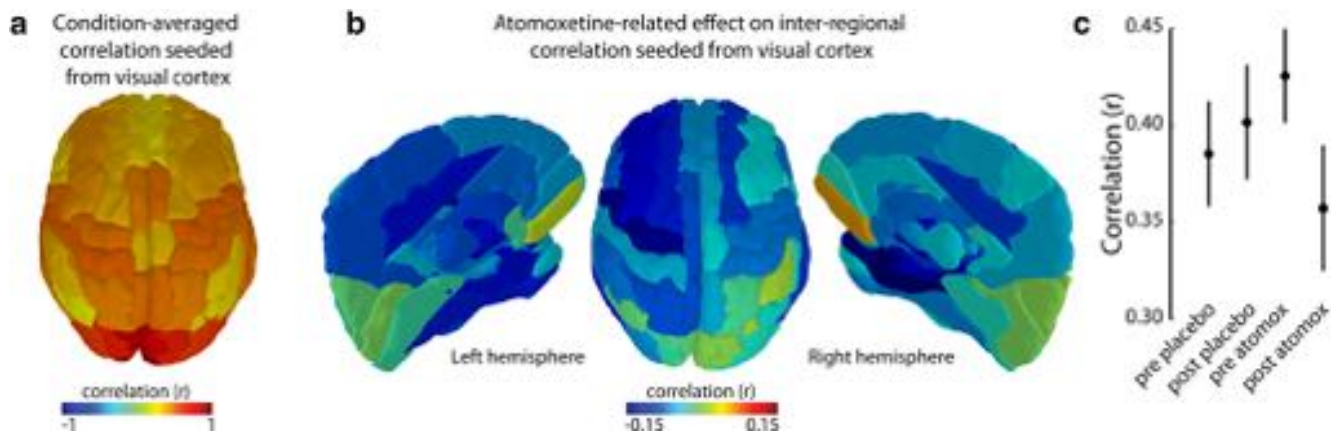


**Figure 4.** Atomoxetine reduces correlation strength between early visual (pericalcarine) cortex and the rest of the brain. *a*, Topography of condition-averaged correlation seeded from left and right early visual cortex. *b*, Topography of atomoxetine-related effects on correlation seeded from left and right early visual cortex. Colors represent the value of the interaction (postatomoxetine – preatomoxetine) minus (postplacebo – preplacebo). *c*, Median correlation values across the brain seeded from left and right early visual cortex. Error bars indicate the SEM.

receive relatively sparse noradrenergic innervation (Aston-Jones et al., 1984), and with findings that atomoxetine has little effect on DA levels within the basal ganglia of rodents (Bymaster et al., 2002). Indeed, unlike in the cortex, in the basal ganglia there is an abundance of DA transporter (Sulzer et al., 2016), so DA reuptake is not dependent on the NE transporter. Thus, our finding that atomoxetine reduced the strength of inter-regional correlations in (predominantly visual) cortical areas is consistent with the specific effect of atomoxetine on synaptic catecholamine levels within the cortex.

In sum, atomoxetine lowered the strength of correlations between visual cortical brain regions (Fig. 3*c*), regions that on average showed strong connectivity (Figs. 1*b*, 2*a*). This raises the question whether the atomoxetine-induced change in connectivity was dependent on the baseline level of connectivity between any pair of brain regions. To address this question, we correlated weighted coupling strength collapsed across the preplacebo and preatomoxetine conditions (i.e., baseline connectivity) with the coupling change following atomoxetine (controlling for regression toward the mean with permutation testing). The observed correlation between baseline connectivity strength and the change with atomoxetine was significant ( $r = -0.22$ ,  $p = 0.029$ ; Fig. 3*e*). This indicates that the strongest functional connections tended to show the largest connectivity reductions after atomoxetine, and vice versa.

#### Atomoxetine induces decoupling of early visual cortex from the rest of the brain

As noted above, atomoxetine reduced correlations between occipital brain regions. To establish whether these occipital regions also showed reduced coupling to the rest of the brain, as suggested by visual inspection (Fig. 3*b*), we computed a summary statistic (median) of correlation strength between early visual (pericalcarine) cortex and all other AAL atlas regions. There were no differences between left and right early visual cortex, so we collapsed the data across hemispheres.

Average connectivity seeded from early visual cortex is shown in Figure 4*a*. Atomoxetine reduced connectivity between early visual cortex and the rest of the brain, as reflected by a significant interaction between treatment and time ( $F_{(1,23)} = 5.31$ ,  $p = 0.031$ ; Fig. 4*b,c*). The only significant pairwise comparison was postatomoxetine versus preatomoxetine ( $t_{(23)} = 2.34$ ,  $p = 0.028$ ). Together, these results suggest that the early visual cortical areas

not only decoupled from each other following atomoxetine (Fig. 3*c*) but also from the rest of the brain.

The results of our analyses at the level of individual connections between brain regions converge with those at the global level and at the level of networks of brain regions, showing that atomoxetine decreased functional connectivity. In addition, the results show that atomoxetine modulated functional connectivity in a highly regionally specific fashion, with more robust changes in visual cortex than in other brain areas.

#### Excluding alternative explanations

In five sets of control analyses, we ruled out the possibility that the atomoxetine-related changes in inter-regional correlations were driven either by local changes in BOLD variance, by retinal effects due to pupil dilation associated with atomoxetine, by head motion, by saccade-related retinal transients, or by atomoxetine-induced changes in physiology (heart rate and breath rate). First, the correlation coefficient between two signals is their covariance normalized by the signals' variances. Thus, it is possible that the observed changes in inter-regional correlations are caused by local changes in variance alone (Haynes et al., 2005; Freeman et al., 2011), rather than by changes in covariance (i.e., the degree to which the BOLD signals in two regions fluctuated together). If this is the case, then the atomoxetine-related change in average inter-regional correlation and the atomoxetine-related change in BOLD signal variance should be negatively correlated across brain regions. Instead, we found a positive relationship between changes in inter-regional correlation and changes in BOLD variance, which was consistent across participants ( $t_{(23)} = 3.36$ ,  $p = 0.003$ ; Fig. 5), ruling out variance as a confound. Moreover, there was no interaction between treatment and time in overall BOLD variance ( $F_{(1,23)} = 0.71$ ,  $p = 0.40$ ), or in variance for only the occipital brain regions that showed reduced atomoxetine-related inter-regional correlation ( $F_{(1,23)} = 0.41$ ,  $p = 0.53$ ).

Second, because atomoxetine increased the size of the pupil (Fig. 6*a*), it is conceivable that this peripheral effect, rather than the effect of atomoxetine on central catecholamine levels, was driving the changes in inter-regional correlation in visual cortex (Haynes et al., 2004). To examine this potential confound, we binned inter-regional correlation by pupil size in the postatomoxetine condition, focusing on those correlations that showed a significant reduction under atomoxetine. If larger pupil size is responsible for the reduction in correlations, then time periods

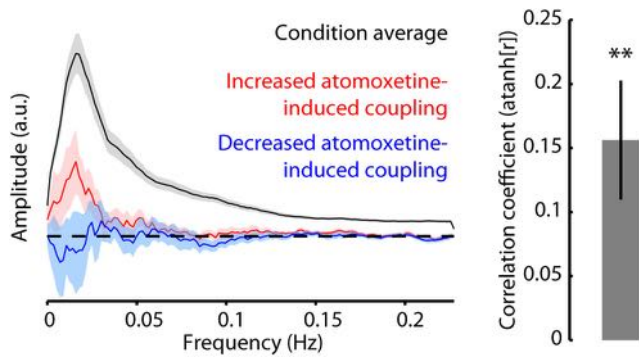


**Figure 5.** Spectral BOLD characteristics and the relation with inter-regional correlations. Left, Atomoxetine-induced changes in spectral amplitude for AAL brain regions that showed an atomoxetine-induced increase (red) and decrease (blue) in inter-regional correlation strength. Brain region and condition-averaged amplitude areas shown in black. Right, Mean correlation between the region-averaged atomoxetine-induced change in coupling strength and fractional amplitude of low-frequency BOLD fluctuations. Error bars indicate the SEM.  $^{**}p < 0.01$ .

during which the pupil is large should be associated with weaker correlations than time periods during which the pupil is small. Interestingly, we found the opposite pattern (Fig. 6*b,c*): stronger correlations for large pupil ( $t_{(18)} = 2.84$ ,  $p = 0.010$ ), ruling out an interpretation in terms of pupil size.

Third, head motion can have a strong influence on the strength of inter-regional correlations (Van Dijk et al., 2012). To rule out the possibility that our key finding of atomoxetine-related changes in inter-regional correlation was driven by head motion, we first compared head motion between conditions. Neither mean head motion nor mean absolute head motion differed between conditions (all  $p$  values  $>0.05$ ). No participant's head motion exceeded 2 mm, indicating that overall there was little head motion. However, general mild head motion tends to increase correlations between proximate areas and decrease connectivity between distant areas (Van Dijk et al., 2012). Thus, head motion can potentially lead to spatially heterogeneous effects on connectivity in a manner that is related to the distance between brain areas. To rule out the possibility that the spatial structure of atomoxetine-related changes in connectivity was driven by subtle (nonsignificant) differences in head motion between conditions, we correlated Euclidean distance between the center of mass of each pair of AAL brain areas and the strength of functional connectivity between those areas, for each participant and each condition. We then compared the distribution of Fisher-transformed correlation coefficients between conditions. If head motion is responsible for the observed change in connectivity between conditions, then the correlation between Euclidean distance and strength of connectivity should also differ between conditions. However, we did not find any differences between conditions (all  $p$  values  $>0.05$ ), ruling out head motion as a confound.

Fourth, it is possible that the atomoxetine-related reduction in the strength of correlation between visual cortical areas occurred due to differences between conditions in saccade-related retinal transients. To rule out this possibility, we extracted several eye movement metrics from the eye tracker gaze position data using the EYE-EEG toolbox (Dimigen et al., 2011). There was no interaction between treatment and time for any of the metrics: the number of saccades ( $F_{(1,18)} = 0.47$ ,  $p = 0.50$ ), median saccade amplitude ( $F_{(1,18)} = 0.45$ ,  $p = 0.51$ ), median saccade duration ( $F_{(1,18)} = 0.11$ ,  $p = 0.74$ ), or median saccade peak velocity ( $F_{(1,18)} = 3.32$ ,  $p = 0.085$ ). This latter trend was driven by a numeric difference between the preplacebo and postplacebo

conditions. Preatomoxetine and postatomoxetine did not differ significantly in saccade peak velocity ( $t_{(18)} = -0.43$ ,  $p = 0.67$ ). Together, these results show that our key result of an atomoxetine-related reduction in the strength of correlation between visual cortical regions was unlikely to be driven by saccade-related retinal transients.

Finally, atomoxetine significantly increased breath rate ( $F_{(1,23)} = 8.96$ ,  $p = 0.007$ ) and heart rate ( $F_{(1,23)} = 4.66$ ,  $p = 0.041$ ), as reflected by a significant interactions between treatment and time. We therefore corrected the BOLD time series using the RETROICOR method (see Materials and Methods) (Glover et al., 2000). The average  $R^2$  of the physiology regressors was relatively low (0.034), indicating that physiology accounted for a small proportion of the total BOLD variance (which was likely the result of artifact removal by FMRIB's ICA-based X-noiseifier) (Griffanti et al., 2014; Salimi-Khorshidi et al., 2014). Nevertheless, to conclusively rule out atomoxetine-related changes in physiology as confounds, we repeated the key analyses on the physiology-corrected data. All three global graph-theoretical measures remained significant and in the same direction as reported above (all  $p$  values  $<0.05$ ). We also found significant reductions in network degree in the same internet-work connections (all  $p$  values  $<0.05$ ). Last, we observed a similar contiguous cluster of significantly reduced inter-regional correlations within visual cortex (all  $p$  values  $<0.005$ , and cluster-corrected at  $p < 0.0001$ ). Thus, our key results were unlikely to be driven by atomoxetine-related changes in physiology.

## Discussion

Using a pharmacological manipulation, we examined the effects of increased extracellular levels of the catecholamines NE and DA on resting-state fMRI connectivity in the human brain. First, we found that our manipulation reduced the strength of inter-regional correlations across three levels of spatial organization, indicating that catecholamines reduce the strength of functional interactions during rest. Second, this modulatory effect on the structure of resting-state correlations exhibited a substantial degree of spatial specificity, indicating that catecholamines differentially reduce spontaneous correlations between select brain regions. These two key findings are surprising in light of the common understanding of the neurophysiology and computational function of catecholaminergic systems. They also identify catecholaminergic neuromodulation as an important factor shaping the spatial structure and strength of intrinsic functional connectivity in the human brain.

Our first key finding is that atomoxetine, a selective NET blocker that increases synaptic NE and DA levels (Bymaster et al., 2002; Devoto et al., 2004; Invernizzi and Garattini, 2004; Swanson et al., 2006; Koda et al., 2010), reduced the strength of inter-regional correlations. Specifically, atomoxetine reduced the strength of connectivity globally (Fig. 1*c*), between nodes belonging to distinct intrinsic connectivity networks (Fig. 2*e*), and between individual brain regions within the visual system (Fig. 3*c*). This consistent pattern of results seems to be at odds with the notion of a facilitative effect of catecholamines on brain-wide signal transmission (Aston-Jones and Cohen, 2005; Eldar et al., 2013). One possible explanation for this discrepancy lies in the fact that, in our experiment, participants did not actively respond to incoming sensory information. According to a recent theory, the effects of NE on neural activity strongly depend on interactions with local glutamate release (Mather et al., 2015). Accordingly, enhanced NE may have qualitatively different effects during task processing, associated with relatively high glutamate

activity, than during states of relative cortical quiescence (i.e., at rest), associated with relatively low glutamate activity. In line with this possibility, Coull et al. (1999) showed dissociable effects of the  $\alpha$ 2-adrenergic agonist clonidine on positron emission tomography effective connectivity obtained during task performance and during rest. Whereas during task performance clonidine increased connectivity between frontal and parietal cortical regions, during rest clonidine reduced connectivity from frontal cortex to thalamus, and in connections to and from visual cortex. Two other studies that used NE drugs also provided evidence for regional reductions in connectivity strength during rest (McCabe and Mishor, 2011; Metzger et al., 2015). These studies, however, only used a small number of seed regions to assess connectivity, and hence did not examine large-scale topographical changes.

Our second key finding is that atomoxetine resulted in spatially heterogeneous changes in inter-regional correlations. For example, atomoxetine caused a reduction in the number of strongly correlated brain regions between (but not within) distinct resting-state networks (Fig. 2*e*). Furthermore, the effect of atomoxetine on inter-regional correlations was dependent on the baseline level of coupling: the strongest functional connections tended to show the largest connectivity reductions after atomoxetine (Fig. 3*d*). How can such spatially structured effects of catecholamines come about? First, recent anatomical tracing work has suggested that the projection profile of the LC is more heterogeneous than once thought (Schwarz and Luo, 2015). For example, even though on the whole there is broad collateralization within the LC-NE system, subpopulations of LC neurons selectively innervate distinct brain regions (Chandler et al., 2014; Schwarz et al., 2015). Moreover, subpopulations of LC neurons that differ in their afferent projection profile also show marked differences in their firing characteristics (Chandler et al., 2014). The firing modes of LC neurons in turn have differentiable effects on neuronal synchronization within the cortex (Safaai et al., 2015). Importantly, LC neurons have been reported to corelease DA (Devoto and Flore, 2006). Thus, spatially selective effects of catecholamines on correlated fluctuations in the brain can be achieved via a heterogeneous cortical innervation by the LC.

Second, heterogeneity in the effect of catecholamines on inter-regional correlations could be achieved by regional differences in the expression of different receptor types. For example, expression of the  $\alpha$ 2 receptor approximately follows an anterior to posterior gradient (Nahimi et al., 2015), with particularly strong expression in primary visual cortex (Zilles and Amunts, 2009). Interestingly, we observed an anterior to posterior gradient in the effect of atomoxetine on the strength of correlations (Fig. 3*b*). Moreover, we found a pronounced reduction in the strength of correlations between regions within visual cortex, and between early visual cortex and the rest of the brain (Fig. 4). The similarity between the spatial distributions of  $\alpha$ 2 receptors and the effects of atomoxetine thus warrants further investigation into the relationship between specific NE receptor types and their influence on correlated activity across the brain.

A number of limitations of the present study should be acknowledged. First, we examined the effects of only one dose (40 mg) of atomoxetine. Dose-dependent pharmacological effects of catecho-

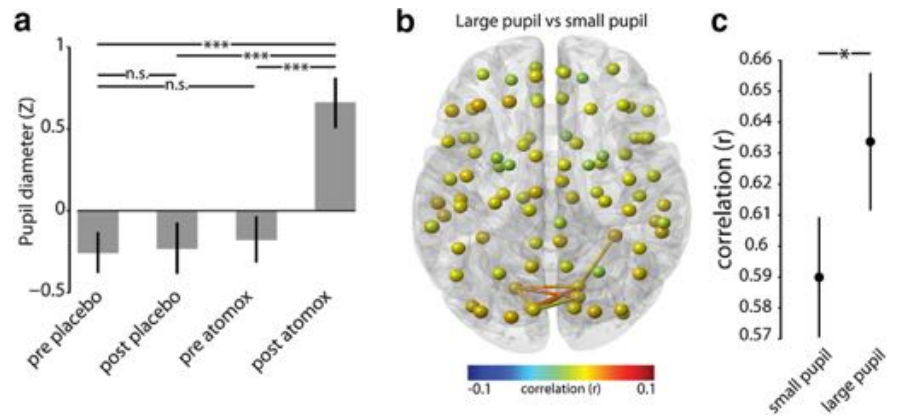


**Figure 6.** *a*, Atomoxetine effect on pupil diameter. *b*, *c*, Correlation strength in the postatomoxetine condition binned by pupil size, only for connections that showed an atomoxetine-related reduction in inter-regional correlation. Error bars indicate the SEM. n.s., Not significant. \* $p < 0.05$ . \*\*\* $p < 0.001$ .

laminergic drugs on neural function are not uncommon (Berridge and Waterhouse, 2003). Future work on the neurochemical basis of functional connectivity will need to examine dose-dependent effects of atomoxetine, and other catecholaminergic drugs, with different pharmacokinetic profiles. Second, we do not know whether atomoxetine would have similar effects on functional connectivity in clinical populations characterized by disturbed catecholaminergic function (e.g., attention deficit hyperactivity disorder and depression). Third, although we used BOLD activity as a proxy for neural activity, the link between neuronal interactions and BOLD activity is not entirely clear (Logothetis, 2008). Models of catecholamine function make predictions about how NE and DA should affect neural communication. However, the translation of these predictions to BOLD correlations is not straightforward. Last, we used an atlas-based brain parcellation to investigate inter-regional correlations. Thus, the spatial resolution of our analyses was restricted by the resolution of the atlas. Future work, using voxel-level approaches, is needed to investigate more fine-grained spatial effects of catecholamine levels on functional connectivity.

The synaptic effects of catecholamines have been relatively well charted (Berridge and Waterhouse, 2003; Winterer and Weinberger, 2004). However, there is considerable uncertainty about how these low-level effects translate to system-wide functional interactions. Recently, Safaai et al. (2015) provided an important first glimpse into how the LC-NE system modulates spontaneous cortical activity and how this modulation in turn affects sensory processing in anesthetized rats. Specifically, they showed that LC bursts can both attenuate and enhance processing of sensory stimuli depending on their timing relative to the stimulus and the cortical activity state. However, the effects of catecholamines on the large-scale communication *between* distant brain areas and their neurophysiological underpinnings remain exceedingly unexplored. Our finding that atomoxetine reduced inter-regional correlations in a spatially structured manner thus calls for novel work on the neural mechanisms that produce such effects.

Theory and evidence indicate that the topography of intrinsic fMRI correlations is dictated to an important extent by the fixed anatomical connectivity of each brain region (Deco et al., 2011, 2013). That is, brain regions that are anatomically strongly connected are more likely to show strong functional coupling than those that are connected weakly or only indirectly. However, within the constraints of physical connectivity, there is substantial room for state-dependent movement in functional topologi-



cal space (Allen et al., 2014; Zalesky et al., 2014; Barttfeld et al., 2015). Our results identify NE and DA as important factors driving these movements, and thus suggest that spontaneous fluctuations of catecholamine levels can serve to flexibly alter the structure of spontaneous correlations both globally and in specific brain regions, around the anatomical backbone.

## References

- Achard S, Bullmore E (2007) Efficiency and cost of economical brain functional networks. *PLoS Comput Biol* 3:e17. [CrossRef Medline](#)
- Allen EA, Damaraju E, Plis SM, Erhardt EB, Eichele T, Calhoun VD (2014) Tracking whole-brain connectivity dynamics in the resting state. *Cereb Cortex* 24:663–676. [CrossRef Medline](#)
- Aston-Jones G, Cohen JD (2005) An integrative theory of locus coeruleus-norepinephrine function: adaptive gain and optimal performance. *Annu Rev Neurosci* 28:403–450. [CrossRef Medline](#)
- Aston-Jones G, Foote SL, Bloom FE (1984) Anatomy and physiology of locus coeruleus neurons: functional implications. In: *Norepinephrine* (Ziegler MG, Lake CR, eds), pp 92–116. Baltimore: Williams and Wilkins.
- Barttfeld P, Uhrig L, Sitt JD, Sigman M, Jarraya B, Dehaene S (2015) Signature of consciousness in the dynamics of resting-state brain activity. *Proc Natl Acad Sci U S A* 112:887–892. [CrossRef Medline](#)
- Berridge CW, Waterhouse BD (2003) The locus coeruleus–noradrenergic system: modulation of behavioral state and state-dependent cognitive processes. *Brain Res Rev* 42:33–84. [CrossRef Medline](#)
- Biswal B, Yetkin FZ, Haughton VM, Hyde JS (1995) Functional connectivity in the motor cortex of resting human brain using echo-planar MRI. *Magn Reson Med* 34:537–541. [CrossRef Medline](#)
- Blondel VD, Guillaume JL, Lambiotte R, Lefebvre E (2008) Fast unfolding of communities in large networks. *J Stat Mech* 10:P10008.
- Bullmore E, Sporns O (2009) Complex brain networks: graph theoretical analysis of structural and functional systems. *Nat Rev Neurosci* 10:186–198. [CrossRef Medline](#)
- Bymaster FP, Katner JS, Nelson DL, Hemrick-Luecke SK, Threlkeld PG, Heiligenstein JH, Morin SM, Gehlert DR, Perry KW (2002) Atomoxetine increases extracellular levels of norepinephrine and dopamine in prefrontal cortex of rat: a potential mechanism for efficacy in attention deficit/hyperactivity disorder. *Neuropsychopharmacology* 27:699–711. [CrossRef Medline](#)
- Chandler DJ, Gao WJ, Waterhouse BD (2014) Heterogeneous organization of the locus coeruleus projections to prefrontal and motor cortices. *Proc Natl Acad Sci U S A* 111:6816–6821. [CrossRef Medline](#)
- Coull JT, Büchel C, Friston KJ, Frith CD (1999) Noradrenergically mediated plasticity in a human attentional neuronal network. *Neuroimage* 10:705–715. [CrossRef Medline](#)
- Craddock RC, James GA, Holtzheimer PE 3rd, Hu XP, Mayberg HS (2012) A whole brain fMRI atlas generated via spatially constrained spectral clustering. *Hum Brain Mapp* 33:1914–1928. [CrossRef Medline](#)
- Deco G, Jirsa VK, McIntosh AR (2011) Emerging concepts for the dynamical organization of resting-state activity in the brain. *Nat Rev Neurosci* 12:43–56. [CrossRef Medline](#)
- Deco G, Ponce-Alvarez A, Mantini D, Romani GL, Hagmann P, Corbetta M (2013) Resting-state functional connectivity emerges from structurally and dynamically shaped slow linear fluctuations. *J Neurosci* 33:11239–11252. [CrossRef Medline](#)
- De Luca M, Smith S, De Stefano N, Federico A, Matthews PM (2005) Blood oxygenation level dependent contrast resting state networks are relevant to functional activity in the neocortical sensorimotor system. *Exp Brain Res* 167:587–594. [CrossRef Medline](#)
- Devoto P, Flore G (2006) On the origin of cortical dopamine: is it a co-transmitter in noradrenergic neurons? *Curr Neuropharmacol* 4:115–125. [CrossRef Medline](#)
- Devoto P, Flore G, Pira L, Longu G, Gessa GL (2004) Alpha2-adrenoceptor mediated co-release of dopamine and noradrenaline from noradrenergic neurons in the cerebral cortex. *J Neurochem* 88:1003–1009. [CrossRef Medline](#)
- Dimigen O, Sommer W, Hohlfield A, Jacobs AM, Kliegl R (2011) Coregistration of eye movements and EEG in natural reading: analyses and review. *J Exp Psychol Gen* 140:552–572. [CrossRef Medline](#)
- Donner TH, Nieuwenhuis S (2013) Brain-wide gain modulation: the rich get richer. *Nat Neurosci* 16:989–990. [CrossRef Medline](#)
- Drew PJ, Duyn JH, Golanov E, Kleinfeld D (2008) Finding coherence in spontaneous oscillations. *Nat Neurosci* 11:991–993. [CrossRef Medline](#)
- Eldar E, Cohen JD, Niv Y (2013) The effects of neural gain on attention and learning. *Nat Neurosci* 16:1146–1153. [CrossRef Medline](#)
- Fox MD, Raichle ME (2007) Spontaneous fluctuations in brain activity observed with functional magnetic resonance imaging. *Nat Rev Neurosci* 8:700–711. [CrossRef Medline](#)
- Fox MD, Snyder AZ, Vincent JL, Corbetta M, Van Essen DC, Raichle ME (2005) The human brain is intrinsically organized into dynamic, anticorrelated functional networks. *Proc Natl Acad Sci U S A* 102:9673–9678. [CrossRef Medline](#)
- Freeman J, Donner TH, Heeger DJ (2011) Inter-area correlations in the ventral visual pathway reflect feature integration. *J Vis* 11:pii15. [CrossRef Medline](#)
- Glover GH, Li TQ, Ress D (2000) Image-based method for retrospective correction of physiological motion effects in fMRI: RETROICOR. *Magn Reson Med* 44:162–167. [CrossRef Medline](#)
- Greicius MD, Srivastava G, Reiss AL, Menon V (2004) Default-mode network activity distinguishes Alzheimer's disease from healthy aging: evidence from functional MRI. *Proc Natl Acad Sci U S A* 101:4637–4642. [CrossRef Medline](#)
- Griffanti L, Salimi-Khorshidi G, Beckmann CF, Auerbach EJ, Douaud G, Sexton CE, Zsoldos E, Ebmeier KP, Filippini N, Mackay CE, Moeller S, Xu J, Yacoub E, Baselli G, Ugurbil K, Miller KL, Smith SM (2014) ICA-based artefact removal and accelerated fMRI acquisition for improved resting state network imaging. *Neuroimage* 95:232–247. [CrossRef Medline](#)
- Haynes JD, Lotto RB, Rees G (2004) Responses of human visual cortex to uniform surfaces. *Proc Natl Acad Sci U S A* 101:4286–4291. [CrossRef Medline](#)
- Haynes JD, Driver J, Rees G (2005) Visibility reflects dynamic changes of effective connectivity between V1 and fusiform cortex. *Neuron* 46:811–821. [CrossRef Medline](#)
- Hiltunen T, Kantola J, Abou Elseoud A, Lepola P, Suominen K, Starck T, Nikkinen J, Remes J, Tervonen O, Palva S, Kiviniemi V, Palva JM (2014) Infra-slow EEG fluctuations are correlated with resting-state network dynamics in fMRI. *J Neurosci* 34:356–362. [CrossRef Medline](#)
- Hipp JF, Hawellek DJ, Corbetta M, Siegel M, Engel AK (2012) Large-scale cortical correlation structure of spontaneous oscillatory activity. *Nat Neurosci* 15:884–890. [CrossRef Medline](#)
- Invernizzi RW, Garattini S (2004) Role of presynaptic alpha2-adrenoceptors in antidepressant action: recent findings from microdialysis studies. *Prog Neuropsychopharmacol Biol Psychiatry* 28:819–827. [CrossRef Medline](#)
- Ishimatsu M, Williams JT (1996) Synchronous activity in locus coeruleus results from dendritic interactions in pericoerulear regions. *J Neurosci* 16:5196–5204. [Medline](#)
- Jenkinson M, Beckmann CF, Behrens TE, Woolrich MW, Smith SM (2012) Fsl. *Neuroimage* 62:782–790. [CrossRef Medline](#)
- Koda K, Ago Y, Cong Y, Kita Y, Takuma K, Matsuda T (2010) Effects of acute and chronic administration of atomoxetine and methylphenidate on extracellular levels of noradrenaline, dopamine and serotonin in the prefrontal cortex and striatum of mice. *J Neurochem* 114:259–270. [CrossRef Medline](#)
- Le Martelot E, Hankin C (2013) Multi-scale community detection using stability optimisation. *Int J Web Based Communities* 9:323–348. [CrossRef](#)
- Leopold DA, Murayama Y, Logothetis NK (2003) Very slow activity fluctuations in monkey visual cortex: implications for functional brain imaging. *Cereb Cortex* 13:422–433. [CrossRef Medline](#)
- Li N, Ma N, Liu Y, He XS, Sun DL, Fu XM, Zhang X, Han S, Zhang DR (2013) Resting-state functional connectivity predicts impulsivity in economic decision-making. *J Neurosci* 33:4886–4895. [CrossRef Medline](#)
- Logothetis NK (2008) What we can do and what we cannot do with fMRI. *Nature* 453:869–878. [CrossRef Medline](#)
- Maslov S, Sneppen K (2002) Specificity and stability in topology of protein networks. *Science* 296:910–913. [CrossRef Medline](#)
- Mather M, Clewett D, Sakaki M, Harley CW (2015) Norepinephrine ignites local hot spots of neuronal excitation: how arousal amplifies selectivity in perception and memory. *Behav Brain Sci* 1–100.
- McCabe C, Mishor Z (2011) Antidepressant medications reduce subcortical-cortical resting-state functional connectivity in healthy volunteers. *Neuroimage* 57:1317–1323. [CrossRef Medline](#)
- Metzger CD, Wieggers M, Walter M, Abler B, Graf H (2015) Local and global

- resting state activity in the noradrenergic and dopaminergic pathway modulated by reboxetine and amisulpride in healthy subjects. *Int J Neuropsychopharmacol* 19:pii080. [CrossRef Medline](#)
- Moises HC, Woodward DJ, Hoffer BJ, Freedman R (1979) Interactions of norepinephrine with Purkinje cell responses to putative amino acid neurotransmitters applied by microiontophoresis. *Exp Neurol* 64:493–515. [CrossRef Medline](#)
- Nahimi A, Jakobsen S, Munk OL, Vang K, Phan JA, Rodell A, Gjedde A (2015) Mapping alpha2 adrenoceptors of the human brain with 11C-yohimbine. *J Nucl Med* 56:392–398. [CrossRef Medline](#)
- Nichols TE, Holmes AP (2002) Nonparametric permutation tests for functional neuroimaging: a primer with examples. *Hum Brain Mapp* 15:1–25. [Medline](#)
- Nir Y, Hasson U, Levy I, Yeshurun Y, Malach R (2006) Widespread functional connectivity and fMRI fluctuations in human visual cortex in the absence of visual stimulation. *Neuroimage* 30:1313–1324. [CrossRef Medline](#)
- Rogawski MA, Aghajanian GK (1980) Modulation of lateral geniculate neurone excitability by noradrenaline microiontophoresis or locus coeruleus stimulation. *Nature* 287:731–734. [CrossRef Medline](#)
- Rubinov M, Sporns O (2010) Complex network measures of brain connectivity: uses and interpretations. *Neuroimage* 52:1059–1069. [CrossRef Medline](#)
- Safaii H, Neves R, Eschenko O, Logothetis NK, Panzeri S (2015) Modeling the effect of locus coeruleus firing on cortical state dynamics and single-trial sensory processing. *Proc Natl Acad Sci U S A* 112:12834–12839. [CrossRef Medline](#)
- Salimi-Khorshidi G, Douaud G, Beckmann CF, Glasser MF, Griffanti L, Smith SM (2014) Automatic denoising of functional MRI data: combining independent component analysis and hierarchical fusion of classifiers. *Neuroimage* 90:449–468. [CrossRef Medline](#)
- Schölvinck ML, Maier A, Ye FQ, Duyn JH, Leopold DA (2010) Neural basis of global resting-state fMRI activity. *Proc Natl Acad Sci U S A* 107:10238–10243. [CrossRef Medline](#)
- Schwarz LA, Luo L (2015) Organization of the locus coeruleus-norepinephrine system. *Curr Biol* 25:R1051–R1056. [CrossRef Medline](#)
- Schwarz LA, Miyamichi K, Gao XJ, Beier KT, Weissbourd B, DeLoach KE, Ren J, Ibanes S, Malenka RC, Kremer EJ, Luo L (2015) Viral-genetic tracing of the input-output organization of a central noradrenaline circuit. *Nature* 524:88–92. [CrossRef Medline](#)
- Seamans JK, Gorelova N, Durstewitz D, Yang CR (2001a) Bidirectional dopamine modulation of GABAergic inhibition in prefrontal cortical pyramidal neurons. *J Neurosci* 21:3628–3638. [Medline](#)
- Seamans JK, Durstewitz D, Christie BR, Stevens CF, Sejnowski TJ (2001b) Dopamine D1/D5 receptor modulation of excitatory synaptic inputs to layer V prefrontal cortex neurons. *Proc Natl Acad Sci U S A* 98:301–306. [CrossRef Medline](#)
- Sepulcre J, Liu H, Talukdar T, Martincorena I, Yeo BT, Buckner RL (2010) The organization of local and distant functional connectivity in the human brain. *PLoS Comput Biol* 6:e1000808. [CrossRef Medline](#)
- Smith SM, Jenkinson M, Woolrich MW, Beckmann CF, Behrens TE, Johansen-Berg H, Bannister PR, De Luca M, Drobnjak I, Flitney DE, Niazy RK, Saunders J, Vickers J, Zhang Y, De Stefano N, Brady JM, Matthews PM (2004) Advances in functional and structural MR image analysis and implementation as FSL. *Neuroimage* 23 [Suppl 1]:S208–S219.
- Sulzer D, Cragg SJ, Rice ME (2016) Striatal dopamine neurotransmission: regulation of release and uptake. *Basal Ganglia* 6:123–148. [CrossRef Medline](#)
- Swanson CJ, Perry KW, Koch-Krueger S, Katner J, Svensson KA, Bymaster FP (2006) Effect of the attention deficit/hyperactivity disorder drug atomoxetine on extracellular concentrations of norepinephrine and dopamine in several brain regions of the rat. *Neuropharmacology* 50:755–760. [CrossRef Medline](#)
- Swanson LW, Hartman BK (1975) The central adrenergic system: an immunofluorescence study of the location of cell bodies and their efferent connections in the rat utilizing dopamine-beta-hydroxylase as a marker. *J Comp Neurol* 163:467–505. [CrossRef Medline](#)
- Tavor I, Parker Jones O, Mars RB, Smith SM, Behrens TE, Jbabdi S (2016) Task-free MRI predicts individual differences in brain activity during task performance. *Science* 352:216–220. [CrossRef Medline](#)
- Tzourio-Mazoyer N, Landeau B, Papathanassiou D, Crivello F, Etard O, Delcroix N, Mazoyer B, Joliot M (2002) Automated anatomical labeling of activations in SPM using a macroscopic anatomical parcellation of the MNI MRI single-subject brain. *Neuroimage* 15:273–289. [CrossRef Medline](#)
- Van Dijk KR, Sabuncu MR, Buckner RL (2012) The influence of head motion on intrinsic functional connectivity MRI. *Neuroimage* 59:431–438. [CrossRef Medline](#)
- van Wijk BC, Stam CJ, Daffertshofer A (2010) Comparing brain networks of different size and connectivity density using graph theory. *PLoS One* 5:e13701. [CrossRef Medline](#)
- Wang J, O'Donnell P (2001) D1 dopamine receptors potentiate NMDA-mediated excitability increase in layer V prefrontal cortical pyramidal neurons. *Cereb Cortex* 11:452–462. [CrossRef Medline](#)
- Waterhouse BD, Moises HC, Woodward DJ (1998) Phasic activation of the locus coeruleus enhances responses of primary sensory cortical neurons to peripheral receptive field stimulation. *Brain Res* 790:33–44. [CrossRef Medline](#)
- Watts DJ, Strogatz SH (1998) Collective dynamics of 'small-world' networks. *Nature* 393:440–442. [CrossRef Medline](#)
- Winterer G, Weinberger DR (2004) Genes, dopamine and cortical signal-to-noise ratio in schizophrenia. *Trends Neurosci* 27:683–690. [CrossRef Medline](#)
- Yeo BT, Krienen FM, Sepulcre J, Sabuncu MR, Lashkari D, Hollinshead M, Roffman JL, Smoller JW, Zöllei L, Polimeni JR, Fischl B, Liu H, Buckner RL (2011) The organization of the human cerebral cortex estimated by intrinsic functional connectivity. *J Neurophysiol* 106:1125–1165. [CrossRef Medline](#)
- Zalesky A, Fornito A, Cocchi L, Gollo LL, Breakspear M (2014) Time-resolved resting-state brain networks. *Proc Natl Acad Sci U S A* 111:10341–10346. [CrossRef Medline](#)
- Zilles K, Amunts K (2009) Receptor mapping: architecture of the human cerebral cortex. *Curr Opin Neurol* 22:331–339. [CrossRef Medline](#)
- Zou QH, Zhu CZ, Yang Y, Zuo XN, Long XY, Cao QJ, Wang YF, Zang YF (2008) An improved approach to detection of amplitude of low-frequency fluctuation (ALFF) for resting-state fMRI: fractional ALFF. *J Neurosci Methods* 172:137–141. [CrossRef Medline](#)

## 4.5. Study 5: Context-dependent neuromodulation of the intrinsic cortical correlation structure

### Author contributions:

1. Conceptualization
  2. Investigation
  3. Formal analysis
  4. Writing – Original draft
  5. Writing – Review
  6. Supervision
- \* Contributed equally

<b>Pfeffer, T.:</b>	<b>1,2,3,4,5</b>
Ponce-Alvarez, A.:	3
Andreas K. Engel:	1
Nolte, G.:	6
Deco, G.:	6
Donner, T.H.:	5,6

**Status:** In preparation

# **A double dissociation between the effects of acetylcholine and catecholamines on frequency-resolved whole-brain correlations during rest and task**

Thomas Pfeffer (1), Adrian Ponce-Alvarez (2), Andreas K. Engel (1), Guido Nolte (1), Gustavo Deco (2), Tobias H. Donner (1,3,4)

1 Department of Neurophysiology and Pathophysiology, University Medical Center Hamburg, Germany

2 Pompeu Fabra, Barcelona, Spain

3 Department of Psychology, University of Amsterdam, The Netherlands

4 Amsterdam Brain and Cognition, University of Amsterdam, The Netherlands

Address for correspondence:

Thomas Pfeffer  
[thms.pffr@gmail.com](mailto:thms.pffr@gmail.com)

Tobias H. Donner  
[t.donner@uke.de](mailto:t.donner@uke.de)

Dept. of Neurophysiology and Pathophysiology  
University Medical Center Hamburg-Eppendorf  
Martinistr. 52, 20246 Hamburg

**Abbreviated title:** Context-dependent neuromodulation of cortical correlation structure

## Introduction

Brain activity exhibits intrinsic fluctuations that are largely independent of external factors (Faisal et al., 2008). These fluctuations exhibit an intricate spatiotemporal structure, reflected in the organization into correlated networks, and provide insights into the fundamental functional architecture of the brain (Fox et al., 2005; Fox and Raichle, 2007; Vincent et al., 2007; Deco et al., 2011; Engel et al., 2013) as well as its malfunctioning in various pathologies (Greicius, 2008; Hawellek et al., 2011, 2013). Despite a surge in the numbers of studies on the correlation patterns of intrinsic fluctuations, the underlying physiological mechanisms are still not well understood. One key candidate for shaping the large-scale correlation pattern of intrinsic brain activity are ascending neuromodulatory systems, such as the noradrenergic and the cholinergic system, which have long been implicated with the regulation of global brain state (Harris and Thiele, 2011; Lee and Dan, 2012; Zagha and DA, 2014) as well as the spatiotemporal coordination of intrinsic fluctuations (Leopold et al., 2003). Neuromodulatory centers, such as the locus coeruleus (noradrenaline) and the nucleus basalis (acetylcholine), have widespread projections covering almost the entire brain (Foote and Morrison, 1987; Aston-Jones and Cohen, 2005; Ballinger et al., 2016), with an innervation profile that has been described as “diffuse” (Woolf, 1991). However, these systems can also act spatially specific (Ballinger et al., 2016). Moreover, neuromodulatory systems can act on both, short as well as long timescales (Aston-Jones and Cohen, 2005; Ballinger et al., 2016). In sum, both the spatial and the temporal profile of neuromodulatory systems enables them to shape brain activity across multiple spatial (from microcircuits to the entire brain) and temporal (from milliseconds to minutes and longer) scales.

Previous research suggests that catecholamines, possibly through changes in the balance



between excitation and inhibition (Murphy and Miller, 2003), increase neural gain, i.e., the responsivity of neurons towards input (Servan-Schreiber et al., 1990). On a network level, these catecholamine-related changes in gain have been shown to result in increases in brain-wide correlations as well as changes in functional network topology during simple cognitive tasks (Eldar et al., 2013; Warren et al., 2016). During rest, on the other hand, a widespread decrease in whole-brain correlations has been observed (van den Brink et al., 2016), pointing towards a “context-dependence” of the effects of catecholamines on brain-wide interactions.

Less is known about the effects of acetylcholine. One important effect of acetylcholine seems to be a boost in the intra-cortical inhibition (Hasselmo and Bower, 1992, 1993). More recent evidence points to a direct inhibition of a specific class of inhibitory interneurons within the cortical microcircuit, possibly resulting in cortical disinhibition (Froemke et al., 2007; Pfeffer et al., 2013; Fu et al., 2014; Letzkus et al., 2015). The net effects of acetylcholine, however, are not well understood. Both multiplicative (Disney et al., 2007), but also divisive and additive gain modulation (Nelson and Mooney, 2016) have been reported in the past. Moreover, the effects of acetylcholine on large-scale brain interactions are unknown.

In the present study, we asked how catecholamines and acetylcholine influence the brain-wide correlation structure of intrinsic neuronal activity. To this end, we pharmacologically manipulated the levels of catecholamines and acetylcholine, combined with MEG recordings of brain activity during both rest (i.e., in absence of external drive) and task (i.e., during constant external drive). Our findings reveal an intricate dissociation between the effects of catecholamines and acetylcholine on large-scale intrinsic correlations: catecholamines strongly increased brain-wide correlations, but only in the presence of strong external drive (i.e., during task), whereas acetylcholine strongly decreased correlations, but only in absence of external drive (i.e., during rest). These results demonstrate a marked context-dependence of the large-scale effects of both

catecholamines as well as acetylcholine.

## Materials and Methods

In the current study, we analyzed a data set that has been described in detail in chapter 3 (see also Fig. 1 of chapter 3) of this thesis. The reader is therefore referred to the respective methods section for details regarding the specifics of the data set and the experimental design. In the following, we will focus on the methodological aspects that are not described in the previous chapter. The approach is also summarized in Figure 1.

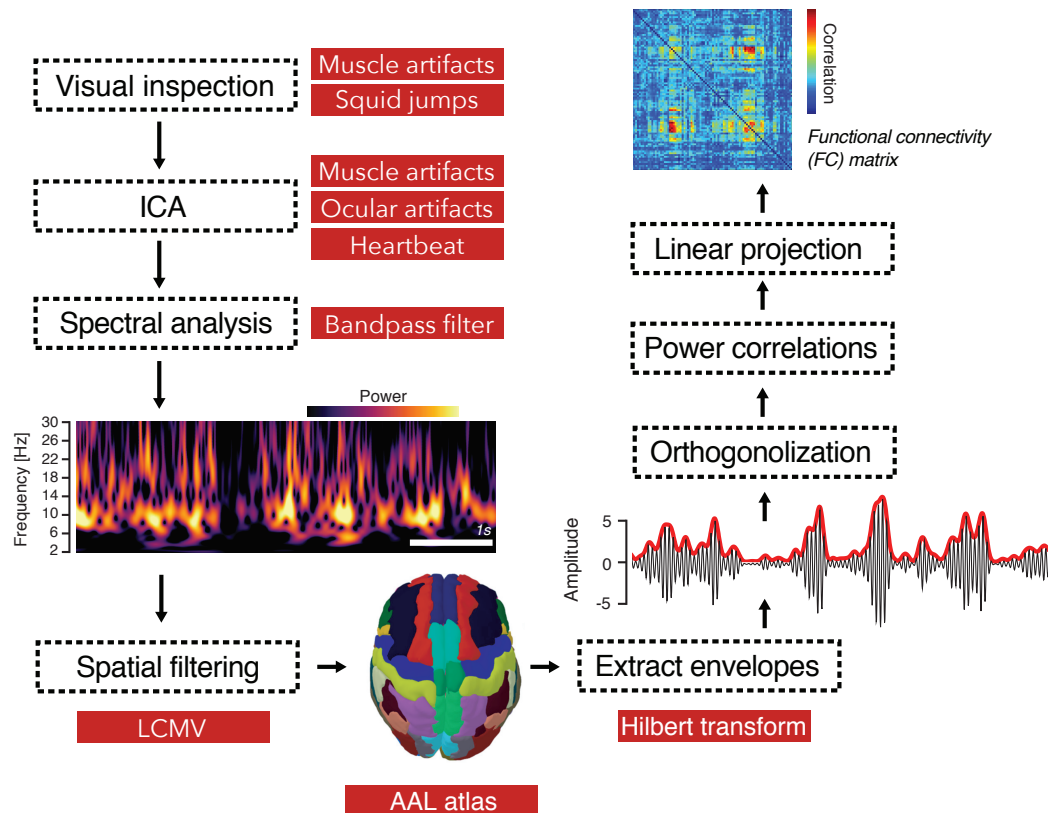


**Figure 1. Methodological approach.** The data were cleaned of extracranial artifacts and filtered into several overlapping frequency-bands of interest. A spatial filtering approach based on LCMV was applied to project the signal onto 90 AAL regions. Phase and amplitude were extracted for each frequency band using Hilbert transformation and the resulting signals were orthogonalized with respect to each other. The orthogonalized signals were then used to compute power envelope correlations. This was repeated for all possible signal combinations, resulting in a 90x90 functional connectivity matrix.

*Band-pass filter.* The cleaned sensor-level signal (see Materials and Methods of chapter 3) was filtered into 13 overlapping frequency-bands of interest, using a 4<sup>th</sup> order Butterworth filter. The center frequencies of the pass-bands were logarithmically spaced from 2 to 128 Hz (rounded to the nearest integer) and the spectral width of each pass-band was defined as half the center frequency. For instance, a center frequency of 4 Hz resulted in a band-width of 2 Hz and a pass-band ranging from 3 Hz to 5 Hz. This ensured that the relation between center frequency and band-width remained constant across all frequency bands.

*Source analysis.* We estimated instantaneous source-level amplitude by means of linear “beamforming” (LCMV; van Veen et al., 1997). LCMV is a linear adaptive spatial filtering technique, where activity from a given source location  $r$  is passed with unit gain, while activity from all other sources is maximally suppressed. The steps described in the following were performed separately for each participant and recording session. For each source location  $r$ , a spatial filter  $A(r, f)$  was derived according to:

$$A(r, f) = \left( L^T(r) C_{real}(f)^{-1} L(r) \right)^{-1} L^T(r) C(f)^{-1} \quad (1)$$

where  $L$  denotes the magnetic leadfield ( $T$  denotes the matrix transpose) and  $C_{real}(f)$  is the real part of the complex frequency-specific sensor-level cross spectral density matrix. The obtained spatial filter contains three orthogonal projections, which were combined into one spatial filter  $B(r, f)$  along the direction of the dominant dipole, using singular value decomposition and the first eigenvector. In order to obtain the the real-valued source level signal for each location  $r$ , the sensor-level signal  $X(t, f)$  was multiplied with the resulting spatial filter:

$$X_{src}(r, t, f) = B(r, f) X(t, f) \quad (3)$$

Finally, the resulting signal was Hilbert-transformed in order to derive complex-valued source-level estimates.

*AAL grid.* To render the results comparable to previously acquired results from fMRI (van den Brink et al., 2016), as well as to reduce the computational load of the following analyses, we projected the signal onto 90 cortical and subcortical AAL regions (Tzourio-Mazoyer et al., 2002). To this end, source locations were first arranged on an equally spaced grid (of 4 mm x 4 mm x 4 mm resolution) covering the entire brain. Time courses for each AAL region  $X_k(t)$  were obtained by means of a weighted sum across all grid points  $M$  covering a given AAL region  $k$  (Brookes et al., 2016). For each grid point  $i$  within a certain AAL region  $k$ , the weights were determined based on distance to the center of mass of region  $k$  according to:

$$X_k(t, f) = \sum_i^M e^{\frac{r_i^2}{400}} X_{src}(i, t, f) \quad (4)$$

Where  $r$  denotes the distance in mm. The full width at half maximum of the weighting corresponded to 17 mm, consistent with a previous report (Brookes et al., 2016). The employed approach ensured that the reconstructed AAL time courses were biased towards their center of mass, hence increasing the contrast between regions. Note that prior to the computation of the weighted sums, the signs of the spatially filtered signal were flipped when necessary, in order to account for the arbitrary polarity which is induced by the source estimation.

*Orthogonalized power envelope correlations.* Power correlations were defined as the correlations of the power envelopes at carrier frequency  $f$  between two regions  $i$  and  $j$ . To this end, we first squared the absolute value of the Hilbert-transformed source-level estimates, yielding the source-level power envelopes, and log-transformed the resulting signal to render the power distribution

more normal. In order to reduce spurious correlations arising from instantaneous signal leakage, we orthogonalized each power envelope with respect to the reference signal (Brookes et al., 2012; Hipp et al., 2012). More specifically, we orthogonalized each signal  $Y$  with respect to signal  $X$  according to:

$$Y_{\perp X}(t, f) = \text{imag} \left( Y(t, f) \frac{X(t, f)^*}{|X(t, f)|} \right) \quad (5)$$

where  $Y_{\perp X}(t, f)$  is the signal  $Y(t, f)$  orthogonalized with respect to signal  $X(t, f)$  and  $*$  denotes the complex conjugate. In principle, the orthogonalization can be computed over the entire signal, but the shortest possible length is recommended (Hipp et al., 2012). In this study, we have chosen to orthogonalize within the smallest window length, i.e., on a sample-by-sample basis. The orthogonalization was done in both directions ( $Y_{\perp X}(t, f)$  as well as  $X_{\perp Y}(t, f)$ ). Next, correlation coefficients were computed for both directions and the resulting values were averaged. The orthogonalization approach has been shown to underestimate true correlations in a signal by a constant factor of  $\sim 0.577$  (Hipp et al., 2012). This factor is not accounted for in this report. The analysis resulted in a “functional connectivity matrix” (subsequently called FC matrix) of size  $N \times N$  (with  $N = 90$  AAL regions), for each frequency band of interest.

*Linear projection.* Peripheral activity, such as changes in heart beat, as well as spontaneous blinks of the eye can introduce spurious correlations between regions (due to muscle activity that is picked up by the sensors). Due to the nearly instantaneous spread of such artifacts, the orthogonalization approach likely eliminates these spurious correlations. However, participants might realize drug-related changes in peripheral signals, such as an increased heart rate. This, in turn, may change the global arousal level of the participant. In order to ensure that the reported effects are independent of such confounds, we additionally employed a linear projection approach. To this end, we sequentially projected out variations in heart beat and blink rate across

subjects from each field in the FC matrix. For each connection  $ij$  (with  $i = 1, \dots, 90$  and  $j = 1, \dots, 90$ ), we first computed and then subtracted the mean across subjects. Next, we computed the residual correlation  $r_{\perp R}$  using orthogonal projection:

$$r_{\perp R} = r_{ij} - (r_{ij}^T x)x, \quad (6)$$

where  $x$  is the reference (i.e., heart beat or blink rate) and  $r$  contains the correlation values for connection  $ij$  across subjects. In this report, only the cleaned matrices are shown. However, the reported results equally hold without the application of the linear projection.

*Statistical tests of changes in whole-brain correlations.* In order to quantify whole-brain changes in power envelope correlations, we have adopted a procedure described previously (Hawellek et al., 2013). For each carrier frequency  $f$ , we statistically compared the (fisher z-transformed) FC matrices, across subjects, between the two drug conditions and placebo, using a paired t-test. Then we counted the number of significantly positively ( $p < 0.05$  and  $t > 0$ ) and the number of significantly negatively altered correlations ( $p < 0.05$  and  $t < 0$ ). This resulting value was divided by the number of possible connections  $M$  (with  $M = (90 \cdot 90 - 90) / 2 = 4005$ ) to obtain the fraction of significantly altered correlations in both directions. This procedure was repeated for all 13 frequencies bands. In order to derive p-values, corrected for multiple comparisons across frequencies, we have employed a single threshold permutation procedure based on ranks (Nichols and Holmes, 2002; Hawellek et al., 2013). In short, for each of  $N$  permutations (with  $N = 20000$ ), the experimental labels were randomly re-assigned within subjects and the aforementioned procedure was repeated. This resulted in a  $N \times 13$  matrix for both effect directions (positive and negative alterations). Next, the matrix was converted into ranks for each column (i.e., across permutations) and the maximum rank was determined for each row (i.e., across frequencies), resulting in a distribution of maximum ranks. For each frequency band, the

distribution of maximum ranks was converted back into a frequency-specific, maximum resample distribution. From this, frequency-specific corrected p-values were obtained. The conversion into a distribution of maximum ranks ensured that the test was not simply biased towards the frequency-bands with the largest magnitudes.

It should be noted that significant alterations in the correlations between two regions can be achieved in different ways. A decrease in correlations, for instance, can mean that a positive correlation becomes weaker, or that a negative correlation becomes more negative. However, only the former would qualify as a meaningful reduction in correlation, whereas the latter correlation gets smaller in number (i.e., more negative), but actually stronger in terms of coupling. Hence, a “significant decrease” does not always carry the same meaning, and same is true for increases. In this study, consistent with many previous reports, the number of positive correlations by far outnumbered the number of negative correlations. In fact, 99% of all connections were positive. Thus, we assume that a decrease (increase) in correlation corresponds to a positive correlation becoming weaker (stronger).

## **Results**

In the current study, we investigated the influence of atomoxetine, which increases the levels of noradrenaline and dopamine, as well as donepezil, which increases the levels of acetylcholine, on frequency-resolved power envelope correlations. Previous studies have reported peaks in power envelope correlations in the alpha- (center frequency 11 Hz) and beta-band (center frequency 16 Hz) (Hipp et al., 2012; Cabral et al., 2013; Brookes et al., 2016). Moreover, in this study, spectral power showed a clear peak in the alpha-band (see chapter 3). Therefore, we first assessed the functional connectivity matrix in the alpha-band.

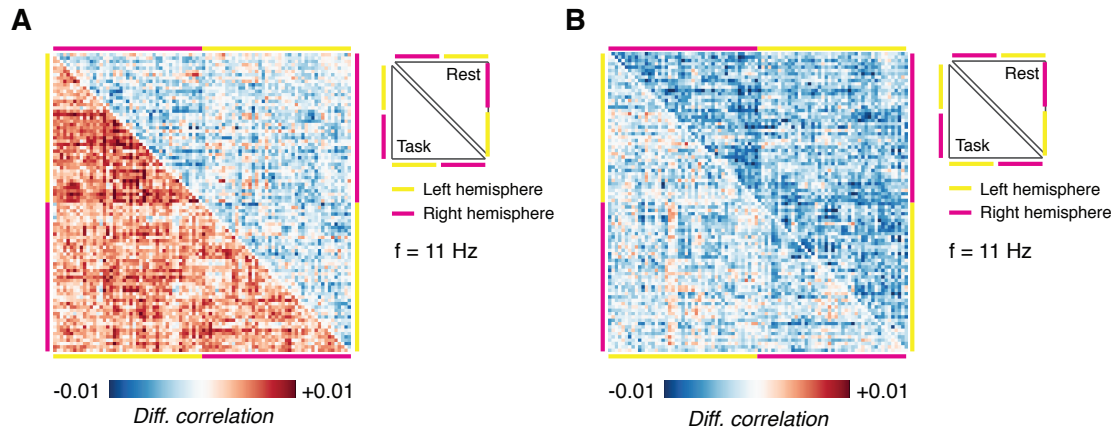


**Figure 2.** Drug-related changes in whole-brain correlations at 11 Hz. **(A)** Atomoxetine-related change in power envelope correlations. *Upper triangular part.* Drug-related changes during task. *Lower triangular part.* Drug-related changes during rest. **(B)** Same as (A), but for donepezil.

During rest, atomoxetine led to a slight decrease in alpha-band correlations, across almost the entire brain (Fig. 2A, upper triangular part of the depicted matrix). During task, on the other hand, atomoxetine increased whole-brain correlations. Again, this increase was spatially widespread (Fig. 2A, lower triangular part of the depicted matrix). We repeated the analysis for donepezil, which increased the levels of acetylcholine. Donepezil decreased power envelope correlations across almost the entire brain in both behavioral contexts, but more strongly during rest (Fig. 2B, upper triangular part of the depicted matrix) than during task (Fig. 2B, lower triangular part of the depicted matrix).

### Double dissociation of effects on whole-brain correlations

We assessed the statistical significance of the observed results collapsed across the entire brain (rather than for each connection separately), but separately for a range of frequencies. To this end, for each frequency, we counted the number of significantly altered (fisher z-transformed) power correlations by means of a paired t-test ( $\alpha = 0.05$ ), separately for positive and negative alterations (see Materials and Methods). During rest, we found no evidence for an effect of



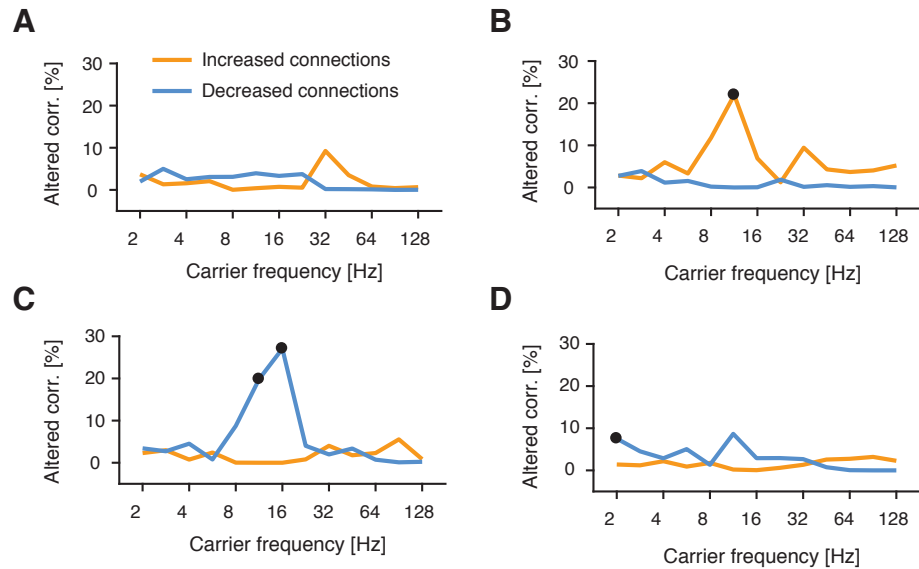


**Figure 3.** Drug-related changes across carrier frequencies. **(A)** Atomoxetine-related changes in the percentage of significantly altered correlations (orange: increased; blue: decreased) during rest. **(B)** Same as (A), but during task. **(C)** Donepezil-related changes in the percentage of significantly altered correlations during rest. **(D)** Same as (C), but during task.

atomoxetine on power envelope correlations, neither positive nor negative ( $p > 0.05$ , two-sided permutation test). In contrast, during task, atomoxetine significantly increased whole-brain power correlations in the alpha-band ( $p = 0.007$ , two-sided permutation test).

In stark contrast to atomoxetine, donepezil led to a significant decrease of whole-brain correlations during rest (Fig 3C). This decrease was most strongly pronounced in the beta-band (center frequency 16 Hz;  $p = 0.001$ ; permutation test), but also present the alpha-band, though slightly weaker in magnitude (center frequency 11 Hz;  $p = 0.011$ ; permutation test). During task, on the other hand, donepezil led to a significant reduction in whole-brain correlations in the delta-band (center frequency 2 Hz;  $p = 0.012$ ; two-sided permutation test), but not in the alpha- and beta-band (Fig. 3D;  $p > 0.05$ ; two-sided permutation test).

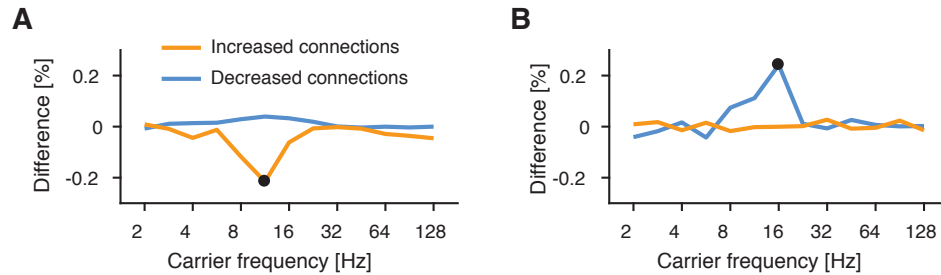


**Figure 4.** Context-dependence across carrier frequencies. **(A)** Context-dependence of atomoxetine-related changes in correlations. **(B)** Same as (A), but for donepezil.

### Context-dependence of neuromodulatory effects

The results obtained thus far point towards a dependence of neuromodulatory effects on whole-brain power envelope correlations on behavioral context (i.e., rest or task), both for atomoxetine as well as donepezil. Therefore, we next assessed the interaction between the drug effects and the behavioral context. Both atomoxetine and donepezil exhibited significant context-dependence: atomoxetine increased whole-brain correlations in the alpha-band significantly more strongly during task compared to rest (Fig. 4A;  $p = 0.008$ ; two-sided permutation test), whereas donepezil significantly decreased whole-brain correlations more strongly during rest compared to task in the beta-band (Fig. 4B; center frequency 16 Hz;  $op = 0.006$ ; two-sided permutation test).

### Discussion

The large-scale correlation structure of intrinsic brain activity has been subject of intense research over the recent decade. Yet, the underlying neurophysiological mechanisms generating the spatiotemporal pattern of correlated brain activity are not yet understood. One important factor is the underlying anatomical connectivity, which provides the scaffold brain activity unfolds upon. Earlier studies have noted a marked resemblance of anatomical connectivity and intrinsic correlations (Honey et al., 2007, 2010). Strong evidence for the causal contribution of anatomical

connectivity to the emergence of correlated spontaneous fluctuations comes from studies on callosotomy, showing that, after the corpus callosum of anesthetized monkeys is cut, spontaneous interhemispheric correlation vanishes (O'Reilly et al., 2013). Anatomy can explain a substantial part of the observed correlation structure especially when considered over long time scales, but the resemblance between anatomical connectivity and whole-brain correlations is markedly reduced on shorter time scales (Honey et al., 2007). Moreover, anatomy cannot account for the profound changes in brain-wide correlations during sleep (e.g. Deco et al., 2013) or under anaesthesia (Supp et al., 2011). These findings clearly indicate that there are other fundamental factors which shape the structure of large-scale correlated brain activity. Here, we investigated the role of two major neuromodulatory systems, the catecholaminergic and the cholinergic system. The innervation profile as well as their temporal characteristics puts those systems in an ideal position to shape coordinated activity within and across large parts of the brain and across multiple time scales. Interestingly, on a local scale (i.e., within microcircuits and cortical regions), both catecholamines and acetylcholine have comparable net effects, resulting in a decrease in low-frequency activity ( $< 10$  Hz) and an increase in high-frequency activity ( $> 20$  Hz) (Bauer et al., 2012; Pinto et al., 2013; Polack et al., 2013; Chen et al., 2015). Our results show that, despite similar effects on local synchronization, the large-scale effects can be strikingly different.

In this study, catecholamines, that is noradrenaline and dopamine, increased whole-brain correlations in the alpha-band during task, but not during rest. This result has important implications for the effects of catecholamines in general as well as on their influence on whole-brain interactions in particular. Catecholamines have been suggested to modulate the gain of neuronal activity multiplicatively (Servan-Schreiber et al., 1990; Aston-Jones and Cohen, 2005), which results in an altered neuronal input-output relation. An increase in multiplicative gain means that a neuron that receives strong input, will respond even stronger, whereas neurons receiving

only weak input, do not change much in output, or even become weaker (Donner and Nieuwenhuis, 2013). On a brain-wide scale, multiplicative gain modulation has been shown to result in wide-spread increases in the interactions between different regions of the brain in a simplified network model (Eldar et al., 2013). This prediction has received experimental support using pharmacological manipulations (Warren et al., 2016), and using pupil dilation as an index of noradrenergic activity (Eldar et al., 2013). These results were obtained while participants were performing a perceptual task. In contrast, during “resting state”, that is, in absence of external input or overt behavior, catecholamines led to a spatially widespread reduction in intrinsic activity correlations in a recent another report (van den Brink et al., 2016). Here, we demonstrate that the discrepancy between these prior reports likely arises from differences in the behavioral context (rest or task), i.e., the level of external/sensory drive. Although we did not observe significant catecholamine-related changes during rest, the sign of the induced change in the alpha-band was consistently negative across many connections (see Fig.2A). However, it should be acknowledged that the transfer of hemodynamic whole-brain correlations (as measured with fMRI) to frequency-specific power correlations (as measured with E/MEG) is far from trivial (Hipp and Siegel, 2015). In contrast to rest, during task, catecholamines led to a pronounced increase in whole-brain interactions (Fig. 2A, Fig. 3A). In previous rodent work, the effects of the catecholamine noradrenaline have been shown to depend on the level of glutamate in the circuit (Polack et al., 2013). It is possible that continuous task/sensory drive, compared to rest, is associated with elevated levels of glutamate, for instance due to feedforward excitation, which locally and globally interacts with noradrenaline (Mather et al., 2015). This idea accounts for the phenomenon that noradrenaline possibly only marginally affects weak neural activity but amplifies strong activity, resulting in multiplicative gain. Notably, strong sensory drive is also associated with an equally strong (Shadlen and Newsome, 1998), or even stronger (Haider et al., 2013), increase in GABAergic inhibition. As of yet, it is unknown if noradrenaline also interacts with the levels of

GABA in the circuit.

In stark contrast to the effects of catecholamines, in this study, increased levels of acetylcholine led to a strong decrease in whole-brain power envelope correlations during rest, with peaks in the alpha- (~11 Hz) and beta-band (~16 Hz) (Fig. 2B/3C). These decreases were spatially widespread and unspecific, possibly reflecting the relatively homogeneous distribution of cholinergic receptors throughout the brain as well as the global innervation profile of cholinergic nuclei in the basal forebrain (Ballinger et al., 2016). Acetylcholine did not alter cortical correlations under external drive (Fig. 3D), that is, during task, and, thus, exhibited significant context-dependence. Notably, this context-dependence was reversed compared to catecholamines, whose effects were strongest during task. Context-dependent effects of acetylcholine have only rarely been assessed and are, consequently, not well understood. Activity in cholinergic centers in the basal forebrain results in cortical disinhibition, for instance in A1 and V1 (Froemke et al., 2007; Fu et al., 2014; Letzkus et al., 2015). This disinhibition is likely the result of the activation of VIP+ interneurons, which in turn decrease the inhibitory effects of SOM+ interneurons on excitatory pyramidal cells (Fu et al., 2014). This circuit mechanism may account for the observed increases in neural gain, associated with focused attention (Thiele et al., 2009) and locomotion (Pi et al., 2013; Fu et al., 2014). Recently, this view has been challenged by several observations, demonstrating that acetylcholine (Kuchibhotla et al., 2016), as well as locomotion (Pakan et al., 2016), activate PV+, SOM+ and VIP+ interneurons in parallel. Most interestingly, these inhibition-related effects of locomotion in V1 exhibit context-dependence (Pakan et al., 2016): during visual stimulation, locomotion resulted in the activation of PV+, VIP+ and SOM+ interneurons, as well as excitatory pyramidal cells. In darkness, however, SOM+ interneurons and pyramidal cells were largely unaffected by locomotion. Thus, it is possible that in the present study, acetylcholine mainly activated PV+ and VIP+ interneurons during rest (i.e., in absence of task/sensory drive). During

task (i.e., strong visual drive), on the other hand, all three interneurons as well as excitatory pyramidal cells were affected. It is unknown how such cell specific effects would affect large-scale cortical activity and interactions across entire regions. Future work should address if and how such local changes can account for the context-dependence of large-scale network alterations as reported here.

## Conclusions

In this study, we provided a quantitative description of the effects of two major neuromodulators, catecholamines and acetylcholine, on the whole-brain correlation structure during both rest and task. Critically, both neuromodulators differed substantially in their effects: catecholamines increased cortical correlations during rest, but not task, whereas acetylcholine decreased cortical correlations during rest, but not during task. These results provide fundamental insights into the physiological mechanisms underlying the generation of large-scale correlated intrinsic activity. Moreover, the reported findings may help to identify novel “neuromodulatory fingerprints” (Schaefer et al., 2014), which can be used to infer disturbances in the functioning of neuromodulatory systems in diseases commonly associated with the malfunctioning of such systems.

## References

- Aston-Jones G, Cohen JD (2005) An integrative theory of locus coeruleus-norepinephrine function: adaptive gain and optimal performance. *Ann Rev Neurosci* 28:403–450.
- Ballinger EC, Ananth M, Talmage DA, Role LW (2016) Basal Forebrain Cholinergic Circuits and Signaling in Cognition and Cognitive Decline. *Neuron* 91:1199–1218.
- Bauer M, Kluge C, Bach D, Bradbury D, Heinze HJ, Dolan RJ, Driver J (2012) Cholinergic enhancement of visual attention and neural oscillations in the human brain. *Curr Biol* 22:397–402.

- Pfeffer et al.: Context-dependent neuromodulation of cortical correlation structure
- Brookes M, Tewarie P, Hunt B, Robson S (2016) A multi-layer network approach to MEG connectivity analysis. *NeuroImage* 132:425-38.
- Brookes MJ, Woolrich MW, Barnes GR (2012) Measuring functional connectivity in MEG: A multivariate approach insensitive to linear source leakage. *NeuroImage* 63:910–920.
- Cabral J, Luckhoo H, Woolrich M, Joensson M, Mohseni H, Baker A, Kringelbach ML, Deco G (2013) Exploring mechanisms of spontaneous MEG functional connectivity: How delayed network interactions lead to structured amplitude envelopes of band-pass filtered oscillations. *NeuroImage* 90:423-35
- Chen N, Sugihara H, Sur M (2015) An acetylcholine-activated microcircuit drives temporal dynamics of cortical activity. *Nat Neurosci* 18:892–902.
- de Pasquale F, Penna S, Snyder AZ, Lewis C, Mantini D, Marzetti L, Belardinelli P, Ciancetta L, Pizzella V, Romani GL, Corbetta M (2010) Temporal dynamics of spontaneous MEG activity in brain networks. *Proc Natl Acad Sci U S A* 107:6040–6045.
- Deco G, Hagmann P, Hudetz AG, Tononi G (2013) Modeling Resting-State Functional Networks When the Cortex Falls Sleep: Local and Global Changes. *Cereb Cortex* 24(12):3180-94.
- Deco G, Jirsa VK, R M Anthony (2011) Emerging concepts for the dynamical organization of resting-state activity in the brain. *Nat Rev Neurosci* 12:43–56.
- Disney AA, Aoki C, Hawken MJ (2007) Gain Modulation by Nicotine in Macaque V1. *Neuron* 56:701–713.
- Donner TH, Nieuwenhuis S (2013) Brain-wide gain modulation: the rich get richer. *Nat Neurosci* 16:989–990.
- Eldar E, Cohen JD, Niv Y (2013) The effects of neural gain on attention and learning. *Nat Neurosci* 16:292–303.
- Footes S, Morrison J (1987) Extrathalamic modulation of cortical function. *Annu Rev Neurosci* 10:67-95.
- Fox MD, Raichle ME (2007) Spontaneous fluctuations in brain activity observed with functional magnetic resonance imaging. *Nat Rev Neurosci* 8:700–711.
- Fox MD, Snyder AZ, Vincent JL, Corbetta M, Essen DC, Raichle ME (2005) The human brain is intrinsically organized into dynamic, anticorrelated functional networks. *Proc Natl Acad Sci U S A* 102:9673–9678.
- Froemke R, Merzenich M, Schreiner C (2007) A synaptic memory trace for cortical receptive field plasticity. *Nature* 450(7168):425-9.

Pfeffer et al.: Context-dependent neuromodulation of cortical correlation structure

- Fu Y, Tucciarone JM, Espinosa SJ, Sheng N, Darcy DP, Nicoll RA, Huang JZ, Stryker MP (2014) A cortical circuit for gain control by behavioral state. *Cell* 156:1139–1152.
- Greicius M (2008) Resting-state functional connectivity in neuropsychiatric disorders. *Curr Opin Neurol* 21:424–430.
- Haider B, Häusser M, Carandini M (2013) Inhibition dominates sensory responses in the awake cortex. *Nature* 493(7430):97-100.
- Harris KD, Thiele A (2011) Cortical state and attention. *Nat Rev Neurosci* 12:509–523.
- Hasselmo M, Bower J (1992) Cholinergic suppression specific to intrinsic not afferent fiber synapses in rat piriform (olfactory) cortex. *J Neurophysiol* 67:1222–1229.
- Hasselmo ME, Bower JM (1993) Acetylcholine and memory. *Trends Neurosci* 16:218–222.
- Hawellek D, Schepers I, Roeder B, Engel A, Siegel M, Hipp J (2013) Altered Intrinsic Neuronal Interactions in the Visual Cortex of the Blind. *J Neurosci* 33:1707217080.
- Hawellek DJ, Hipp JF, Lewis CM, Corbetta M, Engel AK (2011) Increased functional connectivity indicates the severity of cognitive impairment in multiple sclerosis. *Proc Natl Acad Sci U S A* 108:19066–19071.
- Hipp J, Siegel M (2015) BOLD fMRI correlation reflects frequency-specific neuronal correlation. *Curr Biol* 25(10):1368-74.
- Hipp JF, Hawellek DJ, Corbetta M, Siegel M, Engel AK (2012) Large-scale cortical correlation structure of spontaneous oscillatory activity. *Nat Neurosci* 15:884–890.
- Honey CJ, Kötter R, Breakspear M, Sporns O (2007) Network structure of cerebral cortex shapes functional connectivity on multiple time scales. *Proc Natl Acad Sci U S A* 104:10240–10245.
- Honey CJ, Thivierge J-PP, Sporns O (2010) Can structure predict function in the human brain? *NeuroImage* 52:766–776.
- Kuchibhotla KV, Gill JV, Lindsay GW, Papadoyannis ES, Field RE, Sten TA, Miller KD, Froemke RC (2016) Parallel processing by cortical inhibition enables context-dependent behavior. *Nat Neurosci* 20:62–71.
- Lee S, Dan Y (2012) Neuromodulation of brain states. *Neuron* 76: 209–222.
- Leopold DA, Murayama Y, Logothetis NK (2003) Very slow activity fluctuations in monkey visual cortex: implications for functional brain imaging. *Cereb Cortex* 13:422–433.



Pfeffer et al.: Context-dependent neuromodulation of cortical correlation structure

- Letzkus JJ, Wolff SBE, Lüthi A (2015) Disinhibition, a Circuit Mechanism for Associative Learning and Memory. *Neuron* 88:264–276.
- Mather M, Clewett D, Sakaki M, Harley CW (2015) Norepinephrine ignites local hot spots of neuronal excitation: how arousal amplifies selectivity in perception and memory. *Brain Behav Sci*:1–100.
- Murphy BK, Miller KD (2003) Multiplicative gain changes are induced by excitation or inhibition alone. *J Neurosci* 23:10040–10051.
- Nelson A, Mooney R (2016) The Basal Forebrain and Motor Cortex Provide Convergent yet Distinct Movement-Related Inputs to the Auditory Cortex. *Neuron* 90:635–648.
- Nichols T, Holmes A (2002) Nonparametric permutation tests for functional neuroimaging: a primer with examples. *Hum Brain Mapp* 15(1):1-25.
- O'Reilly JX, Crosson PL, Jbabdi S, Sallet J, Noonan MP, Mars RB, Browning PGF, Wilson CRE, Mitchell AS, Miller KL, Rushworth MFS, Baxter MG (2013) Causal effect of disconnection lesions on interhemispheric functional connectivity in rhesus monkeys. *Proc Natl Acad Sci* 110:13982–13987.
- Pakan JM, Lowe SC, Dylida E, Keemink SW, Currie SP, Coutts CA, Rochefort NL (2016) Behavioral-state modulation of inhibition is context-dependent and cell type specific in mouse visual cortex. *Elife* 5.
- Pfeffer CK, Xue M, He M, Huang Z, Scanziani M (2013) Inhibition of inhibition in visual cortex: the logic of connections between molecularly distinct interneurons. *Nat Neurosci* 16:1068–1076.
- Pi H-J, Hangya B, Kvitsiani D, Sanders JI, Huang ZJ, Kepecs A (2013) Cortical interneurons that specialize in disinhibitory control. *Nature* 503:521–524.
- Pinto L, Goard MJ, Estandian D, Xu M, Kwan AC, Lee S-HH, Harrison TC, Feng G, Dan Y (2013) Fast modulation of visual perception by basal forebrain cholinergic neurons. *Nat Neurosci* 16:1857–1863.
- Polack P-OO, Friedman J, Golshani P (2013) Cellular mechanisms of brain state-dependent gain modulation in visual cortex. *Nat Neurosci* 16:1331–1339.
- Schaefer A, Burmann I, Regenthal R, Arélin K, Barth C, Pampel A, Villringer A, Margulies DS, Sacher J (2014) Serotonergic Modulation of Intrinsic Functional Connectivity. *Curr Biol* 24:2314–2318.
- Scholvinck ML, Maier A, Ye FQ, Duyn JH, Leopold DA (2010) Neural basis of global resting-state fMRI activity. *Proc Natl Acad Sci* 107:10238–10243.

Pfeffer et al.: Context-dependent neuromodulation of cortical correlation structure

Servan-Schreiber D, Printz H, Cohen J (1990) A network model of catecholamine effects: gain, signal-to-noise ratio, and behavior. *Science* 249:892–895.

Shadlen MN, Newsome WT (1998) The variable discharge of cortical neurons: implications for connectivity, computation, and information coding. *J Neurosci* 18:3870–3896.

Supp GG, Siegel M, Hipp JF, Engel AK (2011) Cortical Hypersynchrony Predicts Breakdown of Sensory Processing during Loss of Consciousness. *Curr Biol* 21:1988–1993.

Thiele A, Pooresmaeili A, Delicato LS, Herrero JL, Roelfsema PR (2009) Additive Effects of Attention and Stimulus Contrast in Primary Visual Cortex. *Cereb Cortex* 19:2970–2981.

Tzourio-Mazoyer N, Landeau B, Papathanassiou D, Crivello F, Etard O, Delcroix N, Mazoyer B, Joliot M (2002) Automated Anatomical Labeling of Activations in SPM Using a Macroscopic Anatomical Parcellation of the MNI MRI Single-Subject Brain. *NeuroImage* 15:273–289.

van den Brink RL, Pfeffer T, Warren CM, Murphy PR, Tona K-D, van der Wee NJA, Giltay E, van Noorden MS, Rombouts SARB, Donner TH, Nieuwenhuis S (2016) Catecholaminergic Neuromodulation Shapes Intrinsic MRI Functional Connectivity in the Human Brain. *J Neurosci* 36:7865–7876.

Vincent J, Patel G, Fox M, Snyder A, Baker J, Van Essen D, Zempel J, Snyder L, Corbetta M, Raichle M (2007) Intrinsic functional architecture in the anaesthetized monkey brain. *Nature* 447:83–86.

Warren C, Eldar E, van den Brink R (2016) Catecholamine-mediated increases in gain enhance the precision of cortical representations. *J Neurosci* 36(21):5699-708.

Woolf N (1991) Cholinergic systems in mammalian brain and spinal cord. *Prog Neurobiol* 37:475–524.

Zagha E, DA M (2014) Neural control of brain state. *Curr Opin Neurobiol* 0:178-186.

## 5. Abstract

### 5.1. English

Perceptual decision-making is a cognitive operation that results in committing to one perceptual interpretation about the state of the world over a set of alternatives. Studies from psychology and neuroscience have shown that observers accumulate multiple samples of (noisy) perceptual information over time, until a decision threshold is crossed and a choice is made. The accumulation timescale is hypothesized to depend on the strength of recurrent excitation within local cortical circuits as well as their embedding in a large-scale functional network. Decision-making is a highly flexible mechanism, yet little is known about the flexibility of the accumulation timescale and whether it can be strategically adjusted in order to improve performance. Both local circuit dynamics as well as functional network topology fluctuate as a function of brain state, which is under the control of neuromodulators such as noradrenaline and acetylcholine, suggesting an involvement of these systems in temporal accumulation during decision-making.

Through a combination of psychophysics and computational modelling, this thesis provides evidence that the timescale of evidence accumulation is a bounded property with an upper limit, just like working memory capacity. However, below this limit, human observers optimize their performance on a perceptual decision-making task by adjusting the timescale over which they accumulate non-stationary flickering visual evidence that is embedded in noise. This provides evidence for a new type of top-down control in decision-making.

Using pharmacological manipulation and magnetoencephalography (MEG) during rest and task, it is shown in this thesis how such changes could be implemented within cortical circuits: catecholamines (noradrenaline and dopamine) are demonstrated to

increase the local ratio between excitation and inhibition, possibly reflecting an increase in recurrent excitation. Moreover, both acetylcholine and catecholamines are shown here to result in large-scale reconfigurations of the functional network topology of intrinsic brain activity. Thus, the results presented in this thesis argue that (i) the time scale of evidence accumulation is a bounded but adaptive property that can be strategically adjusted by the observer in order to optimize performance, (ii) neuromodulators such as catecholamines and acetylcholine alter both local cortical dynamics and functional network topology, suggesting their involvement in controlling the timescale of evidence accumulation.

## 5.2. German

Perzeptuelle Entscheidungsfindung ist eine kognitive Operation, die darin resultiert, dass eine Wahrnehmungsdeutung über den Zustand der Welt gegenüber anderen alternativen Wahrnehmungsdeutungen abwägt und ausgewählt wird. Frühere Studien aus Psychologie und Neurowissenschaften konnten zeigen, dass Beobachter mehrere Samples verfügbarer Wahrnehmungsinformation über die Zeit akkumulieren, bis eine sogenannte Entscheidungsschwelle überschritten ist und eine Wahl getroffen wird. Dabei wird vermutet, dass die Zeitskala der Akkumulation von der Stärke rekurrenter Erregung innerhalb lokaler kortikaler Schaltkreise, sowie der Einbettung jener in ein großflächiges funktionelles Netzwerk abhängt. Die menschliche Entscheidungsfindung ist ein hochflexibler Prozess, jedoch ist wenig über die Flexibilität der Akkumulationszeitskala bekannt und ob diese vom Beobachter adjustiert werden kann, um Performance zu verbessern. Sowohl die Dynamik lokaler kortikaler Schaltkreise als auch jene funktionaler Netzwerktopologie fluktuieren in Abhängigkeit vom globalen Zustand des Gehirns. Dieser Zustand wird wiederum von Neuromodulatoren wie

Noradrenalin und Acetylcholin reguliert. Dies legt nahe, dass neuromodulatorische Systeme auch bei der zeitlichen Akkumulation sensorischer Information eine Rolle spielen könnten.

Durch eine Kombination von Psychophysik und mathematischer Modellierung wird in dieser Dissertation dargelegt, dass menschliche Beobachter die Zeitskala, über welche sie flackernde visuelle Information in einer perzeptuellen Entscheidungsaufgabe akkumulieren, anpassen, vorausgesetzt dass die verfügbare Information nichtstationär ist und ihre Performance dadurch optimiert werden kann. Die Zeitskala kann dabei jedoch nicht ohne Einschränkung angepasst werden, sondern nur innerhalb eines gewissen Bereichs, der nach oben begrenzt zu sein scheint. Damit zeigt diese Arbeit eine neue Form der top-down Kontrolle in der Entscheidungsfindung auf.

Weiterhin wird durch Anwendung pharmakologischer Manipulationen und Magnetoenzephalographie (MEG) während einer Ruhemessung und während der Bearbeitung einer perzeptuellen Aufgabe zudem gezeigt, wie solche Veränderungen in neuronalen Schaltkreisen implementiert sein könnten: Katecholamine (Noradrenalin und Dopamine) erhöhen das lokale Verhältnis zwischen Erregung und Hemmung, was möglicherweise eine Verstärkung der rekurrenten Erregung innerhalb dieser Schaltkreise widerspiegelt. Des Weiteren wird gezeigt, dass sowohl Acetylcholin als auch Katecholamine zu großräumigen Rekonfigurationen der funktionellen Netzwerktopologie intrinsischer Hirnaktivität führen. Zusammenfassend legen die in dieser Arbeit dargestellten Ergebnisse nahe dass (i) die Zeitskala der Evidenzakkumulation eine adaptive Eigenschaft ist, die innerhalb eines bestimmten Bereichs strategisch angepasst werden kann, um Performance zu optimieren, (ii) Neuromodulatoren wie Katecholamine und Acetylcholin lokale kortikale Schaltkreise

sowie großflächige funktionale Netzwerktopologie verändern, was auf eine Rolle dieser neuromodulatorischen Systeme der bei der zeitlichen Akkumulation von Information nahelegt.

## 6. Acknowledgements

This work would not have been possible without the support of many people. First and foremost, I would like to express my deepest gratitude to my supervisor Tobias Donner, who has profoundly shaped my scientific thinking over the recent years, but has also provided me with the freedom necessary to pursue my own interests. His scientific rigor and enthusiasm will remain as a guiding model for me in the future.

Furthermore, I would like to thank Andreas Engel, without whom large parts of this work would not have been possible and who created an inspiring scientific environment at the Department of Neurophysiology. Moreover, I am deeply grateful to Guido Nolte, for providing profound and instructive methodological support and feedback throughout those years.

Science depends on collaborations and the exchange of ideas and thoughts. Luckily, during my time as a PhD student, I had a number of fantastic collaborators, who I would like to thank. For sharing their knowledge, their ideas, their enthusiasm but also their criticism. In particular, I would like to thank Konstantinos Tsetsos, Marius Usher, Pia Jentgens, Rudy van den Brink, Sander Nieuwenhuis, Klaus Linkenkaer-Hansen, Arthur Avrmiea, Gustavo Deco, Adrian Ponce-Alvarez and Anne Urai.

Scientific work would be only half as enjoyable without the proper social environment. Therefore, I would like to thank my friends and colleagues at the Department of Neurophysiology. For sharing both the joys but also the frustrations of academic life. Special thanks go to my current and former office mates, Marion Höfle, Ina Peiker, Kathrin Müsch, Sarah Bütöf, Arne Ewald and Anke Braun.

Finally, I would like to thank those people who substantially shaped who I am today: my close friends, long-time companions and siblings. For being there when it matters (but also when it doesn't). And for always reminding me that the most important things

in life are to be found outside of academia. Of course, none of this would have been possible without the trust and the almost unconditional support by my parents - I am forever indebted. My final thanks are dedicated to Marie, who I thank for all her support, her input, her optimism, her humor, and her love.



## 7. Curriculum vitae

---

### **Education**

- 01/2012 – current**      PhD student  
University Medical Center Hamburg-Eppendorf  
**Advisors:** Prof. Tobias H. Donner, Prof. Andreas K. Engel
- 2013 – 2014**            MFA student in Fine Arts  
University of the Arts (HfBK) Hamburg
- 2010 - 2012**            MSc student in Brain & Cognitive Sciences  
University of Amsterdam, The Netherlands  
*Graduated with distinction*
- 2006 – 2010**            BSc student in Psychology  
University of Vienna (2006 – 2008)  
University of Magdeburg (2008 – 2010)
- 2004 – 2005**            BSc student in Interactive Media  
University of Applied Sciences Augsburg, Germany

---

### **Research experience**

- 2012 – present**        *Research scientist*  
University Medical Center Hamburg-Eppendorf
- 2016**                    *Visiting scientist (3 months)*  
Universitat Pompeu Fabra, Barcelona, Spain  
**Supervisor:** Prof. Gustavo Deco
- 2011 – 2012**            *Masters student*  
Centre for Integrative Neuroscience (CIN)  
University of Tuebingen, Germany  
**Supervisor:** Dr. Markus Siegel
- 2009**                    *Research intern*  
MPI for Brain and Cognitive Sciences, Leipzig, Germany
- 2008 – 2010**            *Student assistant*  
Institute for Cognitive Neurology and Dementia Research  
University of Magdeburg, Germany
- 2009**                    *Student assistant*  
institute for Biological Psychology  
University of Magdeburg, Germany

## **8. Eidesstattliche Versicherung (Declaration of academic integrity)**

Ich versichere ausdrücklich, dass ich die Arbeit selbständig und ohne fremde Hilfe verfasst, andere als die von mir angegebenen Quellen und Hilfsmittel nicht benutzt und die aus den benutzten Werken wörtlich oder inhaltlich entnommenen Stellen einzeln nach Ausgabe (Auflage und Jahr des Erscheinens), Band und Seite des benutzten Werkes kenntlich gemacht habe.

Ferner versichere ich, dass ich die Dissertation bisher nicht einem Fachvertreter an einer anderen Hochschule zur Überprüfung vorgelegt oder mich anderweitig um Zulassung zur Promotion beworben habe.

Ich erkläre mich einverstanden, dass meine Dissertation vom Dekanat der Medizinischen Fakultät mit einer gängigen Software zur Erkennung von Plagiaten überprüft werden kann.

Unterschrift: .....